The Development of Organelle-localized Hsp90 Isoform-selective Inhibitors

By Vincent Matthew Crowley

Submitted to the graduate degree program in Medicinal Chemistry and the Graduate Faculty of the University of Kansas in partial fulfillment of the requirements for the degree of Doctor of Philosophy.

_____

Co-chairperson: Dr. Brian S. J. Blagg

_____

Co-chairperson: Dr. Apurba Dutta

_____

Dr. Ryan A. Altman

_____

Dr. Mark P. Farrell

_____

Dr. Rick T. Dobrowsky

Date Defended: October 18, 2017

The dissertation committee for Vincent Matthew Crowley certifies that
this is the approved version of the following dissertation:

The Development of Organelle-localized Hsp90 Isoform-selective

Inhibitors

_____

Co-chairperson: Dr. Brian S. J. Blagg

_____

Co-chairperson: Dr. Apurba Dutta

Date Approved: October 18, 2017

ii

Abstract

Molecular chaperones are responsible for the maturation of nascent polypeptides and the re-maturation of denatured proteins. One chaperone family that has emerged as an attractive therapeutic target is the 90 kDa heat shock proteins (Hsp90). Hsp90 is responsible for the maturation of proteins associated with all ten hallmarks of cancer, and its inhibition results in a multidirectional attack on cancer. More than seventeen small molecule inhibitors have entered clinical trials; however, concerns have risen due to toxicities, dosing and scheduling issues, and lack of efficacy as a single agent. Therefore, alternative strategies for Hsp90 inhibition are needed to take advantage of the unique biological role of Hsp90. All of the molecules evaluated in clinical trials exhibit *pan*-Hsp90 inhibition and target all four Hsp90 isoforms with similar affinities.

Humans express four different Hsp90 isoforms: Hsp90α and Hsp90β reside in the cytosol, Grp94 is localized to the endoplasmic reticulum, and TRAP1 is found in the mitochondria. Emerging evidence suggests that each Hsp90 isoform plays a unique role in cancer progression. Therefore, to further study the individual roles of each isoform, the development of Hsp90 isoform-selective inhibitors is highly desirable. However, the development of such inhibitors is hindered by the fact that the N-terminal ATP-binding pocket is >85% identical among all four isoforms.

Described herein is the development of isoform-selective inhibitors of the ER- and mitochondria-localized Hsp90 isoforms, Grp94 and TRAP1, respectively. Grp94-selective inhibitors were evaluated in models of myocilin-associated open angle glaucoma, cancer metastasis, and multiple myeloma. TRAP1-selective inhibitors were evaluated for their ability to induce apoptosis in cancer cells. These isoform-selective inhibitors will serve as invaluable tools to continue to study the roles played by these isoforms in cancer as well as other indications.

Acknowledgements

The last five years have been an experience that I will never forget. Through the highs and the lows, I was lucky to have constant support to help me continue to become a better scientist, friend, and colleague. There have been many people help me that deserve to be recognized.

First, I would like to thank my advisor Dr. Brian Blagg for his mentorship and allowing me to grow and mature as a scientist. I would also like to thank members of the Blagg lab (past and present) that helped make life in lab more enjoyable. Specifically, Dr. Anuj Khandelwal who was a great person to bounce research ideas off of and discuss the Kansas versus Kentucky basketball rivalry. He will be deeply missed and his passion and drive will continue to be a source of motivation throughout my career.

I would like to thank my committee members for taking the time to serve on my committee and helping me continue to develop as a scientist. I would also like to thank Dr. Blake Peterson, Dr. Tom Prisinzano, and their labs for providing me space, equipment, and advice to complete my graduate work. Other members of the Medicinal Chemistry department that deserve a huge thank you are Jane and Norma, their work and organization helped make everything outside class and lab incredibly easy.

My family has been my biggest supporters over the past 5 years. To my parents, brother, and 'new' family: Thank you! You guys have been there for me through it all, provided an amazing support network, and pushed me to be successful at whatever I set my mind to. Lastly, my wife, Rachel, I would not have been able to do it without your support, understanding, and help. I am looking forward what our next chapter together has in store for us.

In addition to the friends and colleagues that I have met throughout my time at KU, I must thank the National Cancer Institute for providing me with financial support in graduate school and in the coming years as a postdoctoral researcher.

Table of Contents

List of Figures

List of Schemes

List of Tables

List of Abbreviations

17-AAG	17-*N*-allylamino-17-demethoxygeldanamycin
A549	Non-small cell lung cancer cell line
AIBN	Azobisisobutyronitrile
CHOP	C/EBP homologous protein
CypD	Cyclophilin D
DBU	1,8-Diazabicyclo[5.4.0]undec-7-ene
DLCs	Delocalized lipophilic cations
DPPA	Diphenylphosphoryl azide
EDCI	1-Ethyl-3-(3-dimethylaminopropyl)carbodiimide Hydrochloride
ER	Endoplasmic reticulum
ERAD	Endoplasmic reticulum associated degradation
FITC	Fluorescein isothiocyanate
GDA	Geldanamycin
GHKL	DNA gyrase, Hsp90, histidine kinase, and mutl
Grp94	Glucose-regulated protein 94
GRPs	Glucose regulated proteins
HCT116	Colorectal cancer cell line
HEK293	Human embryonic kidney cell line
HeLa	Cervical cancer cell line
hERG	Human ether a-go-go-related gene
HOBt	Hydroxybenzotriazole
HOP	Hsp70-Hsp90 organizing co-chaperone
HSF-1	Heat shock factor-1
HSP	Heat shock protein
Hsp90 and Hsp70	Heat shock protein 90 and 70
HSR	Heat shock response
IGF	Insulin-like growth factor
IOP	Intraocular pressure
KD	Knockdown
LDA	Lithium diisopropylamide
LRP6	Low density lipoprotein receptor-related family
MAP	Mitogen activated protein
MDA-MB-231	Triple-negative breast cancer cell line
MMP-2	Matrix-metalloproteinase-2
MOM	Methoxymethyl
MTP	Membrane transition pore
NBS	*N*-Bromosuccinimide
NECA	N-ethylcarboxamideadenosine
PC3-MM2	Prostate cancer cell line
PDB	Protein data bank
POAG	Primary open angle glaucoma
RDA	Radamide

RDC	Radicicol
RuPhos	2- dicyclohexylphosphino-2′,6′-diisopropoxybiphenyl
siRNA	Small interfering RNA
SK-MEL-28	Melanoma cancer cell line
TBAF	Tetra-*n*-butylammonium fluoride
TLR	Toll-like receptor
TM	Trabecular meshwork
TPP	Triphenylphosphonium
TRAP1	Hsp75/tumor necrosis factor receptor associated protein 1
UPR	Unfolded protein response
WT	Wild type
XPhos	2- dicyclohexylphosphino-2′,4′,6′-triisopropylbiphenyl

1. Introduction to Hsp90 Structure, Function, and Isoform-selective Inhibition

Molecular Chaperones

Molecular chaperones are essential for the maintenance of protein homeostasis, assurance of proper folding, stability, activation, trafficking, and the degradation of cellular proteins to preserve a viable cellular environment.[1-4] Molecular chaperones are responsible for responding to and ameliorating the effects of intra- and extracellular stresses. Under stressed conditions, molecular chaperones interact with proteins that have undergone deleterious conformational changes to restore them into their proper biologically-active conformation. Subsets of proteins that demonstrate dependency upon molecular chaperones are referred to as client proteins, with some chaperones displaying more selectivity for their clientele than others.[1, 3]

One specific family of molecular chaperones is the heat shock protein (HSP) family.[5] As suggested by the name, these proteins are responsible for responding to cellular stresses, including elevated temperature. In addition to temperature, HSPs respond to various cellular insults including xenobiotic toxicity, inflammation, hypoxia, nutrient starvation, and protein

Family	Cellular Location	Primary Function
Small HSPs (<50 kDa)	Cytosol	Protein folding, inhibition of apoptosis
60 kDa HSPs	Mitochondria	Client protein folding after mitochondrial import
70 kDa HSPs	Cytosol and ER	Protein folding and thermotolerance
90 kDa HSPs	Cytosol, ER, Mitochondria, Extracellular	Protein activation and stabilization
100 kDa HSPs	Mitochondria, cytosol	Protein aggregate solubilization

Table 1.1. Cellular locations and primary functions of HSP families.

aggregation.[6-8] The HSP family is further characterized by the molecular weight of its members; for example, the 90 kDa heat shock protein is referred to as Hsp90. Members of the HSP family serve roles within various cellular compartments promoting protein homeostasis, as highlighted in **Table 1.1**. Upregulation of these HSPs occurs in many disease states, implicating some of these proteins as potential therapeutic targets.[9-11]

The 90 kDa Heat Shock Protein Family

The 90 kDa heat shock protein (Hsp90) family is responsible for the maturation of nascent polypeptides as well as the refolding of denatured proteins.[12] In fact, over 300 client protein substrates have been identified as Hsp90-dependent for their maturation into biologically active conformations.[13] Hsp90 represents one of the most abundantly expressed proteins within the cell, constituting 1-2% of total cellular protein under normal conditions, and under stressed conditions such as cancer, this can be elevated to as high as 6%.[14] In unstressed cells, Hsp90 promotes homeostasis through transient protein folding, protein trafficking, and protein turnover. Under stressed conditions, especially in cancer, Hsp90 levels are elevated to accommodate the increased demand of protein folding due to upregulated metabolism and constant proliferation.[15-16]

Hsp90 Structure

Hsp90 functions as a homodimer and each monomer is comprised of three domains that support its function (**Figure 1.1**).[12, 17] The N-terminal ATP-binding domain is responsible for binding ATP in an unconventional, bent conformation that is conserved within the GHKL superfamily of proteins (DNA gyrase, Hsp90, histidine kinase, and MutL). This bent conformation, known as a Bergerat fold, is in contrast to the typical extended conformation used by most kinases.[18] Consequently, this domain has been the focus of intense drug discovery research, as the majority
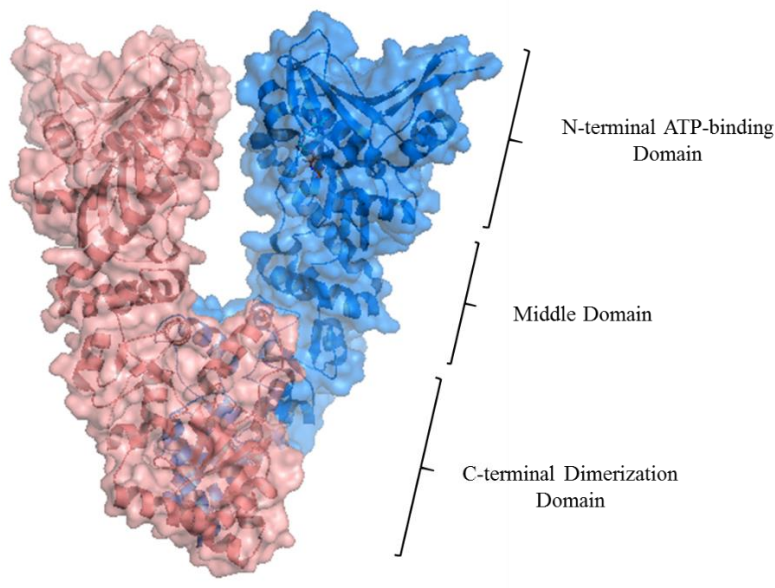
Figure 1.1. Homodimeric state of Hsp90 depicting the three different domains. (PDBID: 2O1U).

of known Hsp90 inhibitors bind competitively versus ATP to this pocket.[19-22] The middle domain

is connected to the N-terminal domain via a charged linker and is important for facilitating protein-

protein interactions with various Hsp90 client proteins and co-chaperones. The C-terminal

dimerization domain is responsible for maintaining the functional Hsp90 homodimer within cells.

In addition to dimerization, this domain also interacts with co-chaperones that facilitate client

protein maturation and progression through the Hsp90 chaperone cycle.[23-25]

Hsp90 Client Proteins

Hsp90 is responsible for the maturation of more than 300 client protein substrates, many of

which are involved in signaling pathways that are commonly hijacked during transformation. In

fact, Hsp90 client proteins are represented in all ten hallmarks of cancer (**Table 1.2**), including the

important anti-cancer targets Her2, Bcr-Abl, Raf, ALK, Src, and Akt, suggesting that Hsp90

inhibition could simultaneously target multiple oncogenic pathways and provide a multi-pronged

approach toward cancer inhibition.[26-28] Due to the high number of Hsp90 client proteins that play

vital roles in cancer progression, the most studied indication for Hsp90 inhibitors has been for the

potential treatment of cancer, however Hsp90 has also been implicated in other pathologies.[22, 29-33]

Hallmarks of Cancer	Hsp90 Client Protein
1. Sustaining Proliferative Signaling	Akt, HER2, BCR-Abl
2. Evading Growth Suppressors	CDK4, CDK6, Myc1
3. Avoiding Immune Destruction	IRAK3
4. Enabling Replicative Immortality	Telomerase
5. Tumor-promoting Inflammation	IL-6, IL-8, IRAK1
6. Activating Invasion & Metastasis	MMP-2, c-MET, Integrins
7. Inducing Angiogenesis	HIF-1α, VEGFR, PI3K
8. Genome Instability & Mutation	NEK8, FANCA, MAFG
9. Resisting Cell Death	p53, Survivin
10. Deregulating Cellular Energetics	ARNT, HMG1

Table 1.2. Hsp90 client proteins are represented in all ten hallmarks of cancer.

Hsp90 Chaperone Cycle

While the Hsp90 chaperone cycle is complex, advances in technology and small molecule probes have provided insight into this catalytic cycle. The cycle begins with the Hsp90 homodimer (**A**, **Figure 1.2**), to which a nascent polypeptide or denatured protein is delivered by Hsp70 (**B**). This process is facilitated by the Hsp70-Hsp90 organizing co-chaperone, HOP. After association with the nascent polypeptide, various immunophilins, co-chaperones, and partner proteins interact with the Hsp90/polypeptide complex to form the heteroprotein complex, **C**.[34] ATP then binds to the N-terminal ATP-binding site, followed by p23 association that stabilizes the closed form of Hsp90 (**D**). ATP hydrolysis provides the requisite energy necessary for maturation of the substrate protein (**E**), as well as release of the mature client protein and regeneration the Hsp90 homodimer, **A**.[35-36]
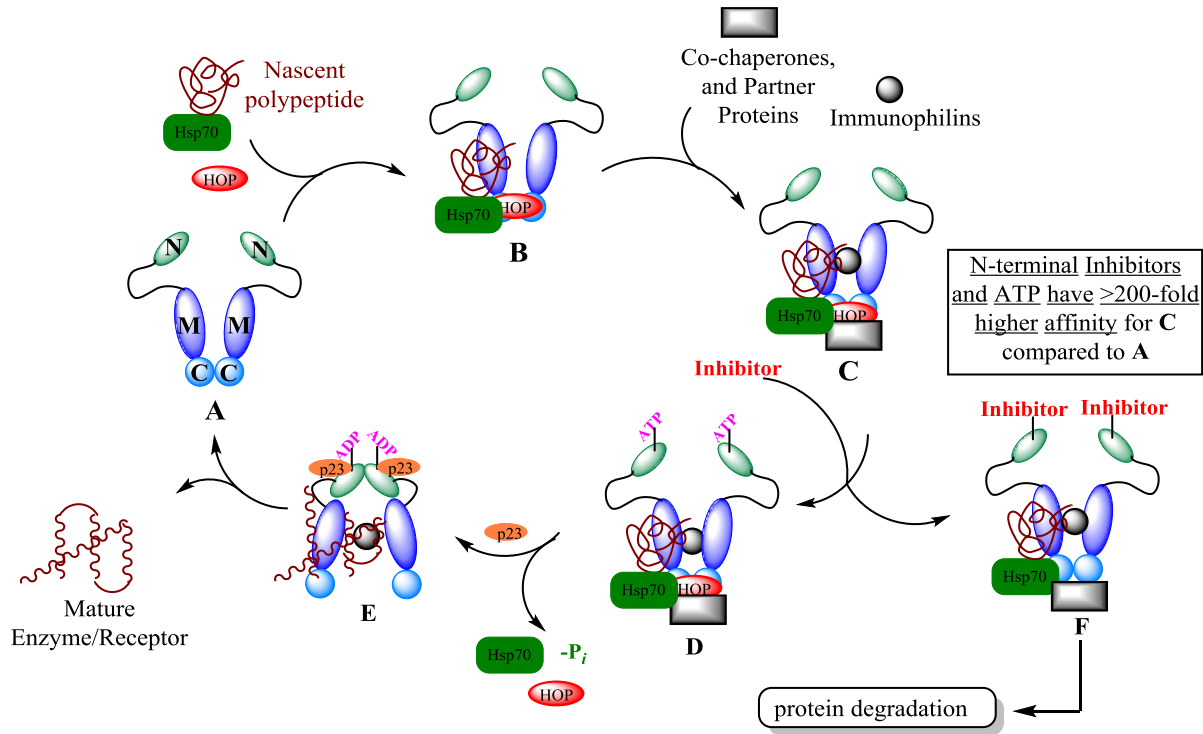
Figure 1.2. The Hsp90 chaperone cycle.

The Hsp90 chaperone cycle can be disrupted through competitive inhibition of the N-terminal ATP-binding domain. In the presence of a competitive, non-hydrolysable inhibitor, ATP is not able to bind the N-terminal ATP-binding pocket, which halts the Hsp90 chaperone cycle and results in the degradation of client protein substrates via the ubiquitin-proteasome pathway (**F**).[37] Malignant cells undergo constant proliferation, resulting in an increased need for the synthesis and maturation of proteins to maintain cell viability. This increased metabolic rate creates a reliance upon Hsp90 for cellular survival, which in turn, results in Hsp90 existing predominantly as the heteroprotein complex (**C**) in oncogenic cells.[38-39] This complex possesses ~200-fold higher affinity for ATP and other small molecules that bind the N-terminal domain, as compared to the Hsp90 homodimer (**A**), resulting in inherent differential selectivities. Consequently, Hsp90 inhibitors accumulate in transformed cells at significantly higher concentrations than normal tissue.

Hsp90 Isoforms

Humans express four different isoforms of Hsp90: Hsp90α and Hsp90β reside in the cytosol, Hsp75/tumor necrosis factor receptor associated protein 1 (TRAP1) is found predominantly in the mitochondria, and glucose regulated protein 94 (Grp94) the endoplasmic reticulum (ER) resident isoform.[12, 40] Deconvolution of the biological processes mediated by of each isoform has proven difficult; however, recent work has begun to delineate these roles.[33, 41-44 45]

Cytosolic Hsp90α/β

The cytosolic Hsp90 isoforms have been the most studied isoforms due to their role in the maturation of many proteins that are both essential to cell viability and reside in this compartment. Numerous crystal and co-crystal structures have been solved for these isoforms, which provides a wealth of structural information that has been used to guide the development of Hsp90 inhibitors.[46-49] These two isoforms are 86% identical over the length of the protein, and their N-terminal ATP-binding domains are 95% identical, differing by only two residues. Many client proteins for these isoforms have been identified and include protein kinases, transcription factors, mutated signaling proteins, and cell cycle regulators.

Distinct roles for Hsp90α and Hsp90β have been difficult to elucidate due to their high sequence identity, antibody cross reactivity, and the presence of Hsp90α/β heterodimers. However, generation of Hsp90α and Hsp90β knockdown cells has assisted in the identification of client proteins that are dependent upon each of these isoforms. Hsp90α knockdown studies have identified the tyrosine-protein kinase, c-Src, and the anti-apoptotic protein, survivin, as client proteins specifically dependent upon this isoform (**Table 1.3**).[41] In addition, Hsp90α is secreted into the extracellular matrix, where it contributes to tumor metastasis by stabilizing matrix-metalloproteinase-2 promoting its proteolytic activity.[50] Hsp90β knockdown studies have also

identified client proteins dependent upon this isoform, including the chemokine receptor, CXCR4, and cell cycle regulators CDK-4 and CDK-6 (**Table 1.3**).[41] In addition to these isoform-specific client proteins, other protein substrates that depend upon both isoforms include the MAP kinase, ERK5, the steroid hormone receptors, and the receptor tyrosine kinase, Her2.[45, 51-52] While client proteins of each cytosolic Hsp90 isoform have been identified, many Hsp90-dependent proteins have not yet been investigated for their isoform-dependency and therefore warrant further investigation to delineate the roles played by each cytosolic isoform.

ER-resident Grp94

Grp94 is the Hsp90 resident isoform in the ER and is a major member of the ER chaperone system along with other glucose regulated proteins (GRPs, e.g. Grp78). The ER chaperone system is responsible for responding to cellular insults, such as redox stress, calcium imbalance, and hypoxia, which result in the unfolded protein response (UPR) or ER stress.[53-54] Compared to Hsp90, Grp94 is only 42-43% identical, but it is ~85% identical within the N-terminal ATP-binding pocket. This difference in the ATP-binding pocket results from a 5 amino acid insertion upstream of the binding pocket, which produces a unique, hydrophobic binding region in the ATP-binding cavity.[55-56] This region can be further divided into two distinct sub-pockets that have been utilized to gain selectivity for Grp94 versus the other Hsp90 isoforms.[45, 57-58] Such Grp94-selective inhibitors and genetic knockdown studies have identified Grp94-dependent client proteins.

Grp94 is responsible for the maturation and trafficking of proteins associated with cell-to-cell signaling and cellular adhesion.[43, 54, 59-61] Additional roles played by Grp94 include embryonic development, calcium binding, and regulation of innate and adaptive immunity.[62] Some Grp94-specific client proteins include select integrins ($\alpha 2$, $\alpha 4$, αL, and $\beta 4$), Toll-like receptors (TLR1, TLR2, TLR4, and TLR9), insulin-like growth factor-I and –II (IGF-I and –II, respectively),

immunoglobulins, low-density lipoprotein receptor-related protein 6 (LRP6), and mutant myocilin (**Table 1.3**).[44-45, 59, 63] Recently, Grp94 has gained interest as a potential therapeutic target for myocilin-associated open angle glaucoma (mutant myocilin), cancer metastasis (integrins), and multiple myeloma (LRP6), which are discussed more thoroughly in Chapters 2, 3, and 4, respectively. [43-44, 58, 63-64]

Mitochondrial TRAP1

The second organelle-specific Hsp90 isoform is the mitochondrial-localized isoform, TRAP1.[65-66] This isoform exhibits the lowest sequence identity to other Hsp90s (~35%); however within its N-terminal ATP-binding site, TRAP1 differs by only four (Hsp90β) and five (Hsp90α) residues from the cytosolic isoforms, making TRAP1 more similar to Hsp90 than Grp94. Few co-crystal structures of TRAP1 are available, and all of these structures are bound to purine-based small molecules (non-hydrolysable ATP mimics and purine-based inhibitors).[67-69] However, these structures provide some insight into TRAP1-structural features that can be utilized to develop selective inhibitors.

TRAP1 is highly expressed in tumorigenic cells and is only expressed at basal (occasionally undetectable) levels in normal tissues.[70] Unlike other Hsp90 isoforms, no co-chaperones have been reported to interact with TRAP1, likely due to predominant localization of TRAP1 to the mitochondrial matrix wherein other Hsp90 co-chaperones do not accumulate as they lack a genetically encoded mitochondrial targeting sequence.[65] TRAP1 was first identified to play a cytoprotective role against mitochondrial apoptosis. Further studies via TRAP1 silencing by small interfering RNA (siRNA) revealed that decreased levels of TRAP1 activated apoptosis, culminating in the release of apoptogenic proteins into the cytosol, including cytochrome c, and activation of caspase induced cell death.[71-72] In addition to its apparent anti-apoptotic function,

Hsp90 Isoform	Identified Isoform-Specific Interactors
Hsp90α	C-Src, Survivin, MMP-2
Hsp90β	CXCR4, CDK-4, CDK-6
Grp94	Integrins ($\alpha2$, $\alpha4$, αL, $\beta4$), IgGs, Toll-like receptors (TLR1, TLR2, TLR4, TLR9), IGF-I and –II, LRP6, mutant myocilin
TRAP1	Cyclophilin D, sorcin, TBP7, β subunit of F_1F_0 ATP synthase, succinate dehydrogenase
Multiple Isoforms	ERK5, Hormone Receptors, Her2

Table 1.3. Some Hsp90 interactors demonstrate specificity towards individual Hsp90 isoforms.

TRAP1 also plays an important role during oxidative stress, by allowing cells to escape activation of reactive oxygen species-mediated apoptosis. Studies aimed at the identification of TRAP1 interactors within the mitochondria revealed cyclophilin D (CypD).[70] CypD is a component of the mitochondrial membrane transition pore (MTP), and formation of the MTP is widely believed to initiate mitochondrial apoptosis. Under normal conditions, TRAP1 antagonizes the actions of CypD, but disruption of this interaction can lead to the initiation of apoptosis. Additional TRAP1 interacting proteins include the calcium binding protein, sorcin, the AAA-ATPase proteasome regulatory protein, TBP7, the β-subunit of F_1F_0 ATP synthase, and succinate dehydrogenase (**Table 1.3**).[73] Low basal expression of TRAP1 in non-transformed cells could represent a mechanism to selectively target cancer via disruption of TRAP1 interactions with apoptogenic proteins.

Pan-Hsp90 Inhibitors in Clinical Trials

Traditionally, Hsp90 inhibitors have been inspired by the endogenous ligand ATP and natural products. The first Hsp90 inhibitor discovered was the benzoquinone ansamycin natural product, geldanamycin (**GDA**, **Figure 1.3**). **GDA** exhibited potent antitumor activity in a variety of cancer cell lines and was identified as an Hsp90 inhibitor in 1994, when Whitesell and co-workers demonstrated that treatment of prostate cancer cells with **GDA** inhibited Hsp90 led to degradation

of the oncogenic client protein, v-Src.[74] Despite the excellent tumor activity exhibited by **GDA**,

its clinical utility was hindered by hepatoxicity, low chemical stability, and poor solubility.[75]

However, structural analogues of **GDA** are currently under clinical investigation, including 17-*N*-

allylamino-17-demethoxygeldanamycin (**17-AAG**). **17-AAG** was the first Hsp90 inhibitor to enter

into clinical trials in 1999 for cancer; however, further development has been hindered by dose-

limiting toxicities.[76]

The resorcinol lactone, radicicol (**RDC**, **Figure 1.3**), was identified as an Hsp90 inhibitor after

it exhibited similar cellular effects and competed with **GDA** for the Hsp90 N-terminal ATP-

binding site.[77] Despite the potent anti-cancer effects in cellular cancer models, **RDC** exhibited no
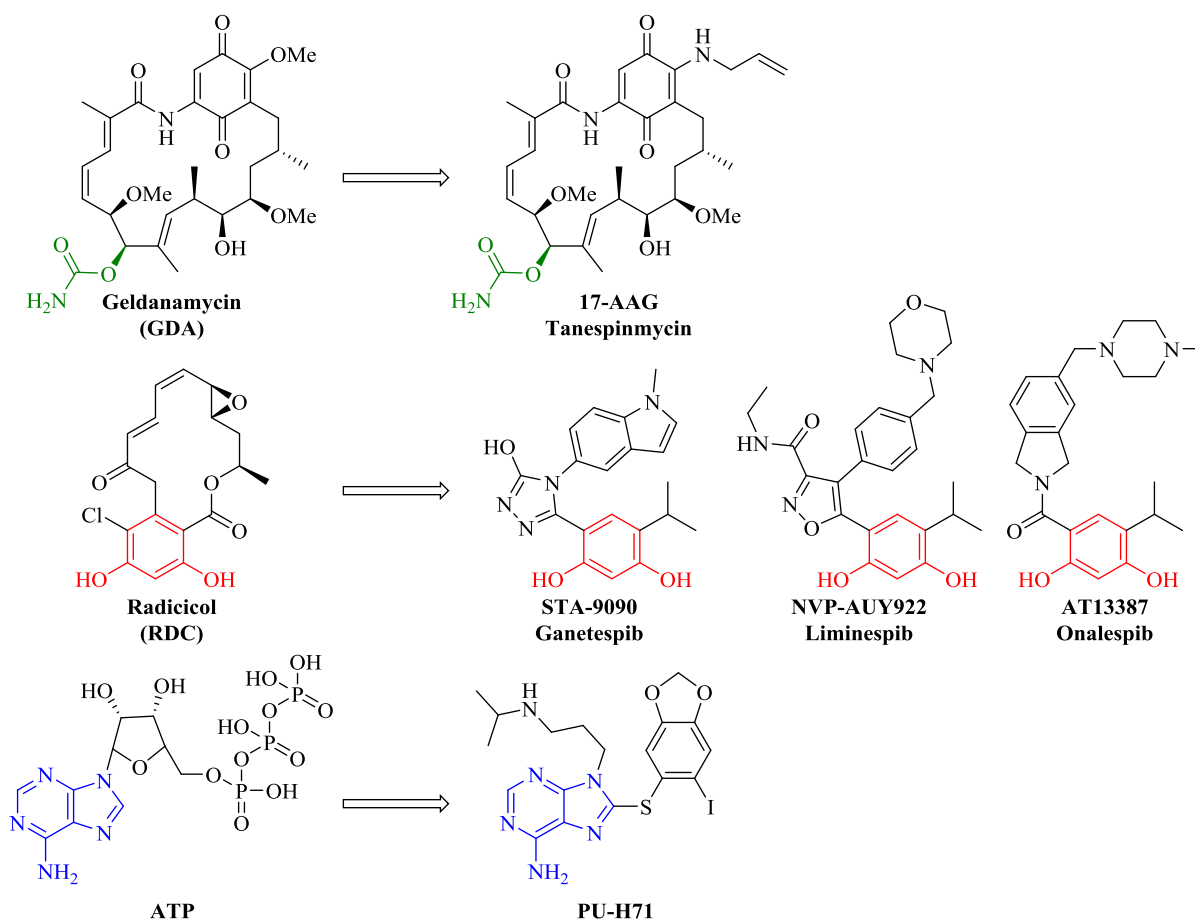
Figure 1.3. *pan*-Hsp90 inhibitory classes and clinical candidates. Pharmacophores are colored by individual classes of inhibitors.

10

activity in animal models due to rapid metabolism to inactive metabolites and its electrophilic nature (allylic epoxide and α,β,γ,δ-unsaturated ketone). Although **RDC** never advanced beyond cellular studies, it did provide a new pharmacophore for development of the resorcinol class of Hsp90 inhibitors. This class of inhibitors possesses the resorcinol ring of **RDC** along with a surrogate of the macrolactone via heterocycles (**STA-9090** and **NVP-AUY922**) or an amide (**AT13387**) that increases affinity and modulates the pharmacokinetic properties.[78-80] Currently, these three resorcinol-based inhibitors are under clinical investigation for various forms of cancer.

In addition to the inspiration derived from natural products **GDA** and **RDC**, the endogenous ligand ATP has served as a starting point for development of the purine-based Hsp90 inhibitor class. Utilizing the purine-core of ATP, Chiosis and co-workers used a structure-based approach to append the purine ring to a non-hydrolysable aryl side chain that could mimic the phosphate group of ATP within the nucleotide-binding site.[81] Optimization of the aryl side chain and the inclusion of a solubilizing amine produced the first purine-based clinical candidate, **PU-H71** (**Figure 1.3**), which remains under Phase 1 clinical evaluation in patients with metastatic solid tumors, lymphoma, or myeloproliferative neoplasms.[75]

Detriments Associated with *pan*-Hsp90 Inhibition

While there have been significant efforts to develop Hsp90 inhibitors for the treatment of cancer, noteworthy challenges have emerged during clinical evaluation. Ocular, hepato-, and cardiotoxicities, as well as scheduling and dosing issues have dampened enthusiasm for the advancement of such inhibitors.

Induction of the Heat Shock Response

The pro-survival heat shock response (HSR) is a natural cellular occurrence to exogenous stresses in which the production of HSPs is increased to restore homeostasis.[82-84] One clinically
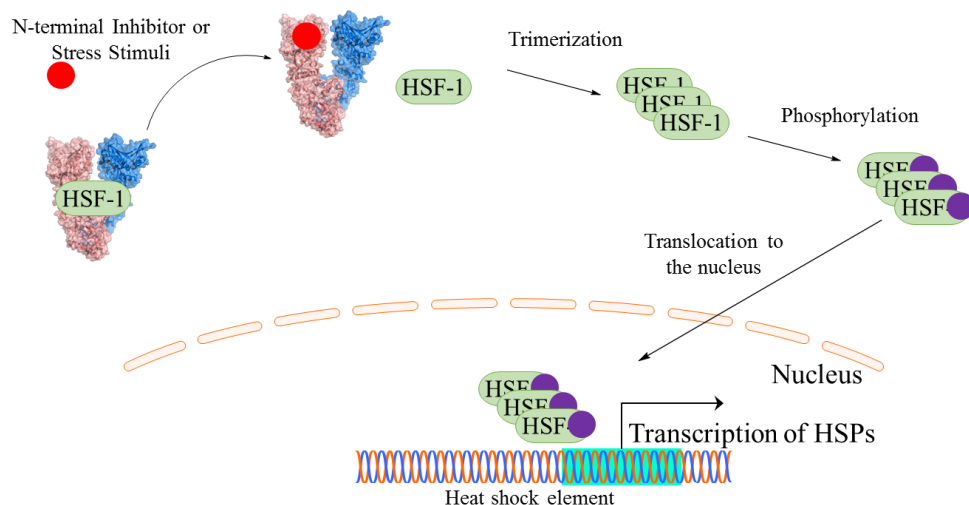
Figure 1.4. N-terminal Hsp90 inhibitors or stress stimuli induce the HSR resulting in increased expression of HSPs.

relevant concern is that administration of N-terminal Hsp90 inhibitors induces the HSR. This effect is mediated through the transcription factor, heat shock factor-1 (HSF-1). Under normal conditions, HSF-1 is associated with Hsp90 in an inactive state.[85-86] However, in the presence of an N-terminal inhibitor or a stress stimulus, HSF-1 dissociates from Hsp90, trimerizes and becomes phosphorylated to generate the activated form of this transcription factor (**Figure 1.4**).[87-89] Upon activation, HSF-1 translocates to the nucleus, where it binds the heat shock element and induces transcription of Hsp90 and other HSPs. Due to the upregulation of Hsp90 and other heat shock proteins that serve a cytoprotective role within the cell, the effects of Hsp90 inhibitors are negated and represent a serious obstacle in the clinical setting. The increased expression of Hsp90 produces severe dosing and scheduling difficulties.[90-91]

Toxicities

Additional challenges were also observed in the clinic, including ocular, hepato-, and cardiotoxicities. It is not well understood whether these toxicities result from on-target effects or are a consequence of the different inhibitory scaffolds. During the clinical evaluation of **17-AAG** (**Figure 1.3**), dose-limiting hepatotoxicities were observed, which is likely scaffold-dependent, as

this molecule contains a redox-active quinone.[90, 92] Quinones are susceptible to oxidation via cytochromes P450, producing reactive intermediates that can result in oxidative damage to the cell.[93-95] In addition, quinones are electrophilic and can react with biological nucleophiles, such as thiols. This reactivity can deplete reducing agents (e.g. glutathione) and produce toxic byproducts that further increase toxicities.[96] These detriments, combined with the modest efficacy exhibited by **17-AAG** as a monotherapy, have tapered enthusiasm for development of the ansamycin-based Hsp90 inhibitors.

A second toxicity observed during clinical trials with Hsp90 inhibitors is cardiotoxicity.[75, 90] A major source of cardiotoxicity during the drug development process results from disruption of the potassium rectifier channel, human ether a-go-go-related gene (hERG) channel, expressed in the heart. The hERG channel is responsible for the repolarization of electrical current in cardiac action potential.[97-98] Inhibition or disruption of this process results in elongation of the QT interval, and potentially death.[98-101] Previous studies have demonstrated that the α-subunit of this channel, which constitutes a major portion of the protein complex, is dependent upon Hsp90 for its maturation and trafficking to the cell surface.[102-103] Treatment of HEK293 cells expressing the hERG channel with **GDA** (**Figure 1.3**) retained immature hERG within the ER, which produced decreased hERG-associated cardiac action potential amplitude.[102] Recently, it was determined that hERG maturation and trafficking to the cell surface are solely dependent upon the Hsp90α isoform, suggesting that inhibition of Hsp90α may contribute to the cardiotoxicities observed in the clinic.[104-105] However, this effect has not been validated with isoform-selective inhibitors to determine whether this is an on-target effect related to Hsp90α inhibition.

Another major toxicity that has emerged from the clinical evaluation of Hsp90 inhibitors is ocular toxicity.[105-106] In particular, in a Phase 1 study with **NVP-AUY922** (**Figure 1.3**), 43% of

patients reported grade 1 or 2 visual adverse effects in a dose-dependent manner.[107] These effects included night blindness, photopsia, blurred vision, and visual impairment, which was reversible upon discontinuation of **NVP-AUY922**. The biological mechanism by which these effects occurred is not well understood; however, **STA-9090** (**Figure 1.3**) does not appear to produce similar effects, suggesting these adverse events may be specific to **NVP-AUY922** (**Figure 1.3**).[108-109] Further investigations into the mechanism by which these ocular toxicities occur is necessary to understand whether these effects are scaffold specific or a consequence of on-target toxicities related to *pan*-Hsp90 inhibition.

Hsp90 Isoform-selective Inhibitors

As a result of these toxicities and the lack of an approved Hsp90 inhibitor nearly 20 years after the first clinical trial was initiated, alternative approaches toward Hsp90 inhibition appear necessary to take advantage of the unique biological role played by Hsp90 in various diseases. One approach that has gained popularity during the last 5 years is the development of Hsp90 isoform-selective inhibitors.[110] This approach could lower toxic liabilities, as compared to *pan*-Hsp90 inhibitors, by reducing the number of client proteins affected by a single agent. The development of such agents has been hindered by the fact that the N-terminal ATP-binding site is >85% identical between the four Hsp90 isoforms. However, in depth analysis of the N-terminal binding pockets of the four isoforms has revealed subtle differences that can be exploited to gain selectivity.

Hsp90α/β N-terminal ATP-binding Site

The cytosolic Hsp90 isoforms possess nearly identical N-terminal binding sites and differ by only two amino acids. Hsp90β contains Ala52 and Leu91, whereas Ser52 and Ile91 are present in Hsp90α (**Figure 1.5**). These residues are buried deep within the binding site and participate in a hydrogen bonding network with Leu48, Asp93, and Thr184 (conserved between the two isoforms)
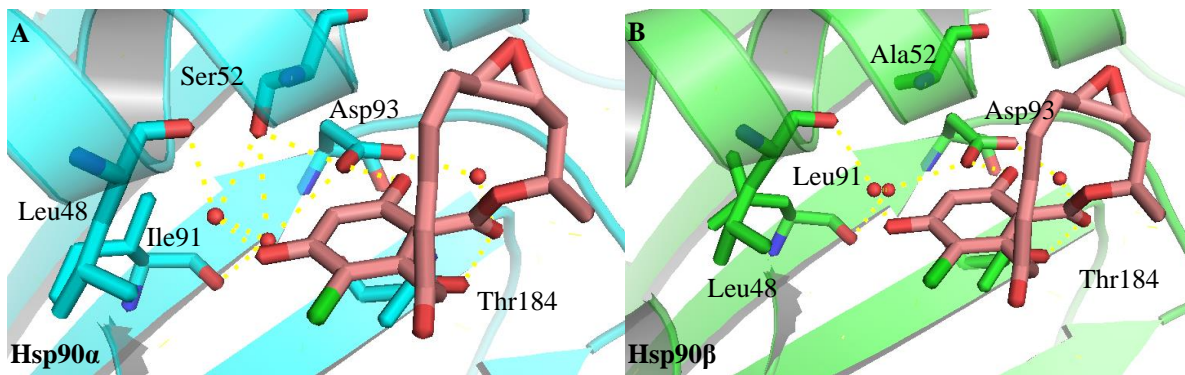
Figure 1.5. Hydrogen bonding network present at the base of the Hsp90 N-terminal ATP-binding site. (**a**) Interactions of **RDC** in the ATP-binding site of Hsp90α. The hydrogen bonding network in this isoform is more extensive than other isoforms due to the presence of Ser52. (**b**) Interactions of **RDC** in the ATP-binding site of Hsp90β. Due to the presence of Leu91 and Ala52, Hsp90β is less sterically demanding and displacement of the conserved water molecules has been utilized for Hsp90β-selective inhibition.

and conserved water molecules. This hydrogen bond network forms interactions with the pharmacophores of Hsp90 inhibitors (see **Figure 1.3**) and induce significant affinity.[111] Although these differences are small, they have been utilized to selectively inhibit each isoform. The presence of Ala52 and Leu91 in Hsp90β results in a small pocket that is typically occupied by water molecules that participate in a hydrogen bonding network. Displacement of these water molecules via **KUNB31** (**Figure 1.6**) afforded 47-fold selectivity for Hsp90β over the other Hsp90 isoforms.[42] Additionally, the presence of Ser52 in Hsp90α increases these hydrogen bond interactions and can be utilized to gain selectivity for this isoform. Hsp90α-selective inhibitors have been proposed to utilize this more extensive hydrogen bonding network in order to produce
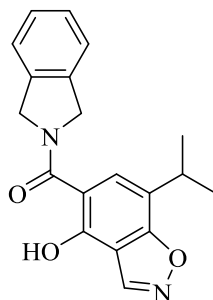
KUNB31
Hsp90β−Selective Inhibitor

Figure 1.6. KUNB31 is the first Hsp90β-selective inhibitor.

15

selectivity. It is important to note that Hsp90α is the only isoform that possesses Ser52, whereas all three other Hsp90 isoforms possess an Ala residue in this location.

Grp94 Binding Site

Grp94 is the most unique of the four isoforms, due to a five amino acid insertion into its primary sequence resulting in access to a secondary binding pocket. This hydrophobic binding pocket can be further divided into two different sub-pockets (S1 and S2).

The S1 sub-pocket is hydrophobic in nature and is found near the solvent exposed region of the Grp94 binding site. The residues that comprise this pocket are Val82, Ile166, Ala167, Phe195, Val197, Phe199, Tyr200, and Trp223. Co-crystallization of radamide (**RDA**, **Figure 1.8**), a *pan*-Hsp90 inhibitor, with Grp94 revealed that the *cis*-amide conformation could project the quinone moiety into the S1 sub-pocket, whereas the co-crystal structure of **RDA** in complex with yHsp82 (yeast ortholog of cytosolic Hsp90s) revealed **RDA** bound solely in the *trans*-amide conformation (**Figure 1.7**).[57] Therefore, the **RDA** scaffold was predisposed to bind in the *cis*-amide conformation via the incorporation of a *cis*-amide bioisostere, imidazole, which led to the development of the first Grp94-selective inhibitor, **BnIm** (**Figure 1.8**).[112] Optimization of **BnIm** for Grp94-selectivity and development of second generation Grp94-selective inhibitors are discussed in Chapters 2 and 3, respectively.[43, 64]
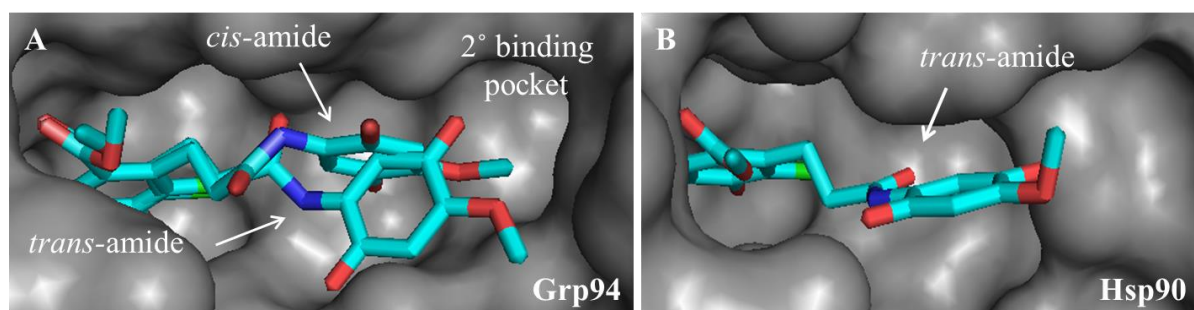
Figure 1.7. RDA bound to Grp94 (**a**) in the *cis*- and *trans*-amide conformations and Hsp90 (**b**) **RDA** was found only in the *trans*-amide conformation.
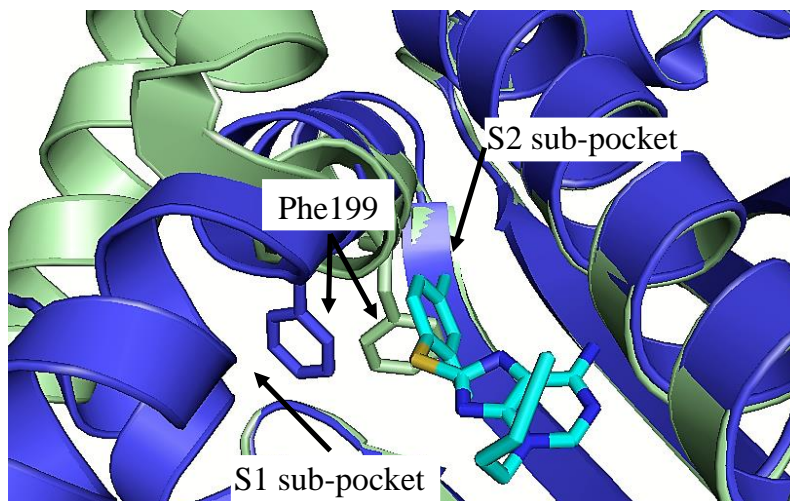
Figure 1.8. Rotation of Phe199 to expose the S2 sub-pocket in Grp94 upon binding of the purine-based inhibitor PU-H54. Green = **RDA** co-crystal structure with Grp94 (PDBID: 2GFD) with the S1 sub-pocket, **RDA** removed for clarity. Blue = **PU-H54** co-crystal structure with Grp94 (PDBID: 2O2F) showing the S2-subpocket.

A high throughput screen of purine-based Hsp90 inhibitors led to the discovery of the S2 sub-pocket, which is distinct from the S1 sub-pocket utilized by **BnIm**. The S2 sub-pocket results from reorganization of helices 1, 4, and 5, which rotates Phe199 and provides access to the S2 sub-pocket (**Figure 1.9**).[45] This pocket is located near the adenine-binding region and buried further into the protein as compared to the S1 sub-pocket. Similar to the S1 sub-pocket, the S2 sub-pocket
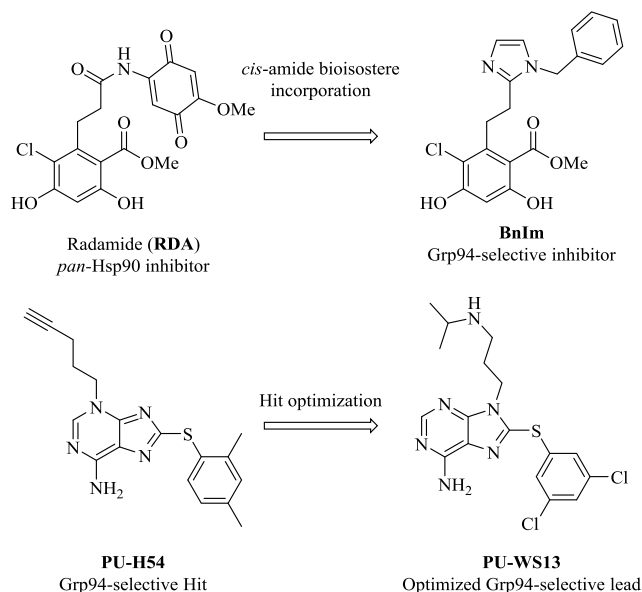
Figure 1.9. Grp94-selective inhibitors.

is outlined by hydrophobic residues and include Leu104, Phe199, Ala202, Trp223, Val211, and Leu249. The S2 sub-pocket has been utilized for Grp94-selecivity by purine-based inhibitors (**PU-H54** and **PU-WS13**, **Figure 1.8**) that preferentially interact with this sub-pocket.[113] Resorcinol-based inhibitors have more recently been developed to bind the S2 sub-pocket for increased selectivity and are discussed in Chapter 4.[58]

TRAP1 Binding Site

When compared to Hsp90, there are considerably fewer crystal structures of TRAP1. The first crystal structure of TRAP1 in complex with a non-hydrolysable ATP mimic was reported in 2014.[67] This structure confirmed a high amino acid identity within the N-terminal ATP-binding pocket to the cytosolic Hsp90 isoforms. Subsequent co-crystal structures revealed a four amino acid difference between TRAP1 and Hsp90β: Asp102(Glu), Gln157(Val), Asn171(Leu), and Ile253(Val).[68-69] The side chain of Gln157 extends away from the binding pocket and exposes the backbone carbonyl and amide NH for interactions with ligands, suggesting this difference cannot be utilized to develop selective inhibitors. The only difference that appears useful for the development of selective inhibitors is Asn171 (**Figure 1.10a** versus **1.10b**), which is located just before the TRAP1 lid that closes over the N-terminal ATP-binding site upon occupancy by ATP. TRAP1 crystal structures revealed the lid (residues 172-201) to be disordered when bound to PU-H71 (**Figure 1.10a**), whereas in the presence of ATP mimics bound to TRAP1, this lid was ordered (**Figure 1.10c**). Therefore, stabilization of this lid could provide a mechanism to selectively inhibit TRAP1 versus other Hsp90 isoforms. Further discussion of the TRAP1 binding site and the development of TRAP1-selective ligands is presented in Chapter 5.

Due to the predominant localization of TRAP1 to the mitochondria, the attachment of mitochondrial targeting moieties to small molecule Hsp90 inhibitors has been utilized to study
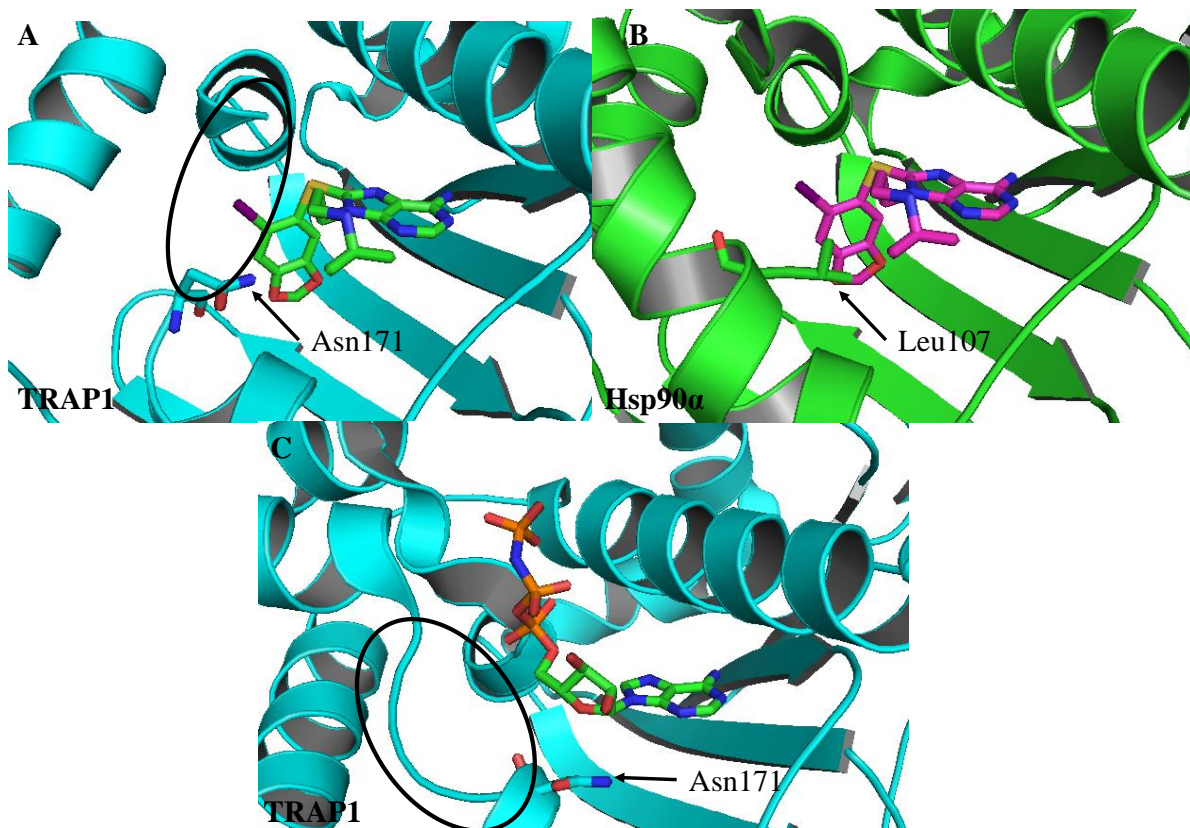
Figure 1.10. TRAP1 co-crystal structures reveal differences that can be utilized for selectivity. (**a**) **PU-H71** bound to TRAP1 depicts the disordered lid region (oval) and Asn171. (**b**) **PU-H71** bound to Hsp90α showing Leu107 in a similar position to Asn171 of TRAP1. (**c**) **ADPNP**, a non-hydrolysable ATP mimic, bound to TRAP1 revealing stabilization of the lid region (oval).

TRAP1. Mitochondria are responsible for production of ATP through oxidative phosphorylation. In order to perform this process, a proton gradient exists across the mitochondrial membrane, resulting in a membrane potential that is used to drive the synthesis of ATP. Delocalized lipophilic cations (DLCs) are capable of penetrating the cellular and mitochondrial membranes due to their lipophilicity and accumulate within the mitochondria due to the negative inner membrane potential of functioning mitochondria.[68, 114-115] The most commonly utilized DLC is the triphenylphosphonium (TPP) cation. Incorporation of this moiety, via a linker, onto the ansamycin scaffold provided the mitochondria-targeted gamitrinib class of inhibitors (**Figure 1.11**).[115] These inhibitors induced mitochondrial apoptosis against a variety of prostate cancer cell lines.
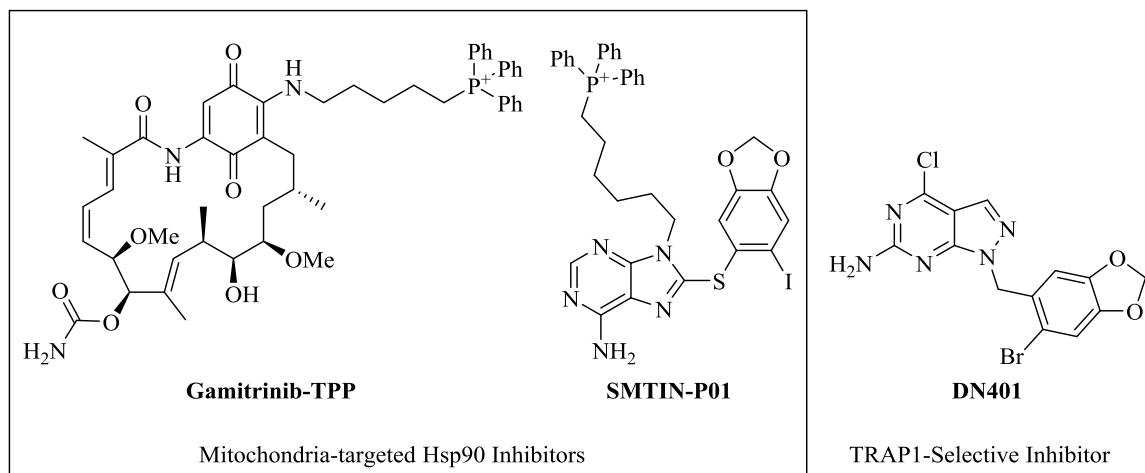
Figure 1.11. Mitochondria-targeted Hsp90 inhibitors (left) and TRAP1-selective inhibitor (right).

Additionally, the TPP moiety has been incorporated into the purine scaffold (**SMTIN-P01**, **Figure 1.11**), and these compounds demonstrated superior efficacy in cell models as compared to the non-TPP conjugated purine inhibitor (**PU-H71**).[68] While this strategy has proven successful for the development of mitochondrial-targeted small molecules, these compounds exhibit reduced drug-like properties that hinder their utilization in the clinic.[116] Therefore, the development of TRAP1-selective inhibitors that do not require a mitochondrial targeting motif are highly sought after. Recently, the small molecule **DN401** (**Figure 1.11**) was reported that utilizes the Asn171 substitution described above for TRAP1-selective inhibition.[69] This compound forms a water-mediated hydrogen bond with Asn171 and exhibited 8-fold selectivity for TRAP1 over Hsp90α. Cellular studies with this inhibitor demonstrated induction of mitochondrial apoptosis; however, western blot analysis at similar concentrations of **DN401** revealed this compound to induce the degradation of the cytosolic Hsp90-dependent client protein, Akt, suggesting that greater TRAP1-selectivity is needed in order to eliminate interactions with other Hsp90 isoforms.

Conclusions and Future Directions for Hsp90 Research

Molecular chaperones are essential to maintaining a viable cellular environment, especially during times of increased cellular stress. The family of Hsp90 isoforms is responsible for restoring and stabilizing the biologically active conformation of more than 300 client proteins. Many of these proteins are essential for cancer progression, making Hsp90 a highly sought after target for the development of anti-cancer therapeutics. To date, more than 17 small molecule Hsp90 inhibitors have entered clinical trials; however, no inhibitor has been approved by the Food and Drug Administration due to the fact that these inhibitors manifest several concerns, including dose-limiting toxicities (ocular, hepato-, and cardiotoxicity), dosing and scheduling problems due to induction of the HSR, and limited efficacy as single agents. These issues have diminished enthusiasm for Hsp90 as a therapeutic target; however, they also demonstrate a need for alternative strategies for Hsp90 inhibition to further understand the biological roles of this molecular chaperone.

One strategy that has gained considerable attention in recent years is the development of isoform-selective inhibitors. Investigations into the roles played by individual isoforms has revealed that some client proteins are dependent upon a specific isoform suggesting that cancers driven by specific oncogenic proteins may depend upon a unique Hsp90 isoform. In addition, isoform-selective inhibitors could reduce the liabilities and issues associated with *pan*-Hsp90 inhibitors and potentially provide superior efficacy for the disease states that are reliant upon a specific isoform.

The development of Hsp90 isoform-selective inhibitors is hindered by the fact that all four isoforms possess >85% identity within their N-terminal ATP-binding site. However, through rational, structure-based drug design, these small differences can be exploited to develop such

inhibitors. Grp94-selective inhibitors have been the most investigated to date, since Grp94 is the most unique isoform. In fact, these inhibitors have demonstrated efficacy in cellular models for glaucoma, cancer metastasis, multiple myeloma, and Her2-positive breast cancers, suggesting a potential for the development of targeted therapies for these diseases. It is hypothesized that isoform-selective inhibitors of the remaining isoforms could demonstrate a similar, if not larger, impact on various disease states.

The development of isoform-selective inhibitors provides an attractive strategy to revive Hsp90 research. In order to fully utilize isoform-selective inhibitors, much work must be done in order to identify client proteins dependent upon specific isoforms since there are currently only a handful of isoform-specific client proteins identified, but the family of Hsp90 proteins is known to interact with more than 300 distinct proteins within the cell. These studies would aid in the identification of disease states that are dependent upon specific isoforms and allow for the development of isoform-selective inhibitors as potential targeted therapies for these indications.

References

1.   Hartl, F. U.; Bracher, A.; Hayer-Hartl, M. Molecular chaperones in protein folding and proteostasis. *Nature* **2011,** *475*, 324-332.

2.   Kim, Y. E.; Hipp, M. S.; Bracher, A.; Hayer-Hartl, M.; Hartl, F. U. Molecular chaperone functions in protein folding and proteostasis. *Annu. Rev. Biochem* **2013,** *82*, 323-355.

3.   Buchberger, A.; Bukau, B.; Sommer, T. Protein quality control in the cytosol and the endoplasmic reticulum: brothers in arms. *Mol. Cell* **2010,** *40*, 238-252.

4.   Walter, S.; Buchner, J. Molecular chaperones--cellular machines for protein folding. *Angew. Chem. Int. Ed. Engl.* **2002,** *41*, 1098-1113.

5. Li, Z.; Srivastava, P. Heat-shock proteins. *Curr. Protoc. Immunol.* **2004,** *Appendix 1*, Appendix 1T.

6. Koller, M.; Hensler, T.; Konig, B.; Prevost, G.; Alouf, J.; Konig, W. Induction of heat-shock proteins by bacterial toxins, lipid mediators and cytokines in human leukocytes. *Zentralbl. Bakteriol.* **1993,** *278*, 365-376.

7. Pockley, A. G. Heat shock proteins, inflammation, and cardiovascular disease. *Circulation* **2002,** *105*, 1012-1017.

8. Benjamin, I. J.; Kroger, B.; Williams, R. S. Activation of the heat shock transcription factor by hypoxia in mammalian cells. *Proc. Natl. Acad. Sci. U. S. A.* **1990,** *87*, 6263-6267.

9. Almeida, M. B.; do Nascimento, J. L.; Herculano, A. M.; Crespo-Lopez, M. E. Molecular chaperones: toward new therapeutic tools. *Biomed. Pharmacother.* **2011,** *65*, 239-243.

10. Soti, C.; Nagy, E.; Giricz, Z.; Vigh, L.; Csermely, P.; Ferdinandy, P. Heat shock proteins as emerging therapeutic targets. *Br. J. Pharmacol.* **2005,** *146*, 769-780.

11. Ciocca, D. R.; Calderwood, S. K. Heat shock proteins in cancer: diagnostic, prognostic, predictive, and treatment implications. *Cell Stress Chaperones* **2005,** *10*, 86-103.

12. Csermely, P.; Schnaider, T.; Soti, C.; Prohaszka, Z.; Nardai, G. The 90-kDa molecular chaperone family: structure, function, and clinical applications. A comprehensive review. *Pharmacol. Ther.* **1998,** *79*, 129-168.

13. Picard, D. Hsp90 Interactors. https://www.picard.ch/downloads.

14. Lai, B. T.; Chin, N. W.; Stanek, A. E.; Keh, W.; Lanks, K. W. Quantitation and intracellular localization of the 85K heat shock protein by using monoclonal and polyclonal antibodies. *Mol. Cell. Biol.* **1984,** *4*, 2802-2810.

15.   Prodromou, C. Strategies for stalling malignancy: targeting cancer's addiction to Hsp90. *Curr. Top. Med. Chem.* **2009,** *9*, 1352-1368.

16.   Bagatell, R.; Whitesell, L. Altered Hsp90 function in cancer: a unique therapeutic opportunity. *Mol. Cancer Ther.* **2004,** *3*, 1021-1030.

17.   Li, J.; Buchner, J. Structure, function and regulation of the hsp90 machinery. *Biomed. J.* **2013,** *36*, 106-117.

18.   McLaughlin, S. H.; Ventouras, L. A.; Lobbezoo, B.; Jackson, S. E. Independent ATPase activity of Hsp90 subunits creates a flexible assembly platform. *J. Mol. Biol.* **2004,** *344*, 813-826.

19.   Centenera, M. M.; Fitzpatrick, A. K.; Tilley, W. D.; Butler, L. M. Hsp90: still a viable target in prostate cancer. *Biochim. Biophys. Acta* **2013,** *1835*, 211-218.

20.   Hong, D. S.; Banerji, U.; Tavana, B.; George, G. C.; Aaron, J.; Kurzrock, R. Targeting the molecular chaperone heat shock protein 90 (HSP90): lessons learned and future directions. *Cancer Treat. Rev.* **2013,** *39*, 375-387.

21.   Messaoudi, S.; Peyrat, J. F.; Brion, J. D.; Alami, M. Heat-shock protein 90 inhibitors as antitumor agents: a survey of the literature from 2005 to 2010. *Expert Opin. Ther. Pat.* **2011,** *21*, 1501-1542.

22.   Trepel, J.; Mollapour, M.; Giaccone, G.; Neckers, L. Targeting the dynamic HSP90 complex in cancer. *Nat. Rev. Cancer* **2010,** *10*, 537-549.

23.   Meyer, P.; Prodromou, C.; Liao, C.; Hu, B.; Mark Roe, S.; Vaughan, C. K.; Vlasic, I.; Panaretou, B.; Piper, P. W.; Pearl, L. H. Structural basis for recruitment of the ATPase activator Aha1 to the Hsp90 chaperone machinery. *EMBO J.* **2004,** *23*, 511-519.

24.   Harris, S. F.; Shiau, A. K.; Agard, D. A. The crystal structure of the carboxy-terminal dimerization domain of htpG, the Escherichia coli Hsp90, reveals a potential substrate binding site. *Structure* **2004,** *12*, 1087-1097.

25.   Wayne, N.; Bolon, D. N. Dimerization of Hsp90 is required for in vivo function. Design and analysis of monomers and dimers. *J. Biol. Chem.* **2007,** *282*, 35386-35395.

26.   Miyata, Y.; Nakamoto, H.; Neckers, L. The therapeutic target Hsp90 and cancer hallmarks. *Curr. Pharm. Des.* **2013,** *19*, 347-365.

27.   Hanahan, D.; Weinberg, R. A. Hallmarks of cancer: the next generation. *Cell* **2011,** *144*, 646-674.

28.   Hanahan, D.; Weinberg, R. A. The hallmarks of cancer. *Cell* **2000,** *100*, 57-70.

29.   Barrott, J. J.; Haystead, T. A. Hsp90, an unlikely ally in the war on cancer. *FEBS J.* **2013,** *280*, 1381-1396.

30.   Blair, L. J.; Sabbagh, J. J.; Dickey, C. A. Targeting Hsp90 and its co-chaperones to treat Alzheimer's disease. *Expert Opin. Ther. Targets* **2014,** *18*, 1219-1232.

31.   Luo, W.; Sun, W.; Taldone, T.; Rodina, A.; Chiosis, G. Heat shock protein 90 in neurodegenerative diseases. *Mol. Neurodegener.* **2010,** *5*, 24.

32.   Dobrowsky, R. T. Targeting the Diabetic Chaperome to Improve Peripheral Neuropathy. *Curr. Diab. Rep.* **2016,** *16*, 71.

33.   Suntharalingam, A.; Abisambra, J. F.; O'Leary, J. C.; Koren, J.; Zhang, B.; Joe, M. K.; Blair, L. J.; Hill, S. E.; Jinwal, U. K.; Cockman, M.; Duerfeldt, A. S.; Tomarev, S.; Blagg, B. S.; Lieberman, R. L.; Dickey, C. A. Glucose-regulated protein 94 triage of mutant myocilin through endoplasmic reticulum-associated degradation subverts a more efficient autophagic clearance mechanism. *J. Biol. Chem.* **2012,** *287*, 40661-40669.

34.   Rohl, A.; Rohrberg, J.; Buchner, J. The chaperone Hsp90: changing partners for demanding clients. *Trends Biochem. Sci.* **2013,** *38*, 253-262.

35.   Prodromou, C. The 'active life' of Hsp90 complexes. *Biochim. Biophys. Acta* **2012,** *1823*, 614-623.

36.   Hall, J. A.; Forsberg, L. K.; Blagg, B. S. Alternative approaches to Hsp90 modulation for the treatment of cancer. *Future Med. Chem.* **2014,** *6*, 1587-1605.

37.   Tillotson, B.; Slocum, K.; Coco, J.; Whitebread, N.; Thomas, B.; West, K. A.; MacDougall, J.; Ge, J.; Ali, J. A.; Palombella, V. J.; Normant, E.; Adams, J.; Fritz, C. C. Hsp90 (heat shock protein 90) inhibitor occupancy is a direct determinant of client protein degradation and tumor growth arrest in vivo. *J. Biol. Chem.* **2010,** *285*, 39835-39843.

38.   Kamal, A.; Thao, L.; Sensintaffar, J.; Zhang, L.; Boehm, M. F.; Fritz, L. C.; Burrows, F. J. A high-affinity conformation of Hsp90 confers tumour selectivity on Hsp90 inhibitors. *Nature* **2003,** *425*, 407-410.

39.   Workman, P. Altered states: selectively drugging the Hsp90 cancer chaperone. *Trends Mol. Med.* **2004,** *10*, 47-51.

40.   Sreedhar, A. S.; Kalmar, E.; Csermely, P.; Shen, Y. F. Hsp90 isoforms: functions, expression and clinical importance. *FEBS Lett.* **2004,** *562*, 11-15.

41.   Liu, W.; Vielhauer, G. A.; Holzbeierlein, J. M.; Zhao, H.; Ghosh, S.; Brown, D.; Lee, E.; Blagg, B. S. KU675, a Concomitant Heat-Shock Protein Inhibitor of Hsp90 and Hsc70 that Manifests Isoform Selectivity for Hsp90alpha in Prostate Cancer Cells. *Mol. Pharmacol.* **2015,** *88*, 121-130.

42.   Khandelwal, A. K., C. N.; Balch, M.; Peng, S.; Mishra, S. J.; Deng, J.; Day, V. W.; Liu, W.; Holzbeierlein, J. M.; Matts, R.; Blagg, B. S. Structure-guided design of the first Hsp90b N-terminal isoform-selective inhibitor. *Nat. Commun.* **2017,** *In Press*.

43.   Crowley, V.; Huard, D.; Lieberman, R.; Blagg, B. Second Generation Grp94-selective Inhibitors Provide Opportunities for the Inhibition of Metastatic Cancer. *Chem. Eur. J.* **2017,** *In press.*

44.   Hua, Y.; White-Gilbertson, S.; Kellner, J.; Rachidi, S.; Usmani, S. Z.; Chiosis, G.; Depinho, R.; Li, Z.; Liu, B. Molecular chaperone gp96 is a novel therapeutic target of multiple myeloma. *Clin. Cancer Res.* **2013,** *19*, 6242-6251.

45.   Patel, P. D.; Yan, P.; Seidler, P. M.; Patel, H. J.; Sun, W.; Yang, C.; Que, N. S.; Taldone, T.; Finotti, P.; Stephani, R. A.; Gewirth, D. T.; Chiosis, G. Paralog-selective Hsp90 inhibitors define tumor-specific regulation of HER2. *Nat. Chem. Biol.* **2013,** *9*, 677-684.

46.   Roe, S. M.; Prodromou, C.; O'Brien, R.; Ladbury, J. E.; Piper, P. W.; Pearl, L. H. Structural basis for inhibition of the Hsp90 molecular chaperone by the antitumor antibiotics radicicol and geldanamycin. *J. Med. Chem.* **1999,** *42*, 260-266.

47.   Wright, L.; Barril, X.; Dymock, B.; Sheridan, L.; Surgenor, A.; Beswick, M.; Drysdale, M.; Collier, A.; Massey, A.; Davies, N.; Fink, A.; Fromont, C.; Aherne, W.; Boxall, K.; Sharp, S.; Workman, P.; Hubbard, R. E. Structure-activity relationships in purine-based inhibitor binding to HSP90 isoforms. *Chem. Biol.* **2004,** *11*, 775-785.

48.   Ernst, J. T.; Liu, M.; Zuccola, H.; Neubert, T.; Beaumont, K.; Turnbull, A.; Kallel, A.; Vought, B.; Stamos, D. Correlation between chemotype-dependent binding conformations of HSP90alpha/beta and isoform selectivity-Implications for the structure-based design of

HSP90alpha/beta selective inhibitors for treating neurodegenerative diseases. *Bioorg. Med. Chem. Lett.* **2014,** *24*, 204-208.

49.   Ernst, J. T.; Neubert, T.; Liu, M.; Sperry, S.; Zuccola, H.; Turnbull, A.; Fleck, B.; Kargo, W.; Woody, L.; Chiang, P.; Tran, D.; Chen, W.; Snyder, P.; Alcacio, T.; Nezami, A.; Reynolds, J.; Alvi, K.; Goulet, L.; Stamos, D. Identification of novel HSP90alpha/beta isoform selective inhibitors using structure-based drug design. demonstration of potential utility in treating CNS disorders such as Huntington's disease. *J. Med. Chem.* **2014,** *57*, 3382-3400.

50.   Song, X.; Wang, X.; Zhuo, W.; Shi, H.; Feng, D.; Sun, Y.; Liang, Y.; Fu, Y.; Zhou, D.; Luo, Y. The regulatory mechanism of extracellular Hsp90{alpha} on matrix metalloproteinase-2 processing and tumor angiogenesis. *J. Biol. Chem.* **2010,** *285*, 40039-40049.

51.   Echeverria, P. C.; Picard, D. Molecular chaperones, essential partners of steroid hormone receptors for activity and mobility. *Biochim. Biophys. Acta* **2010,** *1803*, 641-649.

52.   Citri, A.; Kochupurakkal, B. S.; Yarden, Y. The achilles heel of ErbB-2/HER2: regulation by the Hsp90 chaperone machine and potential for pharmacological intervention. *Cell Cycle* **2004,** *3*, 51-60.

53.   Wang, M.; Kaufman, R. J. The impact of the endoplasmic reticulum protein-folding environment on cancer development. *Nat. Rev. Cancer* **2014,** *14*, 581-597.

54.   Lee, A. S. Glucose-regulated proteins in cancer: molecular mechanisms and therapeutic potential. *Nat. Rev. Cancer* **2014,** *14*, 263-276.

55.   Dollins, D. E.; Warren, J. J.; Immormino, R. M.; Gewirth, D. T. Structures of GRP94-nucleotide complexes reveal mechanistic differences between the Hsp90 chaperones. *Mol. Cell* **2007,** *28*, 41-56.

56.   Immormino, R. M.; Dollins, D. E.; Shaffer, P. L.; Soldano, K. L.; Walker, M. A.; Gewirth, D. T. Ligand-induced conformational shift in the N-terminal domain of GRP94, an Hsp90 chaperone. *J. Biol. Chem.* **2004,** *279*, 46162-46171.

57.   Immormino, R. M.; Metzger, L. E. t.; Reardon, P. N.; Dollins, D. E.; Blagg, B. S.; Gewirth, D. T. Different poses for ligand and chaperone in inhibitor-bound Hsp90 and GRP94: implications for paralog-specific drug design. *J. Mol. Biol.* **2009,** *388*, 1033-1042.

58.   Khandelwal, A. C., V. M.; Blagg, B. S. Resorcinol-Based Grp94-Selective Inhibitors. *ACS Med. Chem. Lett.* **2017,** *8*, 1013-1018.

59.   Marzec, M.; Eletto, D.; Argon, Y. GRP94: An HSP90-like protein specialized for protein folding and quality control in the endoplasmic reticulum. *Biochim. Biophys. Acta* **2012,** *1823*, 774-787.

60.   Ghosh, S.; Shinogle, H. E.; Galeva, N. A.; Dobrowsky, R. T.; Blagg, B. S. Endoplasmic reticulum resident heat shock protein 90 (Hsp90) isoform glucose-regulated protein 94 (Grp94) regulates cell polarity and cancer cell migration by affecting intracellular transport. *J. Biol. Chem.* **2016,** *291*, 8309-8323.

61.   Wu, S.; Hong, F.; Gewirth, D.; Guo, B.; Liu, B.; Li, Z. The molecular chaperone gp96/GRP94 interacts with Toll-like receptors and integrins via its C-terminal hydrophobic domain. *J. Biol. Chem.* **2012,** *287*, 6735-6742.

62.   Wanderling, S.; Simen, B. B.; Ostrovsky, O.; Ahmed, N. T.; Vogen, S. M.; Gidalevitz, T.; Argon, Y. GRP94 is essential for mesoderm induction and muscle development because it regulates insulin-like growth factor secretion. *Mol. Biol. Cell* **2007,** *18*, 3764-3775.

63.   Stothert, A. R.; Suntharalingam, A.; Huard, D. J.; Fontaine, S. N.; Crowley, V. M.; Mishra, S.; Blagg, B. S.; Lieberman, R. L.; Dickey, C. A. Exploiting the interaction between Grp94 and aggregated myocilin to treat glaucoma. *Hum. Mol. Genet.* **2014,** *23*, 6470-6480.

64.   Crowley, V. M.; Khandelwal, A.; Mishra, S.; Stothert, A. R.; Huard, D. J.; Zhao, J.; Muth, A.; Duerfeldt, A. S.; Kizziah, J. L.; Lieberman, R. L.; Dickey, C. A.; Blagg, B. S. Development of Glucose Regulated Protein 94-Selective Inhibitors Based on the BnIm and Radamide Scaffold. *J. Med. Chem.* **2016,** *59*, 3471-3488.

65.   Cechetto, J. D.; Gupta, R. S. Immunoelectron microscopy provides evidence that tumor necrosis factor receptor-associated protein 1 (TRAP-1) is a mitochondrial protein which also localizes at specific extramitochondrial sites. *Exp. Cell Res.* **2000,** *260*, 30-39.

66.   Felts, S. J.; Owen, B. A.; Nguyen, P.; Trepel, J.; Donner, D. B.; Toft, D. O. The hsp90-related protein TRAP1 is a mitochondrial protein with distinct functional properties. *J. Biol. Chem.* **2000,** *275*, 3305-3312.

67.   Lavery, L. A.; Partridge, J. R.; Ramelot, T. A.; Elnatan, D.; Kennedy, M. A.; Agard, D. A. Structural asymmetry in the closed state of mitochondrial Hsp90 (TRAP1) supports a two-step ATP hydrolysis mechanism. *Mol. Cell* **2014,** *53*, 330-343.

68.   Lee, C.; Park, H. K.; Jeong, H.; Lim, J.; Lee, A. J.; Cheon, K. Y.; Kim, C. S.; Thomas, A. P.; Bae, B.; Kim, N. D.; Kim, S. H.; Suh, P. G.; Ryu, J. H.; Kang, B. H. Development of a mitochondria-targeted Hsp90 inhibitor based on the crystal structures of human TRAP1. *J. Am. Chem. Soc.* **2015,** *137*, 4358-4367.

69.   Park, H. K.; Jeong, H.; Ko, E.; Lee, G.; Lee, J. E.; Lee, S. K.; Lee, A. J.; Im, J. Y.; Hu, S.; Kim, S. H.; Lee, J. H.; Lee, C.; Kang, S.; Kang, B. H. Paralog Specificity Determines Subcellular

Distribution, Action Mechanism, and Anticancer Activity of TRAP1 Inhibitors. *J. Med. Chem.* **2017,** *60*, 7569-7578.

70.   Kang, B. H.; Plescia, J.; Dohi, T.; Rosa, J.; Doxsey, S. J.; Altieri, D. C. Regulation of tumor cell mitochondrial homeostasis by an organelle-specific Hsp90 chaperone network. *Cell* **2007,** *131*, 257-270.

71.   Green, D. R.; Kroemer, G. The pathophysiology of mitochondrial cell death. *Science* **2004,** *305*, 626-629.

72.   Masuda, Y.; Shima, G.; Aiuchi, T.; Horie, M.; Hori, K.; Nakajo, S.; Kajimoto, S.; Shibayama-Imazu, T.; Nakaya, K. Involvement of tumor necrosis factor receptor-associated protein 1 (TRAP1) in apoptosis induced by beta-hydroxyisovalerylshikonin. *J. Biol. Chem.* **2004,** *279*, 42503-42515.

73.   Amoroso, M. R.; Matassa, D. S.; Laudiero, G.; Egorova, A. V.; Polishchuk, R. S.; Maddalena, F.; Piscazzi, A.; Paladino, S.; Sarnataro, D.; Garbi, C.; Landriscina, M.; Esposito, F. TRAP1 and the proteasome regulatory particle TBP7/Rpt3 interact in the endoplasmic reticulum and control cellular ubiquitination of specific mitochondrial proteins. *Cell Death Differ.* **2012,** *19*, 592-604.

74.   Whitesell, L.; Mimnaugh, E. G.; De Costa, B.; Myers, C. E.; Neckers, L. M. Inhibition of heat shock protein HSP90-pp60v-src heteroprotein complex formation by benzoquinone ansamycins: essential role for stress proteins in oncogenic transformation. *Proc. Natl. Acad. Sci. U. S. A.* **1994,** *91*, 8324-8328.

75.   Khandelwal, A.; Crowley, V. M.; Blagg, B. S. Natural product inspired N-terminal Hsp90 inhibitors: from bench to bedside? *Med. Res. Rev.* **2016,** *36*, 92-118.

76.   Bhat, R.; Tummalapalli, S. R.; Rotella, D. P. Progress in the discovery and development of heat shock protein 90 (Hsp90) inhibitors. *J. Med. Chem.* **2014,** *57*, 8718-8728.

77.   Schulte, T. W.; Akinaga, S.; Soga, S.; Sullivan, W.; Stensgard, B.; Toft, D.; Neckers, L. M. Antibiotic radicicol binds to the N-terminal domain of Hsp90 and shares important biologic activities with geldanamycin. *Cell Stress Chaperones* **1998,** *3*, 100-108.

78.   Shimamura, T.; Perera, S. A.; Foley, K. P.; Sang, J.; Rodig, S. J.; Inoue, T.; Chen, L.; Li, D.; Carretero, J.; Li, Y. C.; Sinha, P.; Carey, C. D.; Borgman, C. L.; Jimenez, J. P.; Meyerson, M.; Ying, W.; Barsoum, J.; Wong, K. K.; Shapiro, G. I. Ganetespib (STA-9090), a nongeldanamycin HSP90 inhibitor, has potent antitumor activity in in vitro and in vivo models of non-small cell lung cancer. *Clin. Cancer Res.* **2012,** *18*, 4973-4985.

79.   Brough, P. A.; Aherne, W.; Barril, X.; Borgognoni, J.; Boxall, K.; Cansfield, J. E.; Cheung, K. M.; Collins, I.; Davies, N. G.; Drysdale, M. J.; Dymock, B.; Eccles, S. A.; Finch, H.; Fink, A.; Hayes, A.; Howes, R.; Hubbard, R. E.; James, K.; Jordan, A. M.; Lockie, A.; Martins, V.; Massey, A.; Matthews, T. P.; McDonald, E.; Northfield, C. J.; Pearl, L. H.; Prodromou, C.; Ray, S.; Raynaud, F. I.; Roughley, S. D.; Sharp, S. Y.; Surgenor, A.; Walmsley, D. L.; Webb, P.; Wood, M.; Workman, P.; Wright, L. 4,5-diarylisoxazole Hsp90 chaperone inhibitors: potential therapeutic agents for the treatment of cancer. *J. Med. Chem.* **2008,** *51*, 196-218.

80.   Woodhead, A. J.; Angove, H.; Carr, M. G.; Chessari, G.; Congreve, M.; Coyle, J. E.; Cosme, J.; Graham, B.; Day, P. J.; Downham, R.; Fazal, L.; Feltell, R.; Figueroa, E.; Frederickson, M.; Lewis, J.; McMenamin, R.; Murray, C. W.; O'Brien, M. A.; Parra, L.; Patel, S.; Phillips, T.; Rees, D. C.; Rich, S.; Smith, D. M.; Trewartha, G.; Vinkovic, M.; Williams, B.; Woolford, A. J. Discovery   of   (2,4-dihydroxy-5-isopropylphenyl)-[5-(4-methylpiperazin-1-ylmethyl)-1,3-dihydrois oindol-2-yl]methanone (AT13387), a novel inhibitor of the molecular chaperone Hsp90 by fragment based drug design. *J. Med. Chem.* **2010,** *53*, 5956-5969.

81.   Chiosis, G.; Lucas, B.; Shtil, A.; Huezo, H.; Rosen, N. Development of a purine-scaffold novel class of Hsp90 binders that inhibit the proliferation of cancer cells and induce the degradation of Her2 tyrosine kinase. *Bioorg. Med. Chem.* **2002,** *10*, 3555-3564.

82.   Hecker, M.; Schumann, W.; Volker, U. Heat-shock and general stress response in Bacillus subtilis. *Mol. Microbiol.* **1996,** *19*, 417-428.

83.   Conde, R.; Belak, Z. R.; Nair, M.; O'Carroll, R. F.; Ovsenek, N. Modulation of Hsf1 activity by novobiocin and geldanamycin. *Biochem. Cell Biol.* **2009,** *87*, 845-851.

84.   McCollum, A. K.; TenEyck, C. J.; Stensgard, B.; Morlan, B. W.; Ballman, K. V.; Jenkins, R. B.; Toft, D. O.; Erlichman, C. P-Glycoprotein-mediated resistance to Hsp90-directed therapy is eclipsed by the heat shock response. *Cancer Res.* **2008,** *68*, 7419-7427.

85.   Shi, Y.; Mosser, D. D.; Morimoto, R. I. Molecular chaperones as HSF1-specific transcriptional repressors. *Genes Dev.* **1998,** *12*, 654-666.

86.   Zou, J.; Guo, Y.; Guettouche, T.; Smith, D. F.; Voellmy, R. Repression of heat shock transcription factor HSF1 activation by HSP90 (HSP90 complex) that forms a stress-sensitive complex with HSF1. *Cell* **1998,** *94*, 471-480.

87.   Bagatell, R.; Paine-Murrieta, G. D.; Taylor, C. W.; Pulcini, E. J.; Akinaga, S.; Benjamin, I. J.; Whitesell, L. Induction of a heat shock factor 1-dependent stress response alters the cytotoxic activity of hsp90-binding agents. *Clin. Cancer Res.* **2000,** *6*, 3312-3318.

88.   Zuo, J.; Rungger, D.; Voellmy, R. Multiple layers of regulation of human heat shock transcription factor 1. *Mol. Cell. Biol.* **1995,** *15*, 4319-4330.

89.   Xia, W.; Voellmy, R. Hyperphosphorylation of heat shock transcription factor 1 is correlated with transcriptional competence and slow dissociation of active factor trimers. *J. Biol. Chem.* **1997,** *272*, 4094-4102.

90.   Holzbeierlein, J. M.; Windsperger, A.; Vielhauer, G. Hsp90: a drug target? *Curr. Oncol. Rep.* **2010,** *12*, 95-101.

91.   Gao, Z.; Garcia-Echeverria, C.; Jensen, M. R. Hsp90 inhibitors: clinical development and future opportunities in oncology therapy. *Curr. Opin. Drug Discov. Devel.* **2010,** *13*, 193-202.

92.   Biamonte, M. A.; Van de Water, R.; Arndt, J. W.; Scannevin, R. H.; Perret, D.; Lee, W. C. Heat shock protein 90: inhibitors in clinical trials. *J. Med. Chem.* **2010,** *53*, 3-17.

93.   Ishihara, Y.; Ishii, S.; Sakai, Y.; Yamamura, N.; Onishi, Y.; Shimamoto, N. Crucial role of cytochrome P450 in hepatotoxicity induced by 2,3-dimethoxy-1,4-naphthoquinone in rats. *J. Appl. Toxicol.* **2011,** *31*, 173-178.

94.   Ishihara, Y.; Shimamoto, N., A Role of Cytochrome P450 in Quinone-Induced Hepatotoxicity. In *Hepatotoxicity*, John Wiley & Sons, Ltd: 2008; pp 287-297.

95.   Berlin, V.; Haseltine, W. A. Reduction of adriamycin to a semiquinone-free radical by NADPH cytochrome P-450 reductase produces DNA cleavage in a reaction mediated by molecular oxygen. *J. Biol. Chem.* **1981,** *256*, 4747-4756.

96.   Brunmark, A.; Cadenas, E. Redox and addition chemistry of quinoid compounds and its biological implications. *Free Radic. Biol. Med.* **1989,** *7*, 435-477.

97.   Perrin, M. J.; Subbiah, R. N.; Vandenberg, J. I.; Hill, A. P. Human ether-a-go-go related gene (hERG) K+ channels: function and dysfunction. *Prog. Biophys. Mol. Biol.* **2008,** *98*, 137-148.

98.   Vandenberg, J. I.; Walker, B. D.; Campbell, T. J. HERG K+ channels: friend and foe. *Trends Pharmacol. Sci.* **2001,** *22*, 240-246.

99.   Fermini, B.; Fossa, A. A. The impact of drug-induced QT interval prolongation on drug discovery and development. *Nat. Rev. Drug Discov.* **2003,** *2*, 439-447.

100.   Brown, A. M. HERG block, QT liability and sudden cardiac death. *Novartis Found. Symp.* **2005,** *266*, 118-131; discussion 131-115, 155-118.

101.   Wible, B. A.; Hawryluk, P.; Ficker, E.; Kuryshev, Y. A.; Kirsch, G.; Brown, A. M. HERG-Lite: a novel comprehensive high-throughput screen for drug-induced hERG risk. *J. Pharmacol. Toxicol. Methods* **2005,** *52*, 136-145.

102.   Ficker, E.; Dennis, A. T.; Wang, L.; Brown, A. M. Role of the cytosolic chaperones Hsp70 and Hsp90 in maturation of the cardiac potassium channel HERG. *Circ. Res.* **2003,** *92*, e87-100.

103.   Nanduri, J.; Bergson, P.; Wang, N.; Ficker, E.; Prabhakar, N. R. Hypoxia inhibits maturation and trafficking of hERG K(+) channel protein: Role of Hsp90 and ROS. *Biochem. Biophys. Res. Commun.* **2009,** *388*, 212-216.

104.   Peterson, L. B.; Eskew, J. D.; Vielhauer, G. A.; Blagg, B. S. The hERG channel is dependent upon the Hsp90α isoform for maturation and trafficking. *Mol. Pharm.* **2012,** *9*, 1841-1846.

105.   Rajan, A.; Kelly, R. J.; Trepel, J. B.; Kim, Y. S.; Alarcon, S. V.; Kummar, S.; Gutierrez, M.; Crandon, S.; Zein, W. M.; Jain, L.; Mannargudi, B.; Figg, W. D.; Houk, B. E.; Shnaidman, M.; Brega, N.; Giaccone, G. A phase I study of PF-04929113 (SNX-5422), an orally bioavailable heat shock protein 90 inhibitor, in patients with refractory solid tumor malignancies and lymphomas. *Clin. Cancer Res.* **2011,** *17*, 6831-6839.

106.   Wu, W. C.; Wu, M. H.; Chang, Y. C.; Hsieh, M. C.; Wu, H. J.; Cheng, K. C.; Lai, Y. H.; Kao, Y. H. Geldanamycin and its analog induce cytotoxicity in cultured human retinal pigment epithelial cells. *Exp. Eye Res.* **2010,** *91*, 211-219.

107.   Sessa, C.; Shapiro, G. I.; Bhalla, K. N.; Britten, C.; Jacks, K. S.; Mita, M.; Papadimitrakopoulou, V.; Pluard, T.; Samuel, T. A.; Akimov, M.; Quadt, C.; Fernandez-Ibarra, C.; Lu, H.; Bailey, S.; Chica, S.; Banerji, U. First-in-human phase I dose-escalation study of the

HSP90 inhibitor AUY922 in patients with advanced solid tumors. *Clin. Cancer Res.* **2013,** *19*, 3671-3680.

108.   Roman, D.; VerHoeve, J.; Schadt, H.; Vicart, A.; Walker, U. J.; Turner, O.; Richardson, T. A.; Wolford, S. T.; Miller, P. E.; Zhou, W.; Lu, H.; Akimov, M.; Kluwe, W. Ocular toxicity of AUY922 in pigmented and albino rats. *Toxicol. Appl. Pharmacol.* **2016,** *309*, 55-62.

109.   Jhaveri, K.; Chandarlapaty, S.; Lake, D.; Gilewski, T.; Robson, M.; Goldfarb, S.; Drullinsky, P.; Sugarman, S.; Wasserheit-Leiblich, C.; Fasano, J.; Moynahan, M. E.; D'Andrea, G.; Lim, K.; Reddington, L.; Haque, S.; Patil, S.; Bauman, L.; Vukovic, V.; El-Hariry, I.; Hudis, C.; Modi, S. A phase II open-label study of ganetespib, a novel heat shock protein 90 inhibitor for patients with metastatic breast cancer. *Clin. Breast Cancer* **2014,** *14*, 154-160.

110.   Gewirth, D. T. Paralog Specific Hsp90 Inhibitors - A Brief History and a Bright Future. *Curr. Top. Med. Chem.* **2016,** *16*, 2779-2791.

111.   Zubriene, A.; Gutkowska, M.; Matuliene, J.; Chaleckis, R.; Michailoviene, V.; Voroncova, A.; Venclovas, C.; Zylicz, A.; Zylicz, M.; Matulis, D. Thermodynamics of radicicol binding to human Hsp90 alpha and beta isoforms. *Biophys. Chem.* **2010,** *152*, 153-163.

112.   Duerfeldt, A. S.; Peterson, L. B.; Maynard, J. C.; Ng, C. L.; Eletto, D.; Ostrovsky, O.; Shinogle, H. E.; Moore, D. S.; Argon, Y.; Nicchitta, C. V.; Blagg, B. S. Development of a Grp94 inhibitor. *J. Am. Chem. Soc.* **2012,** *134*, 9796-9804.

113.   Patel, H. J.; Patel, P. D.; Ochiana, S. O.; Yan, P.; Sun, W.; Patel, M. R.; Shah, S. K.; Tramentozzi, E.; Brooks, J.; Bolaender, A.; Shrestha, L.; Stephani, R.; Finotti, P.; Leifer, C.; Li, Z.; Gewirth, D. T.; Taldone, T.; Chiosis, G. Structure-activity relationship in a purine-scaffold compound series with selectivity for the endoplasmic reticulum Hsp90 paralog Grp94. *J. Med. Chem.* **2015,** *58*, 3922-3943.

114. Modica-Napolitano, J. S.; Aprille, J. R. Delocalized lipophilic cations selectively target the mitochondria of carcinoma cells. *Adv. Drug Deliv. Rev.* **2001,** *49*, 63-70.

115. Kang, B. H.; Plescia, J.; Song, H. Y.; Meli, M.; Colombo, G.; Beebe, K.; Scroggins, B.; Neckers, L.; Altieri, D. C. Combinatorial drug design targeting multiple cancer signaling networks controlled by mitochondrial Hsp90. *J. Clin. Invest.* **2009,** *119*, 454-464.

116. Lipinski, C. A.; Lombardo, F.; Dominy, B. W.; Feeney, P. J. Experimental and computational approaches to estimate solubility and permeability in drug discovery and development settings. *Adv. Drug Deliv. Rev.* **2001,** *46*, 3-26.

2. Development of Grp94-selective Inhibitors based on the BnIm Scaffold as a Potential Treatment for Myocilin-associated Primary Open Angle Glaucoma

Grp94 Possesses a Unique Secondary Binding Pocket

Glucose regulated protein 94 (Grp94) is the endoplasmic reticulum (ER) resident isoform of the Hsp90 family. Grp94 is responsible for the maturation of proteins associated with cell-to-cell signaling and cell adhesion. Client proteins dependent upon Grp94 have been identified, including select integrins ($\alpha2$, $\alpha4$, αL, and $\beta4$), Toll-like receptors (TLR1, TLR2, TLR4, and TLR9), LRP6, Her2, IGF-I and -II, and mutant myocilin.[1-4] Grp94 is essential only during embryonic development, and therefore, selectively targeting Grp94 may exhibit fewer toxic liabilities than observed with *pan*-Hsp90 inhibitors in the clinic.[5] Recently, mutant myocilin was identified as a Grp94-dependent substrate, and studies have shown that inhibition of Grp94 leads to the disaggregation of mutant myocilin and, consequently, represents a novel target for the treatment of myocilin-associated primary open-angle glaucoma (POAG).[6-8] To date, few Hsp90 isoform-selective inhibitors have been developed, due to the >85% identity within the N-terminal ATP-binding pocket of all four isoforms.

Grp94 is most unique in its N-terminal ATP-binding pocket amongst the Hsp90 isoforms due to a five amino acid insertion (residues 182-186) into its primary sequence.[3] This insertion, while not located directly in the ATP-binding site, produces a hydrophobic binding region within the N-terminal ATP-binding site of Grp94.[9] As such, this unique pocket provides an opportunity to develop Grp94-selective inhibitors. Prior studies, via a high throughput screen, identified **NECA** (**1**, **Figure 2.1**), as a Grp94-selective inhibitor that bound to the S1 sub-pocket of the Grp94 unique secondary pocket.[3, 10] Recently, a library screen identified a series of Grp94-selective inhibitors
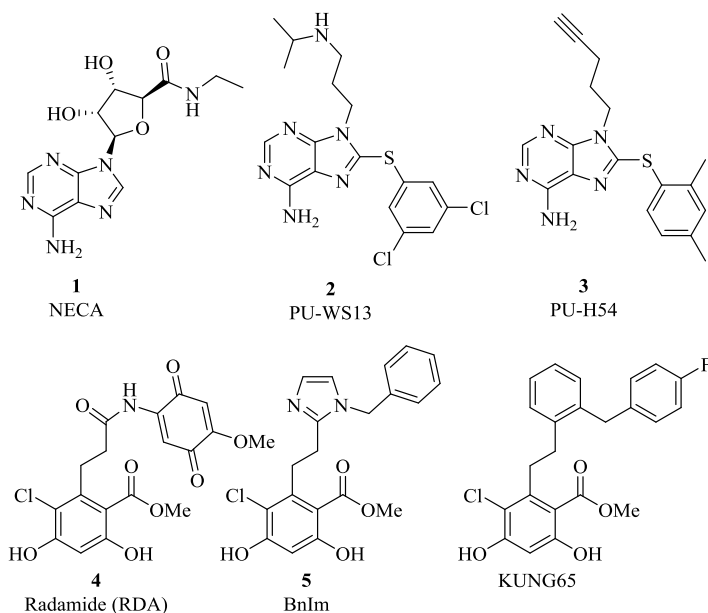
Figure 2.1. Purine-based Grp94-selective inhibitors (**1-3**). Resorcinol-based pan-Hsp90 (**4**) and Grp94-selective (**5**, **KUNG65**) inhibitors.

based on the purine scaffold and subsequent optimization led to the development of **2** and **3,** which preferentially bind the S2 sub-pocket of Grp94 to impart selectivity.[11-12] Co-crystallization of the resorcinol containing *pan*-Hsp90 inhibitor, radamide (**4**, **Figure 2.1**) with canine Grp94 (cGrp94) revealed the amide bond existed in both the *cis*- and *trans*-amide conformations.[13-14] The *cis*-amide conformation projected the quinone moiety directly toward the unique secondary binding pocket of Grp94, while the *trans*-amide did not. Alternatively, when co-crystallized with yeast Hsp82 (yHsp82, yeast ortholog of cytosolic Hsp90 isoforms), **4** bound solely in the *trans*-amide conformation. These data suggested that the predisposition of **4** to bind in the *cis*-amide conformation could lead to selective Grp94 inhibition. Incorporation of a *cis*-amide bioisostere, imidazole, into the scaffold of **4** projects the aryl ring into the unique S1 sub-pocket of Grp94, which led to the discovery of the first Grp94-selective inhibitor, **BnIm** (**5**, **Figure 2.1**).[15] **5** demonstrated Grp94 selectivity via a competitive fluorescence polarization assay and in cells by inhibiting secretion of the Grp94-dependent client protein IGF-II, as well as inhibition of Toll-like

receptor trafficking at concentrations lower than those necessary for cytosolic Hsp90-dependent client protein degradation. **5** provided an excellent lead to pursue Grp94-selective inhibitors that impart improved selectivity and affinity for Grp94.

Design of First Generation Grp94-selective Inhibitors based on the BnIm Scaffold

The co-crystal structure of **4** with cGrp94 revealed the *cis*-amide to project the aryl side chain into the S1 sub-pocket, which is surrounded by hydrophobic amino acids (Val82, Ile166, Ala167, Phe195, Val197, Phe199, Tyr200, and Trp223), suggesting that affinity may be increased through additional hydrophobic interactions with this pocket (**Figure 2.2a**).[13] In contrast, yHsp82 contains the backbone carbonyl of Asn92 and the ε-NH$_2$ of Lys98, which blocks access to these hydrophobic residues, suggesting that modifications to the benzyl side chain of **5** could provide improved Grp94 selectivity (**Figure 2.2b**). Docking of **5** into the co-crystal structure of **4** with Grp94 (PDBID: 2GFD) suggested that substitutions on the aryl side chain could provide additional
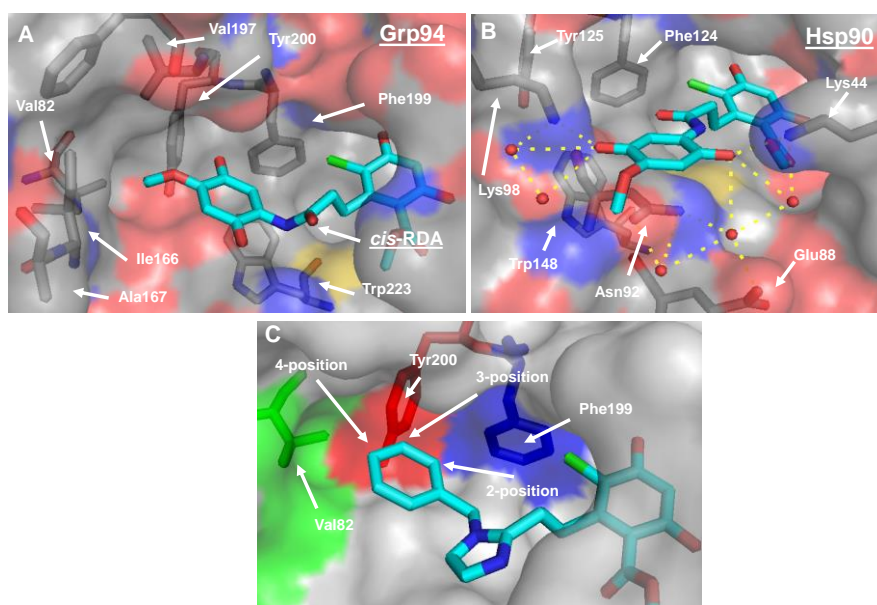
Figure 2.2. Co-crystal structures of **4** with Hsp90 isoforms. (**a**) cGrp94 (PDBID: 2GFD) highlights the hydrophobic and π-rich nature of the unique secondary binding pocket of Grp94. Only the *cis*-amide form of **4** shown for clarity. (**b**) yHsp82 (PDBID: 2FXS) highlighting the hydrogen bonding network present and restricted access to the aromatic residues. Residues are numbered as in their respective proteins. (**c**) **5** docked in to Grp94 highlighting substitution positions on the aryl side chain.

interactions with the S1 sub-pocket of Grp94 and allow for improved Grp94-selective inhibition through optimization of the aryl side chain. Non-polar substitutions at the 4-position were proposed to extend further into the hydrophobic pocket and produce increased affinity and selectivity. However, larger substitutions at this position would likely produce a steric clash with Val82 and exhibit decreased affinity. Due to the close proximity of Tyr200 to the 3-position of the aryl side chain, substitutions at this position appeared detrimental to Grp94 affinity. Substitutions at the 2-position might increase affinity through hydrophobic interactions with the secondary pocket. Based on these observations, the aryl side chain of BnIm was investigated to probe the unique pocket present in Grp94 and to elucidate structure-activity relationships for optimal affinity and selectivity.

Synthesis and Biochemical Evaluation of Modifications to the Benzyl Ring of BnIm

The *cis*-amide bioisostere, imidazole, could be prepared via a multi-component cyclization reaction with a previously reported resorcinolic aldehyde, ammonium bicarbonate, glyoxal, and various benzylamines. Therefore, access to the desired analogues was achieved by varying substitutions on the benzylamine component, which were either commercially available or readily

Scheme 2.1. Synthesis of benzylamines **6a-6f**.
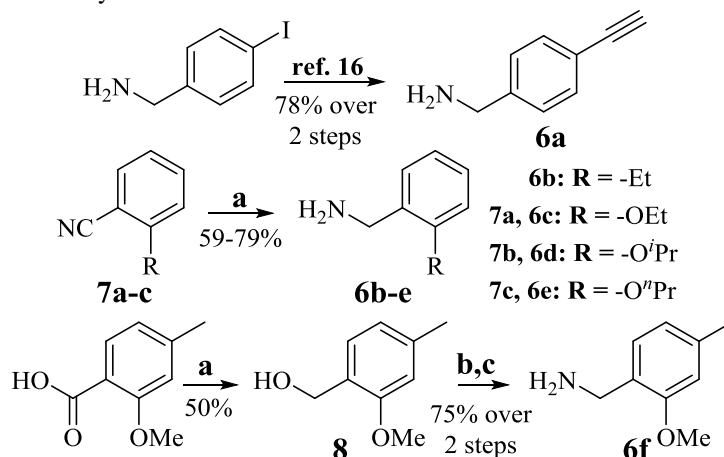
Conditions: **a**) LiAlH$_4$, THF, 0°C to 25°C, 12 h; **b**) DBU, DPPA, Toluene, 0°C to 25°C, 12h; **c**) PPh$_3$, THF:Water (10:1), 25°C, 12h.

Scheme 2.2. Synthesis of first generation Grp94-selective inhibitors **5**, **10-44**, and **50-69**.
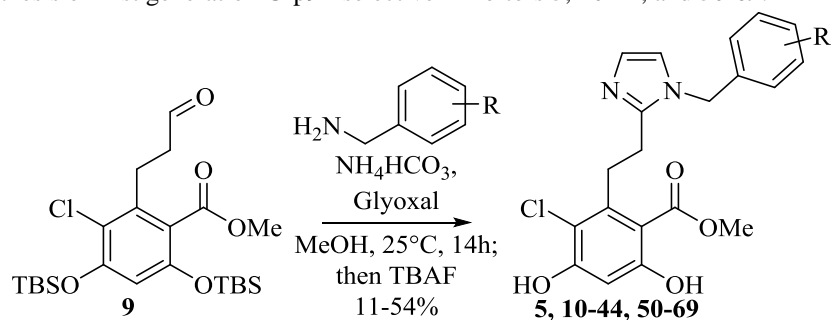
accessible (**Scheme 2.1**). 4-Ethynylbenzylamine (**6a**) was synthesized from 4-iodobenzylamine following literature precedent.[16] Aromatic nitriles were reduced using lithium aluminum hydride to produce the requisite amines (**6b-e**). The substituted benzoic acid was reduced to the corresponding benzyl alcohol, **8**, using lithium aluminum hydride, which was then converted to the benzyl azide and subsequently reduced to the desired amine, **6f**, via Staudinger reduction. The basic amines were then cyclized with aldehyde **9** in the presence of ammonium bicarbonate and glyoxal, followed by desilylation with tetrabutylammonium fluoride to provide the desired analogues, **10-44 (Scheme 2.2)**.[14-15, 17]

Once in hand, the analogues were screened via a competitive binding fluorescence polarization assay using Grp94 or Hsp90α and FITC-labeled geldanamycin (FITC-GDA).[18] Geldanamcyin is a potent, natural product N-terminal, *pan*-Hsp90 inhibitor that competes with these Grp94 inhibitors for the N-terminal ATP-binding site.[19] Analogues were evaluated against Grp94 and Hsp90α in order to determine selectivity. Hsp90α was chosen to evaluate selectivity, because of its similarities to both Hsp90β and TRAP1, and was therefore expected to produce similar selectivity profiles. Analogues were initially screened at 25μM to determine the percent of FITC-GDA (tracer) bound compared to vehicle control (0% tracer displaced, **Table 2.1**).

The 25μM screen provided insight into the structural requirements for binding of the aryl side chain to the Grp94 secondary pocket. Substitutions at the 4-position typically produced similar
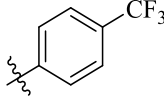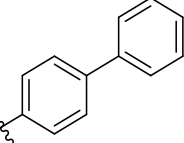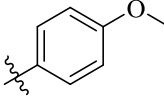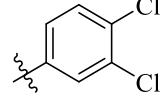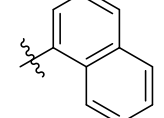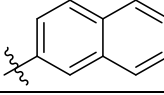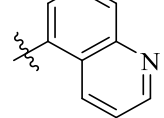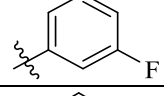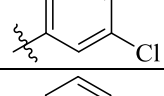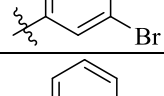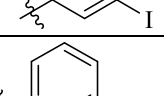
affinity compared to **5**, but provided increased selectivity in several cases. As hypothesized, polar substitutions (**17** and **21**) produced lower affinity due to the hydrophobic nature of the secondary Grp94 binding pocket (**Figure 2.2**). Incorporation of a bicyclic system was not tolerated as the naphthyl (**23** and **24**) and quinoline (**25**) derivatives exhibited decreased affinity for both Grp94 and Hsp90α. Substitutions at the 3-position were not beneficial, as all of the analogues synthesized reduced affinity for both isoforms compared to the parent inhibitor, **5**. Alternatively, substitutions at the 2-position typically increased Grp94 affinity and improved selectivity versus Hsp90α (e.g. **38 – 42**)
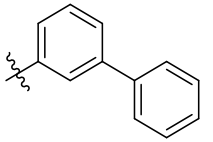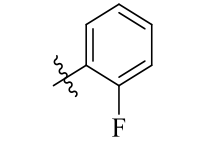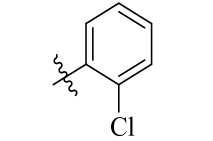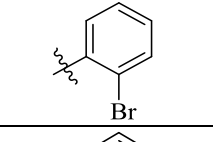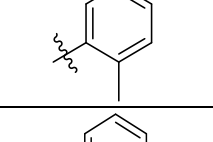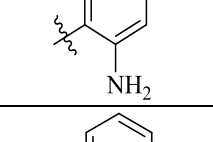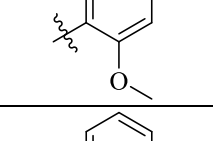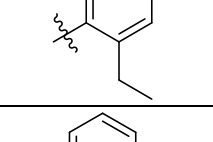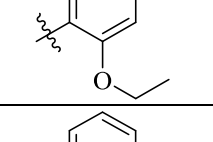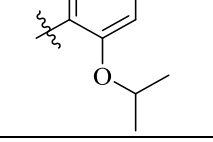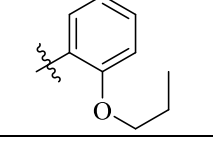
Analogues that displaced ≥ 70% of the tracer, when incubated with Grp94 at 25µM, were subsequently evaluated to determine their apparent K_d values against Grp94 and Hsp90α. Compound **5** manifests an apparent K_d of 1.1 µM for Grp94 and 13.1 µM for Hsp90α, resulting in 12-fold Grp94 selectivity. Substitutions at the 4-position were designed to extend further into the hydrophobic pocket present in Grp94 to increase selectivity over other isoforms. Modest increases in selectivity were observed with these compounds (**11**, **12** and **18**), while increases in affinity were observed with analogues containing halogen substitutions. Incorporation of the hydrophobic methyl group (**14**) substantially increased selectivity for Grp94 as well as increased affinity. Extended alkyl chains (**15** and **16**) were too large to be accommodated into the secondary pocket of Grp94 and decreased affinity, likely due to steric interactions with Val82.
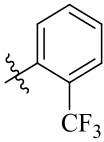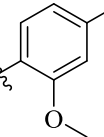
Table 2.1. Apparent K_d values of **5** and **10**-**44** against Grp94 and Hsp90α.
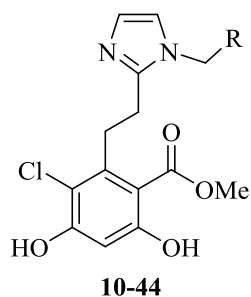
10-44

Entry	R	% Tracer Displaced Grp94[a]	% Tracer Displaced Hsp90α[a]	Apparent K_d Grp94 (µM)	Apparent K_d Hsp90α (µM)	Fold Selective for Grp94
5		98.9 ± 0.2	72.9 ± 1.2	1.14 ± 0.1	13.1 ± 1.1	12
10		90.3 ± 0.5	40.3 ± 3.2	3.2 ± 0.5	23.4 ± 1.2	7
11		99.1 ± 0.5	52.1 ± 2.1	0.81 ± 0.09	12.1 ± 1.6	15
12		1.0 ± 0.4	57.2 ± 3.7	0.96 ± 0.1	12.5 ± 1.8	13
13		43.6 ± 4.4	43.5 ± 2.5	n.d.	n.d.	n.d.
14		98.9 ± 0.8	33.5 ± 4.4	0.73 ± 0.1	25.2 ± 2.1	34
15		24.2 ± 8.7	17.3 ± 5.6	n.d.	n.d.	n.d.
16		23.9 ± 7.7	15.9 ± 6.3	n.d.	n.d.	n.d.
17		75.8 ± 4.1	49.7 ± 3.6	4.7 ± 0.7	18.2 ± 1.1	4
18		89.3 ± 3.2	43.9 ± 2.3	1.4 ± 0.1	15.8 ± 1.0	11

44

Entry	R	% Tracer Displaced Grp94[a]	% Tracer Displaced Hsp90α[a]	Apparent K_d Grp94 (µM)	Apparent K_d Hsp90α (µM)	Fold Selective for Grp94
19	4-CF$_3$-phenyl	52.1 ± 5.5	10.0 ± 12.1	n.d.	n.d.	n.d.
20	biphenyl	18.0 ± 8.5	12.8 ± 6.1	n.d.	n.d.	n.d.
21	4-OMe-phenyl	78.7 ± 4.7	30.1 ± 5.3	6.9 ± 1.3	>150	>22
22	3,4-diCl-phenyl	13.7 ± 7.2	17.1 ± 9.2	n.d.	n.d.	n.d.
23	1-naphthyl	29.5 ± 6.4	9.6 ± 10.3	n.d.	n.d.	n.d.
24	2-naphthyl	34.0 ± 5.7	11.1 ± 9.7	n.d.	n.d.	n.d.
25	quinolinyl	64.2 ± 3.9	35.5 ± 4.7	n.d.	n.d.	n.d.
26	3-F-phenyl	70.9 ± 4.6	57.0 ± 5.6	1.53 ± 0.1	9.63 ± 1.4	6
27	3-Cl-phenyl	56.0 ± 7.1	25.8 ± 6.2	n.d.	n.d.	n.d.
28	3-Br-phenyl	35.6 ± 5.1	25.3 ± 6.7	n.d.	n.d.	n.d.
29	3-I-phenyl	16.5 ± 8.5	14.9 ± 9.4	n.d.	n.d.	n.d.
30	3-OMe-phenyl	27.0 ± 7.2	32.0 ± 6.4	n.d.	n.d.	n.d.
31	3-Me-phenyl	62.4 ± 4.0	39.0 ± 6.7	n.d.	n.d.	n.d.

Entry	R	% Tracer Displaced Grp94[a]	% Tracer Displaced Hsp90α[a]	Apparent K_d Grp94 (μM)	Apparent K_d Hsp90α (μM)	Fold Selective for Grp94
32	biphenyl	67.3 ± 4.3	60.9 ± 4.5	n.d.	n.d.	n.d.
33	F	89.2 ± 3.7	59.8 ± 7.5	1.36 ± 0.1	11.4 ± 1.2	8
34	Cl	86.0 ± 4.2	60.4 ± 2.3	1.39 ± 0.1	8.47 ± 0.9	6
35	Br	84.2 ± 2.1	45.5 ± 5.2	1.60 ± 0.3	21.1 ± 3.7	13
36	CH₃	79.9 ± 2.7	38.8 ± 6.6	3.0 ± 0.8	68.1 ± 8.7	23
37	NH₂	30.8 ± 8.1	20.9 ± 8.3	n.d.	n.d.	n.d.
38	OCH₃	93.5 ± 1.3	36.6 ± 5.8	1.3 ± 0.2	53.9 ± 7.6	41
39	ethyl	99.5 ± 0.1	39.8 ± 7.3	0.81 ± 0.08	38.8 ± 5.3	48
40	O-ethyl	99.6 ± 0.1	57.3 ± 5.8	0.20 ± 0.08	8.1 ± 1.8	41
41	O-isopropyl	99.7 ± 0.1	99.7 ± 0.22	0.09 ± 0.01	0.24 ± 0.03	3
42	O-propyl	99.6 ± 0.1	93.2 ± 1.2	0.25 ± 0.05	2.3 ± 0.2	9

Entry	R	% Tracer Displaced Grp94[a]	% Tracer Displaced Hsp90α[a]	Apparent K_d Grp94 (μM)	Apparent K_d Hsp90α (μM)	Fold Selective for Grp94
43		82.6 ± 3.2	54.8 ± 3.6	1.53 ± 0.23	19.3 ± 2.8	13
44		94.9 ± 1.6	31.0 ± 6.7	2.35 ± 0.31	72.5 ± 8.4	30

[a] % Tracer bound determined when incubated with 25 µM of inhibitors. Data are the average of at least 2 experiments ± SEM n.d. = not determined.

As observed in the 25 µM screen, substitutions at the 3-position (**26**-**32**) did not manifest improved affinity nor selectivity for Grp94 compared to **5**. Alternatively, substitutions at the 2-position provided additional insights into the binding mode for these analogues. Small substitutions at the 2-position were tolerated; however, such substitutions did not increase selectivity or affinity (**33** and **34**). Larger substitutions produced increased selectivity for Grp94 versus Hsp90α, as **38**, **39**, and **40** exhibited >40-fold Grp94 selectivity, potentially due to induction of a conformational shift in the tertiary structure of Grp94.
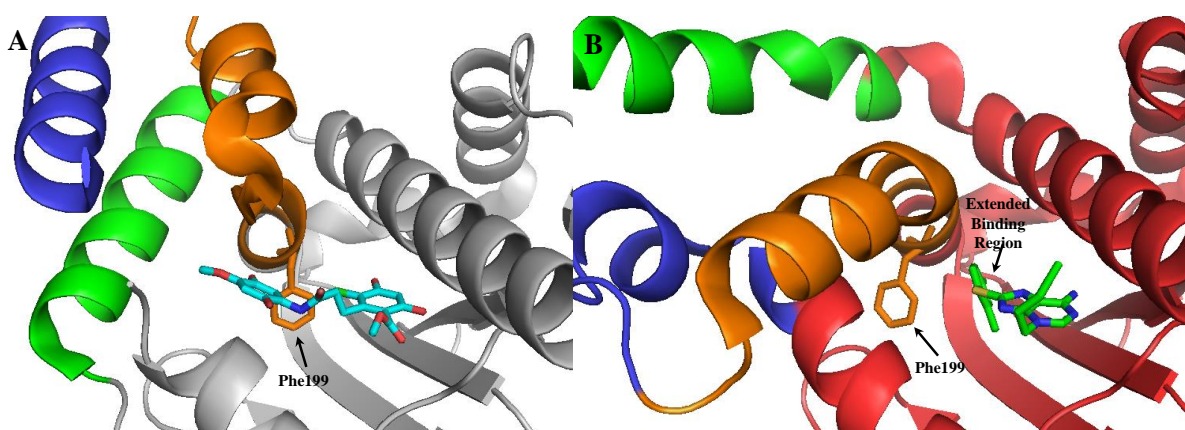
Figure 2.3. Substitutions at the 2-position potentially result in reorganization of Grp94 tertiary structure. (**a**) Tertiary structure of **4** bound to Grp94 (PDBID: 2GFD) showing the open conformation of the N-terminal domain of Grp94. (**b**) Tertiary structure of **3** bound to Grp94 (PDBID: 3O2F) showing the conformational shift (blue, green and orange helices) of the N-terminal domain induced by the inhibitor binding to Grp94 revealing the S2 sub-pocket.

Patel and colleagues previously reported the co-crystallization of **3** with Grp94 (PDBID: 3O2F) in which a conformational shift was observed (compared to **4**, PDBID: 2GFD) to form the S2 sub-pocket within the Grp94 ATP-binding site.[11, 20] This sub-pocket is distinct from the S1 sub-pocket utilized by **1** and **4** (**Figure 2.3a**) due to migration of Phe199. This migration allows access to the S2 sub-pocket that is observed with **3**. Substitutions at the 2-position may also induce a similar conformational change in Grp94. Modeling studies suggested substitutions at this position project into this extended region which could produce increased Grp94 selectivity. In the case of **40** (Grp94 apparent K_d = 0.2 µM; 41-fold selective)**,** the increased selectivity was accompanied by a ~6-fold increase in affinity for Grp94 compared to **5**. Extension or branching of the alkyl ether (**41** and **42**) improved affinity for Grp94, although a loss in selectivity was observed. These larger alkyl ethers did not appear to be accommodated within the S1 or S2 sub-pockets of Grp94, and likely push the benzyl side chain towards the solvent exposed region via ~180° rotation of the imidazole ring to form hydrogen bonds with polar amino acids present in this region (See Chapter 3 for further discussion).[21] These polar residues are conserved in both Grp94 and Hsp90 and provide an explanation for the loss of selectivity and an increase in affinity. In an attempt to combine beneficial substitutions observed with the 2- and 4-positions, **44** was synthesized, however affinity was compromised compared to the parent compounds (**14** and **38**), suggesting the effects of these substitutions are not additive (**Table 2.1**).

Scheme 2.3. Synthesis of heterocyclic amines **6g-6l**.

46b, 6h: X=N, R=H
46c, 6i: X=CH, R=Me

46d, 6j: Y=S
46e, 6k: Y=O
6l: Y=S
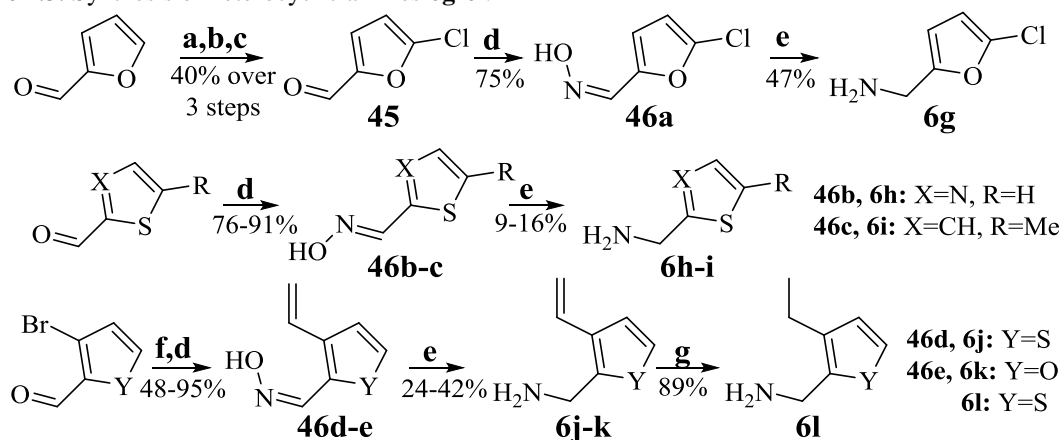
Conditions: **a**) HNO$_3$, H$_2$SO$_4$, Ac$_2$O, 0˚C, 1h; **b**) 50% H$_2$SO$_4$ (aq.), 110˚C, 5 min; **c**) conc. HCl, 40˚C, 12 h; **d**) NH$_2$OH•HCl, NaOAc, MeOH, 25˚C, 8 h; **e**) LiAlH$_4$, THF, 0˚C to 25˚C, 12 h; **f**) Potassium vinyltrifluoroborate, Pd(dppf)Cl$_2$, ^{i}Pr$_2$EtN, Toluene, 110˚C, 14 h; **g**) H$_2$, 10% Pd/C, EtOH, 25˚C, 6 h.

Due to the high density of aromatic amino acids within the unique secondary binding pocket of Grp94, the incorporation of heterocycles was proposed to improve both π-π interactions and affinity for Grp94.[13] The requisite heterocyclic amines (**6g-l**) were synthesized from the corresponding aldehydes through conversion to the oximes (**46a-e**), followed by reduction via lithium aluminum hydride (**Scheme 2.3**). Chlorination of thiophen-2-ylmethanamine via sulfuryl chloride provided **6m** (**Scheme 2.4**). Radical bromination of 5-methylisoxazole followed by conversion to the azide and subsequent Staudinger reduction provided **6n**. Reduction of the substituted furoic acid **48** to the corresponding furfuryl alcohol was achieved using lithium aluminum hydride followed by conversion to the azide and then Staudinger reduction to yield **6o**. Deprotonation of 3-chlorothiophene with *n*-butyllithium followed by the addition of CO$_{2(g)}$ provided a mixture of carboxylate regioisomers which were separable via flash chromatography after reduction to the corresponding alcohols (**49b** and **49c**) with lithium aluminum hydride. These isomers were then converted to the corresponding azides, followed by Staudinger reduction to provide the requisite basic amines, **6p** and **6q** (**Scheme 2.4**). The desired analogues were obtained through the multicomponent reaction detailed in **Scheme 2.2** to produce analogues **50-69**.

Scheme 2.4. Synthesis of heterocyclic amines **6m-6q**.
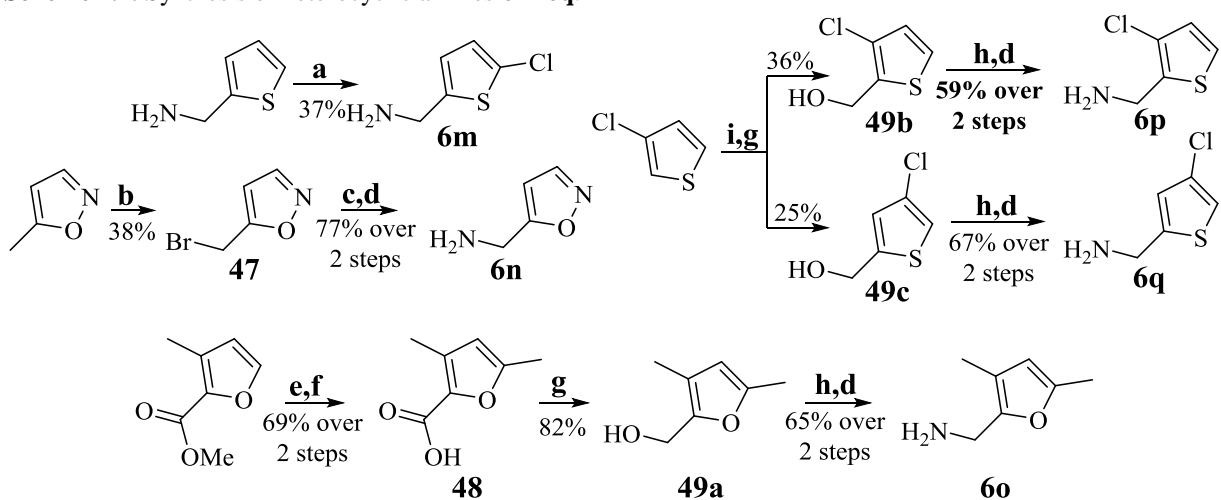
Conditions: **a**) SO$_2$Cl$_2$, 15˚C, AcOH:Et$_2$O (9:1), 1 h; **b**) NBS, AIBN, CCl$_4$, 80˚C, 4 h; **c**) NaN$_3$, MeOH:H$_2$O (10:1), 25˚C, 12 h; **d**) PPh$_3$, THF:H$_2$O (10:1), 25˚C, 12 h; **e**) LiOH, THF:MeOH:H$_2$O (9:1:1), 25˚C, 10 h; **f**) LDA, MeI, THF, -40˚C, 3 h; **g**) LiAlH$_4$, THF, 0˚C to 25˚C, 12 h; **h**) DBU, DPPA, Toluene, 25˚C, 12 h, **i**) n-BuLi, CO$_2$ (g), THF, -78˚C, 2 h.

As can be seen in **Table 2.2**, incorporation of an electron poor (compared to benzene) pyridine ring (**66-69**) decreased selectivity and affinity for Grp94. In contrast, incorporation of electron rich 5-membered heterocycles proved beneficial for Grp94 affinity. Converting the phenyl ring of **5** to the bioisosteric replacement thiophene (**55**) significantly increased affinity for Grp94 compared to **5**. The 2-furan and 2-thiophene (**51** and **55**, respectively) analogues exhibited both increased affinity and selectivity, and consequently, substitutions about these rings were explored. The energy minimized structures of **5** and **51** were overlaid and revealed the 5-position of the heterocycle aligned similarly to the 4-position of the benzyl side chain of **5** (**Figure 2.4**). Therefore, substitutions at the 5-position of both the furan and thiophene rings were sought to increase selectivity and affinity.
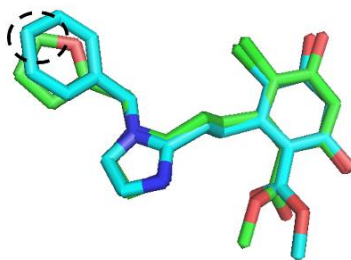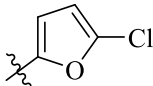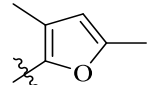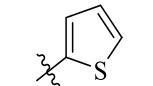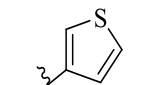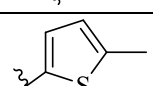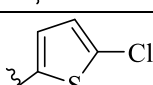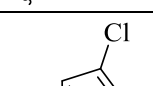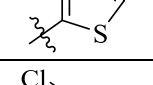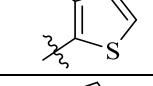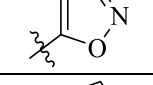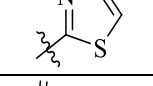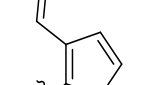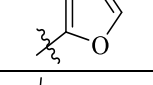
Figure 2.4. Overlay of the minimized structures of **5** (cyan) and **51** (green) highlighting the overlapping 4- and 5-positions, respectively.
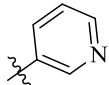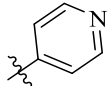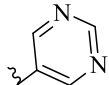
58 exhibited improved selectivity for Grp94 compared to the 3- and 4-chloro substituted thiophene analogues (**59** and **60**), supporting the hypothesis that these 5-substituted heterocycles bind similarly to the 4-substituted phenyl ring. Incorporation of a 5-chloro substitution onto the smaller furan ring (**53**) increased Grp94 selectivity and affinity. In an effort to mimic the 2-substitutions on the benzene ring, modifications to the 3-position of the 5-membered ring were incorporated. Unfortunately, these substitutions exhibited both reduced selectivity and affinity.

Table 2.2. Apparent K_d of heterocyclic analogues **50-69** against Grp94 and Hsp90α.
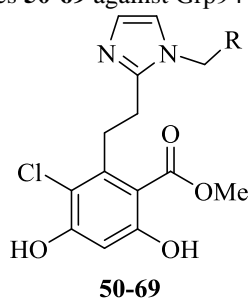
50-69

Entry	R	% Tracer Bound Grp94[a]	%Tracer Bound Hsp90α[a]	Apparent K_d Grp94 (µM)	Apparent K_d Hsp90α (µM)	Fold Selective for Grp94
5		98.9 ± 0.2	72.9 ± 1.2	1.14 ± 0.1	13.1 ± 1.1	12
50		97.4 ± 0.8	78.3 ± 4.7	1.50 ± 0.12	3.77 ± 0.41	3
51		99.2 ± 0.1	75.0 ± 2.3	0.55 ± 0.06	5.91 ± 0.88	11
52		99.1 ± 0.07	73.4 ± 2.3	0.65 ± 0.10	26.6 ± 2.3	41

51

Entry	R	% Tracer Bound Grp94[a]	%Tracer Bound Hsp90α[a]	Apparent K_d Grp94 (μM)	Apparent K_d Hsp90α (μM)	Fold Selective for Grp94
53	(5-chlorofuran-2-yl)	99.3 ± 0.09	91.7 ± 1.2	0.44 ± 0.05	8.31 ± 1.2	19
54	(3,5-dimethylfuran-2-yl)	99.3 ± 0.1	65.1 ± 2.4	0.35 ± 0.06	9.2 ± 1.6	26
55	(thiophen-2-yl)	99.4 ± 0.08	76.7 ± 2.1	0.47 ± 0.07	3.92 ± 0.51	8
56	(thiophen-3-yl)	87.9 ± 1.9	64.5 ± 3.8	2.14 ± 0.22	6.54 ± 0.86	3
57	(5-methylthiophen-2-yl)	99.0 ± 0.2	49.8 ± 6.1	0.68 ± 0.08	5.13 ± 0.42	8
58	(5-chlorothiophen-2-yl)	99.0 ± 0.2	59.2 ± 3.6	0.93 ± 0.09	34.7 ± 2.6	37
59	(4-chlorothiophen-2-yl)	99.1 ± 0.1	97.6 ± 1.1	0.67 ± 0.08	1.8 ± 0.17	3
60	(3-chlorothiophen-2-yl)	99.1 ± 0.08	97.2 ± 1.2	0.76 ± 0.07	3.16 ± 0.41	4
61	(isoxazol-5-yl)	99.3 ± 0.06	99.1 ± 0.08	0.40 ± 0.02	0.81 ± 0.07	2
62	(thiazol-2-yl)	91.7 ± 2.1	62.5 ± 4.0	2.5 ± 0.23	16.0 ± 1.8	6
63	(3-vinylthiophen-2-yl)	99.1 ± 0.2	46.2 ± 7.6	0.75 ± 0.12	36.7 ± 3.2	49
64	(3-vinylfuran-2-yl)	94.8 ± 1.3	59.9 ± 5.0	2.36 ± 0.17	7.5 ± 1.2	3
65	(3-ethylthiophen-2-yl)	99.1 ± 0.1	63.1 ± 3.6	0.72 ± 0.08	6.94 ± 0.94	10
66	(pyridin-2-yl)	82.9 ± 3.3	56.3 ± 5.7	4.94 ± 0.46	9.92 ± 1.5	2

Entry	R	% Tracer Bound Grp94[a]	%Tracer Bound Hsp90α[a]	Apparent K_d Grp94 (μM)	Apparent K_d Hsp90α (μM)	Fold Selective for Grp94
67		93.3 ± 1.5	73.3 ± 4.9	4.04 ± 0.39	5.41 ± 0.67	1
68		62.1 ± 2.7	49.7 ± 4.2	n.d.	n.d.	n.d.
69		73.9 ± 3.9	59.2 ± 5.0	9.18 ± 1.1	9.92 ± 1.6	1

[a] % Tracer bound determined when incubated with 25 μM of inhibitors. Data are the average of at least 2 experiments ± SEM. n.d. = not determined

Co-Crystallization of Grp94 with the Grp94-Selective Inhibitor, 53

The co-crystal structure of the N-terminal domain of Grp94 in complex with **53** was solved to 2.6 Å resolution and supported the proposed docking interactions (**Figure 2.5a**). The structure reveals **53** in the ATP-binding site with the resorcinol ring stabilized by hydrogen bonding interactions with Asp149 (**Figure 2.5b, c**) similar to other resorcinol-based *pan*-Hsp90 inhibitors.[13, 22] Other direct interactions between **53** and the ATP-binding site are mediated through conserved water molecules (**Figure 2.5c**). In contrast to **4**, compound **53** is bound to Grp94 in a single orientation, illustrating the effectiveness of the *cis*-amide bioisostere in reducing binding heterogeneity.

The electron density of **53** was largely continuous for the length of the molecule, with the notable exception of the chlorinated furan moiety (**Figure 2.5d**), which apparently samples multiple conformations within the ATP-binding site and results in low electron density for this region of the molecule. It is possible that the chlorinated furan dwells within the extended hydrophobic region to increase selectivity (as predicted through modeling studies); however, the final binding mode modeled, based on optimal fit to $2F_o$-F_c (**Figure 2.5d**), is one in which the chloride substituent is nestled in an ordered loop (residues 165-170) at the entry to the ATP-
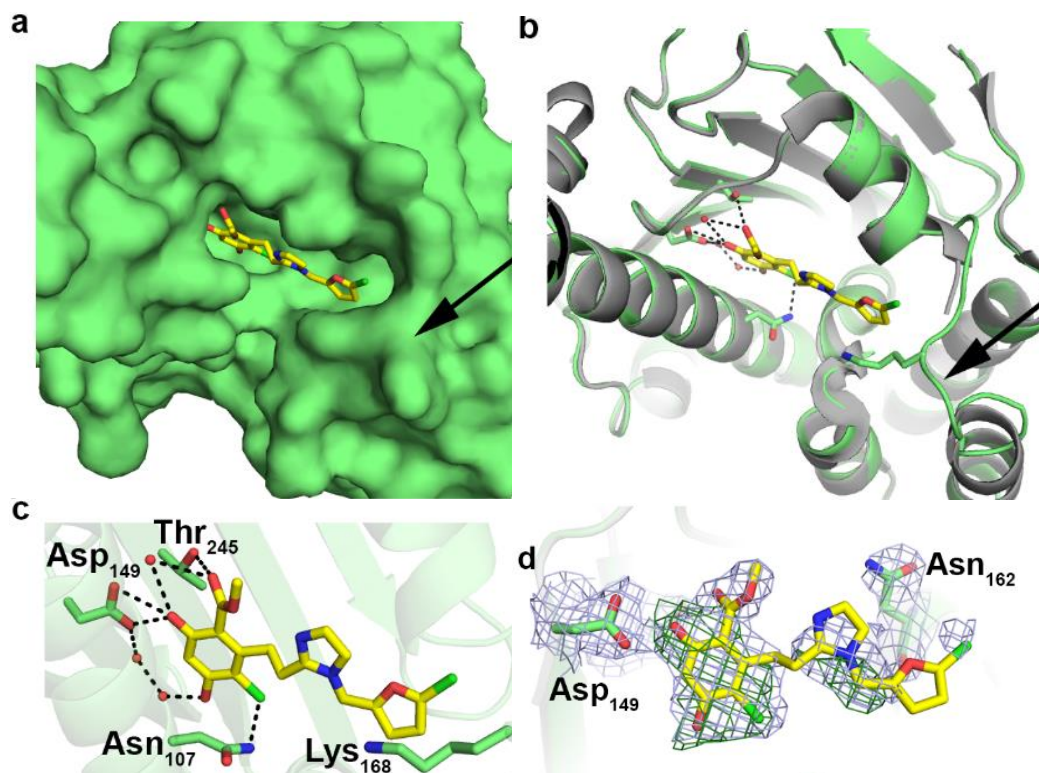
Figure 2.5. Crystal structure of **53** bound to Grp94. (**a**) Surface representation of ATP-binding pocket with **53** as ball and stick. Arrow points to a well ordered loop at the mouth of the active site. (**b**) Cartoon representation of the structure as in (a) highlighting H-bonding interactions (≤ 3.5 Å) and loop configuration. (**c**) Zoomed view of **48** in active site with H-bonding interactions as in (**b**). (**d**) Final $2F_o$-F_c electron density contoured at 1 σ (grey mesh).

binding site (arrow, **Figure 2.5a** and **b**). Notably, this loop is disordered in the structure complexed

with **4** (grey, **Figure 2.5b**). The furan moiety also appears to be involved in a cation-π interaction

with Lys168 to stabilize this loop. In general, phenyl rings form stronger cation-π interactions due

to a larger quadrupole moment compared to furan rings.[23] However, modeling studies suggest that

the phenyl ring of **5** cannot orient in a manner to allow this interaction, which therefore accounts

for the increased affinity manifested by the smaller heterocycles (**50**-**65**). Taken together, **53**, and

by analogy other analogues described within this series, bind to the ATP-binding site of Grp94 in

a mode that manifests increased selectivity over the other Hsp90 isoforms.

Grp94-Selective Inhibition Offers a Potential Treatment for Primary Open Angle Glaucoma
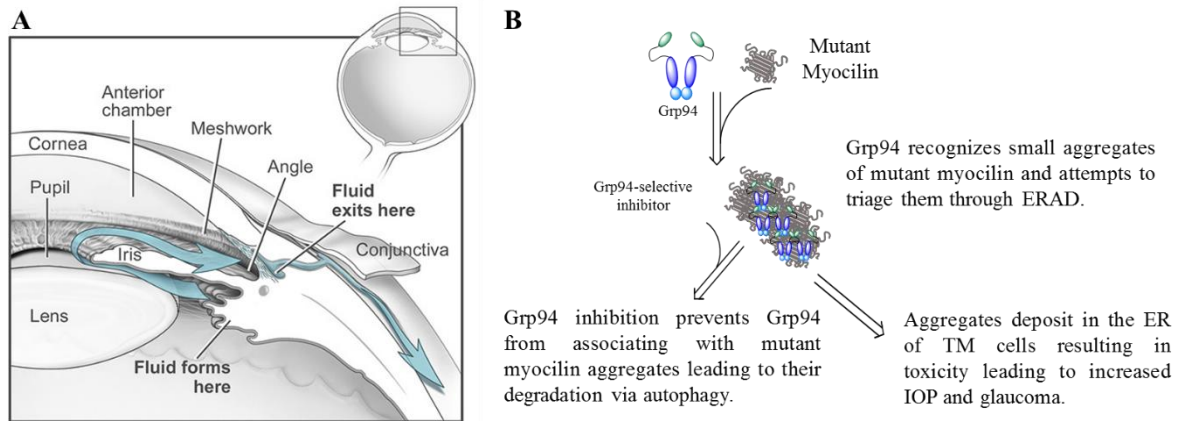
Figure 2.6. Myocilin-associated open angle glaucoma. (**a**) Anatomical diagram of the anterior segment of the eye depicting the normal outflow of aqueous humor. Image courtesy of National Eye Institute, National Institutes of Health. (**b**) Grp94 recognizes small mutant myocilin aggregates and attempts to triage them through ERAD however this results in their deposition in the ER leading to toxicity. In the presence of a Grp94-selective inhibitor, Grp94 is dissociated from mutant myocilin resulting in degradation of mutant myocilin via autophagy and reduction of toxicities.

Glaucoma is the second leading cause of blindness in the world and is characterized by increased intraocular pressure that leads to irreversible optic nerve damage and blindness.[24-26] The clinically observable risk factor of elevated intraocular pressure (IOP) typically results from decreased outflow of the aqueous humor through the trabecular meshwork (TM) in the anterior segment of the eye (**Figure 2.6a**).[27] Nonsynonymous mutations in myocilin, localized to its olfactomedin domain, result in a non-native tertiary structure and promote facile aggregation that leads to TM cell death and ultimately glaucoma and blindness.[28-29] Recently, it was demonstrated that Grp94 associates with amyloid-like aggregates of mutant myocilin but cannot triage these aggregates through the ER-associated degradation (ERAD) pathway (**Figure 2.6b**).[7]

Prior studies showed that Grp94 inhibition allows mutant myocilin degradation through an autophagic mechanism, which decreases intracellular levels of myocilin and, ultimately, reduces toxicity (**Figure 2.6b**).[6] Therefore, these Grp94-selective inhibitors were evaluated for their ability

Figure 2.7. Western blot analysis of HEK293 cells overexpressing myocilin mutants treated with indicated Grp94-selective inhibitors. (**a**) treatment with **12** results in degradation of 5 disease-relevant mutants (**b**) Compounds **KUNG65**, **40**, and **53** produce degradation of myocilin. (**c**) Grp94-selective inhibitors do not induce the heat shock response or result in the degradation of Akt, a cytosolic Hsp90 isoform-dependent client protein. Veh. = DMSO and 17-AAG = 17-(allylamino)-17-demethoxygeldanamycin (*pan*-Hsp90 N-terminal inhibitor).

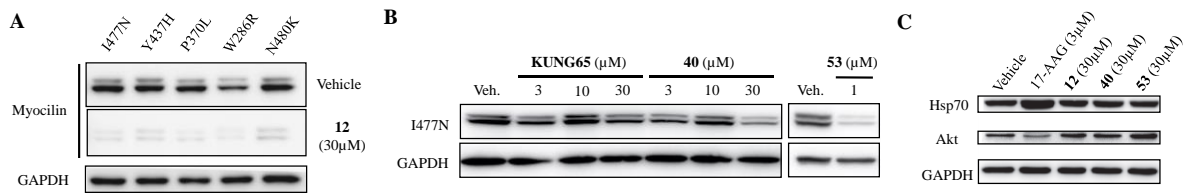to promote mutant myocilin clearance in a cellular model that is transfected to overexpress mutant myocilin. Treatment with **12** produced degradation of five disease relevant mutant forms of myocilin (**Figure 2.7a**). Compound **40** produced similar degradation of mutant myocilin at comparable concentrations to that of **12**, and compound **53** produced significant degradation of mutant myocilin at 1 µM (**Figure 2.7b**). Surprisingly, **KUNG65** (**Figure 2.1**), a second generation Grp94-selective inhibitor (see **Figure 2.1** and Chapter 3), only produces modest degradation of mutant myocilin at 30 µM. Compounds **12**, **40**, and **53** do not induce the pro-survival heat shock response, which is in contrast to the *pan*-Hsp90 inhibitor **17-AAG**. Additionally, these inhibitors do not result in the degradation of the cytosolic Hsp90 isoform-dependent client protein Akt at concentrations similar to those needed to degrade myocilin, suggesting these inhibitors manifest Grp94-selectivity in cells (**Figure 2.7c**).

In order to evaluate the translational potential of Grp94-selective inhibition for the treatment of myocilin-associated glaucoma, **12** was evaluated in a previously characterized Tg-MYOC^{Y437H} mouse model wherein the glaucoma phenotype appears around three months of age.[27] Therefore, treatment was initiated at four months of age. Mice were treated with 300 µM of **12** or vehicle control via eye drops once per day for 12 weeks and IOP measurements were recorded biweekly on each eye. After 8 weeks of treatment, the test group displayed reduced IOP compared to vehicle treated transgenic mice. After 12 weeks, treatment with **12** reduced IOP levels to those that were
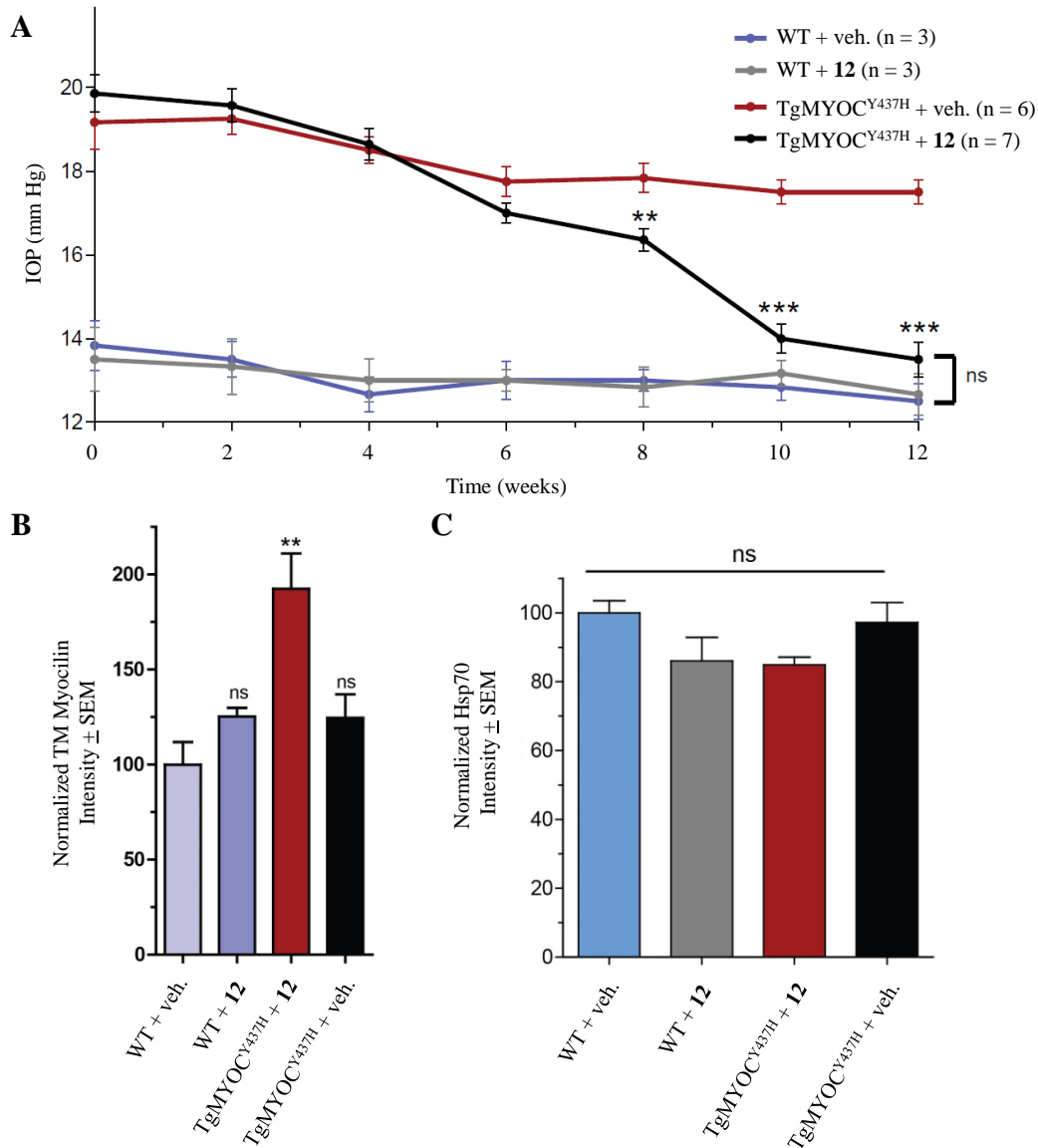
Figure 2.8. *In vivo* evaluation of **12** in a transgenic mutant myocilin mouse model. (**a**) IOP was measured biweekly over 12 weeks of treatment with veh. or **12**. **P < 0.05, ***P < 0.001. Time = 0 = mouse age of 22 weeks. (**b**) Quantification of myocilin levels. **P < 0.01. (**c**) Quantification of Hsp70 levels normalized to WT vehicle-treated controls. No significant difference was observed between groups.

indistinguishable from the WT group (**Figure 2.8a**). Reduced IOP levels were accompanied by a

clearance of mutant myocilin within TM cells after treatment with **12**, recapitulating the clearance

observed in cellular studies (**Figure 2.8b**). In addition to clearance of myocilin, no induction of

the pro-survival heat shock response was observed, as monitored by Hsp70 levels in TM cells

(**Figure 2.8c**). This study represents the first animal model in which a Grp94-selective inhibitor

has demonstrated efficacy and suggests that Grp94-selective inhibition represents a novel mechanism for the treatment of myocilin-associated POAG that does not exhibit the toxic liabilities associated with *pan*-Hsp90 inhibitors.

Conclusions & Future Directions

Structure-activity relationship studies were performed on the aryl side chain of **5**, which interacts with the unique secondary pocket of Grp94 (**Figure 2.9**). Substitutions at the 2- and 4-positions were tolerated within this binding region. Incorporation of an ethoxy group at the 2-position significantly increased affinity, as well as selectivity. **40** exhibited nearly a 10-fold increase in affinity for Grp94 compared to **5** and 40-fold selectivity for Grp94 over the cytosolic Hsp90 isoforms. Replacing the phenyl ring of the side chain with 5-membered heterocycles also increased affinity for Grp94, as observed with **53**. A co-crystal structure of the N-terminal domain of Grp94 with **53** was solved and revealed a cation-π interaction between the furan ring and Lys168. This interaction stabilized a loop of Grp94 (residues 165-170) that was disordered in the co-crystal structure of **4** bound to Grp94, and this stabilization appears to account for the increased affinity observed with the 5-membered heterocycles. Grp94-selective inhibition resulted in the degradation of myocilin aggregates in cells without the liabilities associated with *pan*-Hsp90 inhibitors. Additionally, **12** was evaluated in a mutant myocilin transgenic mouse model and demonstrated restoration of normal IOP levels after 12 weeks of treatment without any apparent toxicities, thus suggesting that Grp94-selective inhibition could serve as a novel treatment for myocilin-associated POAG. Going forward, this scaffold provides an excellent starting point for further modifications that can improve Grp94 selectivity (See Chapter 3). In general, increased ER stress is an emerging characteristic of many forms of glaucoma, suggesting that Grp94-selective inhibition could produce similar effects in non-myocilin-associated forms of glaucoma.[27, 30]

Specifically, ER stress was identified as a causative factor in retinal ganglion cell death following elevated IOP levels, and this increased ER stress was observed in an animal model of steroid-induced glaucoma.[31] These observations suggest that reduction of ER stress may represent a promising treatment opportunity for glaucoma.
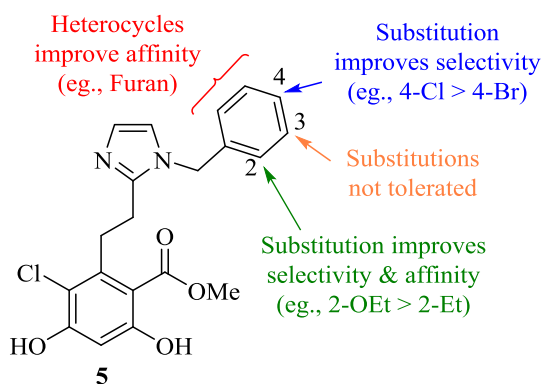
Figure 2.9. Summary of structure-activity relationships for the analogues of **5** for Grp94-selective inhibition.

Experimental Section

Chemistry General. ^{1}H NMR were recorded at 400 (Bruker AVIIIHD 400 MHz NMR with a broadband X-channel detect gradient probe) or 500 MHz (Avance AVIII 500MHz spectrometer with a dual carbon/proton cryoprobe) and ^{13}C were recorded at 125 MHz (Bruker AVIII spectrometer equipped with a cryogenically-cooled carbon observe probe); chemical shifts are reported in δ (ppm) relative to the internal standard (CDCl$_3$, 7.26 ppm or MeOD, 3.31 ppm). HRMS spectra were recorded with a LCT Premier. The purity of compounds was determined by HPLC (Agilent 1100 series quaternary pump; 60% MeCN/40% Water; Agilent C-18 column, 4.6x150mm, 5µM) with UV detection. All biologically tested compounds were determined to be >95% pure. TLC analysis was performed on glass backed silica gel plates and visualized by UV light. All solvents were reagent grade and used without further purification.

General Procedure for multicomponent cyclization reaction. Basic amines (e.g., **6a-6q**, 0.26 mmol, 1 equiv.) were added to a stirred solution of **9** (125 mg, 0.26 mmol, 1 equiv.) in wet MeOH (2 mL) and stirred for 30 minutes at rt followed before the addition of NH_4HCO_3 (0.26 mmol, 1 equiv.) and glyoxal (0.26 mmol, 1 equiv.). After stirring for 12 h, tetrabutylammonium fluoride (0.52 mL of 1 M solution in THF, 0.52 mmol, 2 equiv.) was added and then stirred for 30 minutes before the reaction was quenched with saturated aqueous NH_4Cl (10 mL) and extracted with EtOAc (3x 10 mL). The organic layers were combined, dried (Na_2SO_4), filtered, and concentrated. The residue was purified via flash chromatography (SiO_2, 1:49 MeOH:DCM) to afford the desired product as an amorphous solids:
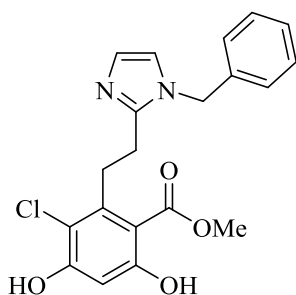
Methyl 2-(2-(1-benzyl-1H-imidazol-2-yl)ethyl)-3-chloro-4,6-dihydroxybenzoate **(5)** 54 mg (54% yield), white amorphous solid. ^1H NMR (500 MHz, $CDCl_3$, MeOD) δ 7.28 – 7.23 (m, 3H), 7.01 – 6.97 (m, 2H), 6.95 (d, J = 1.5 Hz, 1H), 6.81 (d, J = 1.5 Hz, 1H), 6.40 (s, 1H), 5.02 (s, 2H), 3.79 (s, 3H), 3.48 – 3.41 (m, 2H), 2.89 – 2.83 (m, 2H). ^{13}C NMR (126 MHz, $CDCl_3$, MeOD) δ 170.8, 162.1, 158.1, 147.7, 141.7, 136.2, 128.9, 128.0, 126.9, 126.5, 120.1, 114.8, 105.9, 102.5, 52.5, 49.4, 30.8, 26.1. HRMS (ESI) m/z [M–H]$^-$ $C_{20}H_{19}ClN_2O_4$ 385.0955, found 385.0953. t_R = 5.062 min, 99.0%.
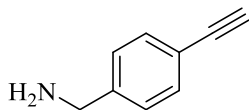
(4-Ethynylphenyl)methanamine **(6a)** was synthesized from 4-iodobenzylamine hydrochloride following procedures detailed in reference 16. 93 mg (78% yield) as a dark yellow oil. ^{1}H NMR (500 MHz, MeOD) δ 7.54 (d, J = 8.2 Hz, 2H), 7.44 (d, J = 8.3 Hz, 2H), 4.13 (s, 2H), 3.60 (s, 1H). ^{13}C NMR (126 MHz, MeOD) δ 133.6, 132.3 (2C), 128.7 (2C), 123.3, 82.1, 78.6, 42.5. HRMS (ESI) *m/z* [M+H]$^+$ for $C_9H_{10}N$: 132.0813, found: 132.0809.

General Procedure for reduction of aromatic nitriles. Benzonitriles (e.g., **7a**-**7c**, 0.7 M in THF, 1 equiv.) were added dropwise to a stirred solution of LiAlH$_4$ (0.5 M in dry THF, 5 equiv.) at 0˚C. The reaction mixture warmed to rt and stirred for 12h. H$_2$O (1 mL/g of LiAlH$_4$) was added dropwise to quench the excess hydride, followed by 4 M NaOH (1 mL/g of LiAlH$_4$), and EtOAc (3 mL/g of LiAlH$_4$). The resulting suspension was filtered through a pad of celite and the celite washed with warm EtOAc (30 mL) and the eluent concentrated. The residue was purified via flash chromatography (SiO$_2$, 1:49, MeOH:DCM to 1:20, MeOH:DCM) to afford the desired product as oils:
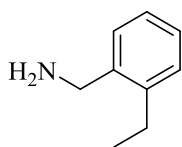
(2-Ethylphenyl)methanamine **(6b)** 653 mg (79% yield) as a colorless oil. ^{1}H NMR (400 MHz, MeOD) δ 6.77 – 6.69 (m, 1H), 6.63 – 6.56 (m, 2H), 6.58 – 6.48 (m, 1H), 4.51 (s, 2H), 2.07 (q, J = 7.6 Hz, 2H), 0.60 (t, J = 7.6 Hz, 3H). ^{13}C NMR (126 MHz, MeOD) δ 143.2, 129.8, 129.4, 129.1, 127.5, 127.0, 42.3, 26.4, 16.0. HRSM (ESI) *m/z* [M+NH$_4$]$^+$ for $C_9H_{17}N_2$: 153.1392, found: 153.1395.
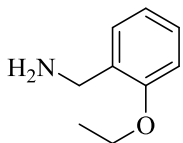
(2-Ethoxyphenyl)methanamine **(6c)** 215 mg (59% yield) as a colorless oil. ^{1}H NMR (400 MHz, CDCl$_3$) δ 7.25 – 7.16 (m, 2H), 6.90 (t, J = 7.4 Hz, 1H), 6.85 (d, J = 8.5 Hz, 1H), 4.07 (q, J = 7.6, 7.1 Hz, 2H), 3.82 (s, 2H), 1.73 (br s, 2H), 1.44 (t, J = 7.0 Hz, 3H). ^{13}C NMR (126 MHz, CDCl$_3$) δ 156.8, 131.8, 128.5, 128.1, 120.4, 111.1, 63.3, 42.9, 15.0. HRMS (ESI) *m/z* [M+H]$^+$ for C$_9$H$_{14}$NO: 152.1075, found: 152.1077.
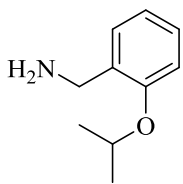
(2-Isopropoxyphenyl)methanamine **(6d)** 243 mg (59% yield) as a colorless oil. ^{1}H NMR (400 MHz, CDCl$_3$) δ 7.19 (t, J = 6.6 Hz, 2H), 6.92 – 6.83 (m, 2H), 4.59 (hept, J = 6.0 Hz, 1H), 3.79 (s, 2H), 1.74 (br s, 2H), 1.36 (d, J = 6.1 Hz, 6H). ^{13}C NMR (126 MHz, CDCl$_3$) δ 155.7, 132.7, 128.7, 128.0, 120.2, 112.5, 69.7, 43.1, 22.2 (2C). MS (EI) *m/z* [M]$^+$ for C$_{10}$H$_{15}$NO: 165.1, found: 165.2.
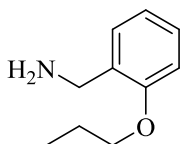
(2-Propoxyphenyl)methanamine **(6e)** 265 mg (67% yield) as a colorless oil. ^{1}H NMR (400 MHz, CDCl$_3$) δ 7.24 – 7.16 (m, 2H), 6.90 (t, J = 7.4 Hz, 1H), 6.85 (d, J = 8.5 Hz, 1H), 3.96 (t, J = 6.4 Hz, 2H), 3.83 (s, 2H), 1.90 – 1.78 (m, 4H), 1.06 (t, J = 7.4 Hz, 3H). ^{13}C NMR (126 MHz, CDCl$_3$) δ 156.9, 131.7, 128.5, 128.1, 120.3, 111.0, 69.3, 42.9, 22.7, 10.8. MS (EI) *m/z* [M]$^+$ for C$_{10}$H$_{15}$NO: 165.1, found: 165.2.

General procedure for Staudinger reduction. PPh₃ (1.1 equiv.) was added to a stirred solution of the benzyl azide (1 equiv.) in THF:H₂O (0.1 M, 10:1) and stirred at rt for 12 h. The reaction mixture was concentrated and the residue was purified via flash chromatography (SiO₂, 1:49, MeOH:DCM to 1:20, MeOH:DCM) to afford the desired product as oils:
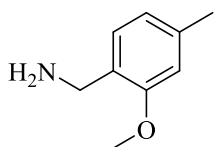

(2-Methoxy-4-methylphenyl)methanamine **(6f)** 99 mg (73% yield) as a colorless oil. ^{1}H NMR (500 MHz, CDCl₃) δ 7.08 (d, J = 7.4 Hz, 1H), 6.72 (d, J = 7.4 Hz, 1H), 6.69 (s, 1H), 3.83 (s, 3H), 3.77 (s, 2H), 2.34 (s, 3H), 1.87 (br s, 2H). ^{13}C NMR (126 MHz, CDCl₃) δ 157.3, 138.2, 128.5, 121.0, 111.2, 74.8, 55.1, 42.4, 21.6. HRMS (ESI) *m/z* [M+H]$^+$ for C₉H₁₄NO: 152.1075, found 152.1076.

General Procedure for Oxime Reduction. Aryl oximes (e.g., **66a-66e**, 0.7 M in THF, 1 equiv.) were added dropwise to a stirred solution of LiAlH₄ (0.5 M in dry THF, 5 equiv.) at 0°C. The reaction mixture warmed to rt and stirred for 12h. H₂O (1 mL/g of LiAlH₄) was added dropwise to quench the excess hydride, followed by 4 M NaOH (1 mL/g of LiAlH₄), and EtOAc (3 mL/g of LiAlH₄). The resulting suspension was then filtered through a pad of celite and the celite washed with warm EtOAc (30 mL) and the eluent was concentrated. The residue was purified via flash chromatography (SiO₂, 1:49, MeOH:DCM to 1:20, MeOH:DCM) to afford the desired products as oils:
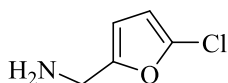
(5-Chlorofuran-2-yl)methanamine **(6g)** 93 mg (47% yield), yellow oil. ^{1}H NMR (500 MHz, CDCl₃) δ 6.12 (d, J = 3.2 Hz, 1H), 6.06 (d, J = 3.2 Hz, 1H), 3.76 (d, J = 0.8 Hz, 2H), 1.58 (br s,

2H). ^{13}C NMR (126 MHz, CDCl$_3$) δ 156.2, 156.2, 135.1, 107.5, 106.6, 39.4. HRMS (ESI) *m/z* [M+H]$^+$ for C$_5$H$_7$ClNS: 147.9988, found: 147.9990. HRMS (ESI) *m/z* [M+H]$^+$ for C$_5$H$_7$ClNO: 132.0216, found: 132.0221.
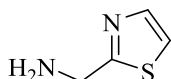

Thiazol-2-ylmethanamine **(6h)** 42 mg (9% yield) as a red oil. ^{1}H NMR (400 MHz, CDCl$_3$) δ 7.72 (d, *J* = 3.1 Hz, 1H), 7.26 (d, *J* = 3.2 Hz, 1H), 4.20 (s, 2H), 1.80 (br, s, 2H). ^{13}C NMR (126 MHz, CDCl$_3$) δ 174.0, 142.6, 118.6, 44.0. HRMS (ESI) *m/z* [M+H]$^+$ for C$_4$H$_7$N$_2$S: 115.0330, found: 115.0331.
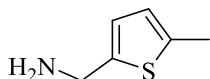
(5-Methylthiophen-2-yl)methanamine **(6i)** 72 mg (16% yield) as a yellow oil. ^{1}H NMR (500 MHz, CDCl$_3$) δ 6.70 (d, *J* = 3.4 Hz, 1H), 6.57 (dd, *J* = 3.3, 1.3 Hz, 1H), 3.96 (s, 2H), 2.72 (br s, 2H), 2.44 (s, 3H). ^{13}C NMR (126 MHz, CDCl$_3$) δ 143.9, 138.9, 124.8, 124.0, 41.2, 15.4. HRMS (ESI) *m/z* [M+H]$^+$ for C$_6$H$_{10}$NS: 128.0534, found: 128.0532. HRMS (ESI) *m/z* [M+H]$^+$ for C$_9$H$_{10}$NS: 164.0534, found: 164.0541.
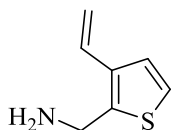
(3-Vinylthiophen-2-yl)methanamine **(6j)** 152 mg (42% yield) as a yellow oil. ^{1}H NMR (400 MHz, CDCl$_3$) δ 7.20 – 7.07 (m, 1H), 6.73 (dd, *J* = 17.5, 11.0 Hz, 1H), 5.54 (dd, *J* = 17.4, 1.3 Hz, 1H), 5.24 (dd, *J* = 11.0, 1.3 Hz, 1H), 4.07 (s, 1H), 2.03 (s, 1H). ^{13}C NMR (126 MHz, CDCl$_3$) δ 142.5, 135.2, 128.8, 125.4, 123.2, 114.2, 38.9. HRMS (ESI) *m/z* [M+H]$^+$ for C$_7$H$_{10}$NS: 140.0534, found: 140.0531.
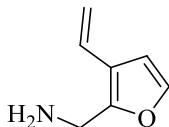
(3-Vinylfuran-2-yl)methanamine **(6k)** 57 mg (24% yield) as a yellow oil. ^{1}H NMR (400 MHz, CDCl$_3$) δ 7.29 (dd, J = 2.0, 0.7 Hz, 1H), 6.57 (dd, J = 17.3, 10.7 Hz, 1H), 6.50 (d, J = 2.0 Hz, 1H), 5.42 (dd, J = 17.4, 1.4 Hz, 1H), 5.14 (dd, J = 10.8, 1.4 Hz, 1H), 3.85 (s, 2H), 1.67 (br s, 2H). ^{13}C NMR (126 MHz, CDCl$_3$) δ 152.8, 141.7, 126.2, 119.3, 113.2, 107.7, 37.1. HRMS (ESI) [M+H]$^+$ for C$_7$H$_{10}$NO: 124.0762, found: 124.0768.
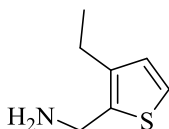
(3-Ethylthiophen-2-yl)methanamine **(6l)** 10% Pd/C (5 mol%) was added to a stirred solution of (3-vinylthiophen-2-yl)methanamine (**6k**, 50 mg, 0.36 mmol) in MeOH (5 mL) and stirred at rt under a hydrogen atmosphere for 12 h. The reaction mixture was filtered through a pad of celite and the eluent was concentrated to produce the title compound which was used without further purification. 45 mg (89% yield) as a yellow oil. ^{1}H NMR (400 MHz, CDCl$_3$) δ 7.16 (d, J = 5.1 Hz, 1H), 6.87 (d, J = 5.2 Hz, 1H), 4.56 (s, 2H), 4.05 (s, 2H), 2.61 (q, J = 7.6 Hz, 2H), 1.20 (t, J = 7.6 Hz, 3H). ^{13}C NMR (126 MHz, CDCl$_3$) δ 141.5, 134.9, 128.6, 123.8, 37.8, 21.5, 15.3. HRMS (ESI) *m/z* [M+H]$^+$ for C$_7$H$_{12}$NS: 147.0690, found: 147.0692.
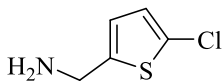
(5-Chlorothiophen-2-yl)methanamine **(6m)** A solution of thiophene-2-ylmethanamine (1 mL, 9.7 mmol, 1 equiv.) in AcOH:Et$_2$O (9:1, 0.5 M) was cooled to 5°C followed by the dropwise addition of SO$_2$Cl$_2$ (1.18 mL, 14.6 mmol, 1.5 equiv.) maintaining the reaction temperature under 20°C. The reaction was stirred at rt for 1 h at which time Et$_2$O (20 mL) was added and stirred for

an additional 30 min. The precipitate (hydrochloride salt of desired product) was filtered and the solid washed with Et_2O. The isolated solid was dissolved in DCM (25 mL) and washed with sat'd $NaHCO_3$ (2 x 30 mL). The organic layer was separated, dried (Na_2SO_4), and concentrated. The residue was purified via flash chromatography (SiO_2, 1:49 MeOH:DCM to 1:20 MeOH:DCM) to provide the title compound. 658 mg (37% yield) as a yellow oil. ^{1}H NMR (400 MHz, MeOD) δ 5.51 (d, J = 3.0 Hz, 1H), 5.40 (d, J = 3.8 Hz, 1H), 2.69 (s, 2H), 1.73 (br s, 2H). ^{13}C NMR (126 MHz, MeOD) δ 134.7, 132.7, 130.6, 127.9, 38.7. HRMS (ESI) m/z [M+H]$^+$ for C_5H_6ClNS: 148.9990, found: 148.9988.
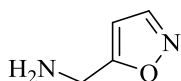
Isoxazol-5-ylmethanamine **(6n)** 159 mg (77% yield) as a colorless oil. ^{1}H NMR (400 MHz, CDCl$_3$) δ 8.17 (s, 1H), 6.13 (s, 1H), 4.00 (s, 2H), 1.53 (br, s, 2H). ^{13}C NMR (126 MHz, CDCl$_3$) δ 172.5, 150.3, 100.0, 37.6. MS (EI) m/z [M]$^+$ for $C_4H_6N_2O$: 98.0, found: 98.1.
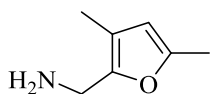
(3,5-Dimethylfuran-2-yl)methanamine **(6o)** 98 mg (65% yield) as a yellow oil. ^{1}H NMR (400 MHz, MeOD) δ 5.78 (s, 1H), 3.70 (s, 2H), 2.17 (s, 3H), 1.92 (s, 3H). ^{13}C NMR (126 MHz, MeOD) δ 152.0, 147.9, 118.5, 110.1, 36.4, 13.4, 9.8. HRMS (ESI) m/z [M+H]$^+$ for $C_7H_{12}NO$: 126.0919, found 126.0924.
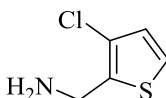
(3-Chlorothiophen-2-yl)methanamine **(6p)** 113 mg (59% yield) as a yellow oil. ^{1}H NMR (400 MHz, CDCl$_3$) δ 7.15 (dd, J = 5.2, 1.2 Hz, 1H), 6.86 (dd, J = 5.3, 1.1 Hz, 1H), 3.98 (s, 2H), 1.79

(br s, 2H). ^{13}C NMR (126 MHz, CDCl$_3$) δ 148.2, 124.5, 123.9, 118.3, 41.5. HRMS (ESI) *m/z* [M+H]$^+$ for C$_5$H$_7$ClNS: 147.9988, found: 147.9990.
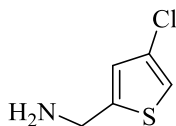
(4-Chlorothiophen-2-yl)methanamine **(6q)** 79 mg (67% yield) as a yellow oil. ^{1}H NMR (400 MHz, CDCl$_3$) δ 6.96 (s, 1H), 6.78 (s, 1H), 3.99 (s, 2H), 1.71 (br s, 2H). ^{13}C NMR (126 MHz, CDCl$_3$) δ 148.24, 124.45, 123.90, 118.33, 41.51. ^{13}C NMR (126 MHz, CDCl$_3$) δ 139.2, 127.9, 127.7, 123.0, 39.2. HRMS (ESI) *m/z* [M+H]$^+$ for C$_5$H$_7$ClNS: 147.9988, found: 147.9995.

General procedure for alkylation of 2-hydroxybenzonitrile. Alkyliodides (3.7 mmol, 1.1 equiv.) and K$_2$CO$_3$ (930 mg, 6.7 mmol, 2 equiv.) were added to a stirred solution of 2-hydroxybenzonitrile (400 mg, 3.4 mmol, 1 equiv.) in DMF (20 mL) at rt and stirred for 4 h. The reaction was quenched with the addition of H$_2$O (20 mL) and EtOAc (40 mL). The organic layer was washed with water (5 x 40 mL), dried (Na$_2$SO$_4$), filtered, and concentrated. The residue was purified by column chromatography (SiO$_2$, 4:1 Hex:EtOAc) to afford the desired alkyl ethers as colorless oils:
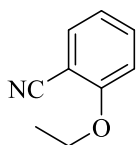
2-Ethoxybenzonitrile **(7a)** 360 mg (71% yield) as a colorless oil. ^{1}H NMR (400 MHz, CDCl$_3$) δ 7.63 − 7.45 (m, 2H), 7.04 − 6.89 (m, 2H), 4.15 (q, *J* = 7.1 Hz, 2H), 1.48 (t, *J* = 7.0 Hz, 3H). ^{13}C NMR (126 MHz, CDCl$_3$) δ 161.0, 134.7, 134.2, 120.9, 117.0, 112.5, 102.4, 65.0, 14.9. MS (EI) *m/z* [M]$^+$ for C$_9$H$_9$NO: 147.1, found: 147.1; [M+H]$^+$ for C$_9$H$_{10}$NO: 148.1, found 148.1.
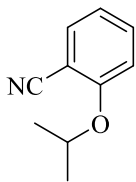
2-Isopropoxybenzonitrile **(7b)** 405 mg (71% yield) as a colorless oil. ^{1}H NMR (400 MHz, CDCl$_3$) δ 7.57 (dt, J = 7.7, 1.5 Hz, 1H), 7.52 (td, J = 7.9, 7.3, 1.5 Hz, 1H), 6.99 (dd, J = 8.2, 5.2 Hz, 2H), 4.68 (hept, J = 6.1 Hz, 1H), 1.43 (d, J = 6.1 Hz, 6H). ^{13}C NMR (126 MHz, CDCl$_3$) δ 159.9, 134.1, 133.9, 120.5, 116.8, 113.6, 103.0, 71.8, 21.9 (2C). MS (EI) m/z [M]$^+$ for C$_{10}$H$_{11}$NO: 161.1, found: 161.1; [M+H]$^+$ for C$_{10}$H$_{12}$NO: 162.1, found: 162.1.
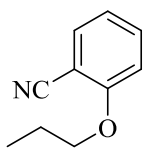
2-Propoxybenzonitrile **(7c)** 385 mg (71% yield) as a colorless oil. ^{1}H NMR (400 MHz, CDCl$_3$) δ 7.55 (d, J = 7.8 Hz, 1H), 7.50 (td, J = 8.1, 7.4, 1.5 Hz, 1H), 7.00 − 6.93 (m, 2H), 4.03 (t, J = 6.5 Hz, 2H), 1.88 (h, J = 7.0 Hz, 2H), 1.08 (t, J = 7.4 Hz, 3H). ^{13}C NMR (126 MHz, CDCl$_3$) δ 160.8, 134.3, 133.8, 120.5, 116.6, 112.2, 102.0, 70.5, 22.3, 10.5. MS (EI) m/z [M]$^+$ for C$_{10}$H$_{11}$NO: 161.1, found: 161.1; [M+H]$^+$ for C$_{10}$H$_{12}$NO: 162.1, found: 162.1.

General procedure for the reduction of carboxylic acids. The aromatic carboxylic acids (e.g., **68**, 0.7 M in THF, 1 equiv.) were added dropwise to a stirred solution of LiAlH$_4$ (0.5M in THF, 5 equiv.) at 0˚C. The reaction warmed to rt and stirred for 12 h. H$_2$O (1 mL/g of LiAlH$_4$) was added, to quench the excess hydride, then 4 M NaOH (1 mL/g of LiAlH$_4$) and EtOAc (3 mL/g of LiAlH$_4$). The resulting suspension was filtered through a pad of celite then the celite was washed with warm EtOAc and the eluent concentrated. The residue was purified via flash chromatography (SiO$_2$, 3:10 EtOAc:Hexanes to 3:5 EtOAc:Hexanes) to provide the desired alcohol as colorless oils:
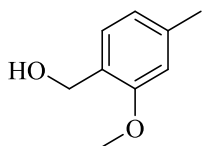
(2-Methoxy-4-methylphenyl)methanol **(8)** 187 mg (50% yield), colorless oil. ^{1}H NMR (400 MHz, CDCl$_3$) δ 7.14 (d, *J* = 7.5 Hz, 1H), 6.78 (dd, *J* = 7.5, 0.8 Hz, 1H), 6.75 (s, 1H), 4.32 (s, 2H), 3.86 (s, 3H), 2.38 (s, 3H). ^{13}C NMR (126 MHz, CDCl$_3$) δ 157.6, 140.1, 130.1, 121.1, 120.8, 111.5, 55.3, 50.0, 21.7. HRSM (ESI) *m/z* [M]$^+$ for C$_9$H$_{12}$O$_2$: 152.0837, found: 152.0846.
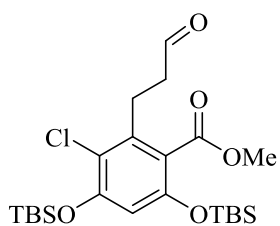
Methyl 4,6-bis((tert-butyldimethylsilyl)oxy)-3-chloro-2-(3-oxopropyl)benzoate **(9)** was synthesized following procedures detailed in references 14 and 17. 1.8 g (68% yield), white amorphous solid. ^{1}H NMR (500 MHz, CDCl$_3$) δ 9.80 (s, 1H), 6.31 (s, 1H), 3.84 (s, 3H), 2.96 – 2.92 (m, 2H), 2.80 – 2.74 (m, 2H), 1.02 (s, 9H), 0.95 (s, 9H), 0.23 (s, 6H), 0.21 (s, 6H). ^{13}C NMR (126 MHz, CDCl$_3$) δ 201.5, 168.4, 153.5, 151.9, 138.1, 121.4, 118.8, 110.2, 110.0, 52.7, 43.8, 26.0 (3C), 25.8 (3C), 18.7, 18.4, -3.9 (2C), -4.00 (2C). HRMS (ESI) *m/z* [M+H]$^+$ for C$_{23}$H$_{40}$ClO$_5$Si$_2$: 487.2103, found 487.2120.
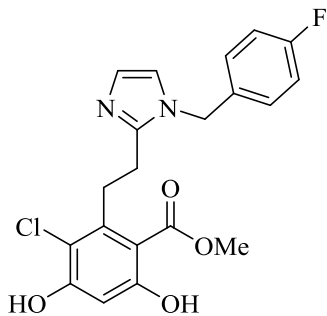
Methyl 3-chloro-2-(2-(1-(4-fluorobenzyl)-1H-imidazol-2-yl)ethyl)-4,6-dihydroxybenzoate **(10)** 22 mg (21% yield), white amorphous solid. ^{1}H NMR (500 MHz, MeOD) δ 7.07–6.94 (m, 5H),

69

6.86 (d, J = 1.4 Hz, 1H), 6.29 (s, 1H), 5.00 (s, 2H), 3.69 (s, 3H), 3.22–3.19 (m, 2H), 2.84 (m, 2H). ^{13}C NMR (126 MHz, MeOD) δ 171.2, 164.8, 162.8, 160.7, 158.8, 148.8, 141.4, 134.2, 130.0, 129.9, 127.3, 121.7, 116.8, 116.6, 112.6 (d, J = 558.4 Hz), 103.3, 52.9, 31.5, 27.3. HRMS (ESI) m/z [M+H] for $C_{20}H_{19}ClFN_2O_4$: 405.1017, found: 405.1009.
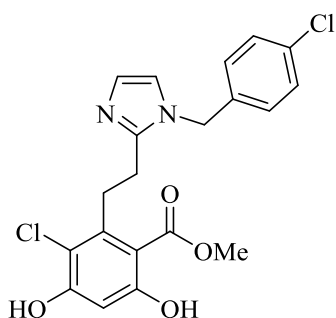
Methyl 3-chloro-2-(2-(1-(4-chlorobenzyl)-1H-imidazol-2-yl)ethyl)-4,6-dihydroxybenzoate **(11)**

28 mg, (25% yield), white amorphous solid. ^{1}H NMR (500 MHz, CDCl[3], MeOD) δ 7.24 (d, J = 8.4 Hz, 2H), 6.98 (d, J = 1.4 Hz, 1H), 6.90 (d, J = 8.4 Hz, 2H), 6.78 (d, J = 1.4 Hz, 1H), 6.40 (s, 1H), 4.97 (s, 2H), 3.81 (s, 3H), 3.46–3.40 (m, 2H), 2.89–2.80 (m, 2H). ^{13}C NMR (126 MHz, CDCl[3], MeOD) δ 170.6, 162.3, 157.7, 147.6, 141.6, 134.6, 134.0, 129.2 (2C), 127.9 (2C), 127.1, 120.0, 114.6, 106.1, 102.7, 52.6, 30.9, 29.7, 26.0 HRMS (ESI) m/z [M+H] for $C_{20}H_{19}Cl_2N_2O_4$: 421.0722, found: 421.0714.
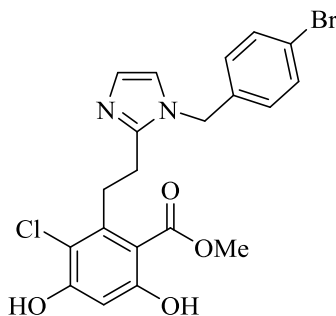
Methyl 2-(2-(1-(4-bromobenzyl)-1H-imidazol-2-yl)ethyl)-3-chloro-4,6-dihydroxybenzoate **(12)**

45 mg (38% yield), off white amorphous solid. ^{1}H NMR (400 MHz, CDCl[3], MeOD) δ 7.36 (d, J = 8.4 Hz, 2H), 6.91 (d, J = 1.4 Hz, 1H), 6.82 (d, J = 8.5 Hz, 2H), 6.77 (d, J = 1.5 Hz, 1H), 6.35 (s,

1H), 4.93 (s, 2H), 3.78 (s, 3H), 3.42 – 3.34 (m, 2H), 2.84 – 2.77 (m, 2H). ^{13}C NMR (101 MHz, CDCl$_3$, MeOD) δ 170.2, 161.4, 157.6, 147.3, 141.1, 134.8, 131.7 (2C), 127.9 (2C), 126.6, 121.6, 119.7, 114.3, 102.1, 100.0, 52.0, 30.4, 25.7. HRMS (ESI) m/z [M + H]$^+$ for C$_{20}$H$_{19}$BrClN$_2$O$_4$: 465.0217, found 465.0237. t_R = 4.17 min, 95.3%.
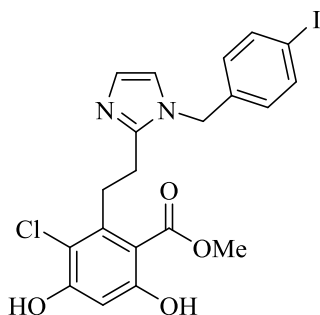
Methyl 3-chloro-4,6-dihydroxy-2-(2-(1-(4-iodobenzyl)-1H-imidazol-2-yl)ethyl)benzoate **(13)**

22 mg (35% yield), white amorphous solid. ^{1}H NMR (400 MHz, CDCl$_3$, MeOD): δ 7.59-7.57 (dd, J=11.6 Hz, 2H), 7.14-7.11 (dd, J=10.0 Hz, 2H), 7.05 (s, 1H), 6.86 (s, 1H), 6.44 (s, 1H), 5.14 (s, 2H), 3.87 (s, 3H), 3.48-3.44 (t, J=16.8, 2H), 2.91-2.87 (t, J=18.4 Hz, 2H.). ^{13}C NMR (125 MHz, CDCl$_3$, MeOD): δ = 170.6, 162.4, 157.6, 147.6, 141.5, 138.1, 128.4, 127.2, 120.0, 114.6, 106.1, 102.7, 93.6, 52.6, 52.2, 49.0, 30.9, 26.1, 25.2, 20.1. HRMS (ESI) m/z [M+H]$^+$ for C$_{20}$H$_{18}$ClIN$_2$O$_4$: 513.0020, found: 513.0070.
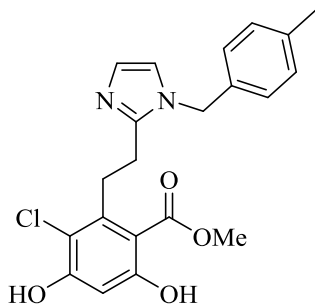
Methyl 3-chloro-4,6-dihydroxy-2-(2-(1-(4-methylbenzyl)-1H-imidazol-2-yl)ethyl)benzoate **(14)**

44 mg (43% yield), off white amorphous solid. ^{1}H NMR (500 MHz, MeOD) δ 7.15 (d, J = 7.9 Hz, 2H), 7.03 (d, J = 1.4 Hz, 1H), 7.00-6.96 (m, 2H), 6.94 (d, J = 1.5 Hz, 1H), 6.39 (s, 1H), 5.05 (s,

2H), 3.77 (s, 3H), 3.37-3.30 (m, 2H), 2.97-2.89 (m, 2H), 2.31 (s, 3H). ^{13}C NMR(125 MHz, MeOD)

δ 171.3, 160.9, 159.0, 148.8, 141.5, 138.9, 135.1, 130.5 (2C), 127.9 (2C), 127.1, 121.8, 115.0,

110.1, 103.3, 52.8, 50.1, 31.5, 27.3, 21.1. HRMS (ESI) *m/z* [M+H]$^+$ for $C_{21}H_{22}ClN_2O_4$: 401.1268,

found: 401.1266.
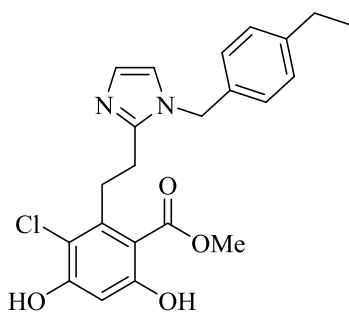
Methyl 3-chloro-2-(2-(1-(4-ethylbenzyl)-1H-imidazol-2-yl)ethyl)-4,6-dihydroxybenzoate (**15**)

37 mg (39% yield), off white amorphous solid. ^{1}H NMR (500 MHz, CDCl$_3$, MeOD) δ 7.14 (d, *J*

= 8.1 Hz, 2H), 7.11-7.08 (m, 1H), 6.98 -6.91 (m, 2H), 6.85 (d, *J* = 1.5 Hz, 1H), 6.44 (s, 1H), 4.96

(s, 3H), 3.54-3.45 (m, 2H), 3.04 (t, *J* = 7.9 Hz, 2H), 2.59 (q, *J* = 7.6 Hz, 2H), 1.17 (td, *J* = 7.6, 1.0

Hz, 3H). ^{13}CNMR (125 MHz, CDCl$_3$,MeOD) δ 170.6, 162.1, 158.2, 147.2, 145.0, 140.9, 132.1,

128.8 (2C), 127.2 (2C), 124.2, 120.6, 114.9, 106.2, 103.0, 50.0, 49.9, 30.7, 28.6, 25.6, 15.6. HRMS

(ESI) *m/z* [M + H]$^+$ for $C_{22}H_{24}ClN_2O_4$: 415.1425, found: 415.1432.

Methyl 3-chloro-4,6-dihydroxy-2-(2-(1-(4-isopropylbenzyl)-1H-imidazol-2-yl)ethyl)benzoate

(**16**) 25 mg (22% yield), white amorphous solid. ^{1}H NMR (500 MHz, CDCl$_3$) δ 7.13 (d, *J* = 8.1

Hz, 2H), 7.03 (s, 1H), 6.90 (d, *J* = 8.2 Hz, 2H), 6.80 (d, *J* = 1.5 Hz, 1H), 6.49 (s, 1H), 4.95 (s, 2H),

3.79 (s, 3H), 3.50 (t, *J* = 7.9 Hz, 2H), 3.00 – 2.92 (m, 2H), 2.82 (hept, *J* = 6.9 Hz, 1H), 1.16 (d, *J* = 7.0 Hz, 6H). ^{13}C NMR (126 MHz, CDCl$_3$) δ 170.6, 162.9, 157.3, 149.3, 147.2, 127.2 (2C), 126.8 (2C), 120.2, 114.5, 106.2, 103.0, 100.0, 52.8, 49.6, 33.8, 30.8, 29.7, 23.9 (2C). HRMS (ESI) *m/z* [M+H]$^+$ for C$_{23}$H$_{26}$ClN$_2$O$_4$: 429.1581, found: 429.1588.

Methyl 3-chloro-2-(2-(1-(4-cyanobenzyl)-1H-imidazol-2-yl)ethyl)-4,6-dihydroxybenzoate (**17**)

37 mg (39% yield), off white amorphous solid. ^{1}H NMR (500 MHz, CDCl$_3$) δ 7.79 (q, *J* = 7.8, 6.0 Hz, 2H), 7.61-7.36 (m, 2H), 7.20-7.12 (m, 1H), 7.05 (s, 1H), 6.57 (s, 1H), 5.44 – 5.25 (m, 2H), 4.00 (s, 3H), 3.57 (q, *J* = 7.7 Hz, 2H), 3.02 (t, *J* = 7.9 Hz, 2H). ^{13}C NMR (125 MHz, CDCl$_3$): 170.4, 161.5, 158.0, 147.8, 142.0, 141.2 132.8, (2C), 127.7, 127.4, 127.0 (2C), 120.2, 118.2, 114.5, 111.6, 102.4, 52.4, 52.3, 30.8, 26.0. HRMS (ESI) *m/z* [M + H]$^+$ for C$_{21}$H$_{19}$ClN$_3$O$_4$: 412.1064, found: 412.1049.
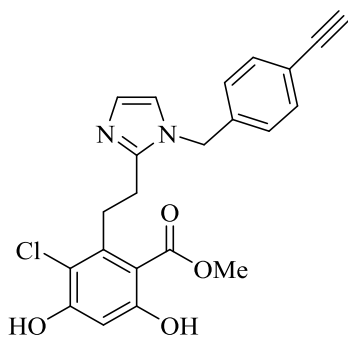
Methyl   3-chloro-2-(2-(1-(4-ethynylbenzyl)-1H-imidazol-2-yl)ethyl)-4,6-dihydroxybenzoate

(**18**). 37 mg (35% yield), tan amorphous solid. ^{1}H NMR (500 MHz, CDCl$_3$) δ 7.46 (d, *J* = 8.3 Hz, 1H), 7.06 (d, *J* = 1.4 Hz, 1H), 7.00 (d, *J* = 8.2 Hz, 1H), 6.86 (d, *J* = 1.4 Hz, 1H), 6.48 (s, 1H), 5.12

(s, 1H), 3.84 (s, 2H), 3.50 (dd, J = 9.3, 6.7 Hz, 1H), 3.09 (s, 1H), 2.94 (dd, J = 9.0, 7.0 Hz, 1H). ^{13}C NMR (126 MHz, CDCl$_3$) δ 170.7, 162.7, 158.4, 147.7, 141.3, 136.7, 132.8, 129.1, 126.8, 126.6, 126.5, 122.1, 120.2, 120.2, 115.0, 105.7, 102.8, 82.9, 52.6, 49.3, 30.9, 26.0. HRMS (ESI) m/z [M+H]$^+$ for C$_{22}$H$_{20}$ClN$_2$O$_4$: 411.1112, found: 411.1121.

Methyl   3-chloro-4,6-dihydroxy-2-(2-(1-(4-(trifluoromethyl)benzyl)-1H-imidazol-2-yl)ethyl)benzoate (**19**). 24 mg (36% yield), white amorphous solid. ^{1}H NMR (400 MHz, CDCl$_3$, MeOD): δ 7.56-.755 (dd, J=9.7 Hz, 2H), 7.15 (s, 1H), 7.10-7.08 (dd, J=11.3 Hz, 2H), 6.86 (s, 1H), 6.44 (s, 1H), 5.06 (s, 2H), 3.86 (s, 3H), 3.47-3.43 (t, J=16.3 Hz, 2H), 3.04-3.00 (t, J=16.3 Hz, 2H). ^{13}C NMR (125 MHz, CDCl$_3$, MeOD): δ 170.2, 162.1, 157.8, 147.3, 140.3, 138.7, 131.1, 130.8, 127.1, 126.3, 126.2, 124.7, 122.6, 120.5, 114.6, 111.4, 106.1, 103.1, 52.9, 30.6, 25.3. HRMS (ESI) m/z [M+H$^+$] for C$_{21}$H$_{18}$ClF$_3$N$_2$O$_4$: 455.0937, found 455.0972.
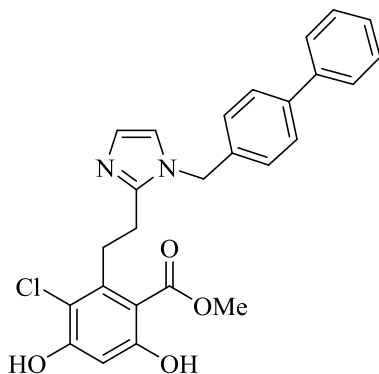
Methyl   2-(2-(1-([1,1'-biphenyl]-4-ylmethyl)-1H-imidazol-2-yl)ethyl)-3-chloro-4,6-dihydroxybenzoate (**20**). 35 mg (29% yield), tan amorphous solid. ^{1}H NMR (500 MHz, CDCl$_3$,

MeOD) δ 7.54 – 7.48 (m, 4H), 7.39 (ddd, *J* = 8.0, 7.0, 1.7 Hz, 2H), 7.31 (td, *J* = 7.2, 1.4 Hz, 1H), 7.07 (dd, *J* = 8.3, 1.6 Hz, 2H), 6.98 (s, 1H), 6.86 (s, 1H), 6.41 (s, 1H), 5.07 (s, 2H), 3.83 (s, 3H), 3.52 – 3.45 (m, 2H), 2.92 – 2.87 (m, 2H). ^{13}C NMR (126 MHz, CDCl$_3$, MeOD) δ 170.8, 162.1, 157.8, 147.7, 141.8, 141.0, 140.2, 135.2, 128.8 (2C), 127.6 (2C), 127.5, 127.2, 127.0 (2C), 127.0 (2C), 120.1, 114.7, 106.1, 102.5, 52.5, 49.6, 30.9, 26.2. HRMS (ESI) *m/z* [M+H]$^+$ for C$_{26}$H$_{23}$ClN$_2$O$_4$: 463.1425, found: 463.1447.
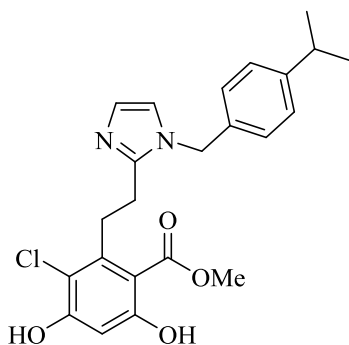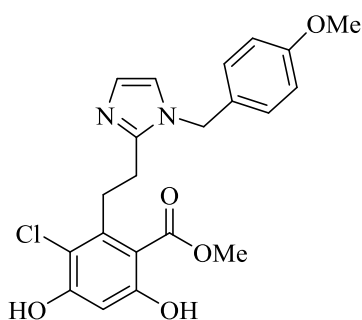

Methyl 3-chloro-4,6-dihydroxy-2-(2-(1-(4-methoxybenzyl)-1H-imidazol-2-yl)ethyl)benzoate **(21)** 25 mg (23% yield), tan amorphous solid. ^{1}H NMR (400 MHz, CDCl$_3$, MeOD) δ 6.86 – 6.84 (m, 1H), 6.82 (d, *J* = 1.4 Hz, 1H), 6.74 – 6.69 (m, 4H), 6.31 (s, 1H), 4.85 (s, 2H), 3.72 (s, 3H), 3.65 (s, 3H), 3.38 – 3.32 (m, 2H), 2.82 – 2.76 (m, 2H). ^{13}C NMR (126 MHz, CDCl$_3$, MeOD) δ 174.6, 165.6, 163.2, 162.1, 151.4, 145.5, 135.4, 132.1 (2C), 132.0, 130.4, 123.9, 118.2 (2C), 110.2, 106.4, 100.0, 59.1, 56.3, 34.6, 30.0. HRMS (ESI) *m/z* [M–H]$^-$ for C$_{21}$H$_{21}$ClN$_2$O$_5$: 415.1061, found: 415.1061.
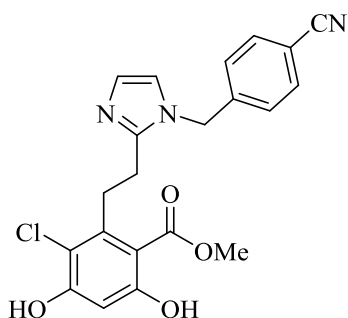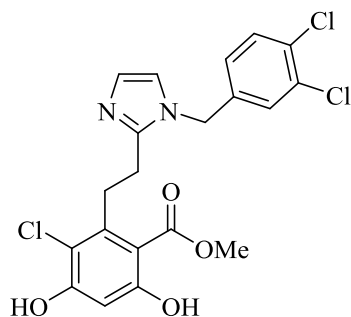
Methyl 3-chloro-2-(2-(1-(3,4-dichlorobenzyl)-1H-imidazol-2-yl)ethyl)-4,6-dihydroxybenzoate

(22) 27 mg (23% yield), tan amorphous solid. ^{1}H NMR (400 MHz, CDCl$_3$, MeOD) δ 7.30 (d, *J* = 8.3 Hz, 1H), 7.05 (d, *J* = 1.9 Hz, 2H), 6.92 (d, *J* = 1.7 Hz, 1H), 6.81 (dd, *J* = 8.3, 2.2 Hz, 1H), 6.32 (s, 1H), 4.94 (s, 2H), 3.76 (s, 3H), 3.36 – 3.29 (m, 2H), 2.95 (t, *J* = 7.8 Hz, 2H). ^{13}C NMR (126 MHz, CDCl$_3$, MeOD) δ 173.6, 164.9, 161.9, 141.3, 137.4, 135.2, 133.1, 130.9, 130.5, 125.3 (2C), 118.4, 116.4, 111.0, 107.0 (2C), 56.5, 53.1, 34.0, 28.9. HRMS (ESI) *m/z* [M+H]$^+$ for C$_{20}$H$_{18}$Cl$_3$N$_2$O$_4$: 455.0332, found: 455.0354.
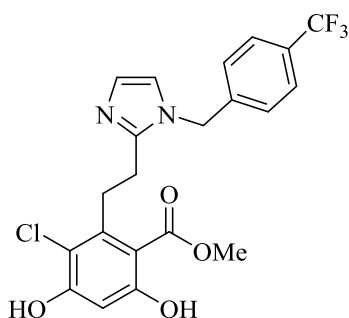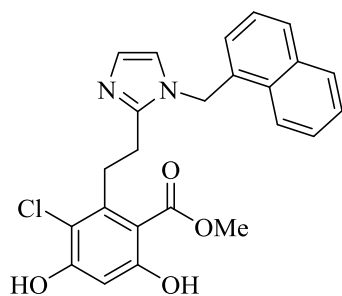

Methyl 3-chloro-4,6-dihydroxy-2-(2-(1-(naphthalen-1-ylmethyl)-1H-imidazol-2-yl)ethyl)benzoate **(23)**. 32 mg (28% yield), tan amorphous solid. ^{1}H NMR (400 MHz, CDCl$_3$, MeOD) δ 7.79 (dd, *J* = 6.8, 2.5 Hz, 1H), 7.71 (dd, *J* = 8.0, 3.9 Hz, 2H), 7.48 – 7.40 (m, 2H), 7.28 (d, *J* = 1.2 Hz, 1H), 6.93 (d, *J* = 1.4 Hz, 1H), 6.72 (d, *J* = 1.5 Hz, 1H), 6.71 – 6.67 (m, 1H), 6.32 (s, 1H), 5.43 (s, 2H), 3.73 (s, 3H), 3.45 – 3.35 (m, 2H), 2.94 – 2.84 (m, 2H). ^{13}C NMR (126 MHz, CDCl$_3$, MeOD) δ 170.6, 161.6, 158.0, 147.9, 141.5, 133.6, 131.6, 130.3, 128.9, 128.7, 126.8 (2C),

126.2, 125.4, 123.9, 122.0, 120.4, 114.6, 106.3, 102.4, 52.3, 47.3, 30.7, 26.2. HRMS (ESI) *m/z* [M+H]$^+$ for C$_{24}$H$_{21}$ClN$_2$O$_4$: 437.1268, found: 437.1250.
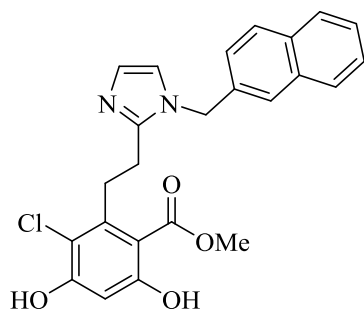
Methyl 3-chloro-4,6-dihydroxy-2-(2-(1-(naphthalen-2-ylmethyl)-1H-imidazol-2-yl)ethyl)benzoate **(24)** 28 mg (25% yield), tan amorphous solid. ^{1}H NMR (400 MHz, DMSO-*d$_6$*) δ 7.88 (dd, *J* = 9.1, 4.0 Hz, 2H), 7.83 − 7.78 (m, 1H), 7.51 − 7.46 (m, 1H), 7.25 (dd, *J* = 8.4, 1.9 Hz, 1H), 7.18 (d, *J* = 1.3 Hz, 1H), 6.85 (d, *J* = 1.3 Hz, 1H), 6.42 (s, 1H), 5.29 (s, 2H), 3.57 (s, 3H), 2.92 − 2.86 (m, 2H), 2.77 − 2.71 (m, 2H). ^{13}C NMR (126 MHz, DMSO-*d$_6$*) δ 167.9, 155.0, 154.5, 146.4, 137.7, 135.2, 132.8, 132.2, 128.4, 127.6 (2C), 127.5, 126.8, 126.4 (2C), 126.0, 124.9, 124.8, 120.6, 113.7, 110.8, 101.7, 51.8, 48.4, 29.9, 26.2. HRMS (ESI) *m/z* [M+H]$^+$ for C$_{24}$H$_{21}$ClN$_2$O$_4$: 437.1268, found: 437.1280.

Methyl 3-chloro-4,6-dihydroxy-2-(2-(1-(quinolin-5-ylmethyl)-1H-imidazol-2-yl)ethyl)benzoate **(25)** 29 mg (25% yield), white amorphous solid. ^{1}H NMR (500 MHz, CDCl$_3$, MeOD) δ 8.87 (dd, *J* = 4.3, 1.6 Hz, 1H), 8.20 − 8.16 (m, 1H), 8.00 (d, *J* = 8.5 Hz, 1H), 7.60 (dd, *J* = 8.5, 7.2 Hz, 1H), 7.49 − 7.44 (m, 1H), 6.99 (s, 1H), 6.86 − 6.83 (m, 1H), 6.76 (s, 1H), 6.36 (s, 1H), 5.48 (s, 2H),

3.83 (s, 3H), 3.48 – 3.44 (m, 2H), 2.95 – 2.89 (m, 2H). ^{13}C NMR (126 MHz, CDCl$_3$, MeOD) δ 170.6, 161.9, 157.9, 150.2, 147.9, 141.6, 132.3, 131.1, 129.5, 129.4, 127.4, 125.6, 124.8, 121.6, 120.1, 114.6, 106.1, 102.5, 100.0, 52.5, 46.6, 30.9, 26.2. HRMS (ESI) *m/z* [M+H]$^+$ for C$_{23}$H$_{21}$ClN$_3$O$_4$: 438.1221, found: 438.1207.

Methyl 3-chloro-2-(2-(1-(3-fluorobenzyl)-1H-imidazol-2-yl)ethyl)-4,6-dihydroxybenzoate (**26**)

26 mg, (25% yield), pale yellow amorphous solid. ^{1}H NMR (500 MHz, CDCl$_3$) δ 7.29 – 7.20 (m, 1H), 7.01 (d, *J* = 1.4 Hz, 1H), 6.92 (m, 1H), 6.82 (d, *J* = 1.4 Hz, 1H), 6.75 (m, 1H), 6.70 – 6.58 (m, 1H), 6.46 (s, 1H), 5.01 (s, 2H), 3.80 (s, 3H), 3.52 – 3.40 (m, 2H), 2.88 – 2.74 (m, 2H). ^{13}C NMR (126 MHz, CDCl$_3$) δ 157.1, 147.6, 141.8, 130.9, 127.8, 122.1, 120.2 (2C), 115.3, 115.1, 113.7, 113.5, 106.7, 103.0 (2C), 100.1, 53.6, 49.0, 31.0, 26.3. HRMS (ESI) *m/z* [M+H] for C$_{20}$H$_{19}$ClFN$_2$O$_4$: 405.1017, found: 405.1009.
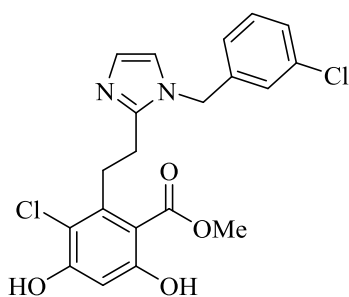
Methyl 3-chloro-2-(2-(1-(3-chlorobenzyl)-1H-imidazol-2-yl)ethyl)-4,6-dihydroxybenzoate (**27**)

47 mg (44 % yield), pale yellow amorphous solid. ^{1}H NMR (500 MHz, CDCl$_3$, MeOD) δ 7.25-7.20 (m, 2H), 7.03 (d, *J* = 1.6 Hz, 1H), 6.99- 6.96 (m, 1H), 6.91-6.84 (m, 2H), 6.40 (s, 1H), 5.00

(s, 2H), 3.82 (s, 3H), 3.49-3.33 (m, 2H), 3.01-2.83 (m, 2H). ^{13}CNMR (125 MHz, CDCl$_3$, MeOD): 170.6, 161.9, 158.2, 147.5, 141.1, 137.7, 135.1, 130.5, 128.5, 126.8, 125.9, 124.9, 120.5, 114.8, 106.2, 102.7, 52.6 (2C), 30.6, 25.8. HRMS (ESI) *m/z* [M+H]$^+$ for C$_{20}$H$_{19}$Cl$_2$N$_2$O$_4$: 421.0722, found: 421.0728.
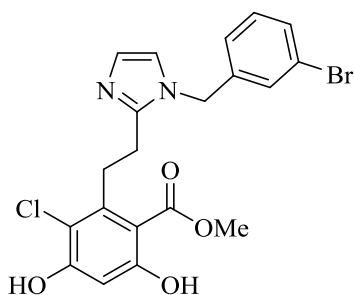
Methyl 2-(2-(1-(3-bromobenzyl)-1H-imidazol-2-yl)ethyl)-3-chloro-4,6-dihydroxybenzoate **(28)**

23 mg, (19% yield), white amorphous solid. ^{1}H NMR (500 MHz, CDCl$_3$, MeOD) δ 7.38 (m, 1H), 7.19 – 7.09 (m, 2H), 6.99 (d, *J* = 1.5 Hz, 1H), 6.91 (m, 1H), 6.84 (d, *J* = 1.5 Hz, 1H), 6.40 (s, 1H), 5.00 (s, 2H), 3.83 (s, 3H), 3.46–3.38 (m, 2H), 2.92 –2.79 (m, 2H). ^{13}C NMR (126 MHz, CDCl$_3$, MeOD) δ 168.0, 159.3, 155.5, 145.0, 138.8, 135.7, 128.7, 128.0, 127.0, 124.1, 122.6, 120.5, 117.6, 112.2, 103.6, 100.0, 50.0, 46.2, 28.1, 23.4. HRMS (ESI) *m/z* [M+H] for C$_{20}$H$_{19}$BrClN$_2$O$_4$: 465.0217, found: 465.0225.
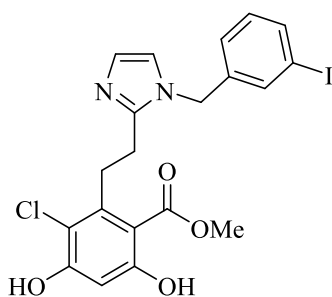
Methyl 3-chloro-4,6-dihydroxy-2-(2-(1-(3-iodobenzyl)-1H-imidazol-2-yl)ethyl)benzoate **(29)**.

4 mg (11% yield), white amorphous solid. ^{1}H NMR (400 MHz, DMSO-*d$_6$*): δ 7.67-7.64 (dd, *J*=7.05 Hz, 1H), 7.43 (s, 1H), 7.18-7.14 (m, 2H), 7.08-7.06 (dd, *J*=9.24 Hz, 1H), 6.86 (s, 1H), 6.47 (s, 1H),

5.14 (s, 2H), 3.68 (s, 3H), 2.92-2.88 (t, *J*=16.3 Hz, 2H), 2.73-2.67 (t, *J*=18.2 Hz, 2H). ^{13}C NMR (125 MHz, DMSO-d_6): δ 167.9, 155.0, 154.5, 146.4, 140.2, 137.7, 136.2, 135.1, 130.9, 126.0, 120.6, 113.8, 110.8, 101.8, 99.5, 95.2, 52.0, 47.4, 29.8, 26.1. HRMS (FAB) m/z [M+H$^+$] for C$_{20}$H$_{18}$ClIN$_2$O$_4$: 513.0023, found 513.0065.

Methyl   2-(2-(1-(3-methoxybenzyl)-1H-imidazol-2-yl)ethyl)-3-chloro-4,6-dihydroxybenzoate

(30). 32 mg (31% yield), white amorphous solid. ^{1}H NMR (400 MHz, CDCl$_3$) δ 7.06 (s, 1H), 6.88 (s, 1H), 6.82 (d, *J* = 9.0 Hz, 1H), 6.62 (d, *J* = 7.7 Hz, 1H), 6.55 (s, 1H), 6.53 (s, 1H), 5.04 (s, 2H), 3.85 (s, 3H), 3.76 (s, 3H), 3.59 – 3.51 (m, 2H), 2.95 – 2.89 (m, 2H). ^{13}C NMR (126 MHz, CDCl$_3$) δ 170.7, 162.9, 160.1, 157.0, 147.5, 141.6, 137.8, 130.1, 127.1, 120.2, 118.7, 114.3, 113.0, 112.5, 106.4, 102.8, 55.3, 52.6, 49.3, 30.9, 26.1. HRMS (ESI) *m/z* [M+H]$^+$ for C$_{21}$H$_{22}$ClN$_2$O$_5$: 417.1217, found: 417.1221.
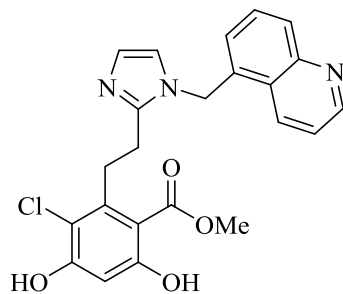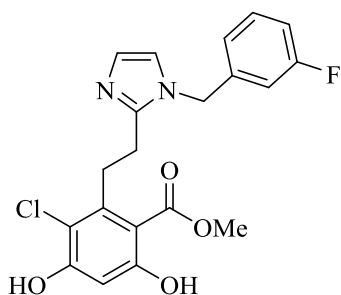

Methyl   3-chloro-4,6-dihydroxy-2-(2-(1-(3-methylbenzyl)-1H-imidazol-2-yl)ethyl)benzoate

(31). 18 mg (17% yield), tan amorphous solid. ^{1}H NMR (500 MHz, CDCl$_3$, MeOD) δ 7.06 (t, *J* = 7.6 Hz, 1H), 6.95 (d, *J* = 7.7 Hz, 1H), 6.85 (d, *J* = 1.5 Hz, 1H), 6.75 (d, *J* = 1.5 Hz, 1H), 6.72 –

6.66 (m, 2H), 6.30 (s, 1H), 4.87 (s, 2H), 3.69 (s, 3H), 3.36 – 3.30 (m, 2H), 2.81 (dd, J = 9.2, 6.9 Hz, 2H), 2.16 (s, 3H). ^{13}C NMR (126 MHz, CDCl$_3$, MeOD) δ 174.5, 165.5, 162.0, 151.4, 145.2, 142.7, 139.6, 132.8 (2C), 131.3, 129.8, 127.7, 124.3, 118.6, 110.3, 106.4, 56.3, 53.5, 34.5, 29.9, 25.1. HRMS (ESI) m/z [M+H]$^+$ for C$_{21}$H$_{22}$ClN$_2$O$_4$: 401.1268, found 401.1255.

Methyl 2-(2-(1-([1,1'-biphenyl]-3-ylmethyl)-1H-imidazol-2-yl)ethyl)-3-chloro-4,6-dihydroxybenzoate (**32**) 46 mg (39% yield), pale yellow amorphous solid. ^{1}H NMR (400 MHz, CDCl$_3$, MeOD) δ 7.53-7.47 (m, 3H), 7.41 (dd, J = 9.1, 7.3 Hz, 3H), 7.38 -7.33 (m, 1H), 7.23 (s, 1H), 7.03 (d, J = 1.3 Hz, 1H), 6.99 (d, J = 7.8 Hz, 1H), 6.89 (d, J = 1.4 Hz, 1H), 6.46 (s, 1H), 5.12 (s, 2H), 3.82 (s, 3H), 3.56-3.46 (m, 2H), 2.97 -2.89 (m, 2H). ^{13}CNMR δ (100 MHz, CDCl$_3$, MeOD): 170.8, 163.0, 157.9, 147.7, 142.4, 141.5, 140.5, 136.6, 129.8 (3C), 129.1(2C), 128.0, 127.3, 127.3, 125.7, 125.6, 120.5, 114.9, 106.3, 103.2, 52.8, 49.9, 31.1, 26.2. HRMS (ESI) m/z [M-H]$^-$ for C$_{26}$H$_{22}$ClN$_2$O$_4$: 461.1268, found: 461.1259.
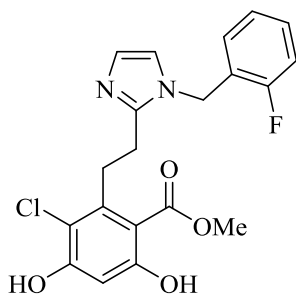
Methyl 3-chloro-2-(2-(1-(2-fluorobenzyl)-1H-imidazol-2-yl)ethyl)-4,6-dihydroxybenzoate (**33**) 23 mg (22% yield), white amorphous solid. ^{1}H NMR (500 MHz, CDCl$_3$, MeOD) δ 7.27 – 7.23 (m,

1H), 7.06 – 6.98 (m, 2H), 6.94 (d, J = 1.4 Hz, 1H), 6.81 (d, J = 1.4 Hz, 1H), 6.78 (dd, J = 7.5, 1.7

Hz, 1H), 6.40 (s, 1H), 5.05 (s, 2H), 3.82 (s, 3H), 3.64 – 3.38 (m, 2H), 3.05 – 2.68 (m, 2H). ^{13}C

NMR (126 MHz, CDCl$_3$, MeOD) δ 170.8, 162.2, 157.8, 147.7, 141.8, 130.0, 128.4, 127.3, 124.6,

123.6, 123.5, 119.9, 115.6 (d, J =21.0 Hz), 114.7, 106.0, 102.6, 52.5, 43.5, 30.8, 26.0. HRMS (ESI)

m/z [M+H] for C$_{20}$H$_{18}$ClFN$_2$O$_4$: 405.1029, found 405.1017.
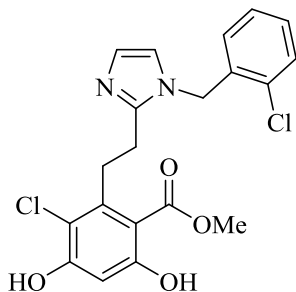
Methyl 2-(2-(1-(2-chlorobenzyl)-1H-imidazol-2-yl)ethyl)-3-chloro-4,6-dihydroxybenzoate **(34)**

23 mg (21% yield), white amorphous solid. ^{1}H NMR (500 MHz, CDCl$_3$, MeOD) δ7.27 (s, 1H),

7.24 – 7.16 (m, 2H), 7.01 (d, J = 1.6 Hz, 1H), 6.94 (dd, J = 1.9, 1.0 Hz, 1H), 6.84 (m, 2H), 6.38

(s, 1H), 4.98 (s, 2H), 3.80 (s, 3H), 3.45 – 3.35 (m, 2H), 2.94 – 2.85 (m, 2H). 13C NMR (126 MHz,

CDCl$_3$, MeOD) δ 170.6, 162.4, 157.4, 147.6, 141.2, 133.5, 132.6, 129.8, 129.6, 127.7, 127.5,

126.2, 120.2, 114.5, 106.2, 102.9, 52.7, 47.5, 30.9, 25.8. HRMS (ESI) m/z [M+H] for

C$_{20}$H$_{19}$Cl$_2$N$_2$O$_4$: 421.0722, found: 421.0714. HRMS (ESI) m/z [M+H] for C$_{20}$H$_{19}$Cl$_2$N$_2$O$_4$:

421.0722, found: 421.0714.
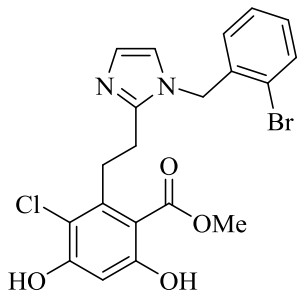
Methyl 2-(2-(1-(2-bromobenzyl)-1H-imidazol-2-yl)ethyl)-3-chloro-4,6-dihydroxybenzoate **(35)**

26 mg (22% yield), white amorphous solid. ^{1}H NMR (500 MHz, CDCl$_3$) δ 7.54 (dd, J = 8.0, 1.3 Hz, 1H), 7.24 – 7.20 (m, 1H), 7.15 (td, *J* = 7.7, 1.7 Hz, 1H), 7.10 (d, *J* = 1.6 Hz, 1H), 6.78 (d, *J* = 1.6 Hz, 1H), 6.67 – 6.57 (m, 1H), 6.48 (s, 1H), 5.06 (s, 2H), 3.85 (s, 3H), 3.48–3.33 (m, 2H), 3.06–2.89 (m, 2H). ^{13}C NMR (126 MHz, CDCl$_3$) δ 170.5, 162.6, 157.8, 147.6, 140.6, 133.2 (2C), 130.1, 128.2 (2C), 122.6, 120.3 (2C), 114.7, 105.9, 103.1, 52.9, 50.2, 30.8, 25.6. HRMS (ESI) *m/z* [M+H] for C$_{20}$H$_{19}$BrClN$_2$O$_4$: 465.0217, found : 465.0231.
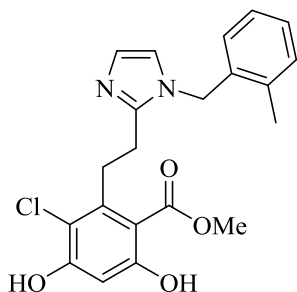
Methyl   3-chloro-4,6-dihydroxy-2-(2-(1-(2-methylbenzyl)-1H-imidazol-2-yl)ethyl)benzoate **(36)**. 32 mg (31% yield), tan amorphous solid. ^{1}H NMR (500 MHz, CDCl$_3$, MeOD) δ 7.25 (s, 1H), 7.08 – 7.02 (m, 2H), 6.88 – 6.83 (m, 1H), 6.66 – 6.58 (m, 1H), 6.47 (t, *J* = 6.7 Hz, 1H), 6.29 (s, 1H), 4.87 (s, 2H), 3.72 (s, 3H), 3.35 – 3.25 (m, 2H), 2.81 (dd, *J* = 10.9, 5.1 Hz, 2H), 2.10 (s, 3H). ^{13}C NMR (126 MHz, CDCl$_3$, MeOD) δ 174.4, 165.5, 162.0, 151.5, 145.1, 139.3, 137.7, 134.5, 132.1, 130.5, 130.1, 129.9, 124.1, 118.5, 110.4, 106.4, 56.3, 51.7, 34.5, 29.9, 22.6. HRMS (ESI) *m/z* [M+H]$^+$ for C$_{21}$H$_{22}$ClN$_2$O$_4$: 401.1268, found: 401.1261.
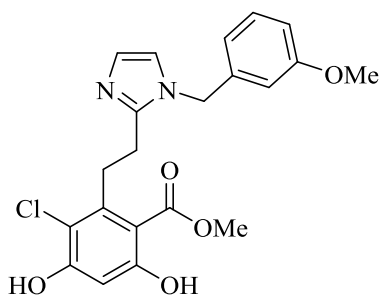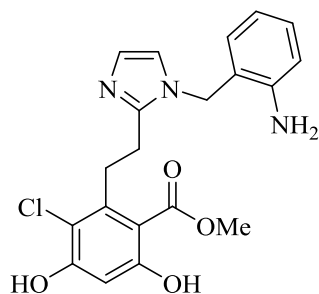
Methyl 2-(2-(1-(2-aminobenzyl)-1H-imidazol-2-yl)ethyl)-3-chloro-4,6-dihydroxybenzoate **(37)**

20 mg (19% yield), white amorphous solid. ^{1}H NMR (500 MHz, MeOD) δ 7.07 (td, *J* = 7.8, 1.6 Hz, 1H), 6.98 (dd, *J* = 7.8, 1.4 Hz, 2H), 6.78 (dd, *J* = 8.0, 1.2 Hz, 1H), 6.65 (td, *J* = 7.5, 1.2 Hz, 1H), 6.52 (dd, *J* = 7.6, 1.5 Hz, 1H), 6.39 (s, 1H), 5.03 (s, 2H), 3.79 (s, 3H), 3.37 − 3.33 (m, 1H), 3.01 − 2.96 (m, 2H). ^{13}C NMR (126 MHz, MeOD) δ 169.9, 159.4, 157.5, 147.6, 145.0, 140.0, 128.6, 127.0, 125.1, 120.4, 120.3, 117.9, 116.0, 113.5, 108.8, 101.9, 51.5, 45.8, 29.9, 25.7. HRMS (ESI) *m/z* [M+H] for $C_{20}H_{20}ClN_3O_4$: 402.1221, found: 402.1230.
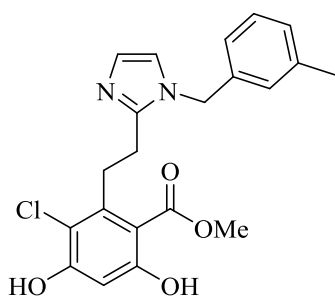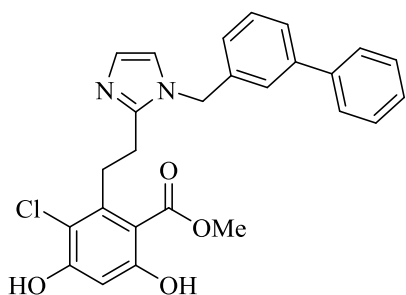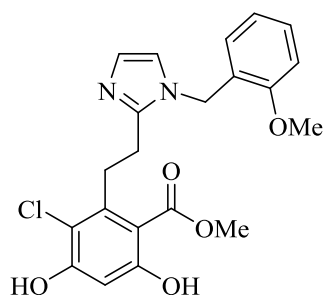

Methyl 3-chloro-4,6-dihydroxy-2-(2-(1-(2-methoxybenzyl)-1H-imidazol-2-yl)ethyl)benzoate **(38)** 46 mg (42% yield), tan amorphous solid. ^{1}H NMR (500 MHz, CDCl$_3$) δ 7.26 − 7.23 (m, 1H), 6.97 (d, *J* = 1.4 Hz, 1H), 6.89 − 6.84 (m, 2H), 6.83 (d, *J* = 1.4 Hz, 1H), 6.70 (dd, *J* = 7.8, 1.7 Hz, 1H), 6.44 (s, 1H), 5.03 (s, 2H), 3.84 (s, 3H), 3.81 (s, 3H), 3.49 − 3.44 (m, 2H), 2.94 − 2.90 (m, 2H). ^{13}C NMR (126 MHz, CDCl$_3$) δ 171.0, 162.4, 157.8, 156.6, 147.7, 141.9, 129.3, 127.6, 126.7, 124.7, 120.7, 120.1, 114.7, 110.3, 105.9, 102.5, 55.3, 52.5, 44.9, 30.9, 26.0. HRMS (ESI) *m/z* [M+H]$^+$ for $C_{21}H_{22}ClN_2O_5$: 417.1217, found: 417.1211.
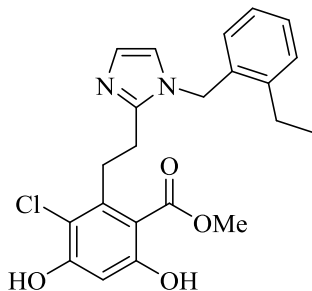
Methyl 3-chloro-2-(2-(1-(2-ethylbenzyl)-1H-imidazol-2-yl)ethyl)-4,6-dihydroxybenzoate **(39)**

33 mg (31% yield), tan amorphous solid. ^{1}H NMR (400 MHz, CDCl$_3$, MeOD) δ 7.43 (d, J = 2.1 Hz, 1H), 7.40 (d, J = 3.0 Hz, 1H), 7.32 − 7.28 (m, 1H), 7.26 (d, J = 7.7 Hz, 1H), 6.83 (d, J = 7.7 Hz, 1H), 6.79 (s, 1H), 6.55 (s, 1H), 4.98 (s, 2H), 4.02 (s, 3H), 3.68 (t, J = 7.3 Hz, 2H), 3.45 (t, J = 7.1 Hz, 3H), 2.52 (q, J = 7.5 Hz, 3H), 1.19 (t, J = 7.6 Hz, 3H). ^{13}C NMR (126 MHz, CDCl$_3$, MeOD) δ 169.9, 162.0, 158.2, 146.2, 145.3, 142.1, 138.9, 129.9, 129.3, 128.2, 127.0, 120.8, 119.1, 114.8, 106.3, 103.5, 53.2, 30.9, 30.0, 25.2, 24.3, 14.5. HRMS (ESI) m/z [M+H]$^+$ for C$_{22}$H$_{24}$ClN$_2$O$_4$: 415.1425, found: 415.1419. t$_R$ = 4.27 min, 95.3%.
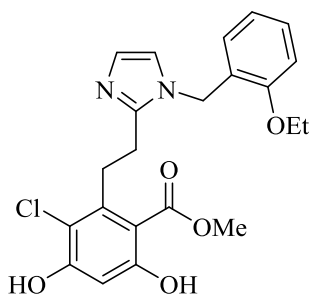
Methyl 3-chloro-2-(2-(1-(2-ethoxybenzyl)-1H-imidazol-2-yl)ethyl)-4,6-dihydroxybenzoate **(40)**. 44 mg (39% yield), tan amorphous solid. ^{1}H NMR (400 MHz, CDCl$_3$, MeOD) δ 7.18 (t, J = 8.0 Hz, 1H), 6.88 (d, J = 1.9 Hz, 1H), 6.83 − 6.76 (m, 3H), 6.67 (d, J = 7.6 Hz, 1H), 6.38 (s, 1H), 4.99 (s, 2H), 3.97 (q, J = 7.7, 6.8 Hz, 2H), 3.80 (s, 3H), 3.45 − 3.39 (m, 2H), 2.88 (t, J = 8.1 Hz, 2H), 1.32 (t, J = 6.8 Hz, 3H). ^{13}C NMR (126 MHz, CDCl$_3$, MeOD) δ 171.0, 162.2, 158.0, 156.0, 147.7, 142.0, 129.3, 127.7, 126.7, 124.6, 120.5, 120.1, 114.7, 111.0, 105.9, 102.4, 63.5, 52.5, 45.0,

30.9, 26.1, 14.7. HRMS (ESI) *m/z* [M+H]$^+$ for C$_{22}$H$_{24}$ClN$_2$O$_5$: 431.1374, found: 431.1378. t$_R$ = 2.71 min, 98.3%.
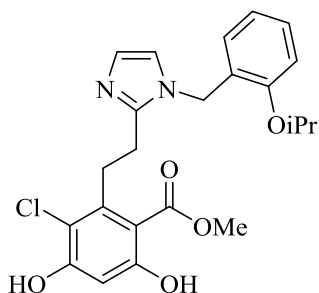

Methyl 3-chloro-4,6-dihydroxy-2-(2-(1-(2-isopropoxybenzyl)-1H-imidazol-2-yl)ethyl)benzoate

(41). 18 mg (16% yield), tan amorphous solid. ^{1}H NMR (400 MHz, CDCl$_3$, MeOD) δ 7.21 (t, *J* = 8.0 Hz, 1H), 6.95 (s, 1H), 6.86 − 6.78 (m, 3H), 6.72 (d, *J* = 7.5 Hz, 1H), 6.44 (s, 1H), 5.00 (s, 2H), 4.56 (hept, *J* = 10.8, 5.3 Hz, 1H), 3.85 (s, 3H), 3.52 − 3.45 (m, 2H), 2.97 − 2.87 (m, 2H), 1.27 (d, *J* = 6.0 Hz, 6H). ^{13}C NMR (126 MHz, CDCl$_3$, MeOD) δ 171.0, 162.2, 158.0, 156.0, 147.7, 142.0, 129.3, 127.7, 126.7, 124.6, 120.5, 120.1, 114.7, 111.0, 105.9, 102.4, 100.0, 63.5, 52.5, 45.0, 30.9, 26.1, 14.7. HRMS (ESI) *m/z* [M+H]$^+$ for C$_{23}$H$_{26}$ClN$_2$O$_5$: 445.1530, found 445.1521. t$_R$ = 2.70 min, 97.7%.
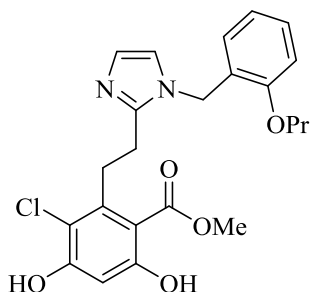
Methyl 3-chloro-4,6-dihydroxy-2-(2-(1-(2-propoxybenzyl)-1H-imidazol-2-yl)ethyl)benzoate

(42). 34 mg (29% yield), tan amorphous solid. ^{1}H NMR (500 MHz, CDCl$_3$) δ 7.29 − 7.26 (m, 1H), 7.02 (d, *J* = 1.4 Hz, 1H), 6.90 − 6.85 (m, 3H), 6.76 − 6.73 (m, 1H), 6.49 (s, 1H), 5.10 (s, 2H), 3.95 (t, *J* = 6.5 Hz, 2H), 3.84 (s, 3H), 3.56 − 3.50 (m, 2H), 3.03 − 2.96 (m, 2H), 1.80 (qt, *J* = 7.4, 6.5

Hz, 2H), 1.01 (t, $J = 7.4$ Hz, 3H). ^{13}C NMR (126 MHz, CDCl$_3$) δ 170.9, 162.9, 157.8, 156.1, 147.6, 141.6, 129.4, 127.8, 126.5, 124.6, 120.6, 120.2, 114.7, 111.0, 105.9, 102.7, 69.5, 52.6, 45.0, 30.9, 26.0, 22.6, 10.6. HRMS (ESI) *m/z* [M+H]$^+$ for C$_{23}$H$_{26}$ClN$_2$O$_5$: 445.1530, found: 445.1539. t$_R$ = 2.73 min, 98.0%.
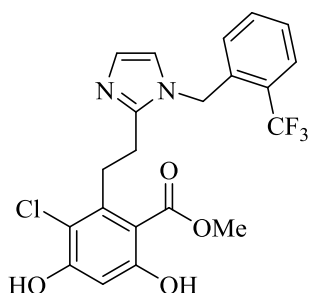
Methyl 3-chloro-4,6-dihydroxy-2-(2-(1-(2-(trifluoromethyl)benzyl)-1H-imidazol-2-yl)ethyl)benzoate **(43)**. 25 mg (21% yield), white amorphous solid. ^{1}H NMR (400 MHz, CDCl$_3$, MeOD) δ 7.65 (d, $J = 7.7$ Hz, 1H), 7.43 (t, $J = 7.6$ Hz, 1H), 7.36 (t, $J = 7.7$ Hz, 1H), 7.02 (s, 1H), 6.79 (s, 1H), 6.57 (d, $J = 7.8$ Hz, 1H), 6.39 (s, 1H), 5.25 (s, 2H), 3.85 (s, 3H), 3.50 – 3.41 (m, 2H), 2.93 – 2.79 (m, 2H). ^{13}C NMR (126 MHz, CDCl$_3$, MeOD) δ 170.7, 162.1, 158.0, 148.1, 141.5, 135.0, 132.6, 128.0, 127.6, 126.9, 126.3 (q, $J = 5.6$ Hz), 125.2, 123.0, 120.2, 114.7, 105.9, 102.5, 52.5, 45.9, 30.9, 25.8. HRMS (ESI) *m/z* [M+H]$^+$ for C$_{21}$H$_{19}$ClF$_3$N$_2$O$_4$: 455.0985, found: 455.0979.
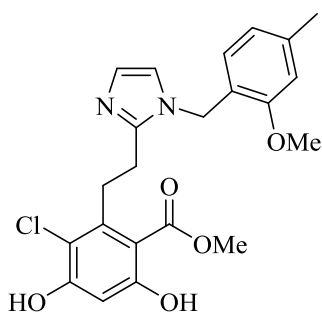
Methyl 3-chloro-4,6-dihydroxy-2-(2-(1-(2-methoxy-4-methylbenzyl)-1H-imidazol-2-yl)ethyl)benzoate **(44)**. 45 mg (40% yield), tan amorphous solid. ^{1}H NMR (400 MHz, CDCl$_3$, MeOD) δ 7.28 (d, $J = 2.1$ Hz, 1H), 6.94 (d, $J = 7.6$ Hz, 1H), 6.85 (d, $J = 2.1$ Hz, 1H), 6.76 (d, $J =$

7.3 Hz, 1H), 6.69 (s, 1H), 6.56 (s, 1H), 4.81 (s, 2H), 3.99 (s, 3H), 3.74 (s, 3H), 3.63 (t, J = 7.4 Hz, 2H), 3.44 (t, J = 7.4 Hz, 2H), 2.34 (s, 3H). ^{13}C NMR (126 MHz, CDCl$_3$, MeOD) δ 169.9, 162.0, 157.1, 151.4, 145.7, 142.0, 140.1, 130.0, 129.5, 121.7, 121.6, 120.5, 118.6, 112.1, 111.9, 55.4, 54.2, 46.6, 30.5, 29.7, 24.0, 21.8. HRMS (ESI) m/z [M+H]$^+$ for C$_{22}$H$_{24}$ClN$_2$O$_5$: 431.1374, found: 431.1370.
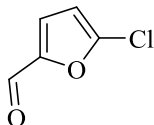
5-Chlorofuran-2-carbaldehyde **(45)** 5-nitrofuran-2-carbaldehyde (730 mg, 5.1 mmol) was stirred in conc. HCl (40 mL) at 40°C for 15 h. The reaction was poured into H$_2$O (80 mL) and extracted with EtOAc (3 x 50 mL). The organic layers were combined, dried (Na$_2$SO$_4$), and concentrated. The residue was purified via flash chromatography (SiO$_2$, 1:4 EtOAc:Hexanes) to provide the title compound. 266 mg (40% yield), yellow oil. ^{1}H NMR (400 MHz, CDCl$_3$) δ 9.53 (s, 1H), 7.23 (d, J = 3.6 Hz, 1H), 6.42 (d, J = 3.6 Hz, 1H). ^{13}C NMR (126 MHz, CDCl$_3$) δ 176.4, 152.0, 144.2, 122.7, 109.8. HRMS (ESI) m/z [M+H]$^+$ for C$_5$H$_4$ClO$_2$: 130.9900, found: 130.9900.

General procedure for oxime formation. NH$_2$OH•HCl (3 equiv.) and NaOAc (3 equiv.) were added to a stirred solution of aromatic aldehydes (1 equiv.) in MeOH (0.2 M) and stirred for 8 h at rt. The reaction was quenched with the addition of H$_2$O (20 mL) and EtOAc (20 mL). The organic layer was washed with H$_2$O (2 x 20 mL), separated, dried (Na$_2$SO$_4$), and concentrated. The residue was purified via flash chromatography (1:10 EtOAc:Hexanes to 1:3 EtOAc:Hexanes) to provide the desired products as amorphous solids:
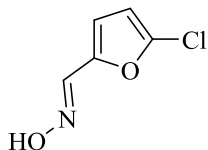
5-Chlorofuran-2-carbaldehyde oxime (**46a**) 225 mg (75% yield) as a white amorphous solid, 1:1 mixture of isomers. ^{1}H NMR (400 MHz, CDCl$_3$) δ 7.91 (s, 1H), 7.46 (s, 1H), 7.35 (d, *J* = 3.5 Hz, 1H), 6.61 (d, *J* = 3.4 Hz, 1H), 6.36 (d, *J* = 3.5 Hz, 1H), 6.26 (d, *J* = 3.4 Hz, 1H). ^{13}C NMR (126 MHz, CDCl$_3$) δ 146.4, 144.4, 139.5, 139.1, 135.9, 121.2, 114.7, 109.8, 109.4, 108.5. HRMS (ESI) *m/z* [M+H]$^+$ for C$_5$H$_5$ClNO$_2$: 146.0009, found: 146.0003.
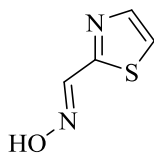
Thiazole-2-carbaldehyde oxime (**46b**) 510 mg (91% yield), white amorphous solid. ^{1}H NMR (400 MHz, CDCl$_3$) δ 8.37 (s, 1H), 7.86 (d, *J* = 3.2 Hz, 1H), 7.33 (dd, *J* = 3.3, 0.9 Hz, 1H). ^{13}C NMR (126 MHz, CDCl$_3$) δ 144.7, 143.2, 142.3, 140.7, 123.5, 120.0. HRMS (ESI) *m/z* [M+H]$^+$ for C$_4$H$_5$N$_2$OS: 129.0123, found: 129.0124.
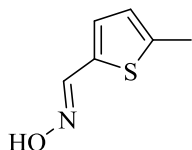
5-Methylthiophene-2-carbaldehyde oxime (**46c**) 491 mg (76% yield), white amorphous solid. ^{1}H NMR (500 MHz, CDCl$_3$) δ 7.62 (s, 1H), 7.21 (d, *J* = 3.7 Hz, 1H), 6.77 (dd, *J* = 3.6, 1.1 Hz, 1H), 2.53 (d, *J* = 1.0 Hz, 3H). ^{13}C NMR (126 MHz, CDCl$_3$) δ 146.8, 141.5, 132.3, 128.9, 124.8, 15.3. HRMS (ESI) *m/z* [M+H]$^+$ for C$_6$H$_8$NOS: 142.0327, found 142.0330.
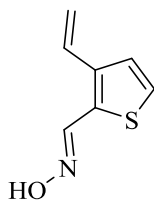
3-Vinylthiophene-2-carbaldehyde oxime (**46d**) 407 mg (95% yield), white amorphous solid, 2:1 mixture of isomers. ^{1}H NMR (400 MHz, CDCl$_3$) δ 8.45 (s, 1H), 8.36 (s, 2H), 7.92 (s, 2H), 7.87 (s, 1H), 7.30 (d, J = 5.3 Hz, 2H), 7.25 (d, J = 5.4 Hz, 2H), 7.20 (d, J = 5.3 Hz, 1H), 7.01 (d, J = 5.4 Hz, 2H), 6.84 (dd, J = 17.4, 10.9 Hz, 1H), 5.65 (d, J = 17.3 Hz, 1H), 5.38 (d, J = 11.0 Hz, 1H). ^{13}C NMR (126 MHz, CDCl$_3$) δ 144.4, 143.7, 140.8, 130.7, 130.3, 130.2, 128.1, 127.5, 127.1, 125.6, 116.9, 113.9. HRMS (ESI) *m/z* [M+H]$^+$ for C$_7$H$_8$NOS: 154.0327, found: 154.0331.
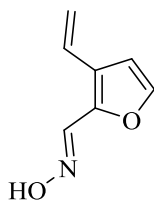
3-Vinylfuran-2-carboxaldehyde oxime (**46e**) 105 mg (48% yield), white amorphous solid. 1H NMR (400 MHz, CDCl$_3$) δ 8.14 (s, 1H), 7.40 (d, J = 1.6 Hz, 1H), 6.76 (dd, J = 17.4, 10.9 Hz, 1H), 6.62 (d, J = 1.9 Hz, 1H), 5.59 (dd, J = 17.5, 1.2 Hz, 1H), 5.32 (dd, J = 10.8, 1.2 Hz, 1H). ^{13}C NMR (126 MHz, CDCl$_3$) δ 144.3, 143.0, 139.6, 126.5, 125.4, 116.6, 108.9. HRMS (ESI) *m/z* [M+H]$^+$ for C$_7$H$_8$NO$_2$: 138.0555, found: 138.0549.
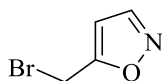
5-(Bromomethyl)isoxazole (**47**) N-bromosuccinimide (2.14 g, 12 mmol, 1 equiv.) and benzoyl peroxide (290 mg, 1.2 mmol, 0.1 equiv.) were added to a stirred solution of 5-methylisoxazole (1 g, 12 mmol, 1 equiv.) in CCl$_4$ (50 mL). The reaction was heated to 80˚C for 5 h then concentrated. The resulting residue was redissolved in EtOAc (30 mL) and washed with H$_2$O (3 x 20 mL). The

organic layer was separated, dried (Na$_2$SO$_4$), and concentrated. The residue was purified via flash chromatography (SiO$_2$, 1:10 EtOAc:Hexanes to 3:10 EtOAc:Hexanes) to provide the title compound. 725 mg (38% yield) as a colorless oil. ^{1}H NMR (400 MHz, CDCl$_3$) δ 8.22 (d, J = 1.6 Hz, 1H), 6.33 (d, J = 1.7 Hz, 1H), 4.49 (s, 2H). ^{13}C NMR (126 MHz, CDCl$_3$) δ 166.9, 150.6, 103.1, 18.3. MS (EI) m/z [M]$^+$ for C$_4$H$_4$BrNO: 160.9, found: 161.0; [M-Br]$^+$ for C$_4$H$_4$NO: 82.0, found 82.0.
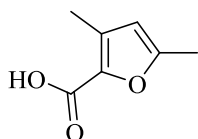
3,5-Dimethylfuran-2-carboxylic acid (**48**) A solution of 3-methylfuran-2-carboxylic acid (1 g, 8 mmol, 1 equiv.) in THF (3 mL) was added to a stirred solution of LDA (1 M in THF, 16 mmol, 2.1 equiv.) at -78˚C and stirred at this temperature for 15 min followed by the addition of iodomethane (1 mL, 16 mmol, 2 equiv.). The reaction was stirred for an additional 15 min at -78˚C before removal of the ice bath and slowly warming to room temperature. The reaction was quenched with the addition of saturated NH$_4$Cl (50 mL). The organic layer was separated and the aqueous layer was extracted with EtOAc (2 x 40 mL). The organic layers were combined, dried (Na$_2$SO$_4$), and concentrated. The residue was purified via flash chromatography (SiO$_2$, 3:10 EtOAc:Hexanes to 3:5 EtOAc:Hexanes) to provide the title compound. 774 mg (69% yield) as a white amorphous solid. ^{1}H NMR (400 MHz, CDCl$_3$) δ 12.35 (br, s, 1H), 6.00 (s, 1H), 2.31 (s, 3H), 2.30 (s, 3H). ^{13}C NMR (126 MHz, CDCl$_3$) δ 164.4, 157.0, 138.0, 135.3, 112.4, 14.0, 11.8. HRMS (ESI) m/z [M+H]$^+$ for C$_7$H$_9$O$_3$: 141.0552, found: 141.0551.
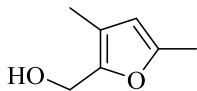
(3,5-Dimethylfuran-2-yl)methanol **(49a)** 575 mg (82% yield), colorless oil. ^{1}H NMR (400 MHz, CDCl$_3$) δ 5.80 (s, 1H), 4.52 (s, 2H), 2.24 (s, 3H), 1.99 (s, 3H), 1.62 (br, s, 1H). ^{13}C NMR (126 MHz, CDCl$_3$) δ 145.2, 124.2, 115.3, 109.0, 61.4, 13.6, 9.7. MS (EI) *m/z* [M+H]$^+$ for C$_7$H$_{11}$O$_2$: 127.1, found 127.1.
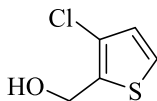
(3-Chlorothiophen-2-yl)methanol **(49b)** 240 mg (36% yield), yellow oil. ^{1}H NMR (400 MHz, CDCl$_3$) δ 7.25 (dd, *J* = 5.4, 1.1 Hz, 1H), 6.90 (dd, *J* = 5.4, 1.1 Hz, 1H), 4.81 (dd, *J* = 6.1, 1.3 Hz, 2H), 2.04 (br s, 1H). ^{13}C NMR (126 MHz, CDCl$_3$) δ 136.0, 127.8, 124.6, 123.0, 57.6. MS (EI) *m/z* [M]$^+$ for C$_5$H$_5$ClOS: 148.0, found 148.0.
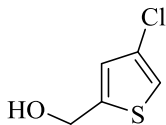
(4-Chlorothiophen-2-yl)methanol **(49c)** 165 mg (25% yield), yellow oil. ^{1}H NMR (400 MHz, CDCl$_3$) δ 7.05 (s, 1H), 6.88 (s, 1H), 4.77 (d, *J* = 5.8 Hz, 2H), 1.92 (br s, 1H). ^{13}C NMR (126 MHz, CDCl$_3$) δ 144.7, 125.5, 124.8, 119.9, 60.1. MS (EI) *m/z* [M]$^+$ for C$_5$H$_5$ClOS: 148.0, found: 148.0; [M+H]$^+$ for C$_5$H$_6$ClOS: 149.0, found 149.0.
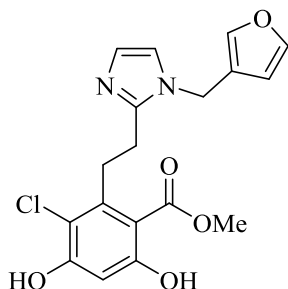
Methyl 3-chloro-2-(2-(1-(furan-3-ylmethyl)-1H-imidazol-2-yl)ethyl)-4,6-dihydroxybenzoate

(**50**) 40 mg (41% yield), off white amorphous solid. ^{1}H NMR (500 MHz, CDCl$_3$, MeOD) δ ^{1}H NMR (500 MHz, CDCl$_3$-MeOD) δ 7.30 (d, *J* = 1.6 Hz, 1H), 7.20 (s, 1H), 6.84 (dd, *J* = 2.7, 1.4 Hz, 1H), 6.78 (d, *J* = 1.4 Hz, 1H), 6.36 (d, *J* = 2.0 Hz, 1H), 6.15 (d, *J* = 1.9 Hz, 1H), 4.80 (s, 2H), 3.78 (d, *J* = 1.9 Hz, 3H), 3.39 (tt, *J* = 8.9, 2.5 Hz, 2H), 2.95 – 2.80 (m, 2H). δ ^{13}CNMR (125 MHz, CDCl$_3$, MeOD): 170.8, 161.8, 158.1, 147.3, 144.1, 141.6, 141.6, 140.1, 126.7, 121.0, 119.6, 114.7, 109.4, 106.2, 102.5, 52.4, 41.0, 30.8, 26.1. HRMS (ESI) *m/z* [M + H]$^+$ for C$_{18}$H$_{18}$ClN$_2$O$_5$: 377.0904, found: 377.0905.
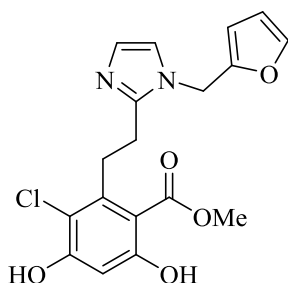
Methyl 3-chloro-2-(2-(1-(furan-2-ylmethyl)-1H-imidazol-2-yl)ethyl)-4,6-dihydroxybenzoate

(**51**) 44 mg (45% yield), off white amorphous solid. ^{1}H NMR (500 MHz, CDCl$_3$, MeOD) δ 7.31 (dt, *J* = 2.4, 1.2 Hz, 1H), 6.87 (dd, *J* = 2.4, 1.4 Hz, 1H), 6.83 (d, *J* = 1.5 Hz, 1H), 6.40 (d, *J* = 1.8 Hz, 1H), 6.26 (dt, *J* = 3.5, 1.7 Hz, 1H), 6.18 (d, *J* = 3.3 Hz, 1H), 4.94 (d, *J* = 1.6 Hz, 2H), 3.82 (d, *J* = 1.9 Hz, 3H), 3.46 (ddd, *J* = 10.2, 6.1, 2.0 Hz, 2H), 2.95 (ddd, *J* = 9.8, 5.9, 1.5 Hz, 2H). ^{13}CNMR (125 MHz, CDCl$_3$, MeOD) δ 170.9, 162.0, 158.2, 149.1, 147.4, 143.2, 141.8, 126.9, 119.7, 114.8,

110.6, 108.8, 106.2, 102.6, 52.6, 42.6, 30.8, 26.1. HRMS (ESI) m/z [M + H]$^+$ for $C_{18}H_{18}ClN_2O_5$: 377.0904, found: 377.0911.
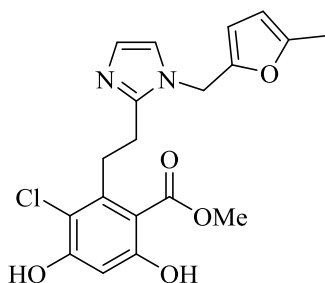
Methyl 3-chloro-4,6-dihydroxy-2-(2-(1-((5-methylfuran-2-yl)methyl)-1H-imidazol-2-yl)ethyl)benzoate (**52**) 46 mg (46% yield), off white amorphous solid. ^{1}H NMR (400 MHz, CDCl$_3$, MeOD) δ 6.87 (d, J = 1.4 Hz, 1H), 6.84 (d, J = 1.4 Hz, 1H), 6.41 (s, 1H), 6.08 (d, J = 3.1 Hz, 1H), 5.84 (dd, J = 3.0, 1.2 Hz, 1H), 4.88 (s, 2H), 3.84 (s, 3H), 3.49-3.42 (m, 2H), 3.08-2.93 (m, 2H), 2.18 (d, J = 1.0 Hz, 3H). ^{13}CNMR (125 MHz, CDCl$_3$, MeOD): 171.0, 162.2, 158.3, 153.1, 147.3, 147.1, 141.9, 126.7, 119.7, 114.9, 109.7, 106.5, 106.1, 102.6, 52.6, 42.7, 30.9, 26.2, 13.5. HRMS (ESI) m/z [M+H]$^+$ for $C_{19}H_{20}ClN_2O_5$: 391.1061, found: 391.1066. t_R = 3.05 min, 95.1%.
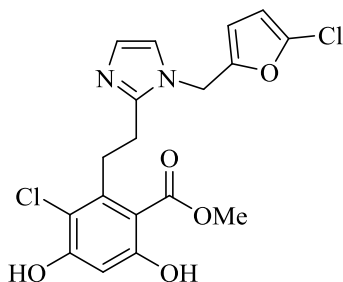
Methyl 3-chloro-2-(2-(1-((5-chlorofuran-2-yl)methyl)-1H-imidazol-2-yl)ethyl)-4,6-dihydroxybenzoate (**53**) 50 mg (47% yield), white amorphous solid. (^{1}H NMR (400 MHz, CDCl$_3$, MeOD) δ 6.91 (s, 2H), 6.31 (s, 1H), 6.23 (d, J = 3.4 Hz, 1H), 5.98 (d, J = 3.3 Hz, 1H), 4.87 (s, 2H), 3.73 (s, 3H), 3.37 − 3.27 (m, 2H), 2.99 (t, J = 7.9 Hz, 2H). ^{13}C NMR (126 MHz, CDCl$_3$, MeOD) δ 173.9, 165.0, 161.9, 151.1, 150.7, 143.8, 141.6, 124.6, 118.5, 116.3, 111.3 (2C), 106.8

(2C), 56.4, 46.9, 34.1, 29.1. HRMS (ESI) *m/z* [M+H]$^+$ for C$_{18}$H$_{17}$Cl$_2$N$_2$O$_5$: 411.0515, found: 411.0527. t$_R$ = 4.15 min, 95.5%.

Methyl 3-chloro-2-(2-(1-((3,5-dimethylfuran-2-yl)methyl)-1H-imidazol-2-yl)ethyl)-4,6-dihydroxybenzoate (**54**). 36 mg (25% yield), off white amorphous solid. ^{1}H NMR (400 MHz, CDCl$_3$, MeOD) δ 7.28 (d, *J* = 2.0 Hz, 1H), 6.92 (s, 1H), 6.44 (s, 1H), 5.77 (s, 1H), 4.80 (s, 2H), 3.89 (s, 3H), 3.59 – 3.48 (m, 2H), 3.37 (t, *J* = 7.1 Hz, 2H), 2.11 (s, 3H), 1.92 (s, 3H). ^{13}C NMR (126 MHz, CDCl$_3$, MeOD) δ 169.9, 162.0, 157.1, 151.4, 145.7, 140.1, 130.0, 121.6, 120.5, 118.9, 118.6, 112.1, 111.9, 55.4, 54.2, 46.6, 30.5, 29.7, 24.0, 21.8. HRMS (ESI) *m/z* [M+H]$^+$ for C$_{20}$H$_{22}$ClN$_2$O$_5$: 405.1217, found: 405.1210. t$_R$ = 3.24 min, 95.5%.
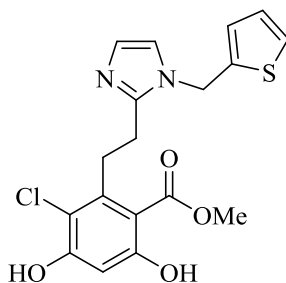
Methyl 3-chloro-4,6-dihydroxy-2-(2-(1-(thiophen-2-ylmethyl)-1H-imidazol-2-yl)ethyl)benzoate (**55**) 37 mg (37% yield), yellow amorphous solid. ^{1}H NMR (400 MHz, CDCl$_3$, MeOD) δ 7.23 (dd, *J* = 5.1, 1.3 Hz, 1H), 6.95 (d, *J* = 1.5 Hz, 1H), 6.92 (dd, *J* = 5.1, 3.5 Hz, 1H), 6.87 (dd, *J* = 3.5, 1.9 Hz, 2H), 6.43 (s, 1H), 5.17 (d, *J* = 0.9 Hz, 2H), 3.84 (s, 3H), 3.56 -3.44 (m, 2H), 3.01-2.92 (m, 2H). ^{13}CNMR (125 MHz, CDCl$_3$, MeOD) δ 170.9, 162.1, 158.2, 147.3, 141.7, 138.5, 127.2, 126.9, 126.4, 126.2, 119.7, 114.9, 106.2, 102.7, 52.6, 44.7, 30.9, 26.2. HRMS (ESI)

m/z [M+H]$^+$ for C$_{18}$H$_{18}$ClN$_2$O$_4$S: 393.0676, found: 393.0674.
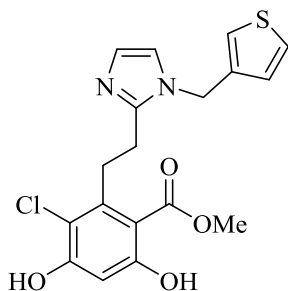
Methyl 3-chloro-4,6-dihydroxy-2-(2-(1-(thiophen-3-ylmethyl)-1H-imidazol-2-yl)ethyl)benzoate **(56)**. 28 mg (27% yield), yellow amorphous solid. ^{1}H NMR (400 MHz, CDCl$_3$, MeOD) δ 7.25 (d, *J* = 4.8 Hz, 1H), 6.98 – 6.92 (m, 2H), 6.83 (d, *J* = 1.5 Hz, 1H), 6.81 – 6.78 (m, 1H), 6.37 (s, 1H), 4.97 (s, 2H), 3.79 (s, 3H), 3.43 – 3.37 (m, 2H), 2.95 – 2.88 (m, 2H). ^{13}C NMR (126 MHz, CDCl$_3$, MeOD) δ 174.5, 165.7, 162.0, 151.1, 145.0, 140.3, 131.3, 130.0, 129.4, 126.7, 124.0, 118.6, 110.2, 106.5, 56.4, 49.3, 34.5, 29.7. HRMS (ESI) *m/z* [M+H]$^+$ for C$_{18}$H$_{18}$ClN$_2$O$_4$S: 393.0676, found: 393.0693.

Methyl 3-chloro-4,6-dihydroxy-2-(2-(1-((5-methylthiophen-2-yl)methyl)-1H-imidazol-2-yl)ethyl)benzoate **(57)**. 23 mg (22% yield), off white amorphous solid. ^{1}H NMR (400 MHz, CDCl$_3$, MeOD) δ 7.34 (d, *J* = 1.8 Hz, 1H), 7.02 – 6.96 (m, 1H), 6.79 (d, *J* = 4.1 Hz, 1H), 6.60 (d, *J* = 2.7 Hz, 1H), 6.48 (s, 1H), 5.03 (s, 2H), 3.95 (s, 3H), 3.58 (t, *J* = 7.2 Hz, 2H), 3.39 (t, *J* = 7.2 Hz, 2H), 2.41 (s, 3H). ^{13}C NMR (126 MHz, CDCl$_3$, MeOD) δ 169.8, 161.9, 158.2, 145.6, 138.8, 131.1, 129.1 (2C), 125.6 (2C), 120.6, 119.1, 106.3, 103.5, 53.2, 46.0, 30.1, 24.2 15.3. HRMS (ESI) *m/z* [M+H]$^+$ for C$_{19}$H$_{20}$ClN$_2$O$_4$S: 407.0832, found: 407.0839.
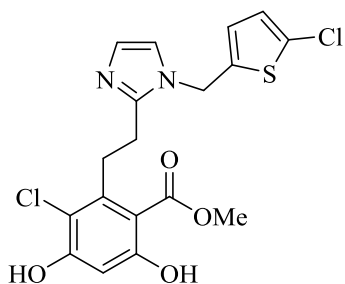
Methyl 3-chloro-2-(2-(1-((5-chlorothiophen-2-yl)methyl)-1H-imidazol-2-yl)ethyl)-4,6-dihydroxybenzoate **(58)**. 20 mg (18% yield), yellow amorphous solid. ^{1}H NMR (500 MHz, CDCl$_3$, MeOD) δ 6.95 (s, 1H), 6.87 (s, 1H), 6.68 (d, *J* = 3.5 Hz, 1H), 6.63 (d, *J* = 3.5 Hz, 1H), 6.37 (s, 1H), 5.03 (s, 2H), 3.81 (s, 3H), 3.47 − 3.37 (m, 2H), 3.02 − 2.92 (m, 2H). ^{13}C NMR (126 MHz, CDCl$_3$, MeOD) δ 174.3, 165.6, 162.0, 150.9, 144.7, 140.2, 134.9, 130.2, 130.1, 129.4, 123.7, 118.6, 110.3, 106.7, 56.5, 48.8, 34.5, 29.6. HRMS (ESI) *m/z* [M+H]$^+$ for C$_{18}$H$_{17}$Cl$_2$N$_2$O$_4$S: 427.0286, found: 427.0292.
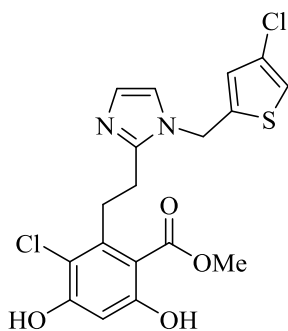
Methyl 3-chloro-2-(2-(1-((4-chlorothiophen-2-yl)methyl)-1H-imidazol-2-yl)ethyl)-4,6-dihydroxybenzoate **(59)**. 23 mg (21% yield), tan amorphous solid. ^{1}H NMR (400 MHz, CDCl$_3$, MeOD) δ 6.97 (s, 1H), 6.90 (s, 1H), 6.83 (s, 1H), 6.67 (s, 1H), 6.38 (s, 1H), 5.07 (s, 2H), 3.81 (s, 3H), 3.45 − 3.39 (m, 2H), 2.88 (t, *J* = 8.2 Hz, 2H). ^{13}C NMR (126 MHz, CDCl$_3$, MeOD) δ 170.6, 161.8, 158.1, 147.3, 141.5, 139.6, 127.3, 126.2, 125.1, 120.1, 119.5, 114.7, 106.0, 102.5, 52.4, 44.4, 30.8, 26.1. HRMS (ESI) *m/z* [M+H]$^+$ for C$_{18}$H$_{17}$Cl$_2$N$_2$O$_4$S: 427.0286, found: 427.0290.
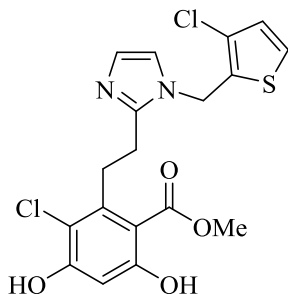
Methyl 3-chloro-2-(2-(1-((3-chlorothiophen-2-yl)methyl)-1H-imidazol-2-yl)ethyl)-4,6-dihydroxybenzoate **(60)**. 17 mg (15% yield), tan amorphous solid. ^{1}H NMR (400 MHz, CDCl$_3$, MeOD) δ 7.21 (dd, *J* = 5.9, 2.3 Hz, 1H), 6.90 (d, *J* = 2.1 Hz, 1H), 6.86 (dt, *J* = 5.2, 1.8 Hz, 2H), 6.41 (s, 0H), 5.09 (s, 0H), 3.84 (s, 2H), 3.54 – 3.45 (m, 2H), 2.96 (dd, *J* = 11.9, 5.4 Hz, 3H). ^{13}C NMR (126 MHz, CDCl$_3$, MeOD) δ 170.8, 162.1, 158.0, 147.2, 141.7, 131.3, 127.9, 127.3, 125.2, 124.2, 119.3, 114.8, 106.0, 102.6, 52.5, 42.0, 30.8, 26.2. HRMS (ESI) *m/z* [M+H]$^+$ for C$_{18}$H$_{16}$Cl$_2$N$_2$O$_4$S: 427.0286, found: 427.0278.
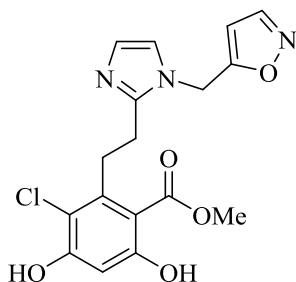
Methyl 3-chloro-4,6-dihydroxy-2-(2-(1-(isoxazol-5-ylmethyl)-1H-imidazol-2-yl)ethyl)benzoate **(61)**. 15 mg (15% yield), tan amorphous solid. ^{1}H NMR (400 MHz, CDCl$_3$, MeOD) δ 8.17 (s, 1H), 6.96 (s, 1H), 6.89 (s, 1H), 6.42 (s, 1H), 6.04 (s, 1H), 5.17 (s, 2H), 3.88 (s, 3H), 3.50 – 3.41 (m, 2H), 2.97 – 2.89 (m, 2H). ^{13}C NMR (126 MHz, CDCl$_3$, MeOD) δ 170.6, 166.3, 158.0, 150.4, 147.6, 141.5, 127.8, 119.7, 114.6, 106.1, 102.6, 102.5, 102.1, 52.6, 41.2, 30.9, 26.0. HRMS (ESI) [M+H]$^+$ for C$_{17}$H$_{17}$ClN$_3$O$_5$: 378.0857, found: 378.0866.
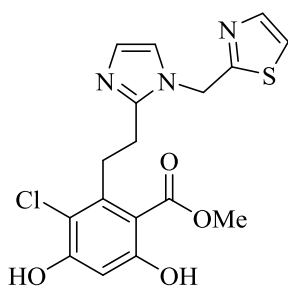
Methyl 3-chloro-4,6-dihydroxy-2-(2-(1-(thiazol-2-ylmethyl)-1H-imidazol-2-yl)ethyl)benzoate

(62). 41 mg (40% yield), tan amorphous solid. ^{1}H NMR (400 MHz, CDCl$_3$, MeOD) δ 7.72 (d, J = 3.2 Hz, 1H), 7.30 (d, J = 3.3 Hz, 1H), 6.99 (s, 1H), 6.95 (s, 1H), 6.43 (s, 1H), 5.35 (s, 2H), 3.87 (s, 3H), 3.51 − 3.46 (m, 2H), 2.98 − 2.91 (m, 2H). ^{13}C NMR (126 MHz, CDCl$_3$, MeOD) δ 170.7, 165.8, 162.1, 157.9, 147.6, 143.1, 141.6, 127.8, 120.3, 119.8, 114.7, 106.0, 102.6, 52.6, 46.8, 30.8, 26.1. HRMS (ESI) *m/z* [M+H]$^+$ for C$_{17}$H$_{17}$ClN$_3$O$_4$S: 394.0628, found: 394.0630.
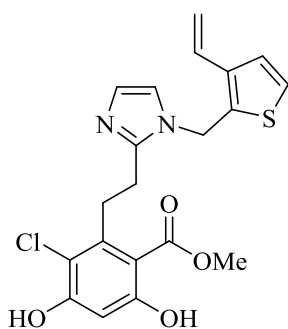
Methyl 3-chloro-4,6-dihydroxy-2-(2-(1-((3-vinylthiophen-2-yl)methyl)-1H-imidazol-2-yl)ethyl)benzoate **(63)**. 35 mg (32% yield), tan amorphous solid. ^{1}H NMR (400 MHz, CDCl$_3$, MeOD) δ 7.19 (d, J = 5.3 Hz, 1H), 7.15 (d, J = 5.3 Hz, 1H), 7.01 (s, 1H), 6.77 (s, 1H), 6.58 (dd, J = 17.3, 10.9 Hz, 1H), 6.45 (s, 1H), 5.56 (d, J = 17.3 Hz, 1H), 5.31 (d, J = 11.0 Hz, 1H), 5.11 (s, 2H), 3.87 (s, 3H), 3.58 − 3.49 (m, 2H), 3.07 (t, J = 7.8 Hz, 2H). ^{13}C NMR (126 MHz, CDCl$_3$, MeOD) δ 170.9, 163.2, 156.1, 142.8, 140.7, 139.8, 138.5, 130.5, 128.7, 128.5, 126.7, 126.5, 126.0, 113.9, 106.7, 102.6, 52.6, 38.4, 34.0, 32.5. HRMS (ESI) *m/z* [M+H]$^+$ for C$_{20}$H$_{20}$ClN$_2$O$_4$S: 419.0832, found: 419.0844.
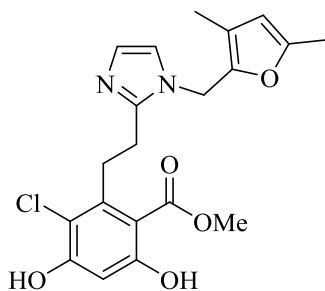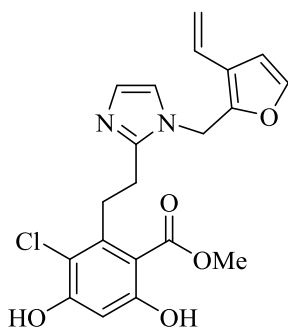
Methyl 3-chloro-4,6-dihydroxy-2-(2-(1-((3-vinylfuran-2-yl)methyl)-1H-imidazol-2-yl)ethyl)benzoate **(64)**. 35 mg (33% yield), off white amorphous solid ^{1}H NMR (400 MHz, CDCl$_3$, MeOD) δ 7.30 (d, *J* = 2.0 Hz, 1H), 6.84 (d, *J* = 1.8 Hz, 1H), 6.51 (d, *J* = 2.0 Hz, 1H), 6.49 (s, 1H), 6.48 − 6.41 (m, 1H), 5.50 (d, *J* = 17.3 Hz, 1H), 5.26 (d, *J* = 11.0 Hz, 1H), 4.94 (s, 2H), 3.91 (s, 3H), 3.59 (t, *J* = 7.6 Hz, 2H), 3.22 (t, *J* = 7.7 Hz, 2H). ^{13}C NMR (126 MHz, CDCl$_3$, MeOD) δ 170.4, 162.1, 158.0, 146.6, 143.6 (2C), 124.5 (2C), 123.7, 119.9 (2C), 116.6, 114.8, 108.3 (2C), 108.2, 106.2, 103.1, 52.8, 41.1, 30.4, 25.2. HRMS (ESI) *m/z* [M+H]$^+$ for C$_{20}$H$_{20}$ClN$_2$O$_5$: 403.1061, found: 403.1069.
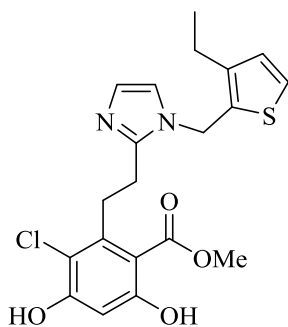
Methyl 3-chloro-2-(2-(1-((3-ethylthiophen-2-yl)methyl)-1H-imidazol-2-yl)ethyl)-4,6-dihydroxybenzoate **(65)**. 43 mg (39% yield), tan amorphous solid. ^{1}H NMR (500 MHz, CDCl$_3$, MeOD) δ 7.16 (d, *J* = 5.2 Hz, 1H), 6.91 (d, *J* = 1.4 Hz, 1H), 6.86 (d, *J* = 5.2 Hz, 1H), 6.73 (d, *J* = 1.5 Hz, 1H), 6.45 (s, 1H), 5.04 (s, 2H), 3.86 (s, 3H), 3.56 − 3.50 (m, 2H), 3.00 − 2.95 (m, 2H), 2.53 (q, *J* = 7.6 Hz, 2H), 1.12 (t, *J* = 7.6 Hz, 3H). ^{13}C NMR (126 MHz, CDCl$_3$, MeOD) δ 170.8, 162.2,

157.9, 147.1, 142.2, 141.8, 130.8, 128.7, 127.0, 124.6, 119.1, 114.7, 106.0, 102.6, 52.6, 42.3, 30.8, 26.3, 21.5, 14.9. HRMS (ESI) m/z [M+H]$^+$ for $C_{20}H_{22}ClN_2O_4S$: 421.0989, found: 421.0995.
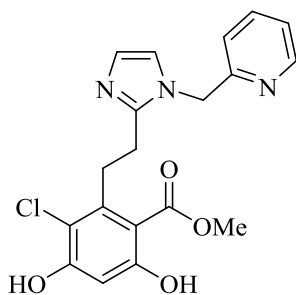
Methyl 3-chloro-4,6-dihydroxy-2-(2-(1-(pyridin-2-ylmethyl)-1H-imidazol-2-yl)ethyl)benzoate

(66). 15 mg (15% yield), tan amorphous solid. ^{1}H NMR (400 MHz, CDCl$_3$) δ 8.57 (d, J = 5.0 Hz, 1H), 7.68 (td, J = 7.7, 1.9 Hz, 1H), 7.13 (d, J = 1.5 Hz, 1H), 6.99 (d, J = 1.6 Hz, 1H), 6.89 (d, J = 7.9 Hz, 1H), 6.51 (s, 0H), 5.23 (s, 1H), 3.89 (s, 1H), 3.52 (t, J = 7.9 Hz, 2H), 3.05 (t, J = 8.0 Hz, 2H). ^{13}C NMR (126 MHz, CDCl$_3$) δ 170.5, 162.8, 157.7, 150.0 (2C), 147.4, 137.5 (3C), 123.4, 121.1, 120.7, 114.6, 106.0, 103.2, 52.9, 51.5, 30.6, 25.4. HRMS (ESI) m/z [M–H]$^-$ for $C_{19}H_{18}ClN_3O_4$: 386.0908, found: 386.0899.
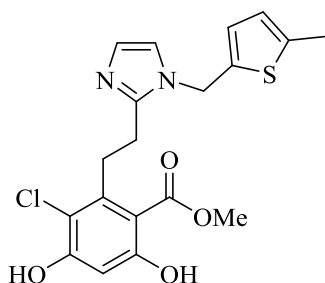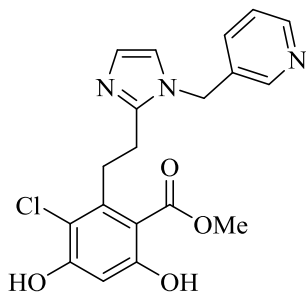

Methyl 3-chloro-4,6-dihydroxy-2-(2-(1-(pyridin-3-ylmethyl)-1H-imidazol-2-yl)ethyl)benzoate

(67). 25 mg (25% yield), yellow amorphous solid. ^{1}H NMR (500 MHz, CDCl$_3$, MeOD) δ 8.44 (d, J = 4.3 Hz, 1H), 8.30 (s, 1H), 7.32 (d, J = 6.0 Hz, 1H), 7.31 – 7.24 (m, 1H), 6.98 (s, 1H), 6.83 (s, 1H), 6.38 (s, 1H), 5.06 (s, 2H), 3.83 (s, 3H), 3.48 – 3.37 (m, 2H), 2.90 – 2.84 (m, 2H). ^{13}C NMR (126 MHz, CDCl$_3$, MeOD) δ 174.4, 165.7, 162.0, 152.9, 152.8, 151.5, 145.2, 138.9, 136.3, 131.1,

128.1, 123.8, 118.6, 110.1, 106.5, 56.4, 50.8, 34.7, 30.0. HRMS (ESI) *m/z* [M–H]⁻ $C_{19}H_{18}ClN_3O_4$: 386.0908, found: 386.0903.
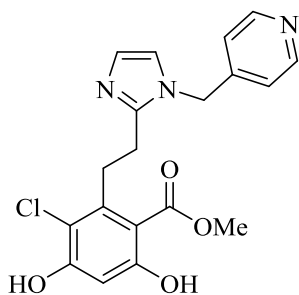
Methyl 3-chloro-4,6-dihydroxy-2-(2-(1-(pyridin-4-ylmethyl)-1H-imidazol-2-yl)ethyl)benzoate **(68)**. 32 mg (30% yield), yellow amorphous solid. ¹H NMR (500 MHz, CDCl₃, MeOD) δ 8.44 – 8.29 (m, 2H), 6.95 (d, *J* = 1.4 Hz, 1H), 6.88 – 6.82 (m, 2H), 6.81 (d, *J* = 1.5 Hz, 1H), 6.30 (s, 1H), 5.03 (s, 2H), 3.78 (s, 3H), 3.40 – 3.28 (m, 2H), 2.78 – 2.71 (m, 2H). ¹³C NMR (126 MHz, CDCl₃, MeOD) δ 170.4, 161.5, 157.9, 149.6 (2C), 147.8, 146.4, 141.1, 127.4, 121.3 (2C), 120.2, 114.5, 106.2, 102.4, 52.3, 30.7, 25.9, 25.1, 19.9. HRMS (ESI) *m/z* [M–H]⁻ $C_{19}H_{18}ClN_3O_4$: 386.0908, found: 386.0912.
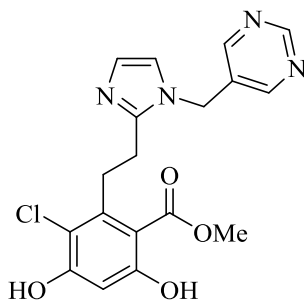
Methyl 3-chloro-4,6-dihydroxy-2-(2-(1-(pyrimidin-5-ylmethyl)-1H-imidazol-2-yl)ethyl)benzoate **(69)**. 45 mg (45% yield), white amorphous solid. ¹H NMR (500 MHz, CDCl₃, MeOD) δ 9.09 (s, 1H), 8.46 (s, 2H), 7.05 (s, 1H), 6.92 (s, 1H), 6.40 (s, 1H), 5.12 (s, 2H), 3.86 (s, 3H), 3.52 – 3.36 (m, 2H), 3.00 – 2.79 (m, 2H). ¹³C NMR (126 MHz, CDCl₃, MeOD) δ 174.1,

165.4, 161.9, 159.5, 159.4, 159.4, 151.4, 144.7, 134.1, 130.8, 123.8, 118.5, 110.4, 106.7, 56.5, 48.8, 34.7, 29.8. HRMS (ESI) *m/z* [M–H]$^-$ C$_{18}$H$_{17}$ClN$_4$O$_4$: 387.0860, found: 387.0861.

Fluorescence polarization. Assay was performed in 96-well format in black, flat bottom plates (Santa Cruz Biotechnology) with a final volume of 100µL. 25µL of assay buffer (20 mM HEPES, pH 7.3, 50 mM KCl, 5 mM MgCl$_2$, 20 mM Na$_2$MoO$_4$, 2 mM DTT, 0.1 mg/mL BGG, and 0.01% NP-40), 25µL of assay buffer containing 6nM FITC-GDA (fluorescent tracer, stock in DMSO and diluted in assay buffer), and 50µL of assay buffer containing 10nM of either Grp94, Hsp90α, or Hsp90β were added to each well. Compounds were tested in triplicate wells (1% DMSO final concentration). For each plate wells containing buffer only (background), tracer in buffer only (low polarization control), and protein and tracer in buffer with 1% DMSO (high polarization control) were included. Plates were incubated at 4˚C with rocking for 24h. Polarization values (in mP units) was measured at 37˚C with an excitation filter at 485nm and an emission filter at 528nm. Polarization values were correlated to % tracer bound and compound concentrations. The apparent K$_d$ of compounds of interest is defined as the concentration at which the tracer was 50% displaced by the inhibitor.

References

1. Lee, A. S. Glucose-regulated proteins in cancer: molecular mechanisms and therapeutic potential. *Nat. Rev. Cancer* **2014,** *14*, 263-276.

2. Stothert, A. R.; Suntharalingam, A.; Huard, D. J.; Fontaine, S. N.; Crowley, V. M.; Mishra, S.; Blagg, B. S.; Lieberman, R. L.; Dickey, C. A. Exploiting the interaction between Grp94 and aggregated myocilin to treat glaucoma. *Hum. Mol. Genet.* **2014,** *23*, 6470-6480.

3. Soldano, K. L.; Jivan, A.; Nicchitta, C. V.; Gewirth, D. T. Structure of the N-terminal domain of GRP94. Basis for ligand specificity and regulation. *J. Biol. Chem.* **2003,** *278*, 48330-48338.

4.   Hua, Y.; White-Gilbertson, S.; Kellner, J.; Rachidi, S.; Usmani, S. Z.; Chiosis, G.; Depinho, R.; Li, Z.; Liu, B. Molecular chaperone gp96 is a novel therapeutic target of multiple myeloma. *Clin. Cancer Res.* **2013,** *19*, 6242-6251.

5.   Wanderling, S.; Simen, B. B.; Ostrovsky, O.; Ahmed, N. T.; Vogen, S. M.; Gidalevitz, T.; Argon, Y. GRP94 is essential for mesoderm induction and muscle development because it regulates insulin-like growth factor secretion. *Mol. Biol. Cell* **2007,** *18*, 3764-3775.

6.   Stothert, A. R.; Suntharalingam, A.; Huard, D. J.; Fontaine, S. N.; Crowley, V. M.; Mishra, S.; Blagg, B. S.; Lieberman, R. L.; Dickey, C. A. Exploiting the interaction between Grp94 and aggregated myocilin to treat glaucoma. *Hum. Mol. Genet.* **2014,** *23*, 6470-6480.

7.   Suntharalingam, A.; Abisambra, J. F.; O'Leary, J. C.; Koren, J.; Zhang, B.; Joe, M. K.; Blair, L. J.; Hill, S. E.; Jinwal, U. K.; Cockman, M.; Duerfeldt, A. S.; Tomarev, S.; Blagg, B. S.; Lieberman, R. L.; Dickey, C. A. Glucose-regulated protein 94 triage of mutant myocilin through endoplasmic reticulum-associated degradation subverts a more efficient autophagic clearance mechanism. *J. Biol. Chem.* **2012,** *287*, 40661-40669.

8.   Stothert, A. R.; Fontaine, S. N.; Sabbagh, J. J.; Dickey, C. A. Targeting the ER-autophagy system in the trabecular meshwork to treat glaucoma. *Exp. Eye Res.* **2016,** *144*, 38-45.

9.   Wassenberg, J. J.; Reed, R. C.; Nicchitta, C. V. Ligand interactions in the adenosine nucleotide-binding domain of the Hsp90 chaperone, GRP94. II. Ligand-mediated activation of GRP94 molecular chaperone and peptide binding activity. *J. Biol. Chem.* **2000,** *275*, 22806-22814.

10.   Rosser, M. F.; Nicchitta, C. V. Ligand interactions in the adenosine nucleotide-binding domain of the Hsp90 chaperone, GRP94. I. Evidence for allosteric regulation of ligand binding. *J. Biol. Chem.* **2000,** *275*, 22798-22805.

11.   Patel, P. D.; Yan, P.; Seidler, P. M.; Patel, H. J.; Sun, W.; Yang, C.; Que, N. S.; Taldone, T.; Finotti, P.; Stephani, R. A.; Gewirth, D. T.; Chiosis, G. Paralog-selective Hsp90 inhibitors define tumor-specific regulation of HER2. *Nat. Chem. Biol.* **2013,** *9*, 677-684.

12.   Patel, H. J.; Patel, P. D.; Ochiana, S. O.; Yan, P.; Sun, W.; Patel, M. R.; Shah, S. K.; Tramentozzi, E.; Brooks, J.; Bolaender, A.; Shrestha, L.; Stephani, R.; Finotti, P.; Leifer, C.; Li, Z.; Gewirth, D. T.; Taldone, T.; Chiosis, G. Structure-activity relationship in a purine-scaffold compound series with selectivity for the endoplasmic reticulum Hsp90 paralog Grp94. *J. Med. Chem.* **2015,** *58*, 3922-3943.

13.   Immormino, R. M.; Metzger, L. E. t.; Reardon, P. N.; Dollins, D. E.; Blagg, B. S.; Gewirth, D. T. Different poses for ligand and chaperone in inhibitor-bound Hsp90 and GRP94: implications for paralog-specific drug design. *J. Mol. Biol.* **2009,** *388*, 1033-1042.

14.   Clevenger, R. C.; Blagg, B. S. Design, synthesis, and evaluation of a radicicol and geldanamycin chimera, radamide. *Org. Lett.* **2004,** *6*, 4459-4462.

15.   Duerfeldt, A. S.; Peterson, L. B.; Maynard, J. C.; Ng, C. L.; Eletto, D.; Ostrovsky, O.; Shinogle, H. E.; Moore, D. S.; Argon, Y.; Nicchitta, C. V.; Blagg, B. S. Development of a Grp94 inhibitor. *J. Am. Chem. Soc.* **2012,** *134*, 9796-9804.

16.   Park, K. D.; Morieux, P.; Salome, C.; Cotten, S. W.; Reamtong, O.; Eyers, C.; Gaskell, S. J.; Stables, J. P.; Liu, R.; Kohn, H. Lacosamide isothiocyanate-based agents: novel agents to target and identify lacosamide receptors. *J. Med. Chem.* **2009,** *52*, 6897-6911.

17.   Hadden, M. K.; Blagg, B. S. Synthesis and evaluation of radamide analogues, a chimera of radicicol and geldanamycin. *J. Org. Chem.* **2009,** *74*, 4697-4704.

18.   Llauger-Bufi, L.; Felts, S. J.; Huezo, H.; Rosen, N.; Chiosis, G. Synthesis of novel fluorescent probes for the molecular chaperone Hsp90. *Bioorg. Med. Chem. Lett.* **2003,** *13*, 3975-3978.

19.   Gorska, M.; Popowska, U.; Sielicka-Dudzin, A.; Kuban-Jankowska, A.; Sawczuk, W.; Knap, N.; Cicero, G.; Bucchieri, F.; Wozniak, M. Geldanamycin and its derivatives as Hsp90 inhibitors. *Front. Biosci.* **2012,** *17*, 2269-2277.

20.   Immormino, R. M.; Dollins, D. E.; Shaffer, P. L.; Soldano, K. L.; Walker, M. A.; Gewirth, D. T. Ligand-induced conformational shift in the N-terminal domain of GRP94, an Hsp90 chaperone. *J. Biol. Chem.* **2004,** *279*, 46162-46171.

21.   Crowley, V.; Huard, D.; Lieberman, R.; Blagg, B. Second Generation Grp94-selective Inhibitors Provide Opportunities for the Inhibition of Metastatic Cancer. *Chem. Eur. J.* **2017,** *In Press.*

22.   Woodhead, A. J.; Angove, H.; Carr, M. G.; Chessari, G.; Congreve, M.; Coyle, J. E.; Cosme, J.; Graham, B.; Day, P. J.; Downham, R.; Fazal, L.; Feltell, R.; Figueroa, E.; Frederickson, M.; Lewis, J.; McMenamin, R.; Murray, C. W.; O'Brien, M. A.; Parra, L.; Patel, S.; Phillips, T.; Rees, D. C.; Rich, S.; Smith, D. M.; Trewartha, G.; Vinkovic, M.; Williams, B.; Woolford, A. J. Discovery of (2,4-dihydroxy-5-isopropylphenyl)-[5-(4-methylpiperazin-1-ylmethyl)-1,3-dihydrois oindol-2-yl]methanone (AT13387), a novel inhibitor of the molecular chaperone Hsp90 by fragment based drug design. *J. Med. Chem.* **2010,** *53*, 5956-5969.

23.   Ma, J. C.; Dougherty, D. A. The Cationminus signpi Interaction. *Chem. Rev.* **1997,** *97*, 1303-1324.

24.   Kingman, S. Glaucoma is second leading cause of blindness globally. *Bull. World Health Organ.* **2004,** *82*, 887-888.

25.   Burns, J. N.; Orwig, S. D.; Harris, J. L.; Watkins, J. D.; Vollrath, D.; Lieberman, R. L. Rescue of glaucoma-causing mutant myocilin thermal stability by chemical chaperones. *ACS Chem. Biol.* **2010,** *5*, 477-487.

26.   Gupta, N.; Yucel, Y. H. Glaucoma as a neurodegenerative disease. *Curr. Opin. Ophthalmol.* **2007,** *18*, 110-114.

27.   Zode, G. S.; Kuehn, M. H.; Nishimura, D. Y.; Searby, C. C.; Mohan, K.; Grozdanic, S. D.; Bugge, K.; Anderson, M. G.; Clark, A. F.; Stone, E. M.; Sheffield, V. C. Reduction of ER stress via a chemical chaperone prevents disease phenotypes in a mouse model of primary open angle glaucoma. *J. Clin. Invest.* **2011,** *121*, 3542-3553.

28.   Hill, S. E.; Donegan, R. K.; Lieberman, R. L. The glaucoma-associated olfactomedin domain of myocilin forms polymorphic fibrils that are constrained by partial unfolding and peptide sequence. *J. Mol. Biol.* **2014,** *426*, 921-935.

29.   Tamm, E. R.; Braunger, B. M.; Fuchshofer, R. Intraocular pressure and the mechanisms involved in resistance of the aqueous humor flow in the trabecular meshwork outflow pathways. *Prog. Mol. Biol. Transl. Sci.* **2015,** *134*, 301-314.

30.   Peters, J. C.; Bhattacharya, S.; Clark, A. F.; Zode, G. S. Increased Endoplasmic Reticulum Stress in Human Glaucomatous Trabecular Meshwork Cells and Tissues. *Invest. Ophthalmol. Vis. Sci.* **2015,** *56*, 3860-3868.

31.   Doh, S. H.; Kim, J. H.; Lee, K. M.; Park, H. Y.; Park, C. K. Retinal ganglion cell death induced by endoplasmic reticulum stress in a chronic glaucoma model. *Brain Res.* **2010,** *1308*, 158-166.

3. Second Generation Grp94-selective Inhibitors Provide Opportunities for the Inhibition of Metastatic Cancer

Introduction

The 90 kDa heat shock protein (Hsp90) family is responsible for the maturation of nascent polypeptides and the re-maturation of denatured proteins. Hsp90 has gained considerable interest as a therapeutic target, because Hsp90-dependent proteins, clients, are directly associated with all ten hallmarks of cancer.[1-2] Therefore, inhibition of Hsp90 results in simultaneous disruption of multiple oncogenic pathways that are essential to cancer progression via a single molecular target. Seventeen small molecule Hsp90 inhibitors have progressed into clinical trials for the treatment of various forms of cancer.[3-4] Unfortunately, these inhibitors have produced various toxicities that have dampened enthusiasm for Hsp90 as a therapeutic target.[5-6] All of these clinical candidates are *pan*-Hsp90 inhibitors and target all four Hsp90 isoforms with similar affinity, which has been suggested to cause some on-target toxicities, such as cardiotoxicity, gastrointestinal toxicity, and ocular toxicity.[7] In addition to these toxicities, *pan*-Hsp90 inhibition induces the pro-survival heat shock response (HSR).[8] The HSR induces the expression of various heat shock proteins, including Hsp90, which results in significant dosing and scheduling issues in the clinic. Therefore, alternative approaches toward Hsp90 inhibition are needed to overcome the potential liabilities associated with *pan*-Hsp90 inhibition.

One approach that has gained considerable interest in recent years is the development of Hsp90 isoform-selective inhibitors.[7, 9-12] The Hsp90 protein family is composed of four isoforms: Hsp90α and Hsp90β reside in the cytosol, TRAP1 is localized to the mitochondria, and Grp94 is found in the endoplasmic reticulum. Grp94 is responsible for the maturation and trafficking of proteins associated with cell signaling and motility.[13] Some Grp94-dependent proteins have been identified

and include some Toll-like receptors, select integrins, IGF-I and -II, LRP6, and mutant myocilin.[13-16] Consequently, Grp94 has been implicated for the treatment of disease states that include metastatic cancer (integrins), glaucoma (mutant myocilin), multiple myeloma (LRP6), and hepatocellular carcinoma (reliance upon a functional ER chaperone system).[10, 14-15, 17] While Grp94 is essential during embryonic development, it is non-essential in developed organisms.[18] Therefore, Grp94 inhibition could provide a therapeutic opportunity that exhibits fewer toxic liabilities than *pan*-Hsp90 inhibition for the treatment of some diseases (e.g. glaucoma). In contrast, some disease states rely more heavily upon a functional ER chaperone system, such as multiple myeloma and hepatocellular carcinoma, wherein Grp94 knockouts decrease the viability of these cancers, highlighting Grp94 as a potential target for these cancers (discussed further in Chapter 4). The development of Hsp90 isoform-selective inhibitors is hindered by >85% identity within the N-terminal ATP-binding site of all four isoforms, which poses a significant challenge to the rational design of Hsp90 isoform-selective inhibitors.[19-21]

Second Generation Grp94-selective Inhibitor Design

The nucleotide binding site of Grp94 is most unique among the four isoforms, due to a five amino acid insertion into its primary sequence which results in secondary binding pockets that can be exploited for selective inhibition. The first Grp94-selective inhibitor was developed via incorporation of a *cis*-amide bioisostere into the **RDA** scaffold (**1**, **Figure 3.1**) to predispose the side chain into the Grp94-exclusive S1 sub-pocket, ultimately leading to the development of **BnIm** (**2**, **Figure 3.1**), which manifested ~12-fold selectivity via a fluorescence polarization assay.[22] Subsequent structure-activity relationship studies on the benzyl side chain of **2** resulted in the development of **KUNG29** (**3**), which exhibited improved affinity and selectivity for Grp94 as compared to **2** (**Figure 3.1**).[10] Interestingly, substitutions at the 2-position of the benzyl side chain
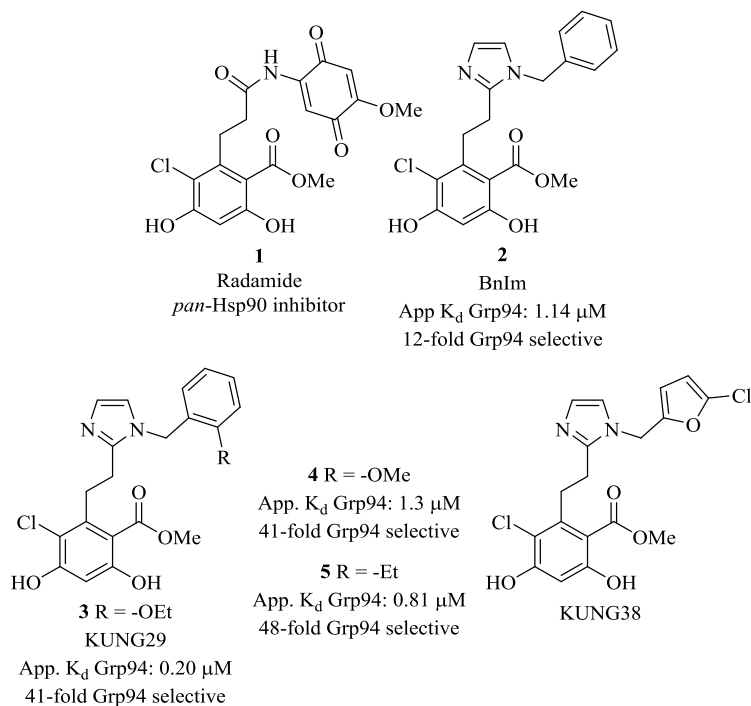
Figure 3.1. First generation Grp94-selective inhibitors.

(**3**-**5**) manifested the greatest Grp94-selectivity (**Figure 3.1**), and suggested that projection of the side chain into this region could improve selectivity. Analysis of the co-crystal structure of **KUNG38** bound to Grp94 suggested that modification of the *cis*-amide bioisostere (imidazole) could orient the side chain to mimic substitutions present in **3-5** and increase both selectivity and affinity.

Replacement of the first generation imidazole with a phenyl ring was hypothesized to serve multiple purposes: **1**) The larger 6-membered ring would reduce the angle between the benzyl side chain and the resorcinol moiety (**Figure 3.2a**) and mimic the binding mode of **3-5** to improve selectivity; **2**) Removal of the polar nitrogen atoms within the imidazole ring could improve interactions with the more hydrophobic binding site present in Grp94 (**Figure 3.2b**);[23] and **3**) The phenyl ring could provide a synthetic handle to identify substituents that interact with polar residues at the solvent exposed region without participation in the extensive hydrogen bond network present in Hsp90 (**Figure 3.2c**). The ortho-substituted phenyl derivative, **6**, reduced the

110
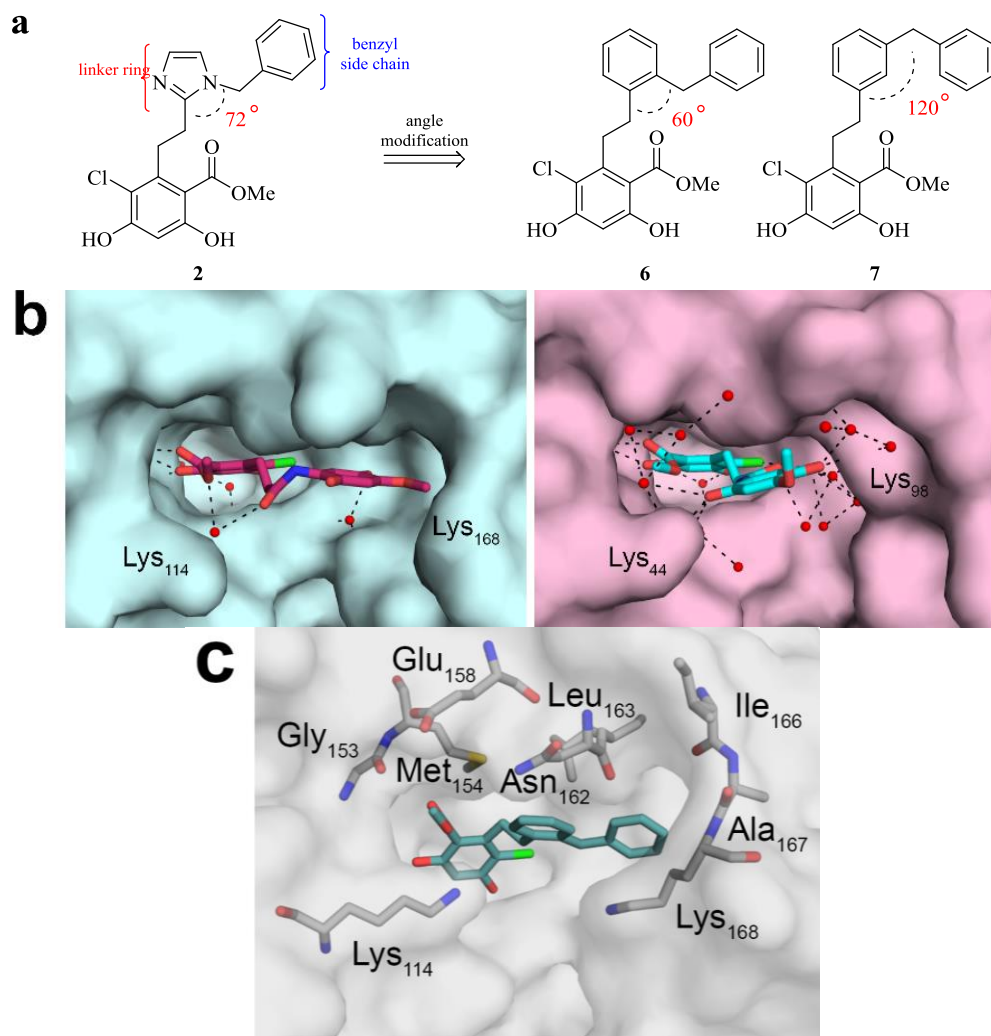
Figure 3.2. Rational design for second generation Grp94-selective inhibitors. (**a**) Replacement of the *cis*-amide linker to decrease (**6**) and increase (**7**) the angle between the benzylic side chain and the resorcinol moiety. (**b**) The water mediated hydrogen bonding network in Hsp90 (right, PDBID: 2FXS) is much more extensive than that of Grp94 (left, PDBID: 2GFD, *trans*-RDA omitted for clarity). (**c**) **6** docked into Grp94 (PDBID: 5IN9) demonstrating that polar residues are present in the region which the linker is proposed to bind can be utilized to increase affinity for Grp94.

angle between the resorcinol moiety and the benzyl side chain (~72˚→ ~60˚), which can mimic 2-substitutions on the benzyl side chain of the first generation Grp94 inhibitors and potentially improve Grp94 selectivity. Alternatively, the meta-substituted phenyl derivative **7** increased the angle between these two substituents (~72˚ → ~120˚), which should reduce Grp94 affinity and selectivity due to steric limitations that result from the backbone carbonyl of Asn162. Herein, the

synthesis and biological evaluation of Grp94-selective inhibitors with replacements for the *cis*-amide bioisostere linker is reported.

Synthesis and Biochemical Evaluation of Second Generation Grp94-selective Inhibitors

Synthesis of the designed analogues, **6** and **7**, was envisioned to occur via a Heck coupling between aryl bromide **8** and 2- or 3-benzylstyrene (**9a** and **9b**, respectively), followed by hydrogenolysis of the benzyl ethers and concomitant reduction of the alkene. This synthetic route allowed for late-stage diversification and provided access to various analogues in a succinct manner (**Scheme 3.1**). Aryl bromide **8** was synthesized from 1-bromo-3,5-dimethoxybenzene in 6 steps, 28% overall yield, and required only one chromatographic separation. The methyl ethers of

Scheme 3.1. Synthesis 2nd Generation Grp94-Selective Inhibitors of **6** and **7**.
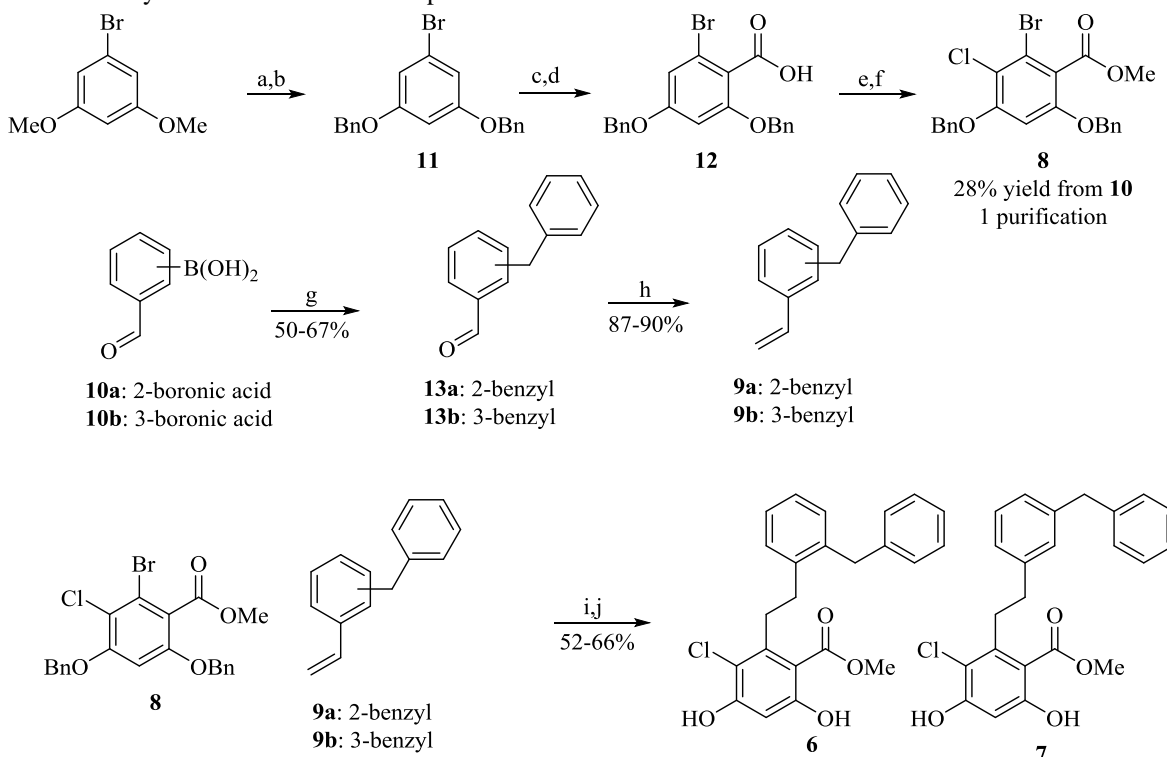
Conditions: (**a**) Py HCl, 220°C; (**b**) BnBr, K$_2$CO$_3$, DMF; (**c**) AgOTf, 1,1-dichloromethyl methyl ether, DCM, -78°C; (**d**) NaClO$_2$, NaH$_2$PO$_4$, 2-methyl-2-butene/^{t}BuOH/H$_2$O; (**e**) LiOH, Me$_2$SO$_4$, THF; (**f**) SO$_2$Cl$_2$, THF, <-30°C; (**g**) BnBr, Pd(PPh$_3$)$_4$, K$_2$CO$_3$; (**h**) MePh$_3$P$^+$Br$^-$, ^{n}BuLi; (**i**) **9a-9b**, Pd(OAc)$_2$, triethanolamine; (**j**) H$_2$, Pd/C, EtOAc

112

1-bromo-3,5-dimethoxybenzene were cleaved via pyridinium hydrochloride, which provided the free phenols after an acidic workup. The phenols were subsequently converted to the benzyl ethers (**11**) upon treatment with benzyl bromide and potassium carbonate. Silver-promoted formylation of **11** and subsequent Pinnick oxidation yielded benzoic acid **12**.[24] Conversion of **12** to the corresponding methyl ester was achieved upon exposure to dimethyl sulfate followed by regioselective chlorination upon reaction with sulfuryl chloride at -30˚C, which provided the desired resorcinol **8** (**Scheme 3.1**).[25] Synthesis of **9a** and **9b** commenced via a palladium-catalyzed cross coupling reaction between commercially available 2- and 3-formylphenyl boronic acid and benzyl bromide to provide the corresponding 2- and 3-benzylbenzaldehydes (**13a** and **13b**, respectively). Subsequent Wittig olefination afforded the 2- and 3-benzylstyrenes (**9a** and **9b**, respectively), which were then subjected to Heck olefination conditions with aryl bromide **8**.[26] Hydrogenolysis of the benzyl ethers and reduction of the olefin under a hydrogen atmosphere provided the desired analogues **6** and **7** (**Scheme 3.1**).

Table 3.1. Evaluation of **6** and **7** via a fluorescence polarization assay against Grp94 and Hsp90α.
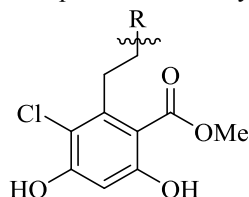
Entry	R	Apparent K_d Grp94 (µM)	Apparent K_d Hsp90α (µM)	Fold Selective for Grp94
2		1.15 ± 0.1	13.1 ± 1.1	12
6		0.63 ± 0.03	20.7 ± 0.5	32
7		10.4 ± 0.2	>100[a]	>10

[a] 100 µM was the highest concentration tested. Apparent K_d values are the average of two independent experiments ± SEM.

Compounds **6** and **7** were evaluated via a fluorescence polarization assay to determine Grp94 affinity and selectivity.[27] As seen in **Table 3.1**, **6** produced an apparent K_d of 0.63 µM along with 32-fold selectivity for Grp94 over Hsp90α, which represented ~2-fold improvement over **2**. In contrast, **7** exhibited a significant reduction in both affinity and selectivity (apparent $K_d = 10.4$ µM and >10-fold selective) for Grp94. These data suggested that reduction of the angle between the resorcinol moiety and the benzyl side chain was beneficial for Grp94 affinity and selectivity. Therefore, structure-activity relationship studies were performed on the phenyl linker of **6** to probe interactions between the phenyl ring and polar residues surrounding this linker.

Scheme 3.2. Synthesis of **16-24** possessing hydrogen bond donating and accepting group substituted linkers.

10c: 5-OMe **13c**: 5-OMe **9c**: 5-OMe
10d: 4-OMe **13d**: 4-OMe **9d**: 4-OMe

14d **13h** **9h**

14a: 3-OMe **13e**: 3-OMe **9e**: 3-OMe
14b: 5-NO₂ **13f**: 5-NO₂ **9f**: 5-NO₂
14c: 4-NO₂ **13g**: 4-NO₂ **9g**: 4-NO₂

15a: 5-OH **13i**: 5-OBn **9i**: 5-OBn
15b: 4-OH **13j**: 4-OBn **9j**: 4-OBn
15c: 3-OH **13k**: 3-OBn **9k**: 3-OBn

8 **16-24**

16: 5-OMe
17: 4-OMe
18: 3-OMe
19: 5-NH₂
20: 4-NH₂
21: 3-pyridyl
22: 5-OH
23: 4-OH
24: 3-OH
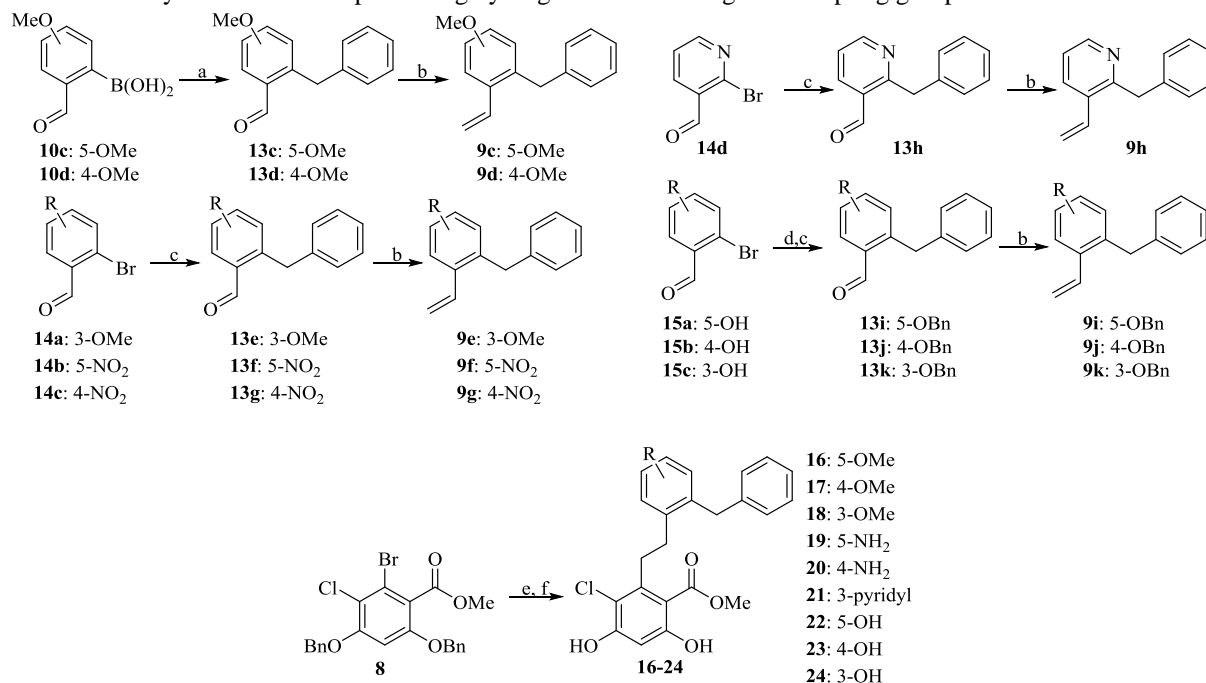
Conditions: (**a**) BnBr, Pd(PPh₃)₄, K₂CO₃; (**b**) MePh₃P⁺Br⁻, ⁿBuLi; (**c**) Potassium benzyltrifluoroborate, Pd(OAc)₂, RuPhos, K₃PO₄; (**d**) BnBr, K₂CO₃; (**e**) **9c-9k**, Pd(OAc)₂, triethanolamine; (**f**) H₂, Pd/C.

As seen in **Figure 3.2c**, the linker was proposed to bind adjacent to polar residues (Glu158 and Asn162) at the solvent exposed region of the binding pocket. Therefore, hydrogen bond donors and acceptors were incorporated onto the linker to improve Grp94 affinity. In addition, a pyridine ring (in lieu of the phenyl linker) was included to investigate the electronic nature of the linker.

Both **9c** and **9d** were synthesized using similar conditions to **9a** and **9b** as outlined in **Scheme 3.1**. As shown in **Scheme 3.2**, commercially available aryl bromides **14a-d** and **15a-c** were subjected to a palladium-catalyzed cross coupling reaction with potassium benzyltrifluoroborate, RuPhos, and palladium (II) acetate to provide benzaldehydes **13e-k**. Conversion of benzaldehydes **13e-k** to the corresponding styrenes **9c-k** was achieved via a Wittig reaction with methyltriphenylphosphonium bromide and *n*-butyllithium. The corresponding alkenes were then subjected to a Heck reaction with **8**, followed by simultaneous cleavage of the benzyl ethers and reduction of the alkene via hydrogen gas and palladium on carbon to provide analogues **16**-**24**.
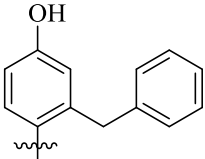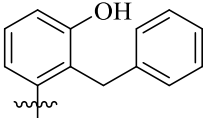
Under hydrogenation conditions, the nitro group was also reduced to the corresponding aniline (**19** and **20**) and hydrogenolysis of the benzyl ethers present on the linker ring produced the free phenols, **22-24**.

Data obtained via a fluorescence polarization assay with these compounds (**Table 3.2**) suggested that incorporation of hydrogen bond acceptors (16-18) did not significantly improve affinity (apparent Kd's = 0.45-0.73 μM). However, hydrogen bond donors (19, 20, 22-24) did improve Grp94 affinity and these compounds exhibited apparent Kd values between 0.24-0.54 μM. Unfortunately, both hydrogen bond acceptors and donors produced a significant loss in Grp94 selectivity. Of these analogues, 18 manifested the highest selectivity (19-fold), which was considerably less than analogue 6 (32-fold selective). Replacement of the phenyl ring with a pyridine linker (21) substantially increased affinity (apparent Kd = 0.18 μM) as compared to 6; however this substitution also produced high affinity for Hsp90α (0.16 μM) and resulted in no selectivity between these two isoforms.

Table 3.2. Evaluation of **16-24** via a fluorescence polarization assay against Grp94 and Hsp90α.
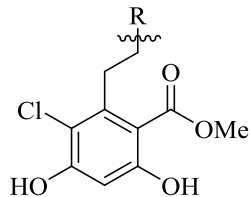
Entry	R	Apparent K_d Grp94 (µM)	Apparent K_d Hsp90α (µM)	Fold Selective for Grp94
6		0.63 ± 0.03	20.7 ± 0.5	32
16		0.45 ± 0.04	2.2 ± 0.2	5
17		0.68 ± 0.04	2.6 ± 0.6	4
18		0.73 ± 0.1	13.7 ± 1.4	19
19		0.28 ± 0.04	1.0 ± 0.1	4
20		0.24 ± 0.04	0.34 ± 0.07	n/a
21		0.18 ± 0.01	0.16 ± 0.02	n/a
22		0.30 ± 0.03	2.1 ± 0.1	7

Entry	R	Apparent K_d Grp94 (µM)	Apparent K_d Hsp90α (µM)	Fold Selective for Grp94
23		0.33 ± 0.01	0.92 ± 0.03	3
24		0.54 ± 0.02	2.0 ± 0.2	4

Apparent K_d values are the average of two independent experiments $\pm$ SEM. n/a = non-selective

Due to the low selectivity produced by **16-24**, additional structure-activity relationship studies were sought to improve both Grp94 selectivity and affinity. **16-24** were synthesized to contain the benzyl side chain of **2** to rapidly evaluate modifications about the linker as the side chain of **2** was previously optimized to achieve >40-fold Grp94-selectivity (see **Figure 3.1**). Incorporation of the Grp94-selective 2-ethoxy- and 2-methoxybenzyl side chains (**3** and **4**) to analogues with a phenyl linker were proposed to further increase Grp94 selectivity. Synthesis of **25** and **26** was achieved through a route similar to that utilized to construct **6** (**Scheme 3.3**). Upon their preparation, these

Scheme 3.3. Synthesis of side chain substituted analogues **25-31**.

13l: 2-OEt
13m: 2-OMe
13n: 2-Cl
13o: 3-Cl
13p: 4-Cl
13q: 4-F

9l: 2-OEt
9m: 2-OMe
9n: 2-Cl
9o: 3-Cl
9p: 4-Cl
9q: 4-F

25: 2-OEt
26: 2-OMe
27: 2-Cl
28: 3-Cl
29: 4-Cl
30: 4-F
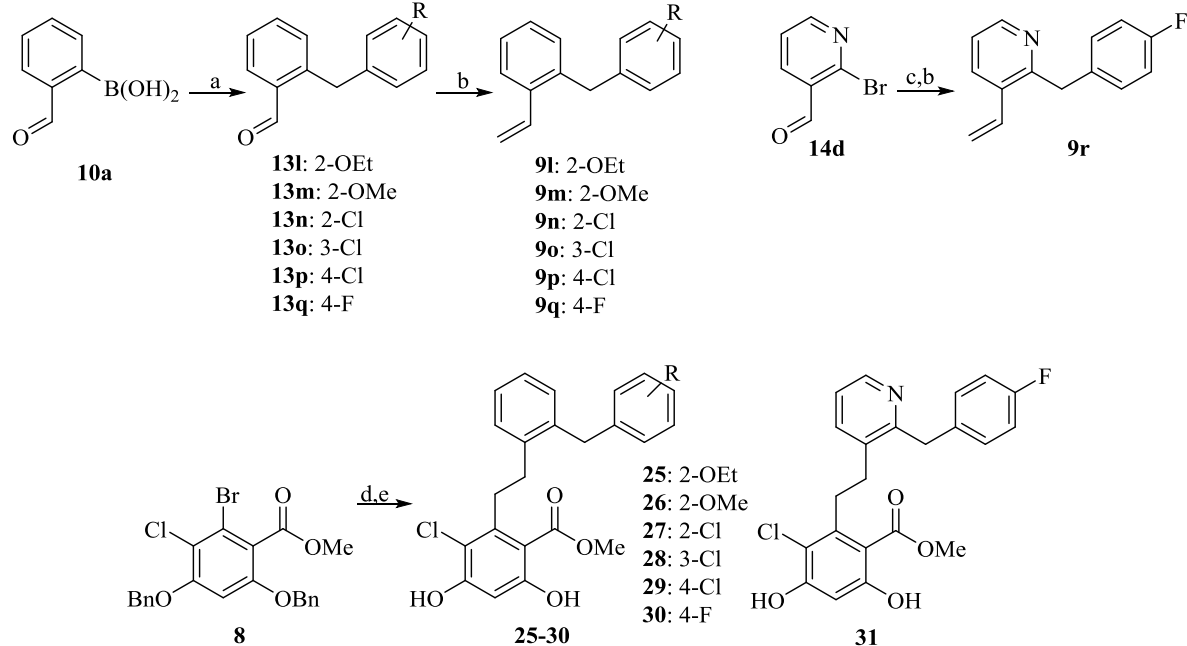
Conditions: (**a**) Pd(PPh$_3$)$_4$, K$_2$CO$_3$, benzyl bromides; (**b**) MePh$_3$P$^+$Br$^-$, ^{n}BuLi; (**c**) Pd(dppf)Cl$_2$, K$_3$PO$_4$, 4-fluorobenzylboronic acid pinacol ester; (**d**) Pd(OAc)$_2$, **9l-9r**, triethanolamine; (**e**) H$_2$, Pd/C.

analogues were evaluated via fluorescence polarization, and demonstrated low affinity (apparent

$K_d = 6.1\,\mu M$ and $7.8\,\mu M$, respectively, **Table 3.3**). The loss in affinity exhibited by **25** (compared

to **3**) suggests the phenyl linker does not bind in a similar manner compared to the first generation

imidazole-linked inhibitors. Therefore, a chloride scan was performed to identify an optimal side

chain for the phenyl-linked analogues. Synthesis of **27-29** was performed in a manner similar to

that used for **25** (**Scheme 3.3**). Once prepared, these analogues were evaluated for Grp94 affinity

and selectivity via the fluorescence polarization assay, and as shown in **Table 3.3**, **27** and **29**

manifested >18- and >24-fold selectivity for Grp94, respectively. However, this gain in selectivity

was accompanied by ~10-fold reduction in Grp94 affinity as compared to **6**, which suggests a

potential steric clash between the chloride-substituted side chains and the hydrophobic pocket of

Grp94. Due to the size difference between the hydrogen of **6** and the chloride of **29**, a fluoride was

incorporated into the 4-position of the side chain to reduce detrimental steric interactions.

Gratifyingly, **30** produced an apparent K_d of $0.54\,\mu M$ and was 73-fold selective for Grp94. The

smaller fluoride substitution (compared to the chloride of **29**) appears to minimize steric

interactions with the hydrophobic pocket and provide a small increase in Grp94 affinity as

compared to **6**.

Table 3.3. Evaluation of **25-31** via a fluorescence polarization assay against Grp94 and Hsp90α.
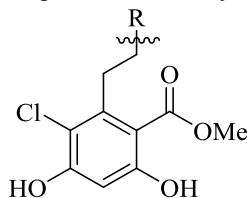
Entry	R	Apparent K_d Grp94 (μM)	Apparent K_d Hsp90α (μM)	Fold Selective for Grp94
6		0.63 ± 0.03	20.7 ± 0.5	32

Entry	R	Apparent K_d Grp94 (μM)	Apparent K_d Hsp90α (μM)	Fold Selective for Grp94
25	OEt	6.1 ± 0.3	>100[a]	>16
26	OMe	7.8 ± 0.4	>100[a]	>13
27	Cl	5.5 ± 0.1	>100[a]	>18
28	Cl	11.9 ± 1.8	44.6 ± 2.0	4
29	Cl	4.2 ± 0.7	>100[a]	24
30	F	0.54 ± 0.05	39.2 ± 2.7	73
31	F	0.36 ± 0.02	0.46 ± 0.03	n/a

[a] 100 μM was the highest concentration tested. Apparent K_d values are the average of two independent experiments ± SEM. n/a = non-selective

Efforts to combine the high affinity produced by the linker of **21** and increased selectivity exhibited by the side chain **30** were pursued in the form of **31**. Synthesis of **31** was accomplished via a palladium-catalyzed cross coupling reaction between **14d** and 4-fluorobenzylboronic acid pinacol ester (**32**)[28] to provide aryl aldehyde **13r**, which was then converted to the corresponding styrene **9r**. A Heck coupling reaction between **9r** and **8** followed by hydrogenolysis of the benzyl ethers and reduction of the alkene provided **31** (**Scheme 3.3**). Evaluation of **31** against Grp94 and Hsp90α via fluorescence polarization gave apparent K_d values of 0.36 μM and 0.46 μM, respectively. Ultimately, the 4-fluoro side chain produced ~2-fold loss in Grp94 affinity (compared to **21**) and a complete loss of selectivity. These data suggest the pyridine linker oriented the side

chain towards the solvent exposed region of the binding pocket in order to avoid repulsive interactions between the pyridine nitrogen and the hydrophobic S1 sub-pocket of Grp94.

Crystallization of 6, 21, and 30 with Grp94 Provides Rationale for Increased Selectivity

Crystal structures of the Grp94 N-terminal domain in complex with **6**, **21**, and **30** revealed binding modes that can explain differences in their selectivity and affinity profiles, as well as the binding interactions for similar compounds within this series (**Figure 3.3a**, **c**, and **e**). The resorcinol ring was anchored within the N-terminal ATP-binding site through direct interactions with Asp149 and Thr245, and a hydrogen bonding network with water molecules (**Figure 3.3b**, **d**, and **f**).[10, 23] Interestingly, **6** and **30** were best modeled via two partially occupied binding modes. The first, termed "benzyl in", aligns with the previously observed binding mode of the first generation Grp94-selective inhibitor, **KUNG38** (PDBID: 5IN9), wherein the benzylic side chain is oriented towards the Grp94-exclusive S1 sub-pocket.[10] When crystallized with **6**, Grp94 loop residues 167-170 which make up a portion of the aforementioned unique binding region, appeared disordered, suggesting that interactions between this loop and the unsubstituted terminal benzene ring of **6** were not stabilizing (**Figure 3.3a**). Alternatively, when crystallized with **30**, the main chain of these loop residues could be built into visible electron density, suggesting that the hydrophobic
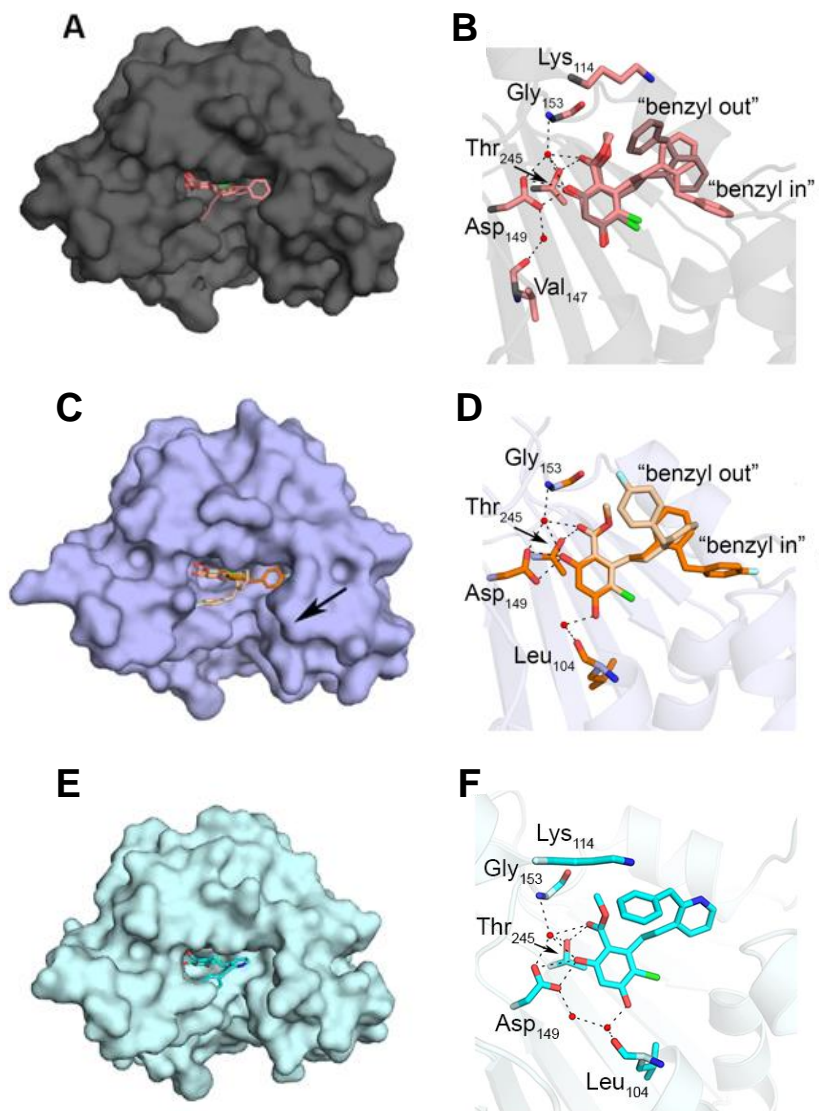
Figure 3.3. Crystal structures of **6** (**a** and **b**, PDBID: 6AOM), **30** (**c** and **d**, PDBID: 6AOL), and **21** (**e** and **f**) bound to Grp94. (**a, c, e**) Surface representation of nucleotide binding pocket of Grp94 occupied by **6** (**a**), **30** (**c**), and **21** (**e**) which are shown as ball and stick. Alternate conformations of **6** and **30** are indicated by off-shade coloration. Arrow in (**c**) indicates loop stabilized at the mouth of the binding pocket through hydrophobic interactions with fluorine substituent of **30**. (**b, d, f**) Hydrogen-bond-mediated protein-inhibitor interactions (dashes) in nucleotide binding pocket between Grp94 and **6** (**b**), **30** (**d**), or **21** (**f**).

interactions mediated by the fluoride substituent stabilized these residues, leading to slightly improved Grp94 binding affinity (**Figure 3.3c**). The second binding mode, termed "benzyl out", positioned the benzyl side chain in the solvent-exposed region of the Grp94 binding pocket. The phenyl linker of **6** is rotated ~180° in this conformation compared to the "benzyl in" conformation,

which orients the terminal benzene ring into the vicinity of the ε-NH$_2$ of Lys114, suggesting a stabilized cation-π interaction (**Figure 3.3b**); direct confirmation of such an interaction is limited by the partial occupancy of **6** in this orientation, but appears likely. Alternatively, the phenyl linker of **30** only rotated ~90˚ and did not appear to orient the terminal benzene ring into position to form this interaction (**Figure 3.3d**). Since Lys114 is conserved amongst Hsp90 isoforms (Lys44 cytosolic Hsp90s), interactions with this residue will likely affect selectivity. In sum, the improved selectivity of **30** appears to result from decreased affinity for Hsp90 rather than a significant improvement in affinity for Grp94. Conversely, non-selective inhibitors, like **21**, appear to favor the binding mode in which Lys114/Lys44 forms a cation-π interaction. When crystallized with Grp94, **21** occupied only one conformation, which was similar to the "benzyl out" conformation (**Figure 3.3f**), and form a cation-π interaction with Lys114, providing some rationale for the increased affinity and non-selective binding profile of this inhibitor.

Integrins are Dependent on Grp94 for their Maturation and Trafficking to the Cell Surface

Integrins are essential to cellular adhesion and the activation of migration/invasion through promoting interactions between the intracellular actin cytoskeleton and the extracellular matrix.[29] Activation of integrin signaling promotes initiation of intracellular signaling pathways that alter gene expression, cell cycle regulation, and actin dynamics, ultimately resulting in cellular migration and invasion away from the primary tumor to form metastatic lesions.[30] Grp94 overexpression has been correlated with tumor aggressiveness and metastatic potential resulting in poor prognoses for patients with increased Grp94 expression.[31] Therefore, Grp94-selective inhibitors were evaluated for their ability to decrease the migration of aggressive cancer cell lines in a model of metastatic cancer. **BnIm, KUNG29**, **KUNG38** (see **Figure 3.1**), and **30** were

evaluated for their ability to decrease cell migration of the metastatic breast cancer cell line, MDA-MB-231.

Evaluation of Grp94-selective inhibitors in a wound healing scratch assay was used to determine the potential of Grp94 inhibitors as anti-metastatic agents. The first Grp94-selective inhibitor, **BnIm**, reduced cell migration against this cell line and led to 73% closure of the wound at 10µM after 24 h (**Figure 3.4**). First generation Grp94-selective inhibitors, **KUNG29** and **KUNG38**, exhibited similar effects (70% and 73%, respectively), but at 20-fold lower concentrations (0.5 µM).[10] Lastly, treatment with **30** resulted in only 40% wound closure at 0.5 µM (**Figure 3.4**). These anti-migratory activities occurred at concentrations well below the anti-proliferative activities of these compounds which, together, demonstrated that Grp94-selective inhibition results in an anti-migratory effect that is not due to decreased proliferation.
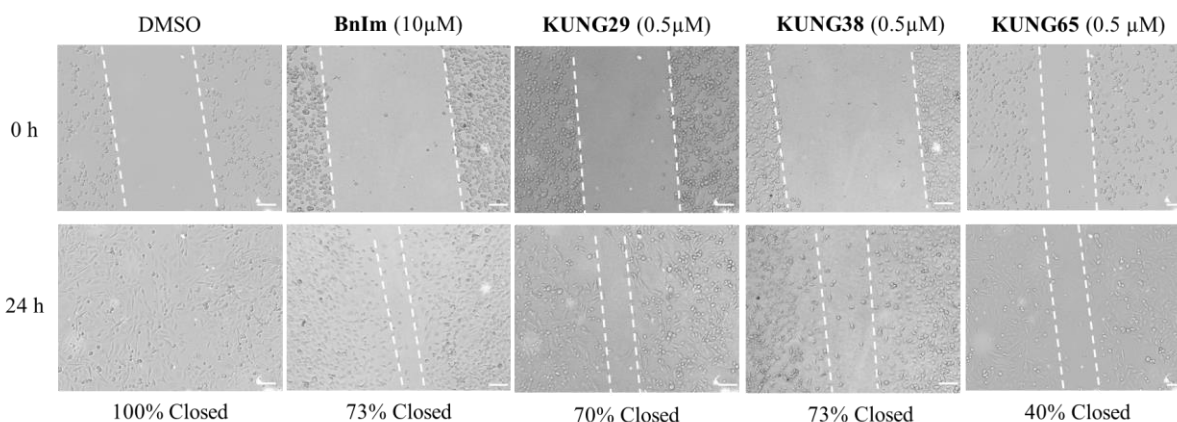
Figure 3.4. Grp94-selective inhibition reduces cellular migration of a metastatic breast cancer cell line (MDA-MB-231) after 24 h. Scale bar = 100 µm.

Based on these results, **30** was evaluated in other aggressive cancer cell lines to determine if Grp94-selective inhibition could be applicable to multiple types of cancer. As seen in **Figure 3.5**, **30** demonstrated a dose-dependent decrease in cell migration against aggressive prostate (PC3-MM2) and melanoma (SK-MEL-28) cell lines. PC3-MM2 cells were similarly susceptible to Grp94-selective inhibition as MDA-MB-231; however, SK-MEL-28 cells demonstrated a reduced
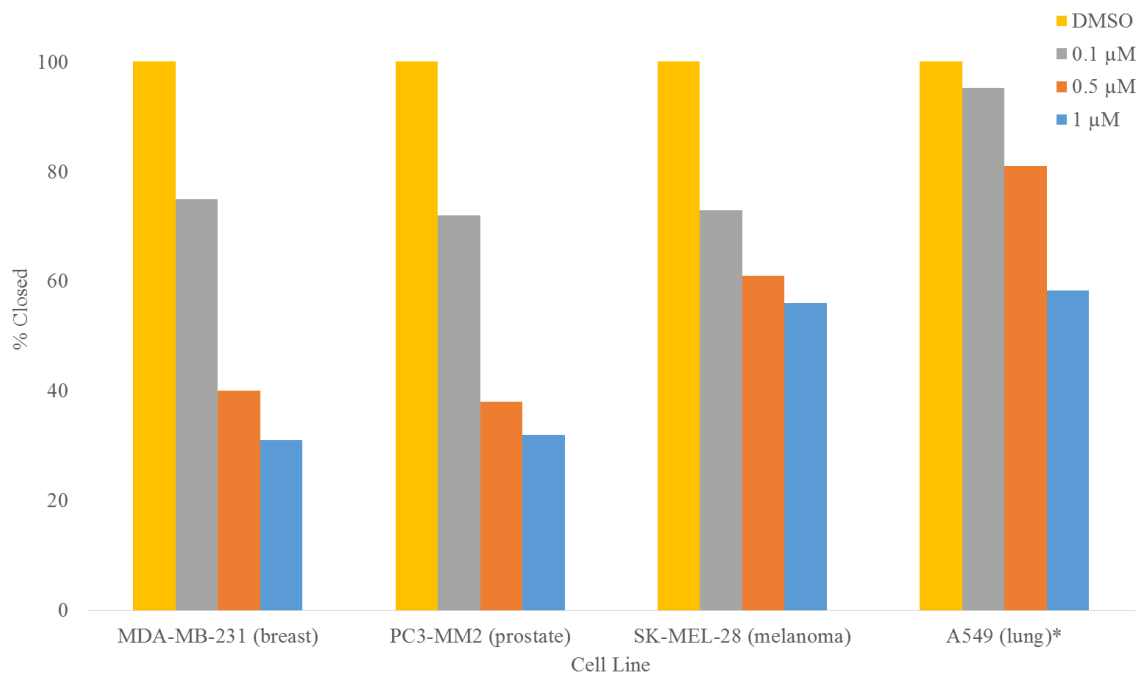
Figure 3.5. Compound **30** inhibits the migration of multiple aggressive cancer cell lines. *Due to the non-aggressive nature of the A549 cell line, the wound only closed 84% in vehicle treated cells. Data for inhibitor treated cells was normalized to the vehicle control = 100%.

susceptibility to Grp94 inhibition after 24 h which suggests that Grp94-dependent integrins are not the major contributor to cellular migration for this cell line. Together, these data suggest that Grp94-selective inhibition represents a new opportunity to inhibit cellular migration of multiple aggressive cell lines.

Increased integrin expression has been positively correlated with increased metastatic aggressiveness for lung squamous cell carcinoma, and therefore, Grp94 inhibition could reduce the metastatic potential of this cancer.[32-33] Grp94-selective inhibition with **30** was evaluated against a non-metastatic lung cancer cell line (A549) and demonstrated an anti-migratory effect at 0.5 µM; however this effect was reduced when compared to the highly metastatic breast, prostate, and melanoma cancers described above as a consequence of the non-aggressive nature of the A549 cell line (**Figure 3.5**). The limited efficacy of Grp94 inhibition in this non-aggressive cancer

suggests that the efficacy of Grp94-selective inhibition correlates directly with the aggressiveness nature of a cancer due to Grp94 overexpression in metastatic cancers.

Grp94-selective Inhibition Results in the Degradation of Integrin α2

The integrin α2 subunit is dependent upon Grp94 for its maturation and trafficking to the cell surface.[34] Integrin α2 is found as a heterodimer with the β1 integrin subunit and is responsible for binding collagen in the extracellular matrix, which promotes cancer metastasis and invasion.[35-36] Increased expression of integrin α2β1 has been reported in both primary and metastatic tissue samples of melanoma from patients, suggesting this cancer utilizes Grp94-dependent integrins to facilitate migration.[37] As shown in **Figure 3.6a**, treatment with first and second generation Grp94-
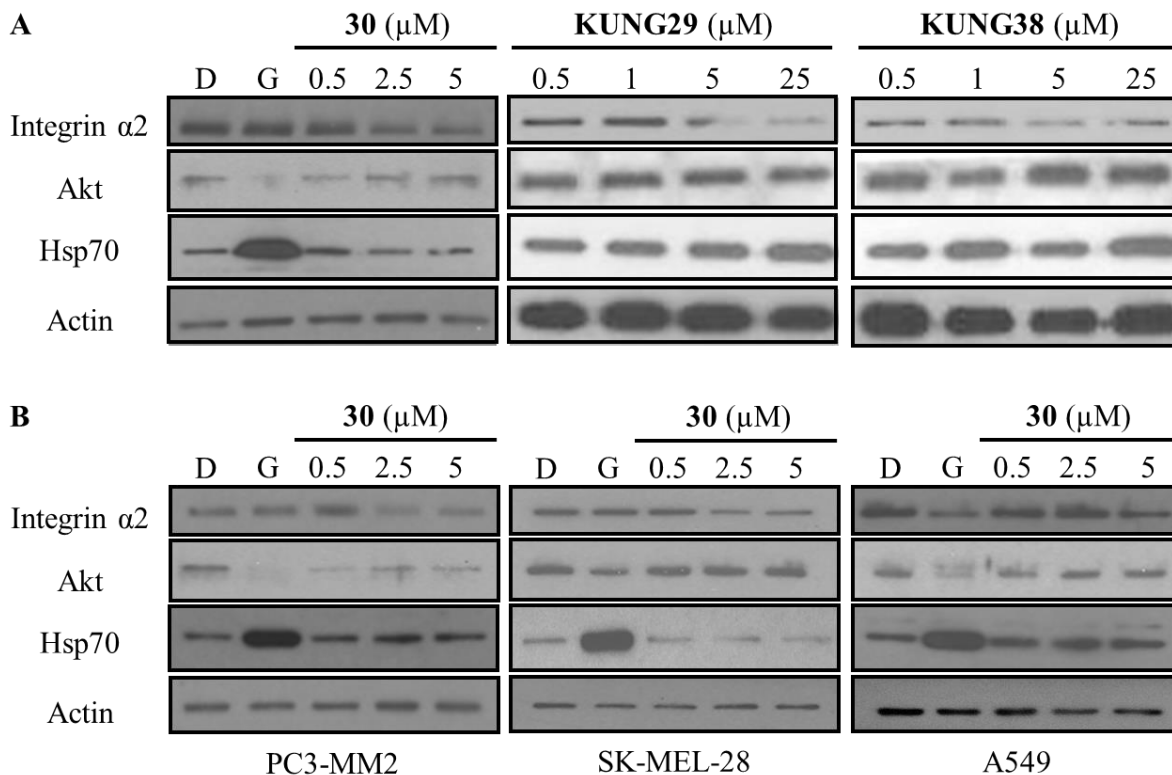
Figure 3.6. Western blot analysis for the Grp94-dependent client protein Integrin α2 after treatment with Grp94-selective inhibitors. (**a**) MDA-MB-231 breast cancer cell line and (**b**) PC3-MM2 (prostate), SK-MEL-28 (melanoma), and A549 (lung) cell lines. D = DMSO, G = geldanamycin, a natural product, *pan*-Hsp90 inhibitor (0.5 μM).

selective inhibitors induced the degradation of integrin α2 in the metastatic breast cancer cell line, MDA-MB-231. Compound **30** demonstrated integrin α2 degradation against other aggressive cell lines (PC3-MM2 and SK-MEL-28). Treatment with **30** also induced the degradation of integrin α2 in the non-aggressive lung cancer cell line A549; however, this effect was not observed until 5 μM, which correlated with the diminished anti-migratory activity exhibited against this cell line (**Figure 3.6b**). Importantly, treatment with Grp94-selective inhibitors did not induce the degradation of Akt, a cytosolic Hsp90-dependent protein, nor did it induce Hsp70 levels. This result contrasts the natural product *pan*-Hsp90 inhibitor geldanamycin (**G**, **Figure 3.6**), which induced the degradation of Akt and increased the levels of Hsp70 in all cell lines. These data demonstrate that these inhibitors selectively target Grp94 and induce the degradation of Grp94-specific client proteins without decreasing the levels of proteins that depend upon the cytosolic Hsp90 isoforms.

Conclusions & Future Directions

Incorporation of a phenyl linker, in lieu of the imidazole ring of **BnIm**, reduced the angle between the resorcinol moiety and the benzyl side chain and led to the identification of **6**, which manifests 0.64 μM Grp94 affinity and 32-fold Grp94 selectivity. Substitutions about the phenyl linker provided compounds with improved affinity; however, in all cases this improved affinity was accompanied by a loss in selectivity. Subsequent modification to the side chain revealed alternative binding modes between the first and second generation of Grp94-selective inhibitors. Structure-activity relationship studies on the side chain of **6** ultimately led to the discovery of **30**, which manifests 0.54 μM affinity and 73-fold selectivity for Grp94 versus other Hsp90 isoforms. Evaluation of first generation Grp94-selective inhibitors **BnIm**, **KUNG29** and **KUNG38**, as well as the second generation Grp94-selective inhibitor **30** in a wound healing scratch assay against

126

aggressive and metastatic cancers (MDA-MB-231, PC3-MM2, and SK-MEL-28) revealed that Grp94-selective inhibition decreased the migratory capabilities of these cells at 500 nM and induced the degradation of the Grp94-dependent protein, integrin α2. When combined, these data suggest that Grp94 inhibition may provide a suitable therapeutic option to reduce the migration/metastasis of many aggressive cancers. Further analysis of these Grp94-selective inhibitors against other aggressive types of cancer would be beneficial to expand the utility of this method for reducing cancer cell migration.

One common trait shared among both first and second generation Grp94-selective inhibitors is that when crystallized with Grp94, they generally adopt multiple conformations within the N-terminal ATP-binding site as a result of the rotational flexibility associated with the ethylene moiety between the resorcinol ring and the linker ring. Therefore, prevention of this flexibility will be beneficial during the development of more selective inhibitors. Furthermore, these inhibitors could utilize the S2 sub-pocket to gain additional selectivity for Grp94, as modifications to the resorcinol ring would project into the S2 sub-pocket. It is not well understood if occupation of both sub-pockets could provide an additive effect for Grp94-selective inhibition or if these pockets are mutually exclusive. The evaluation of such inhibitors would provide a better understanding of the structural requirements for Grp94 selectivity.

Experimental Section

Chemistry General. ^{1}H NMR were recorded at 400 (Bruker AVIIIHD 400 MHz NMR with a broadband X-channel detect gradient probe) or 500 MHz (Avance AVIII 500 MHz spectrometer with a dual carbon/proton cryoprobe), ^{19}F NMR were recorded at 376 MHz (Bruker AVIIIHD 400 MHz NMR equipped with a multinuclear broadband fluorine observe probe), and ^{13}C NMR were recorded at 125 MHz (Bruker AVIII spectrometer equipped with a cryogenically cooled carbon

observe probe); chemical shifts are reported in δ (ppm) relative to the internal standard (CDCl$_3$, 7.26 ppm for ^{1}H and 77.2 for ^{13}C). HRMS spectra were recorded with a LCT Premier with ESI ionization. All biologically tested compounds were determined to be >95% pure. TLC analysis was performed on glass backed silica gel plates and visualized by UV light. All solvents were reagent grade and used without further purification. Synthesis and characterization of compounds is provided in the supplemental information.

Synthetic Procedures
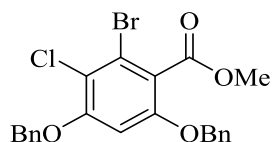
Methyl 4,6-bis(benzyloxy)-2-bromo-3-chlorobenzoate (**8**). 1-bromo-3,5-dimethoxybenzene (5g, 23 mmol, 1 equiv.) was added to a round bottom flask containing pyridinium hydrochloride (20 g, 173 mmol, 7.5 equiv.). The mixture was heated to 220 ˚C for 3h and poured in water (100 mL), diluted with EtOAc (200 mL). The aqueous layer was made acidic via the addition of 3N HCl (100 mL). The aqueous layer was extracted with EtOAc (3 x 100 mL). The organic layers were combined, dried over anhydrous Na$_2$SO$_4$, and concentrated and used as obtained. The residue was diluted in DMF (50 mL) followed by the addition of K$_2$CO$_3$ (11 g) and BnBr (4 mL). The mixture was stirred at rt for 14 h at which point water (200 mL) and EtOAc (300 mL) were added. The organic layer was washed with water (5 x 150 mL), brine (1 x 100 mL), dried over anhydrous Na$_2$SO$_4$, and concentrated to provide **11** as a white amorphous solid which was used without further purification. **11** was dissolved in dry DCM (150 mL) followed by the addition of AgOTf (12.6 g). The mixture was cooled to -78 ˚C and 1,1-dichloromethylmethyl ether (4.4 mL) was added dropwise over 5 min. The reaction mixture was stirred at -78 ˚C for 30 min followed by removal from the cold bath and quenched with sat'd NaHCO$_3$ (150 mL). The mixture was stirred

for 1 h at rt the filtered through a pad of celite. The aqueous layer was extracted with DCM (2 x 100 mL). The organic layers were combined, dried over Na_2SO_4, and concentrated. The residue obtained was used without further purification. The residue was dissolved in a mixture of ^tBuOH:2-methyl-2-butene-water (2:2:1) followed by the addition of $NaClO_2$ (2.4 g) and NaH_2PO_4 (4.7 g). The reaction was stirred at rt for 14 h and quenched with sat'd NaH_2PO_4 (100 mL). The aqueous layer was extracted with EtOAc (3 x 100 mL). The organic layers were combined, dried, and concentrated to provide crude **12**, which was used without further purification. **12** was dissolved in THF (200 mL) followed by the addition of LiOH (0.7 g) and Me_2SO_4 (1.5 mL) and stirred at 50 °C for 8 h (no starting material remaining). Sat'd NH_4Cl (200 mL) was added to the reaction mixture and stirred at 50 °C for 1 h, then cooled to rt, and the aqueous layer was extracted with EtOAc (3 x 100 mL). The organic layers were combined, dried, and concentrated. The resultant residue was dissolved in THF (150 mL) and cooled to -40 °C followed by the addition of SO_2Cl_2 dropwise over 15 min (temperature maintained < -30 °C during addition). The reaction was stirred at -40 °C for 30 min and quenched with sat'd NH_4Cl and extracted with Et_2O (3 x 100 mL). The organic layers were combined, dried, and concentrated. The residue was purified via flash chromatography (SiO_2, 15% EtOAc in Hexanes) to provide **8** was an off white amorphous solid (3 g, 28%). ^1H NMR (400 MHz, $CDCl_3$) δ 7.38-7.34 (m, 7H), 7.32 − 7.28 (m, H), 6.51 (s, 1H), 5.08 (s, 2H), 5.02 (s, 2H), 3.91 (s, 3H). ^{13}C NMR (126 MHz, $CDCl_3$) δ 166.3, 156.1, 155.0, 135.8, 135.6, 128.9 (2C), 128.8 (2C), 128.5, 128.4, 127.1 (2C), 127.0 (2C), 121.4, 121.0, 117.0, 99.6, 71.5, 71.3, 53.0. HRMS [M+H]$^+$ for $C_{22}H_{19}BrClO_4$ 461.0155, found 461.0143.

General Procedure for the synthesis of 13a-13d, 13l-13q

A microwave vial was charged with 2- or 3-formylphenyl boronic acids (**10a-d**, 1 equiv.), tetrakis(triphenylphosphine)palladium(0) (0.025 equiv.), benzyl bromide (**13a-13d**) or substituted

benzyl bromide (**13l-13q**) (1 equiv.) and sealed with a disposable Teflon lined cap. The tube was evacuated and purged with argon (3x) followed by the addition of THF (0.2 M) and 2M K_2CO_3 (3 equiv.). The reaction mixture was heated to 95 ˚C for 12 h, cooled to rt, and diluted with Et_2O (10 mL) and water (15 mL). The aqueous layer was extracted with Et_2O (3 x 10 mL). The organic layers were combined, dried, and concentrated. The resulting residue was purified via flash chromatography (SiO_2, 1:9 EtOAc:Hexanes) to provide the desired benzaldehydes (**13a-13d**, **13l-13q**).
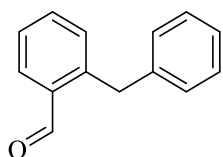
2-Benzylbenzaldehyde (**13a**). Clear oil (220 mg, 67%). ^{1}H NMR (400 MHz, CDCl$_3$) δ 10.26 (s, 1H), 7.87 (dd, J = 7.7, 1.5 Hz, 1H), 7.53 (td, J = 7.5, 1.5 Hz, 1H), 7.42 (t, J = 7.5 Hz, 1H), 7.29 – 7.24 (m, 3H), 7.23 – 7.17 (m, 1H), 7.15 (d, J = 7.6 Hz, 2H), 4.46 (s, 2H). ^{13}C NMR (126 MHz, CDCl$_3$) δ 192.8, 143.4, 140.7, 134.3, 134.3, 132.4, 132.1, 129.2 (2C), 129.0 (2C), 127.4, 126.7, 38.4. HRMS (ESI) [M+H]$^+$ for $C_{14}H_{13}O$ 197.0966, found 197.0976
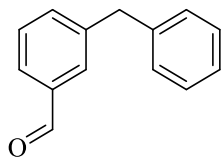
3-Benzylbenzaldehyde (**13b**). Clear oil (165 mg, 50%) ^{1}H NMR (400 MHz, CDCl$_3$) δ 9.98 (s, 1H), 8.01 – 7.91 (m, 1H), 7.72 (d, J = 2.3 Hz, 1H), 7.49 – 7.36 (m, 2H), 7.31 (ddd, J = 7.8, 6.5, 1.9 Hz, 2H), 7.20 (dd, J = 7.7, 6.1 Hz, 3H), 4.06 (d, J = 6.1 Hz, 2H). HRMS (ESI) [M+H]$^+$ for $C_{14}H_{13}O$ 197.0966, found 197.0963
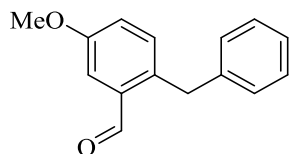
2-Benzyl-5-methoxybenzaldehyde (**13c**). Clear oil (230 mg, 73%). ^{1}H NMR (400 MHz, CDCl$_3$) δ 10.22 (s, 1H), 7.37 (d, J = 2.9 Hz, 1H), 7.27 – 7.21 (m, 2H), 7.17 (d, J = 8.0 Hz, 2H), 7.11 – 7.04 (m, 3H), 4.34 (s, 2H), 3.83 (s, 3H). ^{13}C NMR (126 MHz, CDCl$_3$) δ 191.6, 158.4, 140.6, 135.3, 134.5, 132.8, 128.5 (2C), 128.4 (2C), 126.1, 120.8, 113.9, 55.4, 36.9. HRMS (ESI) [M+Na]$^+$ for C$_{15}$H$_{14}$O$_2$Na 249.0892, found 249.0889
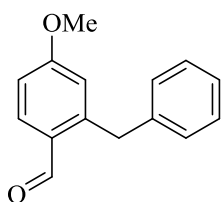
2-Benzyl-4-methoxybenzaldehyde (**13d**). Clear oil (470 mg, 75%). ^{1}H NMR (400 MHz, CDCl$_3$) δ 10.13 (s, 1H), 7.85 (d, J = 8.5 Hz, 1H), 7.29 (d, J = 7.3 Hz, 2H), 7.21 (dd, J = 17.3, 7.4 Hz, 3H), 6.91 (dd, J = 8.6, 2.5 Hz, 1H), 6.75 (d, J = 2.5 Hz, 1H), 4.45 (s, 2H), 3.86 (s, 3H). ^{13}C NMR (126 MHz, CDCl$_3$) δ 191.0, 164.0, 145.7, 140.1, 135.1, 128.9, 128.7, 127.7, 126.4, 117.3, 111.9, 108.6, 100.8, 55.6, 38.3. HRMS (ESI) [M+H]$^+$ for C$_{15}$H$_{15}$O$_2$ 227.1072, found 227.1062
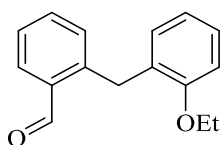
2-(2-Ethoxybenzyl)benzaldehyde (**13l**). Clear oil (275 mg, 43%) ^{1}H NMR (400 MHz, CDCl$_3$) δ 10.38 (s, 1H), 7.88 (dd, J = 7.7, 1.5 Hz, 1H), 7.49 (td, J = 7.5, 1.5 Hz, 1H), 7.42 – 7.33 (m, 1H), 7.31 – 7.25 (m, 2H), 7.18 (td, J = 7.8, 1.8 Hz, 1H), 7.04 – 6.92 (m, 1H), 6.90 – 6.80 (m, 2H), 4.41 (s, 2H), 4.03 (q, J = 7.0 Hz, 2H), 1.36 (t, J = 7.0 Hz, 3H). ^{13}C NMR (126 MHz, CDCl$_3$) δ 192.9,

156.7, 144.0, 134.4, 134.2, 131.8, 130.5, 130.4, 129.3, 128.1, 127.0, 120.8, 111.5, 63.9, 32.2, 15.2. HRMS (ESI) [M+H]$^+$ for C$_{16}$H$_{17}$O$_2$ 241.1229, found 241.1226

2-(2-Methoxybenzyl)benzaldehyde (**13m**). clear oil (230 mg, 51%) ^{1}H NMR (400 MHz, CDCl$_3$) δ 10.36 (s, 1H), 7.88 (dd, J = 7.7, 1.4 Hz, 1H), 7.53 − 7.46 (m, 1H), 7.37 (t, J = 7.5 Hz, 1H), 7.25 − 7.16 (m, 2H), 6.94 (dd, J = 7.4, 1.6 Hz, 1H), 6.91 − 6.82 (m, 2H), 4.40 (s, 2H), 3.81 (s, 3H). ^{13}C NMR (126 MHz, CDCl$_3$) δ 192.3, 156.8, 143.2, 133.9, 133.7, 131.2, 130.1, 129.9, 128.6, 127.6, 126.5, 120.5, 110.1, 55.1, 31.7. HRMS (ESI) [M+H]$^+$ for C$_{15}$H$_{15}$O 227.1076, found 227.1072
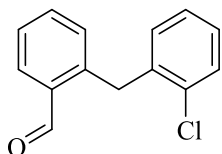
2-(2-Chlorobenzyl)benzaldehyde (**13n**). yellow oil (160 mg, 35%) ^{1}H NMR (400 MHz, CDCl$_3$) δ 10.23 (s, 1H), 7.89 (dd, J = 7.7, 1.5 Hz, 1H), 7.53 (ddd, J = 15.1, 8.1, 1.6 Hz, 2H), 7.46 − 7.38 (m, 2H), 7.20 − 7.10 (m, 3H), 7.02 (td, J = 8.5, 8.0, 7.0 Hz, 1H), 6.94 (dd, J = 7.2, 2.1 Hz, 1H), 4.56 (s, 2H). ^{13}C NMR (126 MHz, CDCl$_3$) δ 192.4, 141.4, 136.9, 133.9, 132.3, 130.9, 130.6, 129.4, 127.8, 127.0, 126.9, 119.7, 117.5, 35.6. HRMS (ESI) [M+H]$^+$ for C$_{14}$H$_{12}$ClO 231.0577, found 231.0581
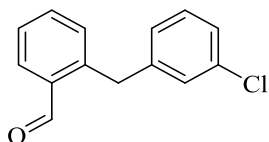
2-(3-Chlorobenzyl)benzaldehyde (**13o**). yellow oil (100 mg, 22%) ^{1}H NMR (400 MHz, CDCl$_3$) δ 10.19 (s, 1H), 7.86 (dd, J = 7.6, 1.5 Hz, 1H), 7.55 (td, J = 7.5, 1.6 Hz, 1H), 7.45 (td, J = 7.6, 1.2

Hz, 1H), 7.30 – 7.24 (m, 1H), 7.23 – 7.15 (m, 2H), 7.12 (d, J = 1.9 Hz, 1H), 7.07 – 7.01 (m, 1H), 4.43 (s, 2H). ^{13}C NMR (126 MHz, CDCl$_3$) δ 192.7, 142.4, 142.0, 134.5, 134.1, 134.0, 133.3, 131.9, 129.9, 129.0, 127.4, 127.2, 126.6, 37.9. HRMS (ESI) [M+H]$^+$ for C$_{14}$H$_{12}$ClO 231.0577, found 231.0574.
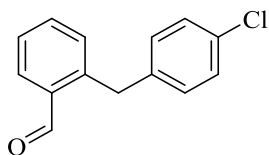
2-(4-Chlorobenzyl)benzaldehyde (**13p**). yellow oil (145 mg, 31%) ^{1}H NMR (400 MHz, CDCl$_3$) δ 10.19 (s, 1H), 7.85 (dd, J = 7.6, 1.5 Hz, 1H), 7.54 (td, J = 7.5, 1.6 Hz, 1H), 7.45 (dd, J = 7.5, 1.2 Hz, 1H), 7.26 (d, J = 1.7 Hz, 1H), 7.25 – 7.23 (m, 2H), 7.08 (d, J = 8.4 Hz, 2H), 4.42 (s, 2H). ^{13}C NMR (126 MHz, CDCl$_3$) δ 192.7, 142.4, 138.9, 134.1, 134.0, 133.3, 132.2, 131.8, 130.3 (2C), 128.8 (2C), 127.4, 37.7. HRMS (ESI) [M+Na]$^+$ for C$_{14}$H$_{12}$ClO 253.0396, found 253.0387.
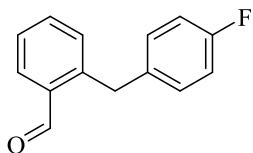
2-(4-Fluorobenzyl)benzaldehyde (**13q**). yellow oil (320 mg, 75%) ^{1}H NMR (400 MHz, CDCl$_3$) δ 10.21 (s, 1H), 7.85 (dd, J = 7.6, 1.5 Hz, 1H), 7.54 (td, J = 7.5, 1.6 Hz, 1H), 7.44 (td, J = 7.5, 1.2 Hz, 1H), 7.25 (d, J = 8.3 Hz, 1H), 7.11 (dd, J = 8.6, 5.5 Hz, 2H), 6.96 (t, J = 8.7 Hz, 2H), 4.42 (s, 2H). ^{19}F NMR (376 MHz, CDCl$_3$) δ -117.0 (s, 1F). ^{13}C NMR (126 MHz, CDCl$_3$) δ 192.7, 142.9, 134.1, 133.0, 131.9, 131.7, 131.2, 130.4, 130.3, 127.3, 122.1, 115.5, 115.4, 37.5. HRMS (ESI) [M+H]$^+$ for C$_{14}$H$_{12}$FO 215.0872, found 215.0880.

General procedure for the synthesis of **13e**-**13h**

A microwave vial was charged with aryl bromides (**14a**-**d**, 1 equiv.), potassium benzyltrifluoroborate (1.5 equiv.), palladium (II) acetate (0.08 equiv.), RuPhos (0.17 equiv.), and K_3PO_4 (5.2 equiv.). The tube was sealed with a disposable Teflon lined lid and evacuate and purged with argon (3x) followed by the addition of mixture of toluene:water (5:1, 0.1 M). The reaction mixture was heated to 115 °C for 16 h, cooled to rt, and diluted with water (10 mL) and EtOAc (20 mL). The aqueous layer was extracted with EtOAc (2 x 20 mL) and the organic layers were combined, dried, and concentrated. The resulting residue was purified via flash chromatography (SiO$_2$, 1:5 EtOAc:Hexanes) to provide the desired benzaldehydes (**13e**-**13h**).
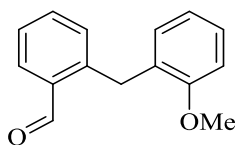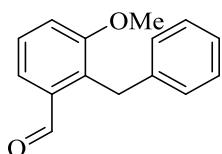

2-Benzyl-3-methoxybenzaldehyde (**13e**). clear oil (110 mg, 70%) ^{1}H NMR (400 MHz, CDCl$_3$) δ 10.30 (s, 1H), 7.50 (d, J = 7.7 Hz, 1H), 7.39 (t, J = 7.9 Hz, 1H), 7.28 – 7.19 (m, 2H), 7.15 (d, J = 7.1 Hz, 4H), 4.50 (s, 2H), 3.86 (s, 3H). ^{13}C NMR (126 MHz, CDCl$_3$) δ 192.3, 157.9, 140.5, 134.9, 131.5, 128.2, 128.2, 127.6, 125.8, 122.8, 121.3, 116.8, 115.9, 55.8, 29.4. HRMS (ESI) [M+Na]$^+$ for $C_{15}H_{15}O_2$ 249.0892, found 249.0890.
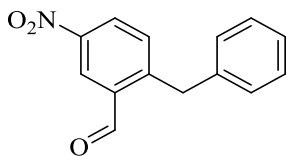
2-Benzyl-5-nitrobenzaldehyde (**13f**). yellow oil (180 mg, 32%) ^{1}H NMR (400 MHz, CDCl$_3$) δ 10.31 (s, 1H), 8.71 (d, J = 2.5 Hz, 1H), 8.34 (dd, J = 8.4, 2.5 Hz, 1H), 7.46 (d, J = 8.4 Hz, 1H), 7.34 – 7.28 (m, 2H), 7.27 – 7.21 (m, 1H), 7.13 (dd, J = 6.9, 1.8 Hz, 2H), 4.54 (s, 2H). ^{13}C NMR (126 MHz, CDCl$_3$) δ 190.1, 150.0, 138.6, 134.7, 133.0, 129.1 (2C), 128.9 (2C), 127.9, 127.1 (2C), 126.7, 38.2. HRMS (ESI) [M+H]$^+$ for $C_{14}H_{12}NO_3$ 242.0817, found 242.0823
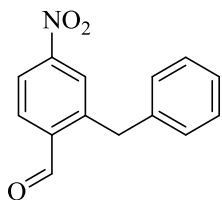
2-Benzyl-4-nitrobenzaldehyde (**13g**). yellow oil (245 mg, 58%) ^{1}H NMR (400 MHz, CDCl$_3$) δ 10.37 (s, 1H), 8.23 (dd, J = 8.5, 2.1 Hz, 1H), 8.13 (s, 1H), 8.05 (d, J = 8.4 Hz, 1H), 7.32 (t, J = 7.5 Hz, 2H), 7.26 (d, J = 4.7 Hz, 2H), 7.14 (d, J = 7.5 Hz, 2H), 4.53 (s, 2H). ^{13}C NMR (126 MHz, CDCl$_3$) δ 190.3, 150.4, 144.7, 138.4, 137.7, 132.3, 128.9, 128.6, 126.9, 126.3, 121.8, 37.7. HRMS (ESI) [M+H]$^+$ for C$_{14}$H$_{12}$NO$_3$ 242.0817, found 242.0825.
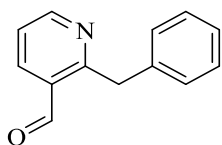
2-Benzylnicotinaldehyde (**13h**). clear oil (145 mg, 68%) ^{1}H NMR (400 MHz, CDCl$_3$) δ 10.34 (s, 1H), 8.77 (dd, J = 4.8, 1.7 Hz, 1H), 8.14 (dt, J = 7.9, 1.5 Hz, 1H), 7.37 (dd, J = 7.8, 4.9 Hz, 1H), 7.31 – 7.16 (m, 5H), 4.60 (s, 2H). ^{13}C NMR (126 MHz, CDCl$_3$) δ 190.8, 162.1, 153.5, 138.8, 138.3, 129.3, 128.6 (2C), 128.5 (2C), 126.5, 122.2, 40.9. HRMS (ESI) [M+H]$^+$ for C$_{13}$H$_{12}$NO 198.0919, found 198.0928.

General procedure for the synthesis of **13i-13k**.

Benzyl bromide (1.1 equiv.) was added to a stirred solution of **15a-15c** (1 equiv.) and K$_2$CO$_3$ (2.5 equiv.) in DMF (0.3 M). The reaction was stirred at rt for 13 h followed by the addition of water (30 mL) and EtOAc (40 mL). The organic layer was washed with water (5 x 30 mL) and brine (1 x 20 mL), dried, and concentrated. The resulting residue was passed through a filter column (SiO$_2$, 1:3 EtOAc:Hexanes) and used as obtained. The residue (1 equiv.) was dissolved in toluene (5 mL) and transferred to a microwave vial that was charged with potassium

benzyltrifluoroborate (1.5 equiv.), palladium (II) acetate (0.08 equiv.), RuPhos (0.17 equiv.), and K$_3$PO$_4$ (5.2 equiv.). The tube was sealed with a disposable Teflon lined lid and the solvent sparged with argon (10 min) followed by the addition of water (0.5 mL). The reaction mixture was heated to 115 ˚C for 16 h, cooled to rt, and diluted with water (10 mL) and EtOAc (20 mL). The aqueous layer was extracted with EtOAc (2 x 20 mL) and the organic layers were combined, dried, and concentrated. The resulting residue was purified via flash chromatography (SiO$_2$, 1:5 EtOAc:Hexanes) to provide the desired benzaldehydes (**13i**-**13j**).
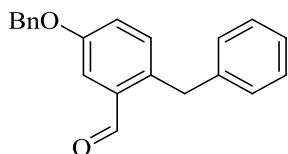
2-Benzyl-5-(benzyloxy)benzaldehyde (**13i**). clear oil (195 mg, 32%) ^{1}H NMR (400 MHz, CDCl$_3$) δ 10.24 (d, J = 1.6 Hz, 1H), 7.48 (q, J = 1.9 Hz, 1H), 7.47 – 7.38 (m, 5H), 7.35 (td, J = 6.8, 1.7 Hz, 1H), 7.31 – 7.25 (m, 1H), 7.19 (t, J = 7.0 Hz, 3H), 7.16 – 7.11 (m, 2H), 5.11 (s, 2H), 4.38 (s, 2H). ^{13}C NMR (126 MHz, CDCl$_3$) δ 191.6, 157.6, 140.6, 136.3, 135.6, 134.5, 132.9, 130.0, 128.6, 128.6, 128.5, 128.1, 127.4, 126.1, 123.6, 122.1, 121.5, 115.1, 113.1, 70.1, 37.0. HRMS (ESI) [M+H]$^+$ for C$_{21}$H$_{19}$O$_2$ 303.1385, found 303.1395
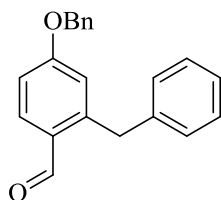
2-Benzyl-4-(benzyloxy)benzaldehyde (**13j**). clear oil (400 mg, 66%) ^{1}H NMR (400 MHz, CDCl$_3$) δ 10.11 (s, 1H), 7.82 (d, J = 8.6 Hz, 1H), 7.43 – 7.33 (m, 5H), 7.31 – 7.27 (m, 2H), 7.23 – 7.17 (m, 1H), 7.17 – 7.13 (m, 2H), 6.96 (dd, J = 8.6, 2.6 Hz, 1H), 6.80 (d, J = 2.5 Hz, 1H), 5.09 (s, 2H), 4.42 (s, 2H). ^{13}C NMR (126 MHz, CDCl$_3$) δ 190.8, 162.8, 145.6, 139.8, 135.8, 134.9, 128.7

(2C), 128.6 (2C), 128.5 (2C), 128.2, 127.5, 127.5 (2C), 126.2, 117.7, 112.6, 70.0, 38.1. HRMS (ESI) [M+H]$^+$ for C$_{21}$H$_{19}$O$_2$ 303.1385, found 303.1400
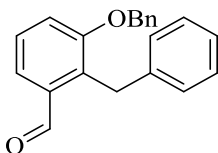
2-Benzyl-3-(benzyloxy)benzaldehyde (**13k**). clear oil (350 mg, 58%) ^{1}H NMR (400 MHz, CDCl$_3$) δ 10.32 (s, 1H), 7.54 – 7.47 (m, 2H), 7.37 – 7.31 (m, 3H), 7.29 – 7.25 (m, 2H), 7.23 – 7.20 (m, 2H), 7.19 – 7.10 (m, 4H), 5.10 (s, 2H), 4.55 (s, 2H). ^{13}C NMR (126 MHz, CDCl$_3$) δ 192.8, 157.5, 141.0, 136.9, 135.6, 132.5, 129.1, 128.9, 128.9, 128.7, 128.6, 128.4, 128.1, 127.9, 127.7, 127.4, 126.3, 123.6, 117.8, 71.0, 30.1. HRMS (ESI) [M+Na]$^+$ for C$_{21}$H$_{18}$O$_2$ 325.1205, found 325.1205.

General procedure for the synthesis of **9a-9r**.

n-butyllithium (2.5 M in hexanes, 1.3 equiv.) was added dropwise to a stirred solution of methytriphenylphosphonium bromide (1.5 equiv.) in dry THF (0.1M) at 0 ˚C. The mixture was stirred for 15 min before the addition of **13a-13r** (1 eq. in 2 mL THF). The reaction was stirred at rt for 8 h at which point water was added dropwise and the aqueous layer was extracted with EtOAc (2 x 10 mL). The combined organic layers were dried, concentrated, and purified via flash chromatography (SiO$_2$, 1:9 EtOAc:Hexanes) to provide the desired styrenes, **9a-9r**.
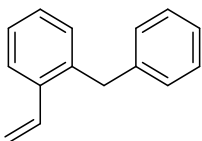
1-Benzyl-2-vinylbenzene (**9a**). clear oil (197 mg, 90%) ^{1}H NMR (400 MHz, CDCl$_3$) δ 7.56 – 7.52 (m, 1H), 7.32 – 7.22 (m, 4H), 7.22 – 7.17 (m, 1H), 7.13 (d, J = 7.5 Hz, 3H), 6.95 (dd, J = 17.4, 11.0 Hz, 1H), 5.64 (d, J = 17.2 Hz, 1H), 5.26 (dd, J = 10.9, 1.6 Hz, 1H), 4.09 (s, 2H). ^{13}C

NMR (126 MHz, CDCl$_3$) δ 141.0, 138.1, 137.4, 135.1, 130.8, 129.0 (2C), 128.8 (2C), 128.3, 127.1, 126.4, 126.3, 116.2, 39.4. HRMS (ESI) [M]$^+$ for C$_{15}$H$_{14}$ 194.1096, found 194.1104.
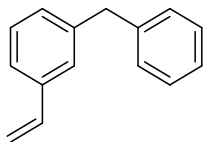
1-Benzyl-3-vinylbenzene (**9b**). clear oil (142 mg, 87%) ^{1}H NMR (400 MHz, CDCl$_3$) δ 7.38 – 7.30 (m, 2H), 7.28 (d, J = 7.5 Hz, 2H), 7.24 (d, J = 2.5 Hz, 2H), 7.22 – 7.17 (m, 3H), 7.12 – 7.06 (m, 1H), 6.69 (dd, J = 17.6, 10.9 Hz, 1H), 5.72 (d, J = 17.6 Hz, 1H), 5.24 (s, 1H), 3.98 (s, 2H). ^{13}C NMR (126 MHz, CDCl$_3$) δ 137.2, 129.3 (2C), 129.0, 128.9, 128.8 (2C), 128.8, 128.7, 127.3, 126.5, 126.3, 124.4, 114.2, 42.3. HRMS (ESI) [M+H]$^+$ for C$_{15}$H$_{14}$ 194.1096, found 194.1093.
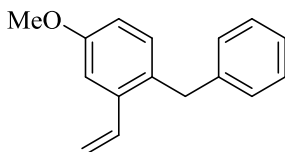
1-Benzyl-4-methoxy-2-vinylbenzene (**9c**). clear oil (217 mg, 95%) ^{1}H NMR (400 MHz, CDCl$_3$) δ 7.30 – 7.22 (m, 3H), 7.17 (t, J = 7.3 Hz, 1H), 7.14 – 7.03 (m, 4H), 6.90 (dd, J = 17.3, 10.9 Hz, 1H), 6.80 (dd, J = 8.4, 2.7 Hz, 1H), 5.63 (dd, J = 17.3, 1.3 Hz, 1H), 5.24 (dd, J = 10.9, 1.3 Hz, 1H), 4.01 (s, 2H), 3.83 (s, 3H). ^{13}C NMR (126 MHz, CDCl$_3$) δ 158.2, 140.9, 137.9, 134.6, 131.4, 130.1, 128.4 (2C), 128.3 (2C), 125.8, 115.7, 113.4, 110.9, 55.2, 38.0. MS (ESI) m/z [M+H]$^+$ for C$_{16}$H$_{17}$O 225.1279, found 225.1285.
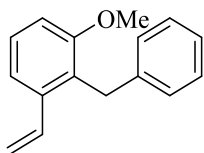
2-Benzyl-1-methoxy-3-vinylbenzene (**9e**). clear oil (84 mg, 77%) ^{1}H NMR (400 MHz, CDCl$_3$) δ 7.29 – 7.20 (m, 3H), 7.18 (d, J = 1.3 Hz, 1H), 7.14 (t, J = 7.0 Hz, 3H), 6.95 (dd, J = 17.4, 11.0 Hz, 1H), 6.86 (d, J = 8.1 Hz, 1H), 5.64 (dd, J = 17.3, 1.5 Hz, 1H), 5.26 (dd, J = 11.0, 1.5 Hz, 1H),

4.14 (s, 2H), 3.80 (d, J = 1.2 Hz, 3H). ^{13}C NMR (126 MHz, CDCl$_3$) δ 157.6, 140.8, 138.4, 134.8, 128.1, 128.1, 127.7, 127.1, 126.4, 125.4, 118.2, 116.1, 110.6, 109.7, 55.6, 31.0. HRMS (ESI) [M+Na]$^+$ for C$_{16}$H$_{16}$O 247.1094, found 247.1090.
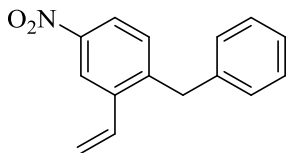
1-Benzyl-4-nitro-2-vinylbenzene (**9f**). yellow oil (157 mg, 88%) ^1H NMR (400 MHz, CDCl$_3$) δ 8.37 (d, J = 2.4 Hz, 1H), 8.05 (dd, J = 8.4, 2.5 Hz, 1H), 7.35 − 7.18 (m, 4H), 7.13 − 7.08 (m, 2H), 6.94 (dd, J = 17.3, 11.0 Hz, 1H), 5.80 (dd, J = 17.3, 0.9 Hz, 1H), 5.45 (dd, J = 11.0, 0.9 Hz, 1H), 4.13 (s, 2H). ^{13}C NMR (126 MHz, CDCl$_3$) δ 147.4, 145.5, 139.1, 138.9, 133.2, 131.6, 129.2 (2C), 129.1 (2C), 127.0, 122.7, 121.4, 119.3, 39.3. HRMS (ESI) m/z [M+H]$^+$ for C$_{15}$H$_{14}$NO$_2$ 242.0817, found 242.0824.
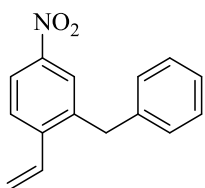
2-Benzyl-4-nitro-1-vinylbenzene (**9g**). yellow oil (230 mg, 95%) ^1H NMR (400 MHz, CDCl$_3$) δ 8.09 (dd, J = 8.6, 2.3 Hz, 1H), 8.01 (d, J = 2.3 Hz, 1H), 7.65 (d, J = 8.6 Hz, 1H), 7.35 − 7.19 (m, 3H), 7.11 (d, J = 7.4 Hz, 2H), 6.96 (dd, J = 17.3, 11.0 Hz, 1H), 5.79 (d, J = 17.4 Hz, 1H), 5.48 (d, J = 11.0 Hz, 1H), 4.14 (s, 2H). ^{13}C NMR (126 MHz, CDCl$_3$) δ 147.6, 143.9, 139.7, 139.2, 133.5, 129.2 (2C), 129.0 (2C), 127.2, 127.0, 125.8, 122.3, 120.3, 39.3. HRMS (ESI) m/z [M+H]$^+$ for C$_{15}$H$_{14}$NO$_2$ 240.1025, found 240.1030
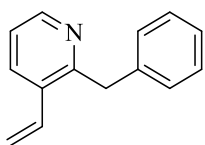
2-Benzyl-3-vinylpyridine (**9h**). yellow oil (97 mg, 68%) ^{1}H NMR (400 MHz, CDCl$_3$) δ 8.50 (dd, J = 4.8, 1.6 Hz, 1H), 7.77 (dd, J = 7.8, 1.6 Hz, 1H), 7.34 – 7.13 (m, 6H), 6.94 (dd, J = 17.4, 11.0 Hz, 1H), 5.64 (d, J = 17.3 Hz, 1H), 5.35 (d, J = 10.9 Hz, 1H), 4.27 (s, 2H). ^{13}C NMR (126 MHz, CDCl$_3$) δ 157.3, 148.4, 139.2, 133.5, 133.0, 132.2, 128.5 (2C), 128.3 (2C), 126.0, 121.9, 117.5, 41.7. HRMS (ESI) [M+H]$^+$ for C$_{14}$H$_{14}$N 196.1126, found 196.1132
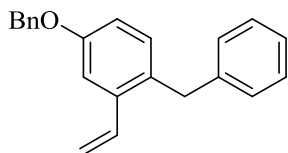
1-Benzyl-4-(benzyloxy)-2-vinylbenzene (**9i**). clear oil (163 mg, 84%) ^{1}H NMR (400 MHz, CDCl$_3$) δ 7.48 (d, J = 8.6 Hz, 1H), 7.42 – 7.35 (m, 4H), 7.35 – 7.25 (m, 3H), 7.24 – 7.17 (m, 1H), 7.15 – 7.10 (m, 2H), 6.92 – 6.84 (m, 2H), 6.74 (d, J = 2.6 Hz, 1H), 5.53 (dd, J = 17.4, 1.4 Hz, 1H), 5.15 (dd, J = 10.9, 1.4 Hz, 1H), 5.03 (s, 2H), 4.03 (s, 2H). ^{13}C NMR (126 MHz, CDCl$_3$) δ 158.3, 140.2, 139.2, 136.8, 133.8, 129.8, 128.6 (2C), 128.5 (2C), 128.3 (2C), 127.8, 127.4 (2C), 126.9, 125.9, 116.5, 113.8, 112.9, 69.8, 39.0. HRMS (ESI) [M+Na]$^+$ for C$_{22}$H$_{20}$O 323.1412, found 323.1419.
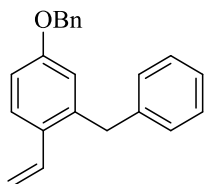
2-Benzyl-4-(benzyloxy)-1-vinylbenzene (**9j**). clear oil (372 mg, 94%) ^{1}H NMR (400 MHz, CDCl$_3$) δ 7.48 (d, J = 8.6 Hz, 1H), 7.43 – 7.35 (m, 4H), 7.34 – 7.30 (m, 1H), 7.29 – 7.23 (m, 3H), 7.23 – 7.16 (m, 1H), 7.15 – 7.10 (m, 2H), 6.96 – 6.83 (m, 2H), 6.74 (d, J = 2.6 Hz, 1H), 5.53 (dd, J = 17.4, 1.4 Hz, 1H), 5.15 (dd, J = 10.9, 1.4 Hz, 1H), 5.03 (s, 2H), 4.03 (s, 2H). ^{13}C NMR (126 MHz, CDCl$_3$) δ 158.9, 140.7, 139.7, 137.3, 134.4, 130.3, 129.1 (2C), 129.0 (2C), 128.8 (2C),

128.3, 127.9 (2C), 127.4, 126.4, 117.1, 114.3, 113.4, 70.3, 39.5. HRMS (ESI) [M+H]$^+$ for C$_{22}$H$_{21}$O 301.1592, found 301.1607.
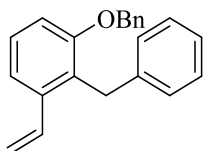
2-Benzyl-1-(benzyloxy)-3-vinylbenzene (**9k**). clear oil (322 mg, 93%) ^{1}H NMR (400 MHz, CDCl$_3$) δ 7.44 – 7.29 (m, 2H), 7.27 – 7.20 (m, 2H), 7.18 – 7.09 (m, 4H), 7.07 (t, J = 6.9 Hz, 3H), 6.91 (dd, J = 17.3, 10.9 Hz, 1H), 6.81 (dd, J = 7.0, 2.2 Hz, 1H), 5.56 (dd, J = 17.3, 1.4 Hz, 1H), 5.19 (dd, J = 11.0, 1.4 Hz, 1H), 4.97 (s, 2H), 4.10 (s, 2H). ^{13}C NMR (126 MHz, CDCl$_3$) δ 156.9, 141.1, 138.9, 137.32, 135.1, 128.7, 128.7, 128.5, 128.5, 128.3, 127.8, 127.7, 127.4, 127.3, 127.2, 127.1, 125.7, 118.7, 116.5, 111.3, 70.3, 31.6. HRMS (ESI) [M+H]$^+$ for C$_{22}$H$_{21}$O 301.1592, found 301.1581.
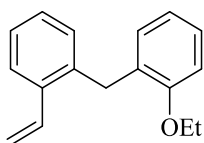
1-Ethoxy-2-(2-vinylbenzyl)benzene (**9l**). clear oil (249 mg, 91%) ^{1}H NMR (400 MHz, CDCl$_3$) δ 7.54 (dd, J = 7.0, 2.2 Hz, 1H), 7.23 – 7.19 (m, 1H), 7.19 – 7.11 (m, 3H), 6.98 (dd, J = 17.5, 11.1 Hz, 1H), 6.90 – 6.78 (m, 3H), 5.63 (dd, J = 17.4, 1.5 Hz, 1H), 5.23 (dd, J = 11.0, 1.5 Hz, 1H), 4.06 (dd, J = 13.6, 6.6 Hz, 4H), 1.41 (t, J = 7.0 Hz, 3H). ^{13}C NMR (126 MHz, CDCl$_3$) δ 156.4, 137.7, 137.0, 134.8, 130.4, 129.7, 129.1, 127.6, 127.0, 126.3, 125.4, 120.1, 115.1, 110.8, 63.4, 32.7, 14.8. HRMS (ESI) [M+Na]$^+$ for C$_{17}$C$_{18}$O 261.1255, found 261.1257.
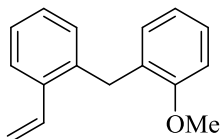
1-Methoxy-2-(2-vinylbenzyl)benzene (**9m**). clear oil (197 mg, 86%) ^{1}H NMR (400 MHz, CDCl$_3$) δ 7.54 (dd, J = 7.1, 1.9 Hz, 1H), 7.24 − 7.15 (m, 3H), 7.13 − 7.06 (m, 1H), 6.95 (dd, J = 17.4, 11.0 Hz, 1H), 6.88 (d, J = 8.2 Hz, 1H), 6.83 (d, J = 4.6 Hz, 2H), 5.64 (dd, J = 17.4, 1.4 Hz, 1H), 5.23 (dt, J = 11.0, 1.2 Hz, 1H), 4.03 (s, 2H), 3.85 (d, J = 1.0 Hz, 3H). ^{13}C NMR (126 MHz, CDCl$_3$) δ 157.5, 138.0, 137.5, 135.2, 130.8, 130.2, 129.3, 128.2, 127.6, 126.9, 126.0, 120.8, 115.7, 110.3, 55.7, 33.1. HRMS (ESI) [M+H][+] for C$_{16}$H$_{17}$O 225.1279, found 225.1280.
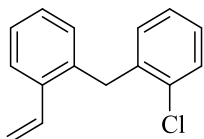
1-Chloro-2-(2-vinylbenzyl)benzene (**9n**). yellow oil (147 mg, 93%) ^{1}H NMR (400 MHz, CDCl$_3$) δ 7.56 (dd, J = 7.5, 1.6 Hz, 1H), 7.40 (dd, J = 7.5, 1.7 Hz, 1H), 7.30 − 7.20 (m, 2H), 7.14 (pd, J = 7.4, 1.8 Hz, 2H), 7.05 (dd, J = 7.5, 1.6 Hz, 1H), 6.91 − 6.81 (m, 2H), 5.65 (dd, J = 17.3, 1.3 Hz, 1H), 5.26 (dd, J = 11.0, 1.4 Hz, 1H), 4.15 (s, 2H). ^{13}C NMR (126 MHz, CDCl$_3$) δ 138.0, 137.1, 136.2, 134.3, 133.9, 130.3, 130.1, 129.2, 127.9, 127.4, 126.8, 126.7, 125.8, 115.9, 36.3. HRMS (ESI) [M][+] for C$_{15}$H$_{13}$Cl 228.0706, found 228.0712.
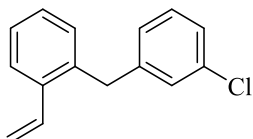
1-(3-Chlorobenzyl)-2-vinylbenzene (**9o**). yellow oil (78 mg, 79%) ^{1}H NMR (400 MHz, CDCl$_3$) δ 7.53 (dd, J = 7.0, 2.1 Hz, 1H), 7.27 − 7.20 (m, 4H), 7.11 (dd, J = 6.9, 2.1 Hz, 1H), 7.07 − 7.02 (m, 2H), 6.88 (dd, J = 17.3, 10.9 Hz, 1H), 5.63 (dd, J = 17.4, 1.4 Hz, 1H), 5.25 (dd, J = 11.0, 1.3 Hz, 1H), 4.03 (s, 2H). 13C NMR (126 MHz, CDCl$_3$) δ 142.6, 136.9, 136.7, 134.3, 134.1, 130.3,

129.5, 128.6, 127.9, 126.9, 126.7, 126.1, 126.0, 116.0, 38.5. HRMS (ESI) m/z [M]$^+$ for C$_{15}$H$_{13}$Cl 228.0706, found 228.0697.
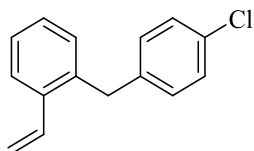
1-(4-Chlorobenzyl)-2-vinylbenzene (**9p**). yellow oil (99 mg, 68%) ^{1}H NMR (400 MHz, CDCl$_3$) δ 7.54 (dd, J = 7.0, 2.2 Hz, 1H), 7.30 − 7.23 (m, 2H), 7.24 − 7.15 (m, 2H), 7.13 − 7.10 (m, 2H), 7.02 − 6.97 (m, 1H), 6.89 (dd, J = 17.3, 11.0 Hz, 1H), 5.64 (dd, J = 17.3, 1.3 Hz, 1H), 5.27 (dd, J = 11.0, 1.3 Hz, 1H), 4.04 (s, 2H). ^{13}C NMR (126 MHz, CDCl$_3$) δ 139.4, 137.6, 137.4, 134.8, 132.1, 130.8, 130.3 (2C), 128.9 (2C), 128.4, 127.4, 126.4, 116.5, 38.8. HRMS [M]$^+$ for C$_{15}$H$_{13}$Cl 228.0706, found 228.0703.
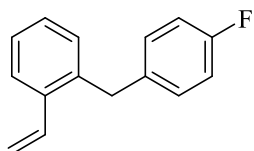
1-(4-Fluorobenzyl)-2-vinylbenzene (**9q**). clear oil (291 mg, 92%) ^{1}H NMR (400 MHz, CDCl$_3$) δ 7.57 − 7.50 (m, 1H), 7.29 − 7.20 (m, 2H), 7.15 − 7.03 (m, 3H), 6.99 − 6.86 (m, 3H), 5.63 (dd, J = 17.4, 1.4 Hz, 1H), 5.25 (dd, J = 11.0, 1.4 Hz, 1H), 4.04 (s, 2H). ^{19}F NMR (376 MHz, CDCl3) δ -117.5 (s, 1F). ^{13}C NMR (126 MHz, CDCl$_3$) δ 138.0, 137.4, 136.6, 136.6, 134.9, 130.7, 130.4, 130.3, 128.4, 127.3, 126.4, 116.3, 115.7, 115.5, 38.6. HRMS (ESI) [M+H]$^+$ for C$_{15}$H$_{14}$F 213.1080, found 213.1077.
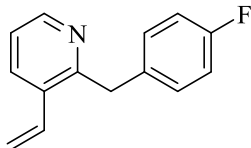
2-(4-Fluorobenzyl)-3-vinylpyridine (**9r**). A microwave vial was charged with **14d** (250 mg, 1.3 mmol, 1 equiv.), 4-fluorobenzylboronicacid pinacol ester (317 mg, 1.3 mmol, 1 equiv.), [1,1′-Bis(diphenylphosphino)ferrocene]dichloropalladium(II) (49 mg, 0.07 mmol, 0.05 equiv.), and K_3PO_4 (560 mg, 4 mmol, 3 equiv.) and capped with a Teflon lined lid. The vial was evacuated and purged with argon (3x) and then dioxane (15 mL) was added. The reaction mixture was heated to 90 °C for 14 h, cooled to rt, and diluted with EtOAc (40 mL) and water (15 mL). The aqueous layer was extracted with EtOAc (2 x 20 mL). The combined organic layers were dried, concentrated and purified via through a filter column (SiO_2, 1:2 EtOAc:Hexanes) and used as obtained. The residue was added to a stirred solution of *n*-butyl lithium (1.5 equiv.) and methyltriphenylphosphonium bromide (1.3 equiv.) at 0 °C. The reaction was stirred for 8 h at rt and quenched with water (10 mL). The aqueous phase was extracted with EtOAc (2 x 15 mL). The combined organic layers were dried, concentrated, and purified via flash chromatography (SiO_2, 1:3 EtOAc:Hexanes) to provide **9r** as a clear oil (73 mg, 26%). ^{1}H NMR (400 MHz, $CDCl_3$) δ 8.51 − 8.46 (m, 1H), 7.82 − 7.72 (m, 1H), 7.16 (ddd, J = 15.5, 8.1, 5.1 Hz, 3H), 6.92 (dt, J = 18.4, 9.7 Hz, 3H), 5.65 (d, J = 17.3 Hz, 1H), 5.36 (d, J = 11.0 Hz, 1H), 4.22 (s, 2H). ^{19}F NMR (376 MHz, $CDCl_3$) δ -117.2 (s, 1F). ^{13}C NMR (126 MHz, $CDCl_3$) δ 162.8, 160.8, 157.5, 149.0, 135.3, 134.1, 133.4, 130.4, 130.3, 122.5, 118.3, 115.7, 115.5, 41.3. HRMS (ESI) [M+H]$^+$ for $C_{14}H_{13}FN$ 214.1032, found 214.1036.

General procedure for the synthesis of **6-7** and **16-31**.

A microwave vial was charged with **8** (200 mg, 2 equiv.), **9a-9r** (1 eq.), and palladium (II) acetate (5 mg, 0.1 equiv.). The tube was sealed with a Teflon lined lid, evacuated and purged with

argon (3x). Triethanolamine (0.8 mL) was added and the reaction was stirred at 115 ˚C for 12 h. The reaction was cooled, partitioned between Et$_2$O (30 mL) and water (10 mL). The aqueous layer was extracted with Et$_2$O (3 x 20 mL). The organic layers were combined, dried, and concentrated. The residue was passed through a filter column (SiO$_2$, 1:1 EtOAc:Hexanes) and concentrated. The residue was dissolved in EtOAc (15 mL), evacuated and purged with argon (3x) before the addition of 10% Pd/C (25 mg). The reaction was then stirred under a hydrogen atmosphere (balloon) for 14 h. The reaction mixture was passed through a pad of celite and washed with DCM and concentrated. The residue was purified by flash chromatography (SiO$_2$, 1:2 EtOAc:Hexanes) to provide the desired analogues **6-7** and **16-31**.
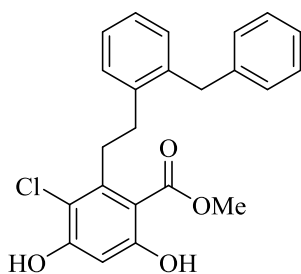
Methyl 2-(2-benzylphenethyl)-3-chloro-4,6-dihydroxybenzoate (**6**). White amorphous solid (45 mg, 52%). ^{1}H NMR (400 MHz, CDCl$_3$) δ 11.40 (s, 1H), 7.31 − 7.22 (m, 2H), 7.20 (q, J = 4.5, 2.8 Hz, 4H), 7.11 (d, J = 7.6 Hz, 3H), 6.58 (s, 1H), 6.05 (s, 1H), 4.11 (s, 2H), 3.91 (d, J = 1.0 Hz, 3H), 3.42 − 3.34 (m, 2H), 2.91 − 2.80 (m, 2H). ^{13}C NMR (126 MHz, CDCl$_3$) δ 170.8, 163.1, 156.0, 142.6, 140.6, 139.7, 138.3, 130.4, 129.0, 128.6, 128.3, 126.6, 126.4, 125.9, 113.7, 106.6, 102.5, 52.5, 38.3, 33.9, 32.3. HRMS (ESI) [M]$^+$ for C$_{23}$H$_{21}$ClO$_4$ 396.1128, found 396.1122.
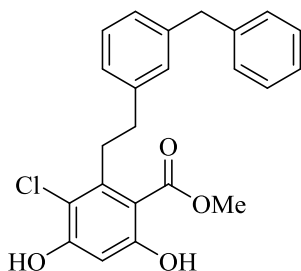
Methyl 2-(3-benzylphenethyl)-3-chloro-4,6-dihydroxybenzoate (**7**). White amorphous solid (57 mg, 66%) ^{1}H NMR (400 MHz, CDCl$_3$) δ 11.45 (s, 1H), 7.36 – 7.26 (m, 3H), 7.22 (t, J = 7.5 Hz, 3H), 7.09 (t, J = 8.1 Hz, 2H), 7.03 (s, 1H), 6.57 (s, 1H), 6.06 (s, 1H), 4.00 (s, 2H), 3.83 (s, 3H), 3.38 – 3.30 (m, 2H), 2.87 – 2.70 (m, 2H). ^{13}C NMR (126 MHz, CDCl$_3$) δ 170.9, 163.1, 156.1, 142.6, 141.7, 141.3, 140.9, 128.9 (2C), 128.7, 128.5, 128.4 (2C), 126.7, 126.0, 125.9, 113.6, 106.5, 102.4, 52.3, 41.8, 35.4, 35.0. HRMS (ESI) [M+H]$^+$ for C$_{23}$H$_{22}$ClO$_4$ 397.1207, found 397.1230.
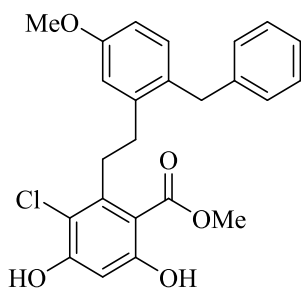
Methyl 2-(2-benzyl-5-methoxyphenethyl)-3-chloro-4,6-dihydroxybenzoate (**16**). White amorphous solid (25 mg, 27%) ^{1}H NMR (400 MHz, CDCl$_3$) δ 11.40 (s, 1H), 7.24 (s, 2H), 7.17 (t, J = 7.2 Hz, 1H), 7.09 (d, J = 7.6 Hz, 2H), 7.03 (d, J = 8.4 Hz, 1H), 6.84 (d, J = 2.7 Hz, 1H), 6.74 (dd, J = 8.3, 2.7 Hz, 1H), 6.57 (s, 1H), 6.05 (s, 1H), 4.04 (s, 2H), 3.91 (d, J = 1.0 Hz, 3H), 3.81 (s, 3H), 3.41 – 3.33 (m, 2H), 2.85 – 2.74 (m, 2H). ^{13}C NMR (126 MHz, CDCl$_3$) δ 171.3, 163.5, 158.6, 156.5, 143.1, 141.5, 141.5, 131.9, 131.1, 129.0 (2C), 128.8 (2C), 126.3, 115.6, 114.2, 111.5, 107.1, 103.0, 55.6, 53.0, 38.1, 34.23, 33.0. HRMS (ESI) [M+Na]$^+$ for C$_{24}$H$_{23}$ClO$_5$Na 449.1132, found 449.1126.
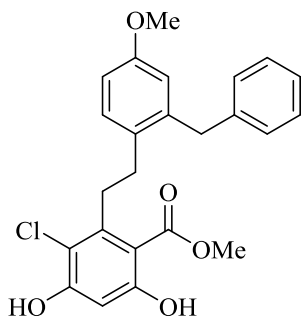
Methyl 2-(2-benzyl-4-methoxyphenethyl)-3-chloro-4,6-dihydroxybenzoate (**17**). White amorphous solid (83 mg, 90%) ^{1}H NMR (400 MHz, CDCl$_3$) δ 11.40 (s, 1H), 7.26 (d, J = 1.2 Hz, 1H), 7.19 (d, J = 8.2 Hz, 2H), 7.12 (d, J = 7.5 Hz, 2H), 6.78 (d, J = 8.5 Hz, 1H), 6.66 (s, 1H), 6.57 (s, 1H), 6.04 (s, 1H), 4.08 (s, 2H), 3.91 (s, 3H), 3.76 (s, 3H), 3.39 – 3.32 (m, 2H), 2.81 (d, J = 8.7 Hz, 2H). ^{13}C NMR (126 MHz, CDCl$_3$) δ 163.5, 158.5, 156.5, 143.2, 140.9, 140.1, 132.4, 130.5, 129.1 (2C), 128.9 (2C), 126.5, 116.5 (2C), 114.2, 112.2, 107.1, 103.0, 55.6, 53.0, 39.0, 34.7, 32.2. HRMS (ESI) [M+Na]$^+$ for C$_{24}$H$_{23}$ClO$_5$ 449.1132, found 449.1128.
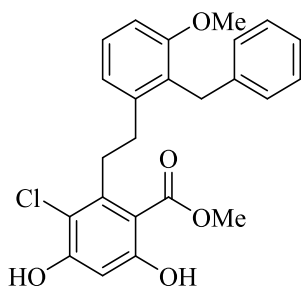
Methyl 2-(2-benzyl-3-methoxyphenethyl)-3-chloro-4,6-dihydroxybenzoate (**18**). White amorphous solid (57 mg, 64%) ^{1}H NMR (400 MHz, CDCl$_3$) δ 11.43 (d, J = 11.6 Hz, 1H), 7.25 – 7.18 (m, 2H), 7.15 – 7.11 (m, 1H), 7.08 (d, J = 7.6 Hz, 2H), 6.93 (d, J = 7.6 Hz, 1H), 6.88 – 6.77 (m, 2H), 6.56 (d, J = 1.1 Hz, 1H), 4.18 (s, 2H), 3.89 (s, 3H), 3.78 (s, 3H), 3.39 – 3.28 (m, 2H), 2.85 (dd, J = 10.7, 6.0 Hz, 2H). ^{13}C NMR (126 MHz, CDCl$_3$) δ 171.3, 163.5, 156.5, 142.9, 134.1, 131.0, 130.7, 128.4, 127.6, 127.6, 127.1, 125.4, 124.5, 123.5, 114.3, 111.7, 111.3, 107.2, 103.0, 69.9, 56.65, 52.5, 35.0, 33.1. HRMS (ESI) [M]$^+$ for C$_{24}$H$_{23}$ClO$_5$ 426.1234, found 426.1234
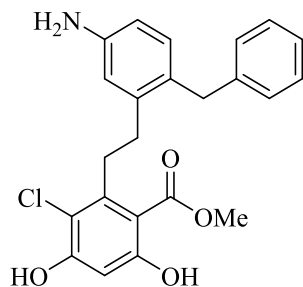
Methyl 2-(5-amino-2-benzylphenethyl)-3-chloro-4,6-dihydroxybenzoate (**19**). Tan amorphous solid (41 mg, 46%). ^{1}H NMR (400 MHz, CDCl$_3$) δ 11.40 (s, 1H), 7.31 – 7.25 (m, 2H), 7.23 – 7.17 (m, 1H), 7.15 – 7.10 (m, 3H), 6.71 (dd, J = 8.2, 2.8 Hz, 1H), 6.57 (s, 1H), 6.54 (d, J = 2.7 Hz, 1H), 6.07 (s, 1H), 4.05 (s, 2H), 3.91 (s, 3H), 3.41 – 3.30 (m, 2H), 2.84 – 2.73 (m, 2H). ^{13}C NMR (126 MHz, CDCl$_3$) δ 170.8, 163.0, 156.0, 153.8, 142.7, 140.2, 140.0, 131.9, 130.2, 128.7 (2C), 128.4 (2C), 126.0, 116.9, 113.4, 106.6, 102.5, 52.5, 38.3, 34.1, 31.7. HRMS (ESI) [M+H]$^{+}$ for C$_{23}$H$_{23}$ClNO$_4$ 412.1316, found 412.1303.
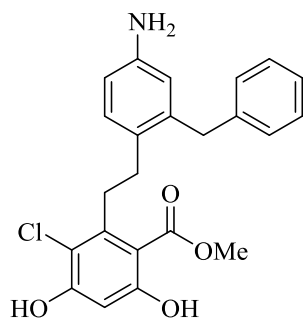
Methyl 2-(4-amino-2-benzylphenethyl)-3-chloro-4,6-dihydroxybenzoate (**20**). Tan amorphous solid (38 mg, 43%). ^{1}H NMR (400 MHz, CDCl$_3$) δ 7.25 – 7.19 (m, 2H), 7.17 – 7.13 (m, 1H), 7.09 (d, J = 7.7 Hz, 2H), 7.05 (d, J = 7.9 Hz, 1H), 6.56 (dd, J = 8.2, 2.5 Hz, 1H), 6.41 (dd, J = 4.9, 1.9 Hz, 2H), 4.00 (s, 2H), 3.86 (s, 3H), 3.34 – 3.22 (m, 2H), 2.75 – 2.67 (m, 2H), 2.63 (br s, 2H). ^{13}C NMR (126 MHz, CDCl$_3$) δ 171.5, 162.6, 157.9, 144.6, 143.6, 141.2, 139.8, 130.9, 130.4, 129.1,

148

129.1, 128.7, 128.7, 126.2, 117.7, 114.9, 114.2, 106.3, 102.4, 52.7, 38.7, 34.6, 32.1. HRMS (ESI) [M+H]$^+$ for C$_{23}$H$_{23}$ClNO$_4$ 412.1316, found 412.1302.
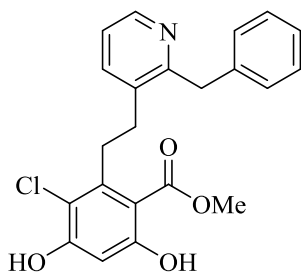
Methyl 2-(2-(2-benzylpyridin-3-yl)ethyl)-3-chloro-4,6-dihydroxybenzoate (**21**). White amorphous solid (81 mg, 94%). ^{1}H NMR (400 MHz, CDCl$_3$) δ 11.34 (s, 1H), 8.49 (d, J = 4.9 Hz, 1H), 7.51 (d, J = 7.7 Hz, 1H), 7.23 (d, J = 7.2 Hz, 2H), 7.19 – 7.13 (m, 4H), 6.58 (d, J = 1.1 Hz, 1H), 6.40 (s, 1H), 4.30 (s, 2H), 3.86 (d, J = 1.0 Hz, 3H), 3.50 – 3.35 (m, 2H), 3.04 – 2.83 (m, 2H). ^{13}C NMR (126 MHz, CDCl$_3$) δ 170.8, 163.3, 158.5, 156.5, 147.5, 142.2, 139.5, 137.1, 135.1, 128.7 (2C), 128.6 (2C), 126.4, 122.1, 114.1, 106.7, 103.0, 52.7, 41.3, 33.4, 31.8. HRMS (ESI) [M+H]$^+$ for C$_{22}$H$_{21}$ClNO$_4$ 398.1159, found 398.1154.
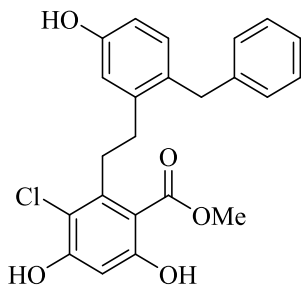
Methyl 2-(2-benzyl-5-hydroxyphenethyl)-3-chloro-4,6-dihydroxybenzoate (**22**). White amorphous solid (42 mg, 47%). ^{1}H NMR (400 MHz, CDCl$_3$) δ 11.37 (s, 1H), 7.24 (s, 2H), 7.18 (d, J = 7.3 Hz, 1H), 7.09 (d, J = 7.5 Hz, 2H), 6.97 (d, J = 8.2 Hz, 1H), 6.79 (d, J = 2.4 Hz, 1H), 6.66 (d, J = 8.4 Hz, 1H), 6.58 (s, 1H), 6.04 (s, 1H), 4.02 (s, 2H), 3.90 (s, 3H), 3.40 – 3.32 (m, 2H), 2.86 – 2.73 (m, 2H). ^{13}C NMR (126 MHz, CDCl$_3$) δ 171.2, 163.5, 156.5, 154.5, 143.0, 141.8,

141.5, 132.0, 131.2, 129.0 (2C), 128.8 (2C), 126.4, 116.2, 113.7, 107.1, 103.0, 53.0, 38.1, 34.1, 32.8. HRMS (ESI) [M+H]$^+$ for C$_{23}$H$_{22}$ClO$_5$ 413.1156, found 413.1150.
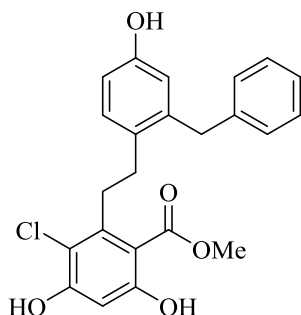
Methyl 2-(2-benzyl-4-hydroxyphenethyl)-3-chloro-4,6-dihydroxybenzoate (**23**). White amorphous solid (38 mg, 42%). ^{1}H NMR (400 MHz, CDCl$_3$) δ 11.40 (s, 1H), 7.27 (d, J = 8.4 Hz, 2H), 7.22 − 7.17 (m, 1H), 7.16 − 7.11 (m, 3H), 6.71 (dd, J = 8.2, 2.8 Hz, 1H), 6.57 (s, 1H), 6.54 (d, J = 2.7 Hz, 1H), 6.07 (s, 1H), 4.05 (s, 2H), 3.91 (s, 3H), 3.40 − 3.32 (m, 2H), 2.87 − 2.73 (m, 2H). ^{13}C NMR (126 MHz, CDCl$_3$) δ 171.3, 163.5, 156.5, 154.4, 143.2, 140.7, 140.5, 132.4, 130.7, 129.2 (2C), 128.9 (2C), 126.6, 117.4, 113.9, 107.1, 103.0, 53.0, 38.8, 34.6, 32.2. HRMS (ESI) [M+H]$^+$ for C$_{23}$H$_{22}$ClO$_5$ 413.1156, found 413.1175.
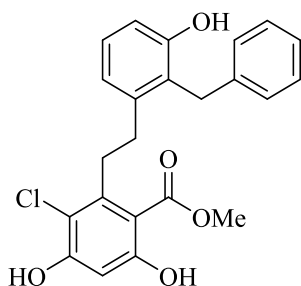
Methyl 2-(2-benzyl-3-hydroxyphenethyl)-3-chloro-4,6-dihydroxybenzoate (**24**). White amorphous solid (25 mg, 28%) ^{1}H NMR (400 MHz, CDCl$_3$) δ 11.40 (s, 1H), 7.24 (d, J = 0.9 Hz, 2H), 7.18 (d, J = 7.9 Hz, 1H), 7.14 (dd, J = 7.9, 1.5 Hz, 3H), 6.95 − 6.91 (m, 1H), 6.74 (d, J = 1.2 Hz, 1H), 6.56 (s, 1H), 6.03 (s, 1H), 4.62 (s, 1H), 4.19 (s, 2H), 3.89 (s, 3H), 3.39 − 3.26 (m, 2H), 2.93 − 2.79 (m, 2H). ^{13}C NMR (126 MHz, CDCl$_3$) δ 171.1, 163.3, 156.3, 154.4, 142.8, 142.0,

139.9, 128.8 (2C), 128.1 (2C), 127.7, 126.4, 124.9, 122.0, 114.0, 114.0, 106.8, 102.8, 52.7, 34.4, 33.0, 31.5. HRMS (ESI) [M]$^+$ for $C_{23}H_{21}ClO_5$ 412.1078, found 412.1073.
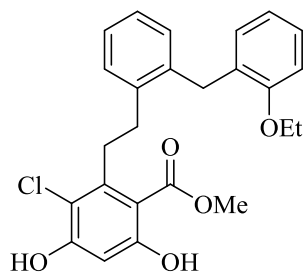
Methyl 3-chloro-2-(2-(2-ethoxybenzyl)phenethyl)-4,6-dihydroxybenzoate (**25**). Tan amorphous solid (61 mg, 64%). ^{1}H NMR (400 MHz, CDCl$_3$) δ 11.46 (s, 1H), 7.29 (dd, J = 7.6, 1.6 Hz, 2H), 7.22 (td, J = 7.4, 1.6 Hz, 1H), 7.17 (td, J = 7.7, 2.2 Hz, 2H), 7.09 (dd, J = 7.5, 1.5 Hz, 1H), 6.90 – 6.80 (m, 3H), 6.57 (s, 1H), 6.04 (d, J = 1.2 Hz, 1H), 4.09 (s, 2H), 4.03 (q, J = 7.0 Hz, 2H), 3.93 (s, 3H), 3.40 – 3.30 (m, 2H), 2.94 – 2.72 (m, 2H), 1.35 (t, J = 7.0 Hz, 3H). ^{13}C NMR (126 MHz, CDCl$_3$) δ 171.0, 163.1, 156.5, 156.0, 142.9, 139.9, 138.3, 130.2, 129.6, 129.2, 128.9, 127.1, 126.3, 126.3, 120.1, 113.8, 110.7, 106.5, 102.4, 63.3, 52.5, 34.0, 32.5, 32.4, 14.8. HRMS (ESI) [M+H]$^+$ for $C_{25}H_{26}ClO_5$ 441.1469, found 441.1449.
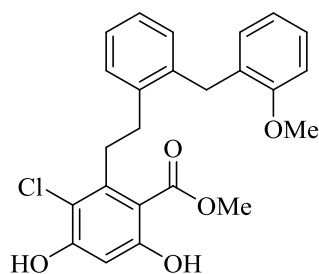
Methyl 3-chloro-4,6-dihydroxy-2-(2-(2-methoxybenzyl)phenethyl)benzoate (**26**). White amorphous solid (52 mg, 56%). ^{1}H NMR (400 MHz, CDCl$_3$) δ 11.50 (s, 1H), 7.31 (d, J = 7.5 Hz, 1H), 7.25 (d, J = 6.0 Hz, 1H), 7.20 (q, J = 8.3, 7.3 Hz, 2H), 7.09 (d, J = 7.5 Hz, 1H), 6.89 (d, J = 8.2 Hz, 1H), 6.86 – 6.81 (m, 2H), 6.58 (s, 1H), 6.12 (s, 1H), 4.10 (s, 2H), 3.95 (s, 3H), 3.83 (s, 3H), 3.45 – 3.29 (m, 2H), 2.97 – 2.69 (m, 2H). ^{13}C NMR (126 MHz, CDCl$_3$) δ 171.5, 163.5, 157.6,

156.6, 143.3, 140.4, 138.6, 130.7, 130.0, 129.6, 129.5, 127.7, 126.8, 126.8, 120.8, 114.3, 110.3, 107.0, 102.9, 55.6, 52.9, 34.5, 32.9, 32.7. HRMS (ESI) [M+Na]$^+$ for C$_{24}$H$_{23}$ClO$_5$ 449.1132, found 449.1124.
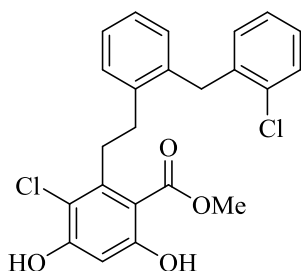
Methyl 3-chloro-2-(2-(2-chlorobenzyl)phenethyl)-4,6-dihydroxybenzoate (**27**). Clear oil (27 mg, 29%). ^{1}H NMR (400 MHz, CDCl$_3$) δ 11.41 (s, 1H), 7.40 (dd, J = 7.6, 1.7 Hz, 1H), 7.33 (dd, J = 7.6, 1.6 Hz, 1H), 7.30 – 7.24 (m, 1H), 7.22 – 7.09 (m, 3H), 7.01 (dd, J = 7.6, 1.3 Hz, 1H), 6.88 – 6.80 (m, 1H), 6.57 (s, 1H), 6.06 (s, 1H), 4.20 (s, 2H), 3.96 (s, 3H), 3.41 – 3.30 (m, 2H), 2.91 – 2.72 (m, 2H). ^{13}C NMR (126 MHz, CDCl$_3$) δ 170.8, 163.0, 156.1, 142.5, 140.0, 138.3, 136.7, 134.1, 130.1, 130.1, 129.2, 129.2, 127.5, 126.8, 126.7, 126.6, 113.8, 106.5, 102.5, 52.5, 36.0, 334.0, 32.4. HRMS (ESI) [M+H]$^+$ for C$_{23}$H$_{21}$Cl$_2$O$_4$ 431.0817, found 431.0836.
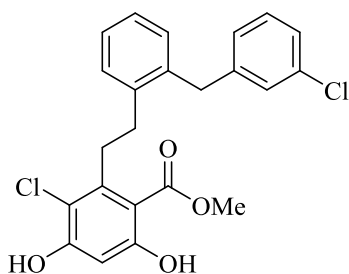
Methyl 3-chloro-2-(2-(3-chlorobenzyl)phenethyl)-4,6-dihydroxybenzoate (**28**). Clear oil (35 mg, 37%). ^{1}H NMR (400 MHz, CDCl$_3$) δ 11.38 (s, 1H), 7.28 (dd, J = 3.0, 1.8 Hz, 1H), 7.25 – 7.21 (m, 1H), 7.20 – 7.16 (m, 2H), 7.10 (dd, J = 7.4, 1.5 Hz, 1H), 7.07 (dt, J = 1.8, 1.0 Hz, 1H), 7.02 – 6.97 (m, 1H), 6.58 (s, 1H), 6.08 (d, J = 5.2 Hz, 2H), 4.08 (s, 2H), 3.93 (s, 3H), 3.43 – 3.31 (m, 2H), 2.91 – 2.74 (m, 2H). ^{13}C NMR (126 MHz, CDCl$_3$) δ 170.7, 163.0, 156.1, 142.7, 142.5, 139.6,

137.4, 134.2, 130.5, 129.6, 129.1, 128.6, 126.9, 126.7, 126.6, 126.2, 113.7, 106.6, 102.6, 52.5, 38.0, 33.8, 32.3. HRMS (ESI) [M+H]$^+$ for C$_{23}$H$_{20}$Cl$_2$O$_4$ 431.0817, found 431.0835.
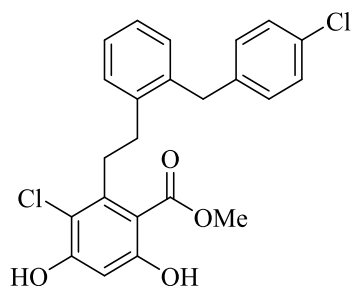
Methyl 3-chloro-2-(2-(4-chlorobenzyl)phenethyl)-4,6-dihydroxybenzoate (**29**). Clear oil (25 mg, 27%). ^{1}H NMR (400 MHz, CDCl$_3$) δ 11.37 (s, 1H), 7.30 – 7.26 (m, 2H), 7.23 (d, J = 8.4 Hz, 2H), 7.21 – 7.16 (m, 1H), 7.16 – 7.07 (m, 2H), 7.07 – 7.00 (m, 2H), 6.58 (s, 1H), 6.07 (s, 1H), 4.07 (s, 2H), 3.92 (s, 3H), 3.44 – 3.34 (m, 2H), 2.90 – 2.76 (m, 2H). ^{13}C NMR (126 MHz, CDCl$_3$) δ 170.7, 163.0, 156.0, 142.5, 139.6, 139.1, 137.8, 130.4, 129.8, 129.1, 129.0, 128.6, 128.4, 128.3, 126.8, 126.5, 125.9, 106.6, 102.6, 52.5, 37.7, 33.9, 32.3. HRMS (ESI) [M+H]$^+$ for C$_{23}$H$_{21}$Cl$_2$O$_4$ 431.0817, found 431.0814.
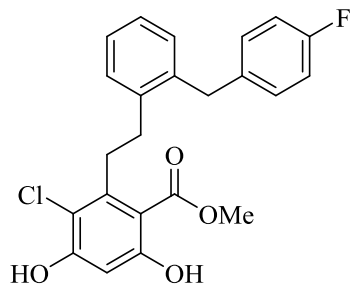
Methyl 3-chloro-2-(2-(4-fluorobenzyl)phenethyl)-4,6-dihydroxybenzoate (**30**). White amorphous solid (44 mg, 49%). ^{1}H NMR (400 MHz, CDCl$_3$) δ 11.38 (s, 1H), 7.29 (dd, J = 7.5, 1.9 Hz, 1H), 7.24 – 7.16 (m, 2H), 7.13 – 7.02 (m, 3H), 6.99 – 6.92 (m, 2H), 6.58 (s, 1H), 6.07 (s, 1H), 4.07 (s, 2H), 3.92 (s, 3H), 3.41 – 3.35 (m, 2H), 2.90 – 2.78 (m, 2H). ^{19}F NMR (376 MHz, CDCl$_3$) δ -117.4 (s, 1F). ^{13}C NMR (126 MHz, CDCl$_3$) δ 170.7, 163.0, 162.2 (d, *J* = 244.0 Hz), 156.0,

142.5, 139.6, 138.2, 136.2, 136.2, 130.3, 129.9, 129.1, 126.7, 126.5, 115.2, 115.0, 113.7, 106.6, 102.5, 52.5, 37.5, 33.8, 32.3. HRMS (ESI) [M+H] for $C_{23}H_{21}ClFO_4$ 415.1112, found 415.1103.
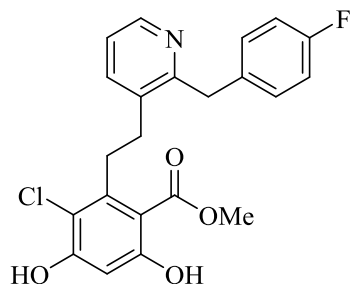
Methyl 3-chloro-2-(2-(2-(4-fluorobenzyl)pyridin-3-yl)ethyl)-4,6-dihydroxybenzoate (**31**). Clear oil (37 mg, 41%). ^{1}H NMR (400 MHz, CDCl$_3$) δ 8.42 (t, J = 4.2 Hz, 1H), 7.54 (dd, J = 7.6, 1.6 Hz, 1H), 7.17 (dd, J = 7.7, 4.9 Hz, 1H), 7.09 (t, J = 6.6 Hz, 2H), 6.90 (td, J = 8.6, 2.0 Hz, 2H), 6.47 (d, J = 3.9 Hz, 1H), 4.24 (s, 2H), 3.86 (s, 3H), 3.42 − 3.29 (m, 2H), 2.92 − 2.77 (m, 2H). ^{19}F NMR (376 MHz, CDCl$_3$) δ -117.03 (s, 1F). ^{13}C NMR (126 MHz, CDCl$_3$) δ 170.6, 163.2, 162.6 (d, J = 244 Hz), 156.7, 142.0, 130.1 (2C), 130.1 (2C), 122.3, 115.5 (2C), 115.4 (2C), 114.2, 106.7, 103.1 (2C), 52.7, 33.4, 31.7, 29.9. HRMS (ESI) [M+H]$^+$ for $C_{22}H_{20}ClFNO_4$ 416.1065, found 416.1050.

Fluorescence Polarization. The assay was performed in 96-well black, flat-bottom plates with a final volume of 100 µL. 25 µL of assay buffer (20 mM HEPES, pH 7.3, 50 mM KCl, 5 mM MgCl$_2$, 20 mM Na$_2$MoO$_4$, 2 mM DTT, 0.1 mg/mL BGG, and 0.01% NP-40) were added, followed by 25 µL of assay buffer containing 6 nM FITC-GDA (fluorescent tracer, stock in DMSO, diluted in assay buffer) and 50 µL of assay buffer containing 10 nM of either Grp94 or Hsp90α were added to each well. For each plate, wells containing buffer only (background), tracer in buffer only (low polarization control) and protein, tracer, and 1% DMSO (final concentration, high polarization control) were included. Compounds were then added with a final concentration of DMSO = 1%. Plates were incubated at 4 °C with rocking for 24 h. Polarization values (in mP units) were measured at 37 °C with an excitation filter at 485 nm and an emission filter at 528 nm. Polarization

values were correlated to % tracer bound and compound concentrations. The concentration at which the tracer was 50% displaced by compound of interested were calculated and reported as apparent Kd's.

Docking Studies. The Surlfex-Docking module in Sybyl v8.0 was used for docking studies using the crystal structure of KUNG38 bound to Grp94 (PDBID: 5IN9). Pymol was used for visualization of the results.

Cell Culture. MDA-MB-231, PC3-MM2, SK-MEL-28, and A549 cells were grown in a water jacketed incubator at 37 °C with 5% CO_2 in DMEM (MDA-MB-231 and PC3-MM2), EMEM (SK-MEL-28) or F-12K (A549) media supplemented with 10% FBS and 1% penicillin/streptomycin.

Anti-proliferation. cells were counted via Trypan blue exclusion and seeded in 96-well plates at 2,000 cells/0.1 mL/well then returned to the incubator for 24 h. Compounds or vehicle were administered in DMSO (1% DMSO final concentration) and the plates were placed back in the incubator. After 72 h, the % viable cells were determined using the MTS/PMS cell proliferation kit (Promega) per the manufacturer's instructions. Cells treated with vehicle were normalized to 100% viable and compound treated wells were adjusted accordingly. GI_{50} values were calculated via GraphPad Prism and reported as the average of 2 or more independent experiments ± SEM.

Wound Healing Scratch Assay. Cells were counted via Trypan blue exclusion and seeded in 12-well plates at 200,000 cells/mL/well and returned to the incubator for 24 h. Scratches were made with a 0.1-10 µL pipette tip, then cells were washed with PBS and fresh media was added. Compound or DMSO control were then added (0.25% DMSO final concentration) and 0 h pictures taken with a camera-mounted Olympus IX-71 microscope (10X objective). Plates were returned to the incubator until 24 h pictures were taken. Images were processed and % migration determined via ImageJ. All experiments were performed in quadruplicate.

Western Blot Analysis. Cells were counted via Trypan blue exclusion and were seeded at 100,000 cells/mL in 10 cm dishes and placed back in the incubator for 24 h. Compounds or vehicle were dosed (0.25% DMSO final concentration) and incubated together for 24 h. Cells were harvested in cold PBS and lysed using MPER (Thermo Scientific) supplemented with protease inhibitors (Roche) according the manufacturer's instructions. Cell lysates were obtained by centrifugation at 15,000 rpm for 10 min at 4 °C. Protein concentrations were determined using the Pierce BCA assay kit following the manufacturer's instructions. Equal amounts of protein were separated via gel electrophoresis under reducing conditions (10% acrylamide gels) then transferred to PVDF membranes and immunoblotted with the corresponding primary antibodies. Membranes were then incubated with the correct HRP-labeled secondary antibody, developed with a chemiluminescent substrate, and visualized.

References

1. Hanahan, D.; Weinberg, R. A. Hallmarks of cancer: the next generation. *Cell* **2011,** *144*, 646-674.

2. Miyata, Y.; Nakamoto, H.; Neckers, L. The therapeutic target Hsp90 and cancer hallmarks. *Curr. Pharm. Des.* **2013,** *19*, 347-365.

3. Travers, J.; Sharp, S.; Workman, P. HSP90 inhibition: two-pronged exploitation of cancer dependencies. *Drug Discov. Today* **2012,** *17*, 242-252.

4. Khandelwal, A.; Crowley, V. M.; Blagg, B. S. Natural product inspired N-terminal Hsp90 inhibitors: from bench to bedside? *Med. Res. Rev.* **2016,** *36*, 92-118.

5. Neckers, L.; Workman, P. Hsp90 molecular chaperone inhibitors: are we there yet? *Clin. Cancer Res.* **2012,** *18*, 64-76.

6.   Taipale, M.; Jarosz, D. F.; Lindquist, S. HSP90 at the hub of protein homeostasis: emerging mechanistic insights. *Nat. Rev. Mol. Cell Biol.* **2010,** *11*, 515-528.

7. Ernst, J. T.; Liu, M.; Zuccola, H.; Neubert, T.; Beaumont, K.; Turnbull, A.; Kallel, A.; Vought, B.; Stamos, D. Correlation between chemotype-dependent binding conformations of HSP90alpha/beta and isoform selectivity-Implications for the structure-based design of HSP90alpha/beta selective inhibitors for treating neurodegenerative diseases. *Bioorg. Med. Chem. Lett.* **2014,** *24*, 204-208.

8.   Whitesell, L.; Bagatell, R.; Falsey, R. The stress response: implications for the clinical development of hsp90 inhibitors. *Curr. Cancer Drug Targets* **2003,** *3*, 349-358.

9. Gewirth, D. T. Paralog Specific Hsp90 Inhibitors - A Brief History and a Bright Future. *Curr. Top. Med. Chem.* **2016,** *16*, 2779-2791.

10.   Crowley, V. M.; Khandelwal, A.; Mishra, S.; Stothert, A. R.; Huard, D. J.; Zhao, J.; Muth, A.; Duerfeldt, A. S.; Kizziah, J. L.; Lieberman, R. L.; Dickey, C. A.; Blagg, B. S. Development of Glucose Regulated Protein 94-Selective Inhibitors Based on the BnIm and Radamide Scaffold. *J. Med. Chem.* **2016,** *59*, 3471-3488.

11.   Patel, H. J.; Patel, P. D.; Ochiana, S. O.; Yan, P.; Sun, W.; Patel, M. R.; Shah, S. K.; Tramentozzi, E.; Brooks, J.; Bolaender, A.; Shrestha, L.; Stephani, R.; Finotti, P.; Leifer, C.; Li, Z.; Gewirth, D. T.; Taldone, T.; Chiosis, G. Structure-activity relationship in a purine-scaffold compound series with selectivity for the endoplasmic reticulum Hsp90 paralog Grp94. *J. Med. Chem.* **2015,** *58*, 3922-3943.

12.   Patel, P. D.; Yan, P.; Seidler, P. M.; Patel, H. J.; Sun, W.; Yang, C.; Que, N. S.; Taldone, T.; Finotti, P.; Stephani, R. A.; Gewirth, D. T.; Chiosis, G. Paralog-selective Hsp90 inhibitors define tumor-specific regulation of HER2. *Nat. Chem. Biol.* **2013,** *9*, 677-684.

157

13.   Marzec, M.; Eletto, D.; Argon, Y. GRP94: An HSP90-like protein specialized for protein folding and quality control in the endoplasmic reticulum. *Biochim. Biophys. Acta* **2012,** *1823*, 774-787.

14.   Hua, Y.; White-Gilbertson, S.; Kellner, J.; Rachidi, S.; Usmani, S. Z.; Chiosis, G.; Depinho, R.; Li, Z.; Liu, B. Molecular chaperone gp96 is a novel therapeutic target of multiple myeloma. *Clin. Cancer Res.* **2013,** *19*, 6242-6251.

15.   Stothert, A. R.; Suntharalingam, A.; Huard, D. J.; Fontaine, S. N.; Crowley, V. M.; Mishra, S.; Blagg, B. S.; Lieberman, R. L.; Dickey, C. A. Exploiting the interaction between Grp94 and aggregated myocilin to treat glaucoma. *Hum. Mol. Genet.* **2014,** *23*, 6470-6480.

16.   Wu, S.; Hong, F.; Gewirth, D.; Guo, B.; Liu, B.; Li, Z. The molecular chaperone gp96/GRP94 interacts with Toll-like receptors and integrins via its C-terminal hydrophobic domain. *J. Biol. Chem.* **2012,** *287*, 6735-6742.

17.   Rachidi, S.; Sun, S.; Wu, B. X.; Jones, E.; Drake, R. R.; Ogretmen, B.; Cowart, L. A.; Clarke, C. J.; Hannun, Y. A.; Chiosis, G.; Liu, B.; Li, Z. Endoplasmic reticulum heat shock protein gp96 maintains liver homeostasis and promotes hepatocellular carcinogenesis. *J. Hepatol.* **2015,** *62*, 879-888.

18.   Randow, F.; Seed, B. Endoplasmic reticulum chaperone gp96 is required for innate immunity but not cell viability. *Nat. Cell Biol.* **2001,** *3*, 891-896.

19.   Chen, B.; Piel, W. H.; Gui, L.; Bruford, E.; Monteiro, A. The HSP90 family of genes in the human genome: insights into their divergence and evolution. *Genomics* **2005,** *86*, 627-637.

20.   Taldone, T.; Patel, P. D.; Patel, M.; Patel, H. J.; Evans, C. E.; Rodina, A.; Ochiana, S.; Shah, S. K.; Uddin, M.; Gewirth, D.; Chiosis, G. Experimental and structural testing module to analyze

paralogue-specificity and affinity in the Hsp90 inhibitors series. *J. Med. Chem.* **2013,** *56*, 6803-6818.

21.   Song, H. Y.; Dunbar, J. D.; Zhang, Y. X.; Guo, D.; Donner, D. B. Identification of a protein with homology to Hsp90 that binds the type 1 tumor necrosis factor receptor. *J. Biol. Chem.* **1995,** *270*, 3574-3581.

22.   Duerfeldt, A. S.; Peterson, L. B.; Maynard, J. C.; Ng, C. L.; Eletto, D.; Ostrovsky, O.; Shinogle, H. E.; Moore, D. S.; Argon, Y.; Nicchitta, C. V.; Blagg, B. S. Development of a Grp94 inhibitor. *J. Am. Chem. Soc.* **2012,** *134*, 9796-9804.

23.   Immormino, R. M.; Metzger, L. E. t.; Reardon, P. N.; Dollins, D. E.; Blagg, B. S.; Gewirth, D. T. Different poses for ligand and chaperone in inhibitor-bound Hsp90 and GRP94: implications for paralog-specific drug design. *J. Mol. Biol.* **2009,** *388*, 1033-1042.

24.   Ohsawa, K.; Yoshida, M.; Doi, T. A direct and mild formylation method for substituted benzenes utilizing dichloromethyl methyl ether-silver trifluoromethanesulfonate. *J. Org. Chem.* **2013,** *78*, 3438-3444.

25.   Dutton, B. L.; Kitson, R. R.; Parry-Morris, S.; Roe, S. M.; Prodromou, C.; Moody, C. J. Synthesis of macrolactam analogues of radicicol and their binding to heat shock protein Hsp90. *Org. Biomol. Chem.* **2014,** *12*, 1328-1340.

26.   Li, H. J. W., L. Triethanolamine as an Efficient and Reusable Base, Ligand and Reaction Medium for Phosphane-Free Palladium-Catalyzed Heck Reactions. *Eur. J. Org. Chem.* **2006,** *2006*, 5099-5102.

27.   Hu, T.; Xie, N.; Qin, C.; Wang, J.; You, Y. Glucose-regulated protein 94 is a novel glioma biomarker and promotes the aggressiveness of glioma via Wnt/beta-catenin signaling pathway. *Tumour Biol.* **2015,** *36*, 9357-9364.

28.   Giroux, A. Synthesis of benzylic boronates via palladium-catalyzed cross-coupling reaction of bis(pinacolato)diboron with benzylic halides. *Tetrahedron Lett.* **2003,** *44*, 233-235.

29.   Luo, B. H.; Carman, C. V.; Springer, T. A. Structural basis of integrin regulation and signaling. *Annu. Rev. Immunol.* **2007,** *25*, 619-647.

30.   Ganguly, K. K.; Pal, S.; Moulik, S.; Chatterjee, A. Integrins and metastasis. *Cell Adh. Migr.* **2013,** *7*, 251-261.

31.   Wang, Q.; He, Z.; Zhang, J.; Wang, Y.; Wang, T.; Tong, S.; Wang, L.; Wang, S.; Chen, Y. Overexpression of endoplasmic reticulum molecular chaperone GRP94 and GRP78 in human lung cancer tissues and its significance. *Cancer Detect. Prev.* **2005,** *29*, 544-551.

32.   Guo, L.; Zhang, F.; Cai, Y.; Liu, T. Expression profiling of integrins in lung cancer cells. *Pathol. Res. Pract.* **2009,** *205*, 847-853.

33.   Gogali, A.; Charalabopoulos, K.; Constantopoulos, S. Integrin receptors in primary lung cancer. *Exp. Oncol.* **2004,** *26*, 106-110.

34.   Ghosh, S.; Shinogle, H. E.; Galeva, N. A.; Dobrowsky, R. T.; Blagg, B. S. Endoplasmic Reticulum-resident Heat Shock Protein 90 (HSP90) Isoform Glucose-regulated Protein 94 (GRP94) Regulates Cell Polarity and Cancer Cell Migration by Affecting Intracellular Transport. *J. Biol. Chem.* **2016,** *291*, 8309-8323.

35.   Naci, D.; Vuori, K.; Aoudjit, F. α2β1 integrin in cancer development and chemoresistance. *Semin. Cancer Biol.* **2015,** *35*, 145-153.

36.   Haidari, M.; Zhang, W.; Caivano, A.; Chen, Z.; Ganjehei, L.; Mortazavi, A.; Stroud, C.; Woodside, D. G.; Willerson, J. T.; Dixon, R. A. Integrin α2β1 mediates tyrosine phosphorylation of vascular endothelial cadherin induced by invasive breast cancer cells. *J. Biol. Chem.* **2012,** *287*, 32981-32992.

37. Schadendorf, D.; Gawlik, C.; Haney, U.; Ostmeier, H.; Suter, L.; Czarnetzki, B. M. Tumour progression and metastatic behaviour in vivo correlates with integrin expression on melanocytic tumours. *J. Pathol.* **1993,** *170*, 429-434.

4. Resorcinol-based Grp94-selective Inhibitors Exhibit Activity against Multiple Myeloma

Introduction

The 90kDa heat shock proteins (Hsp90) are responsible for the maturation of more than 300 nascent polypeptides into their biologically active conformations as well as the re-maturation of denatured proteins.[1-3] Many protein substrates dependent upon Hsp90 are associated with signaling pathways that are commonly hijacked during malignant transformation, including Her2, Akt, and Raf. In fact, Hsp90-dependent client proteins are represented in all ten hallmarks of cancer.[4-5] Consequently, Hsp90 inhibition provides a combinatorial attack against cancer via a single molecular target. Hsp90 is a homodimeric protein and each monomer contains: An N-terminal ATP-binding motif, a middle domain that is important for protein-protein interactions, and a C-terminal dimerization domain.[6] Binding and hydrolysis of ATP at the N-terminus provides the requisite source of energy for client protein folding, but inhibition or disruption of this process results in ubiquitination of the substrate which signals its degradation via the proteasome.

Seventeen small molecule, ATP-competitive N-terminal inhibitors have been introduced into clinical trials for the treatment of various types of cancer.[7-9] Unfortunately, these trials have revealed cardiotoxicity, hepatotoxicity, ocular toxicity, hypoglycemia, and/or limited efficacy as a single agent in many cases.[10] In addition, all of these inhibitors induce the pro-survival heat shock response (HSR), in which the heat shock proteins (Hsp90, Hsp70, Hsp27, etc.) are upregulated at the same concentrations required for client protein degradation, requiring patients to receive increasingly higher doses that push the patient toward the maximum tolerated dose and toxicity. These detriments have produced concerns about Hsp90 as a therapeutic target and support the need for alternative strategies of Hsp90 inhibition.

The Hsp90 family of chaperones is comprised of four isoforms: Hsp90α and Hsp90β reside in the cytosol, TRAP1 is localized to the mitochondria, and Grp94 is found in the endoplasmic reticulum. All of the Hsp90 clinical candidates are *pan*-Hsp90 inhibitors and manifest similar affinity against all four Hsp90 isoforms. Each Hsp90 isoform appears to play a distinct role in cancer progression, and therefore, targeting a specific isoform may induce the degradation of a smaller subset of client proteins and reduce the liabilities associated with *pan*-Hsp90 inhibition. All four Hsp90 isoforms share high identity within their N-terminal ATP-binding site, hindering the development of Hsp90 isoform-selective inhibitors.[11-13] The most unique isoform is Grp94, which contains a five amino acid insertion into its primary sequence that results in a unique secondary binding pocket within the ATP-binding site.

Grp94 is the ER resident isoform of the Hsp90 protein family and is responsible for the maturation and trafficking of proteins associated with cell signaling and cellular adhesion.[14] Grp94 plays a key role in the maturation and intracellular trafficking of integrins as well as maintenance of cell polarity.[15] Other Grp94-dependent client proteins include Her2, LRP6, IGF-I and –II, Toll-like receptors, integrins, and mutant myocilin.[16-19] Due to the dependency of integrins on Grp94 for their maturation and trafficking to the cell surface, Grp94-selective inhibitors may represent a non-toxic method to inhibit cancer metastasis.[20-22] Inhibition of Grp94 has also been implicated in other diseases, such as myocilin-associated open angle glaucoma.[23-25] Since Grp94 is only essential during embryonic development, Grp94 may represent a non-toxic target that can be inhibited to treat these diseases while reducing the liabilities associated with *pan*-Hsp90 inhibitors. Conversely, some cancers exhibit an increased dependence upon a functional ER and the ER chaperone system for survival due to increased metabolic rate (hepatocellular carcinoma) or the

unfolded protein response as a result of elevated ER stress (multiple myeloma), and these circumstances render Grp94 inhibition as a potential strategy to combat these cancers.[23-24]

Rationale of Resorcinol-based Grp94-selective inhibitor that utilize the S2 sub-pocket

As a consequence of the five amino acid insertion into its primary sequence, the Grp94 N-terminal ATP-binding pocket contains a unique hydrophobic pocket, which can be divided into two distinct sub-pockets that are not present in other isoforms. Sub-pocket 1 (S1) is located near the solvent-exposed region of the binding pocket, but it is hydrophobic in nature and surrounded by Ile166, Ala167, Phe195, Val197, and Tyr200. The corresponding residues in cytosolic Hsp90s (Hsp90α and Hsp90β) are similar, but access to this region is blocked by Asn92 and Lys90. The S1 sub-pocket has been utilized previously for the development of Grp94-selective inhibitors, as evidenced by the rational design of **BnIm** and its subsequent analogue, **KUNG38** (**Figure 4.1a**).[21, 26-27] These resorcinol-based inhibitors orient the benzylic side chain into the S1 sub-pocket to
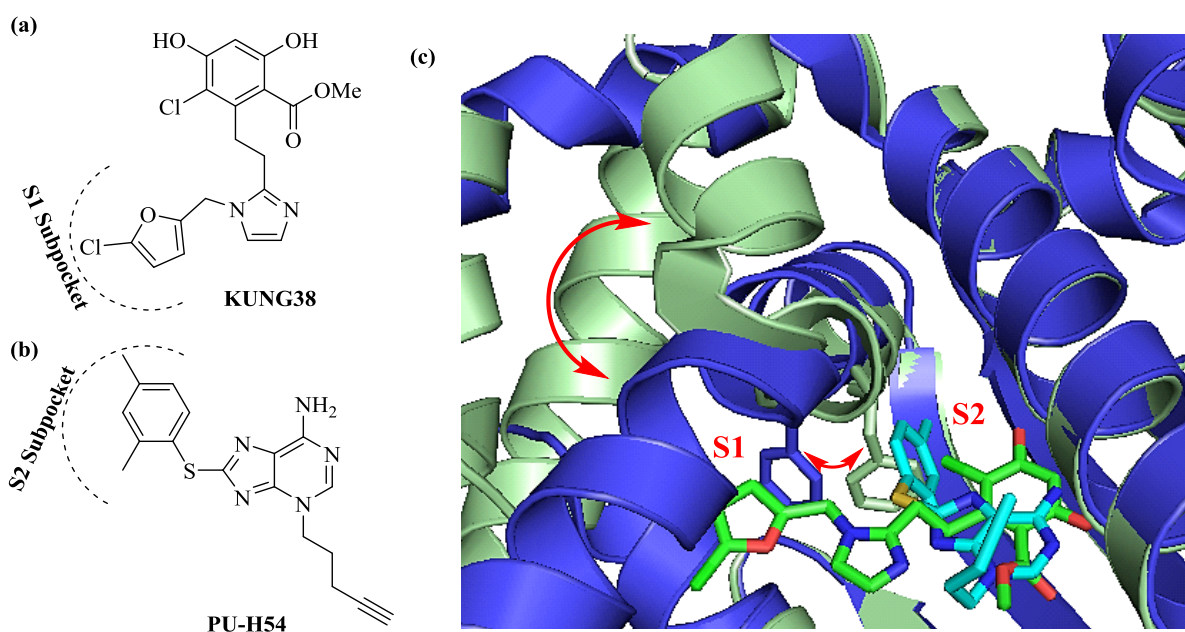
Figure 4.1. Grp94-selective scaffolds utilize different sub-pockets to gain selectivity. (a) Structure of **KUNG38** and its interaction with the S1 sub-pocket of Grp94. (b) Structure of **PU-H54** and its interaction with the S2 sub-pocket of Grp94. (c) Overlay of **KUNG38** (green, PDBID: 5IN9) and **PU-H54** (blue, PDBID: 3O2F) co-crystal structures demonstrating the different binding modes between two Grp94-selective scaffolds. Red arrows indicate helix reorganization upon ligand binding resulting in Phe199 moving to allow access to S2 sub-pocket.

164

impart selectivity for Grp94 (**Figure 4.1c**). Recently, a small library of purine-based inhibitors was screened for Grp94-inhibition which identified **PU-H54** as a Grp94-selective inhibitor (**Figure 4.1b**).[17, 28] The co-crystal structure of **PU-H54** bound to Grp94 identified a second Grp94-exclusive sub-pocket (S2) near the adenine binding region of the N-terminal ATP-binding pocket (**Figure 4.1c**). The S2 sub-pocket results from rotation of Phe199 in Grp94 (red arrow, **Figure 4.1c**) as helices 1, 4, and 5 reorganize upon ligand binding (red arrow, **Figure 4.1c**). Surprisingly, access to the S2 sub-pocket is obstructed in the crystal structure of **KUNG38** bound to Grp94. To date, no resorcinol-based inhibitor has been shown to bind the S2 sub-pocket in order to gain Grp94 selectivity. Therefore, resorcinol-based inhibitors were designed to selectively interact with the S2 sub-pocket in an effort to identify the optimal sub-pocket for the development of Grp94-selective inhibitors.

Design, Synthesis, and Biochemical Evaluation of Resorcinol-based Grp94-selective inhibitors

The resorcinol containing isoindoline **1** was chosen as a starting point to probe the S2 sub-pocket of Grp94 (**Figure 4.2a**) because it contains the resorcinolic pharmacophore present in the *pan*-Hsp90 inhibitor **AT13387**, which remains under clinical investigation.[29-30] As shown in **Figure 4.2b**, an overlay of **1** docked to both Grp94 and Hsp90α provides insight into the development of Grp94-selective inhibitors. The 5-position of the resorcinol ring projects directly toward the hydrophobic S2 sub-pocket that is surrounded by Leu104, Phe199, Ala202, Val211, Trp223, and Leu249 (**Figure 4.2c**). The Hsp90α binding site possesses a pocket that extends towards the solvent exposed region of the ATP-binding pocket (Site-1, **Figure 4.2d**), which has been utilized
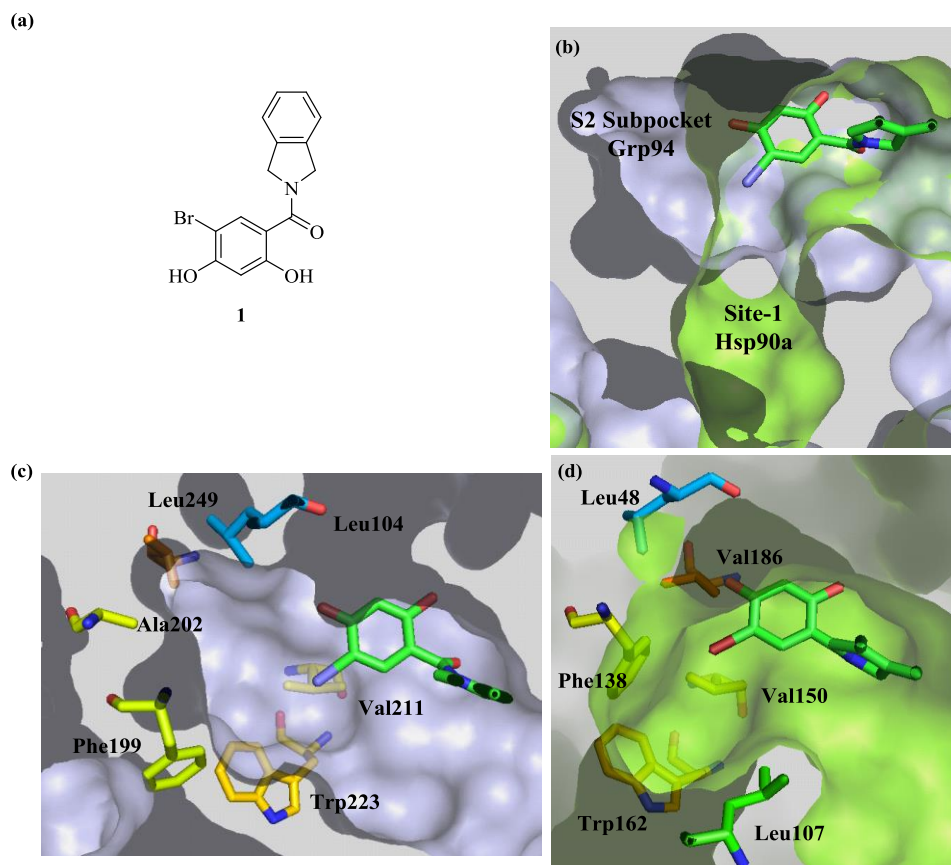
Figure 4.2. Grp94-selective inhibitor design. (a) Structure of **1**. (b) Proposed binding model of **1** in Hsp90α (green) and Grp94 (blue). PDBIDs: 3O2F (Grp94), 3O2I (Hsp90α). Br = light blue (c) Key hydrophobic residues comprising the S2 sub-pocket of Grp94. (d) Key hydrophobic residues comprising Site-1 of Hsp90α. Isoindoline ring omitted for clarity.

previously to develop *pan*-Hsp90inhibitors. The S2 sub-pocket extends deeper into the protein and away from the solvent exposed region compared to Site-1. In order to transform **1** into a Grp94-selective inhibitor, substitutions at the 5-position must exhibit a preference for interacting with the S2 sub-pocket of Grp94 versus Site-1 of Hsp90α (**Figure 4.2b**). Molecular modeling studies suggested that direct attachment of an aryl group to the 5-position of the resorcinol ring (**3**) would produce detrimental steric interactions with the S2 sub-pocket. However, it appeared that a single atom linker could alleviate this steric clash and, instead, produce compounds that selectively interact with the S2 sub-pocket to exhibit Grp94 selectivity. Molecules that connect a phenyl (proposed to bind to the S2 sub-pocket) and resorcinol ring via a sulfur atom (**4**) or methylene

Scheme 4.1. Synthesis of compounds **3-6**.
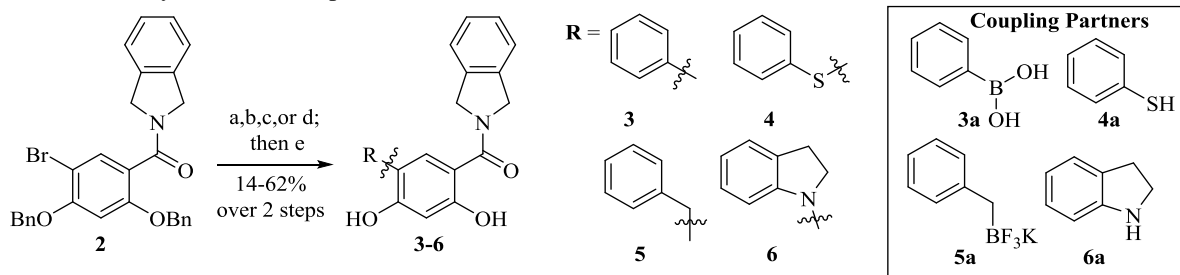
Conditions: (**a**) **3a**, Pd(dppf)Cl$_2$, Toluene/EtOH; (**b**) **4a**, Pd$_2$(dba)$_3$, NaO^{t}Bu, XPhos, Toluene; (**c**) **5a**, Pd(OAc)$_2$, RuPhos, K$_3$PO$_4$, Toluene; (**d**) **6a**, Pd$_2$(dba)$_3$, RuPhos, NaO^{t}Bu, Toluene; (**e**) BBr$_3$, DCM.

group (**5**) were proposed. In addition, a ring-constrained nitrogen-linked analogue (**6**) was also sought to limit rotation about the linker moiety, while projecting the aromatic ring into the S2 sub-pocket for selective inhibition of Grp94.

Synthesis of the proposed analogues began via the preparation of **2** following literature procedures.[31] Subsequent treatment of **2** with boron tribromide afforded resorcinol **1**. Compounds **3-6** were prepared via palladium-catalyzed cross-coupling reactions between **2** and the corresponding coupling partners (**3a-6a**). Resorcinol **3** was synthesized via a Suzuki cross-coupling reaction with phenyl boronic acid (**3a**), followed by cleavage of the benzyl ethers upon exposure to boron tribromide. Coupling of **2** with thiophenol (**4a**) was achieved via the enlistment of tris(dibenzylideneacetone)dipalladium(0), sodium *tert*-butoxide, and XPhos to provide the corresponding thioether, which was then exposed to boron tribromide to provide **4**. Coupling of potassium benzyltrifluoroborate (**5a**) with **2** was performed using palladium (II) acetate, RuPhos, and potassium phosphate tribasic followed by cleavage of the benzyl ethers to afford **5**. Coupling of indoline (**6a**) with resorcinol ring **2** was achieved via a palladium-catalyzed cross-coupling reaction followed by cleavage of the benzyl ethers to yield **6** (**Scheme 4.1**).

Table 4.1. Evaluation of compounds **1** and **3 – 6** via fluorescence polarization against Grp94 and Hsp90α.
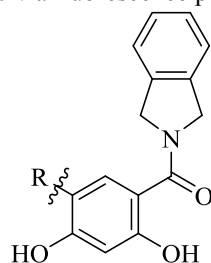
Entry	R	Grp94 (μM)	Hsp90α(μM)	Fold Grp94 Selective
1	-Br	0.02 ± 0.005	0.025 ± 0.007	n/a
3		>100	>100	n/a
4		0.013 ± 0.002	0.026 ± 0.002	2
5		0.015 ± 0.003	0.066 ± 0.006	4
6		9.89 ± 1.1	>50	5

Data are the average of at least two independent experiments ± SEM. n/a = non-selective

Upon their preparation, compounds **1** and **3-6** were evaluated in a fluorescence polarization assay to measure their affinity for both Grp94 and Hsp90α.[32] The results from these studies are summarized in **Table 4.1**. The parent compound, **1**, demonstrated good affinity but no selectivity between Grp94 and Hps90α, which was expected due to the bromide substitution not projecting into the S2 sub-pocket of Grp94 or Site-1 of Hsp90α. As predicted by modeling, direct attachment of an aryl appendage to the resorcinol ring was detrimental, as evidenced by **3** which did not produce any measurable affinity up to 100 μM against both Grp94 and Hsp90α. However, incorporation of a linker (**4** and **5**) proved that the S2 sub-pocket could be exploited with the resorcinol scaffold to gain Grp94 selectivity with these analogues, resulting in 2- or 4-fold selectivity for Grp94, respectively. Thioether **4** and methylene analogue **5** exhibited excellent affinities of 13 nM and 15 nM for Grp94, respectively. However, the low selectivity exhibited by
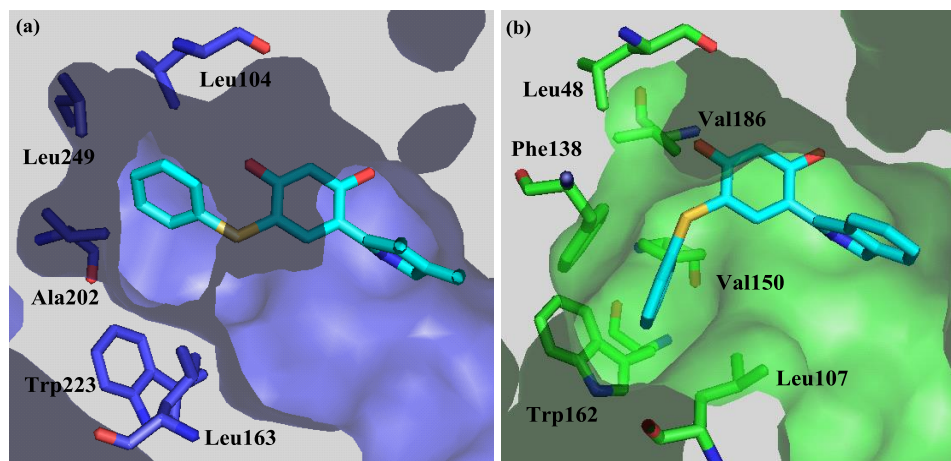
Figure 4.3. Proposed binding mode of **4**. (**a**) Grp94 (blue) and (**b**) Hsp90α (green).

these analogues suggested that rotation about the linker produced similar affinities for Hsp90α. Therefore, reduction of the rotational freedom about the linker atom was pursued via the incorporation of an indoline ring (**6**), which produced 5-fold selectivity. However, this selectivity was accompanied by a significant loss of affinity for Grp94 with an apparent K_d of 9.9 µM.

Compounds containing sulfur and methylene linkers (**4** and **5**) also produced low selectivity for Grp94, but maintained good affinity. Lack of selectivity for these analogues was not too surprising, as rotation about the linker atoms could project the phenyl ring into either the S2 sub-pocket of Grp94 or Site-1 of Hsp90α (**Figure 4.3**). Similar rotational freedom has been observed for the sulfide linked purine-based Grp94-selective inhibitors that target the S2 sub-pocket of

Scheme 4.2. Synthesis of sulfide-containing analogues **10 – 14**.

7a: X = 2-OMe   10a: X = 2,4-dimethyl
8a: X = 3-OMe   11a: X = 2,5-dimethyl
9a: X = 4-OMe
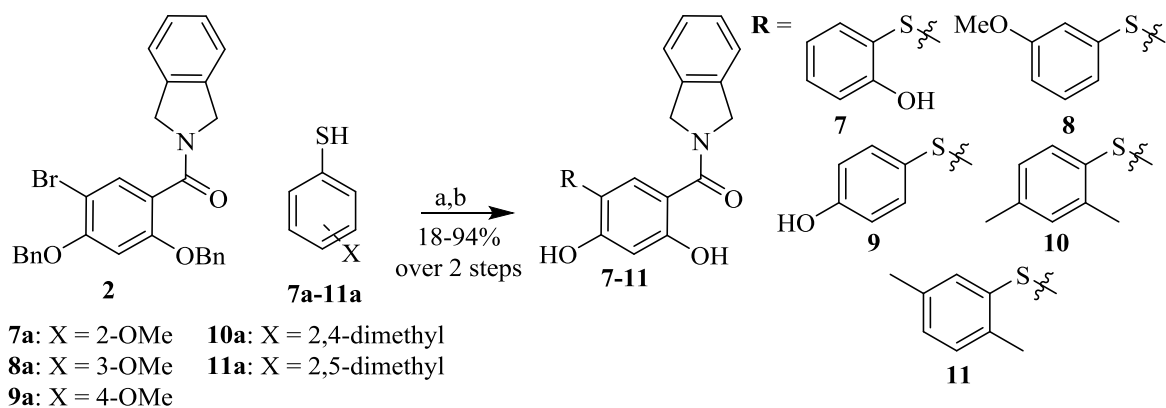
Conditions: (a) Pd$_2$(dba)$_3$, XPhos, **7a-11a**, NaO^{t}Bu, Toluene; (b) BBr$_3$, DCM

169

Table 4.2. Evaluation of **7 – 11** in a fluorescence polarization assay against Grp94 and Hsp90α.
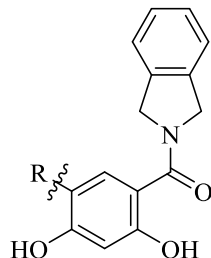
Entry	R	Grp94(μM)	Hsp90α(μM)	Fold Grp94 Selective
4		0.013 ± 0.002	0.026 ± 0.002	2
7		0.029 ± 0.004	0.065 ± 0.01	2
8		0.034 ± 0.002	0.037 ± 0.002	n/a
9		0.07 ± 0.002	0.052 ± 0.007	n/a
10		0.03 ± 0.002	0.07 ± 0.002	2
11		0.029 ± 0.001	0.031 ± 0.002	n/a

Data are the average of at least two independent experiments ± SEM. n/a = non-selective.

Grp94; however these purine-based inhibitors appear to possess some preference for binding the S2 sub-pocket for reasons that remain unclear. In an effort to improve the selectivity profile of these inhibitors, substitutions on the aryl side chain of **4** and **6** were explored.

Analysis of the crystal structures of Hsp90α and Grp94 indicated that both Site-1 of Hsp90α and the S2 sub-pocket of Grp94 are comprised of similar, hydrophobic amino acid residues, but these residues orient differently around the aryl side chain of these inhibitors (**Figure 4.3**). Furthermore, the S2 sub-pocket of Grp94 appears to be sterically less demanding compared to Site-1 of Hsp90α. Therefore, it was proposed that these subtle differences could be exploited to improve Grp94 selectivity by the introduction of substituents onto the aryl side chain. Selection of substituents

was guided by docking studies and prior structure-activity relationship studies observed for the purine-based Grp94-selective inhibitors, due to the potential for overlapping binding modes.[28, 33] Compounds **7 – 9** , which contain electron donating groups at the 2'-, 3'-, and 4'-positions were considered (**Scheme 4.2**) as well as dimethyl (**10** and **11**) substituents on the aryl side chain as mechanisms to reduce affinity for the smaller Site-1 binding region. The 2'-methyl group was hypothesized to produce detrimental steric interactions with the smaller Site-1 of Hsp90α and produce favorable interactions with the larger and more hydrophobic residues present in the S2 sub-pocket of Grp94. **7 – 11** were prepared via the synthetic route described for **4**, but instead, utilized coupling partners **7a – 11a**, followed by cleavage of the benzyl ethers with boron tribromide to provide the desired analogues.

  Once synthesized, **7 – 11** were evaluated for affinity and selectivity via a fluorescence polarization assay, which provided information regarding the binding modes for these analogues (**Table 4.2**). While these substitutions provided compounds with excellent affinity for Grp94 (K_ds ≤70 nM), many of these analogues did not exhibit the anticipated selectivity for Grp94 (eg, **8**, **9**, and **11**). Lack of selectivity is likely due to Site-1 of Hsp90α possessing a higher degree of flexibility than originally suspected and observed via docking studies. Alteration of the electronic nature of the phenyl ring did not improve selectivity, as neither electron donating (**8**) nor electron neutral (**11**) substitutions provided enhanced selectivity. Additionally, the low selectivity exhibited by analogues **10** and **11** (2-fold and non-selective, respectively) suggests the aryl side chains of these resorcinol-based Grp94-selective inhibitors orients differently than the aryl side chains of the previously reported purine-based Grp94-selective inhibitors. Substitutions similar to **10** and **11** in the purine-scaffold exhibited high selectivity for Grp94 over the cytosolic Hsp90 isoforms. Therefore, these resorcinol-based Grp94 inhibitors resulted in new structure-activity relationships.

Scheme 4.3. Synthesis of methylene-linked analogues **12 – 15**.
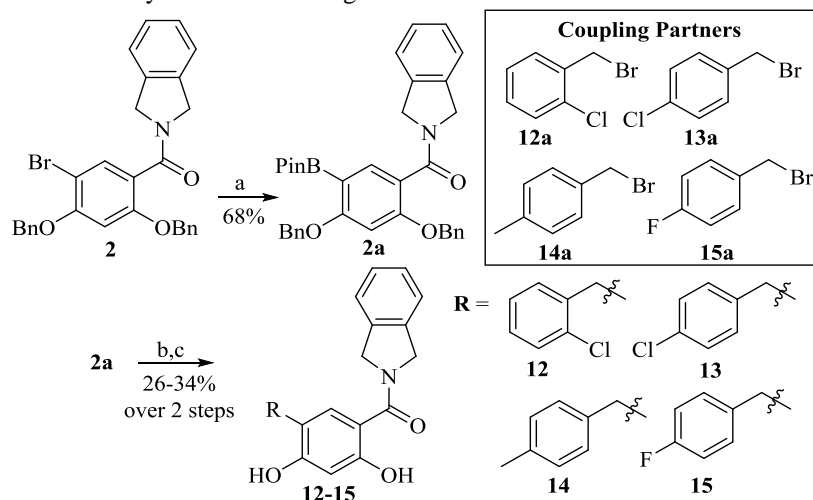
Conditions: (a) (BPin)$_2$, Pd$_2$(dba)$_3$, PCy$_3$, KOAc, Dioxane; (b) **12a-15a**, Pd(PPh$_3$)$_4$, 2M K$_2$CO$_3$, THF; (c) BBr$_3$, DCM

Due to poor selectivity manifested by the analogues containing a sulfide linker (**7 – 11**), attention turned toward modification of **6** to improve selectivity for Grp94. Compounds **7** and **10** possess substitutions at the 2'- and 4'-positions and were the only analogues that demonstrated Grp94-selectivity, suggesting that these modifications are necessary to improve selectivity. Therefore, **12** and **13** were sought to elucidate substituents that could further enhance Grp94 selectivity versus other Hsp90 isoforms. These analogues were synthesized via a palladium-catalyzed cross-coupling reaction between boronic acid pinacol ester **2a** and 2-chloro- or 4-chlorobenzyl bromide (**12a** and **13a**, respectively), followed by treatment with boron tribromide to ultimately produce **12** and **13** (**Scheme 4.3**).

Evaluation of these analogues via a fluorescence polarization assay revealed **13** to manifest 5-fold selectivity for Grp94 and improved affinity as compared to sulfide analogues **7 – 11**, whereas **12** exhibited a similar affinity and selectivity profile to the sulfide analogues (**Table 4.3**). Due to the difference in size between the sulfur atom and the methylene group, substitutions at the 4'-position did not exhibit similar affinities or selectivity profiles (e.g. **9** versus **13**). Consequently, substitutions at the 4'-position were further explored and ultimately led to the identification of **14**

172

and **15**. It was determined that increasing the size of the substituent from chloro (**13**) to methyl

(**14**) reduced selectivity and a 3-fold decrease in affinity, as compared to **13**. In contrast, decreasing

the size to a fluorine (**15**), led to ~10-fold selectivity for Grp94 and <10 nM affinity and warranted

further evaluation in cellular models of Grp94-dependent processes.

Table 4.3. Evaluation of **12 – 15** in a fluorescence polarization assay against Grp94 and Hsp90α.
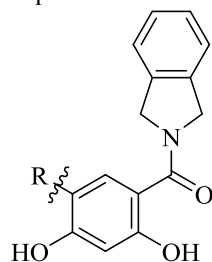
Entry	R	Grp94(μM)	Hsp90α(μM)	Fold Grp94 Selective
5		0.015 ± 0.003	0.066 ± 0.006	4
12		0.06 ± 0.01	0.20 ± 0.01	3
13		0.013 ± 0.004	0.06 ± 0.01	5
14		0.04 ± 0.001	0.04 ± 0.002	n/a
15		0.008 ± 0.001	0.077 ± 0.004	10

Data are the average of at least two independent experiments ± SEM. n/a = non-selective

Evaluation of Grp94-selective inhibitors against Multiple Myeloma

ER chaperones are upregulated in multiple myeloma as a consequence of the unfolded protein

response that leads to plasma cell differentiation and pathogenesis.[33] Grp94 is critical for the

development of multiple myeloma and its genetic deletion led to inhibition of cell growth.[24] Li and

coworkers demonstrated this phenomenon to occur through loss of the canonical Wnt signaling

pathway. LRP6, a Frizzled co-receptor, was identified as a Grp94-specific client, and genetic

knockdown of Grp94 led to degradation of LRP6 and reduction of Wnt signaling, ultimately leading to cell death via activation of caspase 9. Consequently, these Grp94-selective inhibitors were evaluated for their ability to decrease the proliferation of multiple myeloma cells.

Table 4.4. Evaluation of resorcinol-based inhibitors against the multiple myeloma cell line, RPMI8226.

Entry	R	GI$_{50}$ (µM) RPMI8226
Geldanamycin	n/a	0.003 ± 0.0006
BnIm	n/a	10.2 ± 0.5
3		>25
5		3.7 ± 0.8
11		1.9 ± 0.2
13		3.0 ± 0.4
14		2.7 ± 0.4
15		1.4 ± 0.1

Data are the average of at least two independent experiments ± SEM

Grp94-selective inhibitors (**5**, **13**, **15**), non-selective inhibitors (**11**, **14**), and an inactive control (**3**) were evaluated for anti-proliferative activity against a multiple myeloma cell line (RPMI8226) as summarized in

Table 4.4. In general, compounds that demonstrated affinity via fluorescence polarization exhibited low micromolar GI_{50} values against these cells. The Grp94-selective inhibitor **15** exhibited a GI_{50} value of 1.4 µM and was selected for further evaluation via western blot analysis of RPMI8226 cell lysates. As predicted via Grp94 KD studies, treatment with **15** demonstrated reduction of LRP6 levels (**Figure 4.4**), and this effect was seen at concentrations that mirrored cell viability, linking Grp94 inhibition to cell viability. Analysis of downstream Wnt signaling demonstrated that survivin, an anti-apoptotic protein, was degraded in a dose-dependent manner, which suggested that **15** activated apoptosis through decreased Wnt signaling. Importantly, degradation of Akt, a cytosolic Hsp90 isoform-dependent client protein, was not observed until the highest concentration. Similarly, induction of Hsp70, a hallmark of the pro-survival HSR and *pan*-Hsp90 inhibition, was not observed until the highest concentration. This result contrasted the natural product *pan*-Hsp90 inhibitor, geldanamycin (**G**), which induced Hsp70 levels at low
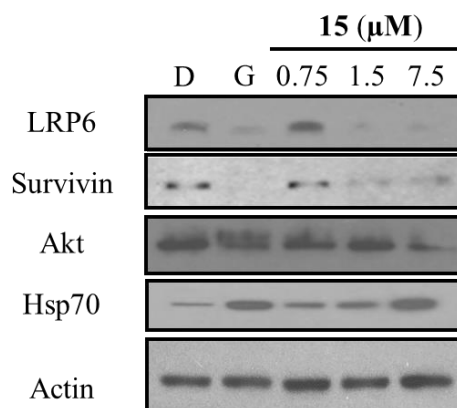
Figure 4.4. Western blot analysis of RPMI8226 cell lysates after treatment with **15**. **G** = geldanamycin (a natural product, *pan*-Hsp90 inhibitor, 0.5 µM) and D = DMSO (vehicle control, 0.1% final concentration).

concentrations. Together, these data suggest that **15** manifests Grp94-selective inhibition in cells and represents a new scaffold for future development.

Conclusions & Future Directions

Recently, Grp94-selective inhibition has emerged as a therapeutic target for the treatment of glaucoma, multiple myeloma, and metastatic cancer. Therefore, the development of new Grp94-selective scaffolds is highly desirable. In this study, a resorcinol-based, non-selective Hsp90 inhibitory scaffold was modified through a rational, structure-based drug design approach to probe an exclusive S2 sub-pocket present in Grp94, which had not been previously accessed with the resorcinol class of Hsp90 inhibitors. Structure-activity relationship studies resulted in the Grp94-selective inhibitor **15**, which manifested low nanomolar affinity and ~10-fold selectivity for Grp94 via fluorescence polarization. This work demonstrates that the S2 sub-pocket of Grp94 can be utilized to develop inhibitors that are selective for Grp94. Compound **15** also demonstrated a low micromolar GI_{50} value against the multiple myeloma cell line, RPMI8226. Further analysis via western blot demonstrated that treatment of multiple myeloma cells with **15** induced degradation of the Grp94-specfic client protein LRP6, without the degradation of the cytosolic Hsp90-dependent client protein Akt, demonstrating that **15** selectively inhibited Grp94 within cells. In addition, compound **15** did not induce the HSR at concentrations similar to those needed to degrade LRP6, which contrasts the *pan*-Hsp90 inhibitors in the clinic. These data suggest that Grp94-selective inhibition could provide an attractive therapeutic option for the treatment of multiple myeloma. Based on the success of converting the non-selective inhibitor **1** into a Grp94-selective inhibitor that takes advantage of the Grp94-exclusive S2 sub-pocket, a structure-based approach to modify other resorcinol-based *pan*-Hsp90 inhibitors could lead to more efficacious Grp94-selective inhibitors.

Experimental Section

Chemistry General. ^{1}H NMR were recorded at 400 (Bruker AVIIIHD 400 MHz NMR with a broadband X-channel detect gradient probe) or 500 MHz (Avance AVIII 500 MHz spectrometer with a dual carbon/proton cryoprobe), ^{19}F NMR were recorded at 376 MHz (Bruker AVIIIHD 400 MHz NMR equipped with a multinuclear broadband fluorine observe probe), and ^{13}C NMR were recorded at 125 MHz (Bruker AVIII spectrometer equipped with a cryogenically cooled carbon observe probe); chemical shifts are reported in δ (ppm) relative to the internal standard (CDCl$_3$, 7.26 ppm). HRMS spectra were recorded with a LCT Premier with ESI ionization. All biologically tested compounds were determined to be >95% pure via ^{1}H and ^{13}C NMR. TLC analysis was performed on glass backed silica gel plates and visualized by UV light. All solvents were reagent grade and used without further purification.

3
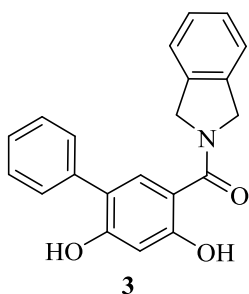
(4,6-Dihydroxy-[1,1'-biphenyl]-3-yl)(isoindolin-2-yl)methanone (**3**). A microwave vial was charged with **2** (100 mg, 0.19 mmol, 1 equiv.), phenyl boronic acid (549 mg, 0.39 mmol, 2.0 equiv.), and [1,1′-Bis(diphenylphosphino)ferrocene]dichloropalladium (27 mg, 0.038 mmol, 0.2 equiv.). The tube was sealed with a cap lined with a disposable Teflon septum. The tube was evacuated and purged with nitrogen (3 times), before the addition of a solvent mixture of toluene (1.0 mL), ethanol (1.0 mL), and saturated sodium bicarbonate solution (1.0 mL) by syringe. The resulting mixture was heated at 80 °C for 14 h, cooled to rt, and filtered through a small pad of celite (elution with ethyl acetate). Solvent was removed and the residue purified by flash

chromatography (SiO$_2$, 1:3 ethyl acetate/hexanes) to give the corresponding 5-substituted product, which was used further as obtained, and taken in dichloromethane (2 mL), cooled to 0 °C before the addition of 1 M solution of boron tribromide (0.5 mL). The resulting mixture was stirred for 6 h, quenched with saturated sodium bicarbonate solution (5 mL) and extracted with dichloromethane (2 × 10 mL). The combined organic layers were washed with saturated sodium chloride solution (15 mL), dried over anhydrous sodium sulfate, filtered, and concentrated. The residue purified with flash chromatography (SiO$_2$, 1:3 ethyl acetate/hexanes) to give the desired product **3** as white amorphous solid (31 mg, 49 %). ^{1}H NMR (500 MHz, CDCl$_3$) δ 11.67 (s, 1H), 7.57 (s, 1H), 7.56 – 7.41 (m, 5H), 7.34 – 7.28 (m, 4H), 6.63 (s, 1H), 5.78 (s, 1H), 5.11 (s, 4H). ^{13}C NMR (125 MHz, CDCl$_3$) δ 170.7, 162.6, 156.8, 136.6, 136.0 (2), 130.4, 129.7 (4), 128.1 (3), 128.0, 122.8, 119.7, 110.4, 104.5, 55.2, 53.4. HRMS (ESI-) m/z [M-H$^+$] calcd for C$_{21}$H$_{16}$NO$_3$, 330.1130, found 330.1124.

4
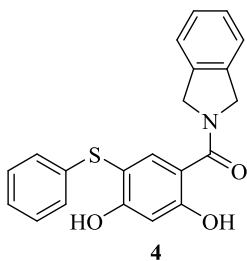
(2,4-Dihydroxy-5-(phenylthio)phenyl)(isoindolin-2-yl)methanone (**4**). A microwave vial was charged with **2** (100 mg, 0.19 mmol, 1 equiv.), thiophenol (0.02 mL, 0.19 mmol, 1.0 equiv.), Tris(dibenzylideneacetone)dipalladium(0) (90 mg, 0.01 mmol, 0.05 equiv.), 1,1′-Ferrocenediyl-bis(diphenylphosphine) (110 mg, 0.02 mmol, 0.1 equiv.), and diisopropyethylamine (0.04 mL, 0.21 mmol, 1.1 equiv.). The tube was sealed with a cap lined with a disposable Teflon septum. The tube was evacuated and purged with nitrogen (3 times), before the addition of toluene (4.0 mL) by syringe. The resulting mixture was heated at 115 °C for 14 h, cooled to rt, and filtered

through a small pad of celite (elution with ethyl acetate). Solvent was removed and the residue passed through a filter column (SiO$_2$, 1:3 ethyl acetate/hexanes) to give the corresponding 5-substituted product, which was used further as obtained, and taken in dichloromethane (5 mL), cooled to 0 °C before the addition of 1 M solution of boron tribromide (0.8 mL). The resulting mixture was stirred for 6 h, quenched with water (5 mL) and extracted with dichloromethane (2 × 10 mL). The combined organic layers were washed with saturated sodium chloride solution (15 mL), dried over anhydrous sodium sulfate, filtered, and concentrated. The residue purified with flash chromatography (SiO$_2$, 1:3 ethyl acetate/hexanes) to give the desired product **4** as yellow amorphous solid (43 mg, 62 %). ^{1}H NMR (400 MHz, CDCl$_3$) δ 12.09 (s, 1H), 7.91 (s, 1H), 7.29 (dd, J = 9.7, 2.4 Hz, 5H), 7.18 (t, J = 7.3 Hz, 1H), 7.11 – 7.05 (m, 2H), 6.76 (s, 1H), 6.71 (s, 1H), 5.07 (s, 4H). ^{13}C NMR (126 MHz, CDCl$_3$) δ 169.9, 165.5, 161.2, 137.7 (2C), 136.3, 129.5 (2C), 128.1, 126.4 (2C), 126.4 (2C), 122.7, 111.2 (2C), 105.9, 104.2 (2C), 77.4 (2C). HRMS (ESI) [M+H]$^+$ for C$_{21}$H$_{18}$NO$_3$S: 364.1007, found 364.0996.
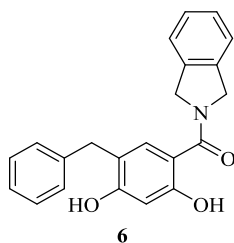

6

(5-Benzyl-2,4-dihydroxyphenyl)(isoindolin-2-yl)methanone (**5**). A microwave vial was charged with **2** (100 mg, 0.19 mmol, 1 equiv.), potassium benzyltrifluoroborate (60 mg, 0.3 mmol, 1.5 equiv.), RuPhos (15 mg, 0.03 mmol, 0.17 equiv.), palladium (II) acetate (3 mg, 0.015 mmol, 0.08 equiv.), and potassium phosphate tribasic (215 mg, 1 mmol, 5.2 equiv.). The tube was sealed with a cap lined with a disposable Teflon septum. The tube was evacuated and purged with nitrogen (3 times), before the addition of toluene (1.7 mL) and water (0.3 mL) by syringe. The resulting mixture was heated at 115 °C for 16 h, cooled to rt, and filtered through a small pad of celite

(elution with ethyl acetate). Solvent was removed and the residue purified through a filter column (SiO$_2$, 1:3 ethyl acetate/hexanes) to give the corresponding 5-substituted product, which was used further as obtained, and taken in dichloromethane (5 mL), cooled to 0 °C before the addition of 1 M solution of boron tribromide (0.7 mL). The resulting mixture was stirred for 6 h, quenched with water (5 mL) and extracted with dichloromethane (2 × 10 mL). The combined organic layers were washed with saturated sodium chloride solution (15 mL), dried over anhydrous sodium sulfate, filtered, and concentrated. The residue purified with flash chromatography (SiO$_2$, 1:2 ethyl acetate/hexanes) to give the desired product **5** as white amorphous solid (37 mg, 56 %). ^{1}H NMR (400 MHz, CDCl$_3$) δ 11.71 (s, 1H), 7.36 (dd, J = 8.5, 6.7 Hz, 2H), 7.32 – 7.26 (m, 5H), 7.24 (d, J = 9.4 Hz, 3H), 6.43 (s, 1H), 4.91 (br s, 4H), 3.97 (s, 2H). ^{13}C NMR (126 MHz, CDCl$_3$) δ 170.4, 161.4, 157.4, 139.8, 130.8, 130.5, 129.0 (2C), 128.7 (2C), 128.6 (2C), 127.6, 126.4, 122.4, 117.9, 109.3, 103.8 (2C), 68.1, 38.6, 35.1. HRMS (ESI) [M+H]$^{+}$ for C$_{22}$H$_{20}$NO$_3$: 346.1143, found: 346.1146.
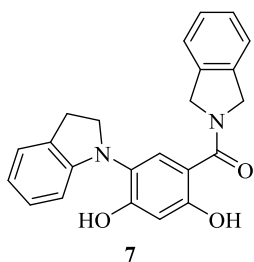

7

(2,4-Dihydroxy-5-(indolin-1-yl)phenyl)(isoindolin-2-yl)methanone (**6**). A microwave vial was charged with **2** (150 mg, 0.36 mmol, 1 equiv.), indoline (0.06 mL, 0.55 mmol, 1.5 equiv.), RuPhos (15 mg, 0.03 mmol, 0.09 equiv.), Tris(dibenzylideneacetone)dipalladium(0) (35 mg, 0.033 mmol, 0.09 equiv.), and sodium *tert*-butoxide (55 mg, 0.55 mmol, 1.5 equiv.). The tube was sealed with a cap lined with a disposable Teflon septum. The tube was evacuated and purged with nitrogen (3 times), before the addition of toluene (3 mL) by syringe. The resulting mixture was heated at 115

°C for 16 h, cooled to rt, and filtered through a small pad of celite (elution with ethyl acetate). Solvent was removed and the residue purified through a filter column (SiO$_2$, 1:3 ethyl acetate/hexanes) to give the corresponding 5-substituted product, which was used further as obtained, and taken in dichloromethane (5 mL), cooled to 0 °C before the addition of 1 M solution of boron tribromide (0.4 mL). The resulting mixture was stirred for 6 h, quenched with water (5 mL) and extracted with dichloromethane (2 × 10 mL). The combined organic layers were washed with saturated sodium chloride solution (15 mL), dried over anhydrous sodium sulfate, filtered, and concentrated.   The residue purified with flash chromatography (SiO$_2$, 1:2 ethyl acetate/hexanes) to give the desired product **6** as white amorphous solid (19 mg, 14 %). ^{1}H NMR (400 MHz, CDCl$_3$) δ 7.50 (s, 1H), 7.32 – 7.27 (m, 3H), 7.24 (d, J = 7.6 Hz, 2H), 7.10 (td, J = 7.7, 1.2 Hz, 1H), 6.86 (td, J = 7.4, 1.0 Hz, 1H), 6.69 (s, 1H), 6.39 (d, J = 7.9 Hz, 1H), 4.99 (s, 4H), 3.67 (s, 2H), 3.20 (t, J = 8.1 Hz, 2H). ^{13}C NMR (151 MHz, CDCl$_3$) δ 170.3, 163.0, 161.3, 157.7, 155.9, 151.5, 130.5, 128.8, 128.3, 127.5, 125.3, 124.9, 124.1, 122.9, 121.3, 120.8, 120.1, 109.6, 103.4, 56.8, 53.4, 29.6, 29.1. HRMS (ESI) [M+Na]$^+$ for C$_{23}$H$_{20}$N$_2$O$_3$Na: 395.1372, found: 395.1383.
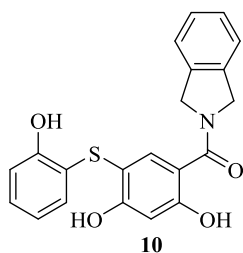

10

(2,4-Dihydroxy-5-((2-hydroxyphenyl)thio)phenyl)(isoindolin-2-yl)methanone   (**7**).   A microwave vial was charged with **2** (100 mg, 0.19 mmol, 1 equiv.), 2-methoxythiophenol (0.02 mL, 0.19 mmol, 1.0 equiv.), Tris(dibenzylideneacetone)dipalladium(0) (90 mg, 0.01 mmol, 0.05 equiv.), 1,1′-Ferrocenediyl-bis(diphenylphosphine) (110 mg, 0.02 mmol, 0.1 equiv.), and diisopropyethylamine (0.04 mL, 0.21 mmol, 1.1 equiv.). The tube was sealed with a cap lined with a disposable Teflon septum. The tube was evacuated and purged with nitrogen (3 times), before

the addition of toluene (4.0 mL) by syringe. The resulting mixture was heated at 115 °C for 14 h, cooled to rt, and filtered through a small pad of celite (elution with ethyl acetate). Solvent was removed and the residue passed through a filter column (SiO$_2$, 1:3 ethyl acetate/hexanes) to give the corresponding 5-substituted product, which was used further as obtained, and taken in dichloromethane (5 mL), cooled to 0 °C before the addition of 1 M solution of boron tribromide (0.8 mL). The resulting mixture was stirred for 6 h, quenched with water (5 mL) and extracted with dichloromethane (2 × 10 mL). The combined organic layers were washed with saturated sodium chloride solution (15 mL), dried over anhydrous sodium sulfate, filtered, and concentrated. The residue purified with flash chromatography (SiO$_2$, 1:3 ethyl acetate/hexanes) to give the desired product **7** as yellow amorphous solid (69 mg, 92 %). ^{1}H NMR (400 MHz, CDCl$_3$) δ 7.70 (s, 1H), 7.35 – 7.27 (m, 3H), 7.26 (m, 3H), 6.98 (dd, J = 8.1, 1.3 Hz, 1H), 6.91 (td, J = 7.5, 1.2 Hz, 1H), 6.59 (s, 1H), 4.96 (s, 4H). ^{13}C NMR (126 MHz, CDCl$_3$) δ 169.6, 163.7, 159.6, 155.3, 134.9 (2C), 133.6 (2C), 130.5 (2C), 127.8, 122.5, 121.5 (2C), 120.2, 115.7, 110.6, 108.9, 104.0, 60.4 (2C). HRMS (ESI) [M+H]$^+$ for C$_{21}$H$_{18}$NO$_4$S: 380.0957, found 380.0976.

11

(2,4-Dihydroxy-5-((3-methoxyphenyl)thio)phenyl)(isoindolin-2-yl)methanone (**8**). A microwave vial was charged with **2** (100 mg, 0.19 mmol, 1 equiv.), 3-methoxythiophenol (0.03 mL, 0.19 mmol, 1.0 equiv.), Tris(dibenzylideneacetone)dipalladium(0) (90 mg, 0.01 mmol, 0.05 equiv.), 1,1′-Ferrocenediyl-bis(diphenylphosphine) (110 mg, 0.02 mmol, 0.1 equiv.), and diisopropyethylamine (0.04 mL, 0.21 mmol, 1.1 equiv.). The tube was sealed with a cap lined with a disposable Teflon septum. The tube was evacuated and purged with nitrogen (3 times), before

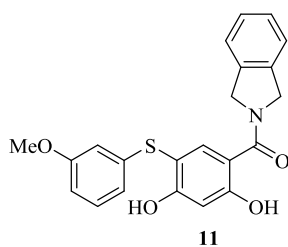the addition of toluene (4.0 mL) by syringe. The resulting mixture was heated at 115 °C for 14 h, cooled to rt, and filtered through a small pad of celite (elution with ethyl acetate). Solvent was removed and the residue passed through a filter column (SiO$_2$, 1:3 ethyl acetate/hexanes) to give the corresponding 5-substituted product, which was used further as obtained, and taken in dichloromethane (5 mL), cooled to 0 °C before the addition of 1 M solution of boron tribromide (1.0 mL). The resulting mixture was stirred for 6 h, quenched with water (5 mL) and extracted with dichloromethane (2 × 10 mL). The combined organic layers were washed with saturated sodium chloride solution (15 mL), dried over anhydrous sodium sulfate, filtered, and concentrated. The residue purified with flash chromatography (SiO$_2$, 1:3 ethyl acetate/hexanes) to give the desired product **8** as yellow amorphous solid (68 mg, 94 %). ^{1}H NMR (400 MHz, CDCl$_3$) δ 7.71 (d, J = 1.3 Hz, 1H), 7.26 (m, 4H), 7.07 (td, J = 8.0, 1.3 Hz, 1H), 6.67 – 6.63 (m, 1H), 6.61 – 6.58 (m, 1H), 6.57 (d, J = 1.3 Hz, 1H), 6.50 (q, J = 1.8 Hz, 1H), 4.96 (s, 4H), 2.79 (s, 3H). ^{13}C NMR (126 MHz, CDCl$_3$) δ 169.4, 162.5, 160.7, 157.4, 137.4 (2C), 136.8 (2C), 129.9 (2C), 127.6, 122.4, 118.1 (2C), 113.3, 113.2, 111.5, 107.2, 103.4, 66.8, 55.1, 53.1. HRMS (ESI) [M]$^{+}$ for C$_{22}$H$_{19}$NO$_4$S: 393.1035, found: 393.1041.

12

(2,4-Dihydroxy-5-((4-hydroxyphenyl)thio)phenyl)(isoindolin-2-yl)methanone (**9**). A microwave vial was charged with **2** (100 mg, 0.19 mmol, 1 equiv.), 4-methoxythiophenol (0.03 mL, 0.19 mmol, 1.0 equiv.), Tris(dibenzylideneacetone)dipalladium(0) (90 mg, 0.01 mmol, 0.05

equiv.), 1,1′-Ferrocenediyl-bis(diphenylphosphine) (110 mg, 0.02 mmol, 0.1 equiv.), and diisopropyethylamine (0.04 mL, 0.21 mmol, 1.1 equiv.). The tube was sealed with a cap lined with a disposable Teflon septum. The tube was evacuated and purged 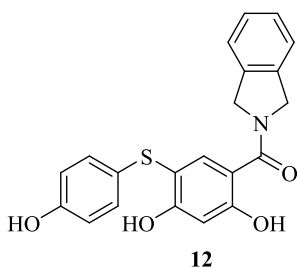with nitrogen (3 times), before the addition of toluene (4.0 mL) by syringe. The resulting mixture was heated at 115 °C for 14 h, cooled to rt, and filtered through a small pad of celite (elution with ethyl acetate). Solvent was removed and the residue passed through a filter column (SiO_2, 1:3 ethyl acetate/hexanes) to give the corresponding 5-substituted product, which was used further as obtained, and taken in dichloromethane (5 mL), cooled to 0 °C before the addition of 1 M solution of boron tribromide (1.0 mL). The resulting mixture was stirred for 6 h, quenched with water (5 mL) and extracted with dichloromethane (2 × 10 mL). The combined organic layers were washed with saturated sodium chloride solution (15 mL), dried over anhydrous sodium sulfate, filtered, and concentrated. The residue purified with flash chromatography (SiO_2, 1:3 ethyl acetate/hexanes) to give the desired product **9** as yellow amorphous solid (53 mg, 74 %). ^{1}H NMR (400 MHz, $CDCl_3$) δ 11.95 (s, 1H), 7.87 (s, 1H), 7.30 (m, 4H), 7.07 (s, 2H), 6.83 (s, 1H), 6.77 (d, J = 8.7 Hz, 2H), 6.67 (s, 1H), 5.06 (s, 4H). ^{13}C NMR (126 MHz, $CDCl_3$) δ 170.2, 165.2, 161.0, 155.3, 137.4 (2C), 129.8 (2C), 128.3, 127.0, 123.0, 118.0, 116.9 (2C), 111.3 (2C), 108.3, 104.3 (2C), 60.9 (2C). HRMS (ESI) [M]$^+$ for $C_{21}H_{17}NO_4S$ 379.0878, found: 379.0876.

13

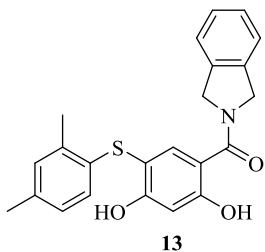*(5-((2,4-Dimethylphenyl)thio)-2,4-dihydroxyphenyl)(isoindolin-2-yl)methanone* (**10**). A microwave vial was charged with **2** (100 mg, 0.19 mmol, 1 equiv.), 2,4-dimethylthiophenol (0.03 mL, 0.19 mmol, 1.0 equiv.), Tris(dibenzylideneacetone)dipalladium(0) (90 mg, 0.01 mmol, 0.05

equiv.), 1,1′-Ferrocenediyl-bis(diphenylphosphine) (110 mg, 0.02 mmol, 0.1 equiv.), and diisopropyethylamine (0.04 mL, 0.21 mmol, 1.1 equiv.). The tube was sealed with a cap lined with a disposable Teflon septum. The tube was evacuated and purged with nitrogen (3 times), before the addition of toluene (4.0 mL) by syringe. The resulting mixture was heated at 115 °C for 14 h, cooled to rt, and filtered through a small pad of celite (elution with ethyl acetate). Solvent was removed and the residue passed through a filter column (SiO$_2$, 1:3 ethyl acetate/hexanes) to give the corresponding 5-substituted product, which was used further as obtained, and taken in dichloromethane (5 mL), cooled to 0 °C before the addition of 1 M solution of boron tribromide (0.8 mL). The resulting mixture was stirred for 6 h, quenched with water (5 mL) and extracted with dichloromethane (2 × 10 mL). The combined organic layers were washed with saturated sodium chloride solution (15 mL), dried over anhydrous sodium sulfate, filtered, and concentrated. The residue purified with flash chromatography (SiO$_2$, 1:3 ethyl acetate/hexanes) to give the desired product **10** as yellow amorphous solid (43 mg, 58 %). ^{1}H NMR (400 MHz, CDCl$_3$) δ 12.06 (s, 1H), 7.83 (s, 1H), 7.31 (m, 4H), 7.03 (m, 1H), 6.89 (dd, J = 8.0, 1.9 Hz, 1H), 6.70 (s, 1H), 6.69 (s, 1H), 6.62 (d, J = 8.0 Hz, 1H), 5.05 (s, 4H), 2.43 (s, 3H), 2.28 (s, 3H). ^{13}C NMR (126 MHz, CDCl$_3$) δ 169.6, 164.9, 160.8, 137.2 (2C), 135.9, 135.2, 131.5, 131.3 (2C), 127.7, 127.5 (2C), 125.6, 122.4, 111.0, 105.7, 103.9 (2C), 55.4, 53.5, 20.7, 19.8. HRMS (ESI) [M+H]$^+$ for C$_{23}$H$_{22}$NO$_3$S: 392.1320, found: 392.1336.

15

(5-((2,5-Dimethylphenyl)thio)-2,4-dihydroxyphenyl)(isoindolin-2-yl)methanone (**11**). A microwave vial was charged with **2** (100 mg, 0.19 mmol, 1 equiv.), 2,5-dimethylthiophenol (0.03

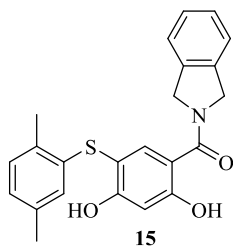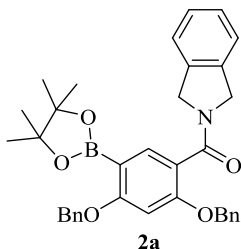mL, 0.19 mmol, 1.0 equiv.), Tris(dibenzylideneacetone)dipalladium(0) (90 mg, 0.01 mmol, 0.05 equiv.), 1,1′-Ferrocenediyl-bis(diphenylphosphine) (110 mg, 0.02 mmol, 0.1 equiv.), and diisopropyethylamine (0.04 mL, 0.21 mmol, 1.1 equiv.). The tube was sealed with a cap lined with a disposable Teflon septum. The tube was evacuated and purged with nitrogen (3 times), before the addition of toluene (4.0 mL) by syringe. The resulting mixture was heated at 115 °C for 14 h, cooled to rt, and filtered through a small pad of celite (elution with ethyl acetate). Solvent was removed and the residue passed through a filter column (SiO$_2$, 1:3 ethyl acetate/hexanes) to give the corresponding 5-substituted product, which was used further as obtained, and taken in dichloromethane (5 mL), cooled to 0 °C before the addition of 1 M solution of boron tribromide (0.8 mL). The resulting mixture was stirred for 6 h, quenched with water (5 mL) and extracted with dichloromethane (2 × 10 mL). The combined organic layers were washed with saturated sodium chloride solution (15 mL), dried over anhydrous sodium sulfate, filtered, and concentrated. The residue purified with flash chromatography (SiO$_2$, 1:3 ethyl acetate/hexanes) to give the desired product **11** as yellow amorphous solid (48 mg, 65 %). ^{1}H NMR (400 MHz, CDCl$_3$) δ 12.08 (s, 1H), 7.84 (s, 1H), 7.31 (dt, J = 6.5, 3.6 Hz, 3H), 7.08 (d, J = 7.6 Hz, 1H), 6.95 − 6.89 (m, 1H), 6.72 (m, 2H), 6.53 − 6.47 (m, 1H), 5.06 (s, 4H), 2.42 (s, 3H), 2.20 (s, 3H). ^{13}C NMR (126 MHz, CDCl$_3$) δ 169.9, 165.2, 161.2, 137.6 (2C), 136.9, 135.0, 132.3, 130.5 (2C), 128.0, 126.9, 125.7, 122.7, 111.3, 105.5, 104.2 (2C), 55.7, 53.8, 21.3, 19.6. HRMS (ESI) [M+H]$^+$ for C$_{23}$H$_{22}$NO$_3$S: 392.1320, found: 392.1310.

2a

(2,4-Bis(benzyloxy)-5-(4,4,5,5-tetramethyl-1,3,2-dioxaborolan-2-yl)phenyl)(isoindolin-2-yl)methanone (**2a**). A microwave vial was charged with **2** (100 mg, 0.19 mmol, 1 equiv.), bis(pinacolato)diboron (74 mg, 0.29 mmol, 1.5 equiv.), Tris(dibenzylideneacetone)dipalladium(0) (9 mg, 0.01 mmol, 0.05 equiv.), tricylcohexylphosphine (7 mg, 0.02 mg, 0.12 equiv.), and potassium acetate (29 mg, 0.29 mmol, 1.5 equiv.). The tube was sealed with a cap lined with a disposable Teflong septum. The tube was evacuated and purged with nitrogen (3 times) before the addition of dioxane (2 mL) by syringe. The resulting mixture was heated to 115 °C for 16 h, cooled to rt, and filtered through a small pad of celite (elution with EtOAc). The solvent was removed and the residue purified by flash chromatography (SiO$_2$, 3:10 EtOAc:Hexanes) to afford **2a** as a gold oil (73 mg, 68%). ^{1}H NMR (400 MHz, CDCl$_3$) δ 7.74 (s, 1H), 7.58 (ddd, J = 7.4, 1.4, 0.7 Hz, 2H), 7.44 − 7.36 (m, 3H), 7.35 − 7.28 (m, 6H), 7.25 − 7.21 (m, 2H), 7.09 (d, J = 7.3 Hz, 1H), 6.55 (s, 1H), 5.16 (s, 2H), 5.09 (s, 2H), 4.97 (s, 2H), 4.62 (s, 2H), 1.33 (s, 12H). ^{13}C NMR (151 MHz, CDCl$_3$) δ 168.7, 166.0, 158.7, 137.4, 137.1, 137.0, 136.9, 136.7, 128.9 (2C), 128.9, 128.6 (2C), 128.3, 127.9, 127.9, 127.7, 127.3 (2C), 127.1 (2C), 123.4, 122.8, 120.5, 98.8, 83.8, 75.4, 70.9, 70.6, 53.8, 52.4, 25.3 (2C), 25.2 (2C). HRMS (ESI) [M+H]$^+$ for C$_{35}$H$_{37}$BNO$_5$ 562.2765, found 562.2778.

18

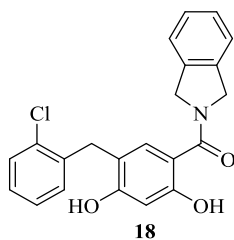*(5-(2-Chlorobenzyl)-2,4-dihydroxyphenyl)(isoindolin-2-yl)methanone* (**12**). A microwave vial was charged with **2a** (100 mg, 0.18 mmol, 1 equiv.), 2-chlorobenzyl bromide (0.02 mL, 0.18 mmol, 1.0 equiv.), and tetrakis(triphenylphosphine)palladium(0) (5 mg, 0.004 mmol, 0.025 equiv.). The tube was sealed with a cap lined with a disposable Teflon septum. The tube was evacuated and

purged with nitrogen (3 times), before the addition of tetrahydrofuran (2 mL) and 2M potassium

carbonate (0.3 mL, 0.5 mmol, 3 equiv.) by syringe. The resulting mixture was heated at 95 °C for

18 h, cooled to rt, and filtered through a small pad of celite (elution with ethyl acetate). Solvent

was removed and the residue purified by flash chromatography (SiO$_2$, 1:3 ethyl acetate/hexanes)

to give the corresponding 5-substituted product, which was used further as obtained, and taken in

dichloromethane (2 mL), cooled to 0 °C before the addition of 1 M solution of boron tribromide

(0.7 mL). The resulting mixture was stirred for 6 h, quenched with water (5 mL) and extracted

with dichloromethane (2 × 10 mL). The combined organic layers were washed with saturated

sodium chloride solution (15 mL), dried over anhydrous sodium sulfate, filtered, and concentrated.

The residue purified with flash chromatography (SiO$_2$, 1:2 ethyl acetate/hexanes) to give the

desired product **12** as white amorphous solid (23 mg, 34 %). ^{1}H NMR (400 MHz, CDCl$_3$) δ 11.75

(s, 1H), 7.47 – 7.42 (m, 1H), 7.30 (m, 4H), 7.26 – 7.20 (m, 4H), 7.20 (d, J = 0.8 Hz, 1H), 6.44 (s,

1H), 5.03 – 4.83 (m, 4H), 4.07 (s, 2H). ^{13}C NMR (151 MHz, CDCl$_3$) δ 162.0, 159.4, 157.9, 138.2,

131.6, 131.1, 130.9, 130.6, 129.9, 128.6, 128.4, 127.5, 124.6, 123.8, 116.7, 109.8, 104.2, 103.7,

90.7, 50.3 (2C), 33.1. HRMS (ESI) [M+H]$^+$ for C$_{22}$H$_{19}$ClNO$_3$ 380.1053, found 380.1046.

19
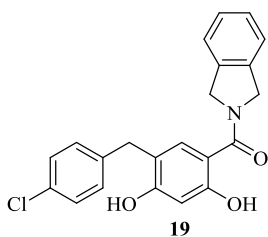
(5-(4-Chlorobenzyl)-2,4-dihydroxyphenyl)(isoindolin-2-yl)methanone (**13**). A microwave vial

was charged with **2a** (100 mg, 0.18 mmol, 1 equiv.), 4-chlorobenzyl bromide (34 mg, 0.18 mmol,

1.0 equiv.), and tetrakis(triphenylphosphine)palladium(0) (5 mg, 0.004 mmol, 0.025 equiv.). The

tube was sealed with a cap lined with a disposable Teflon septum. The tube was evacuated and

purged with nitrogen (3 times), before the addition of tetrahydrofuran (2 mL) and 2M potassium

carbonate (0.3 mL, 0.5 mmol, 3 equiv.) by syringe. The resulting mixture was heated at 95 °C for 18 h, cooled to rt, and filtered through a small pad of celite (elution with ethyl acetate). Solvent was removed and the residue purified by flash chromatography (SiO$_2$, 1:3 ethyl acetate/hexanes) to give the corresponding 5-substituted product, which was used further as obtained, and taken in dichloromethane (2 mL), cooled to 0 °C before the addition of 1 M solution of boron tribromide (0.3 mL). The resulting mixture was stirred for 6 h, quenched with water (5 mL) and extracted with dichloromethane (2 × 10 mL). The combined organic layers were washed with saturated sodium chloride solution (15 mL), dried over anhydrous sodium sulfate, filtered, and concentrated. The residue purified with flash chromatography (SiO$_2$, 1:2 ethyl acetate/hexanes) to give the desired product **13** as white amorphous solid (18 mg, 26 %). ^{1}H NMR (400 MHz, CDCl$_3$) δ 7.26 (s, 4H), 7.25 – 7.10 (m, 5H), 6.36 (s, 1H), 4.89 (s, 4H), 3.91 (s, 2H). ^{13}C NMR (126 MHz, CDCl$_3$) δ 170.6, 161.6, 158.0, 139.1 (2C), 132.2, 130.6 (2C), 130.5 (2C), 128.8 (2C), 127.9 (2C), 122.6 (2C), 118.0, 109.3, 103.9, 50.3, 50.1, 34.6. HRMS (ESI) [M+H]$^+$ for C$_{22}$H$_{19}$ClNO$_3$ 380.1053, found 380.1071.

20

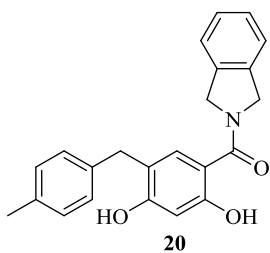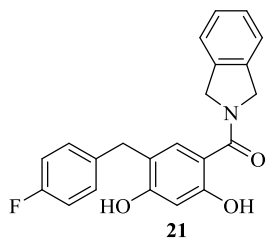*(2,4-Dihydroxy-5-(4-methylbenzyl)phenyl)(isoindolin-2-yl)methanone* (**14**). A microwave vial was charged with **2a** (100 mg, 0.18 mmol, 1 equiv.), 4-methylbenzyl bromide (48 mg, 0.18 mmol, 1.0 equiv.), and tetrakis(triphenylphosphine)palladium(0) (5 mg, 0.004 mmol, 0.025 equiv.). The tube was sealed with a cap lined with a disposable Teflon septum. The tube was evacuated and purged with nitrogen (3 times), before the addition of tetrahydrofuran (2 mL) and 2M potassium carbonate (0.3 mL, 0.5 mmol, 3 equiv.) by syringe. The resulting mixture was heated at 95 °C for

18 h, cooled to rt, and filtered through a small pad of celite (elution with ethyl acetate). Solvent was removed and the residue purified by flash chromatography (SiO$_2$, 1:3 ethyl acetate/hexanes) to give the corresponding 5-substituted product, which was used further as obtained, and taken in dichloromethane (2 mL), cooled to 0 °C before the addition of 1 M solution of boron tribromide (0.3 mL). The resulting mixture was stirred for 6 h, quenched with water (5 mL) and extracted with dichloromethane (2 × 10 mL). The combined organic layers were washed with saturated sodium chloride solution (15 mL), dried over anhydrous sodium sulfate, filtered, and concentrated. The residue purified with flash chromatography (SiO$_2$, 1:2 ethyl acetate/hexanes) to give the desired product **14** as white amorphous solid (18 mg, 26 %). ^{1}H NMR (400 MHz, CDCl$_3$) δ 11.68 (s, 1H), 7.30 (m, 3H), 7.25 (m, 2H), 7.19 – 7.12 (m, 4H), 6.43 (s, 1H), 4.93 (s, 4H), 3.93 (s, 2H), 2.35 (s, 3H). HRMS (ESI) [M+Na]$^+$ for C$_{23}$H$_{21}$NO$_3$Na 382.1419, found 382.1423.

21

(5-(4-Fluorobenzyl)-2,4-dihydroxyphenyl)(isoindolin-2-yl)methanone (**15**). A microwave vial was charged with **2a** (100 mg, 0.18 mmol, 1 equiv.), 4-methylbenzyl bromide (48 mg, 0.18 mmol, 1.0 equiv.), and tetrakis(triphenylphosphine)palladium(0) (5 mg, 0.004 mmol, 0.025 equiv.). The tube was sealed with a cap lined with a disposable Teflon septum. The tube was evacuated and purged with nitrogen (3 times), before the addition of tetrahydrofuran (2 mL) and 2M potassium carbonate (0.3 mL, 0.5 mmol, 3 equiv.) by syringe. The resulting mixture was heated at 95 °C for 18 h, cooled to rt, and filtered through a small pad of celite (elution with ethyl acetate). Solvent was removed and the residue purified by flash chromatography (SiO$_2$, 1:3 ethyl acetate/hexanes) to give the corresponding 5-substituted product, which was used further as obtained, and taken in

dichloromethane (2 mL), cooled to 0 °C before the addition of 1 M solution of boron tribromide (0.3 mL). The resulting mixture was stirred for 6 h, quenched with water (5 mL) and extracted with dichloromethane (2 × 10 mL). The combined organic layers were washed with saturated sodium chloride solution (15 mL), dried over anhydrous sodium sulfate, filtered, and concentrated. The residue purified with flash chromatography (SiO$_2$, 1:2 ethyl acetate/hexanes) to give the desired product **15** as white amorphous solid (18 mg, 26 %). ^{1}H NMR (400 MHz, CDCl$_3$) δ 11.70 (s, 1H), 7.31 (m, 3H), 7.25 – 7.18 (m, 4H), 7.08 – 7.00 (m, 2H), 6.42 (s, 1H), 4.94 (s, 4H), 3.94 (s, 2H). ^{19}F NMR (376 MHz, CDCl$_3$) δ – 117.4 (s, 1F). ^{13}C NMR (126 MHz, CDCl$_3$) δ 170.7, 161.7, 157.6, 130.6 (2C), 130.5, 130.2, 130.2, 128.4, 128.0, 124.0 (d, J = 87.1 Hz), 118.1, 115.7 (2C), 115.5 (2C), 109.6, 104.1, 103.6, 53.6, 50.1, 34.5. HRMS (ESI) [M+H]$^+$ for C$_{22}$H$_{19}$FNO$_3$ 364.1349, found 364.1366.

Biological Protocols

Fluorescence Polarization. The assay was performed in 96-well black, flat-bottom plates with a final volume of 100 µL. 25 µL of assay buffer (20 mM HEPES, pH 7.3, 50 mM KCl, 5 mM MgCl$_2$, 20 mM Na$_2$MoO$_4$, 2 mM DTT, 0.1 mg/mL BGG, and 0.01% NP-40) were added, followed by 25 µL of assay buffer containing 6 nM FITC-GDA (fluorescent tracer, stock in DMSO, diluted in assay buffer) and 50 µL of assay buffer containing 10 nM of either Grp94 (Enzo) or Hsp90α (Dickey Lab) were added to each well. For each plate, wells containing buffer only (background), tracer in buffer only (low polarization control) and protein, tracer, and 1% DMSO (final concentration, high polarization control) were included. Compounds were then added with a final concentration of DMSO = 1%. Plates were incubated at 4 ˚C with rocking for 24 h. Polarization values (in mP units) were measured at 37 ˚C with an excitation filter at 485 nm and an emission filter at 528 nm. Polarization values were correlated to % tracer bound and compound

concentrations. The concentration at which the tracer was 50% displaced by compound of interested were calculated and reported as apparent K_d's.

Cell Culture and Western blot. RPMI8226 cells (ATCC) were grown in a water jacketed incubator at 37 °C with 5% CO_2 in RPMI1640 media supplemented with 10% FBS (Corning) and 1% penicillin/streptomycin (Gibco). For anti-proliferation, cells were seeded in 96-well plates at 2000 cell/well and 0.1 mL/well. Then placed in the incubator for 24 h. Compounds or vehicle were administered in DMSO (0.5% DMSO final concentration). After 72 h, the % viable cells were determined using the MTS/PMS cell proliferation kit (Promega) per the manufacturer's instructions. Cells treated with vehicle were normalized to 100% viable and values adjusted accordingly. GI_{50} values were calculated via GraphPad Prism and reported as the average of >2 independent experiments ± SEM. For western blot analysis, RPMI8226 cells were seeded at 100,000 cells/mL in 10 cm dishes and placed back in the incubator for 24 h. Compounds or vehicle were dosed (0.1% DMSO final concentration) and incubated together for 24 h. Cells were harvested in cold PBS and lysed using MPER (Thermo Scientific) supplemented with protease inhibitors (Roche) according the manufacturer's instructions. Cell lysates were obtained by centrifugation at 15,000 rpm for 10 min at 4 °C. Protein concentrations were determined using the Pierce BCA assay kit following the manufacturer's instructions. Equal amounts of protein were separated via gel electrophoresis under reducing conditions (10% acrylamide gels) then transferred to PVDF membranes (Invitrogen) and immunoblotted with the corresponding primary antibodies for 4h at room temperature. Primary antibody sources: LRP6 (Cell Signaling Technology, 2560); Survivin (Santa Cruz Biotechnology, sc-10811), Akt (Santa Cruz Biotechnology, sc-8312), and Actin (Santa Cruz Biotechnology, sc-1616); Hsp70 (Enzo Life Sciences, ADI-SPA-811). Membranes were then incubated with the correct HRP-labeled secondary antibody for 2h at room

temperature (anti-Rabbit, Cell Signaling Technology, 7074). Membranes were then developed with a chemiluminescent substrate (Clarity, Bio-Rad), and visualized using autoradiography film (MidSci).

References

1. Taipale, M.; Jarosz, D. F.; Lindquist, S. HSP90 at the hub of protein homeostasis: emerging mechanistic insights. *Nat. Rev. Mol. Cell Biol.* **2010,** *11*, 515-528.

2. Picard, D. Hsp90 Interactors. https://www.picard.ch/downloads.

3. Trepel, J.; Mollapour, M.; Giaccone, G.; Neckers, L. Targeting the dynamic HSP90 complex in cancer. *Nat. Rev. Cancer* **2010,** *10*, 537-549.

4. Miyata, Y.; Nakamoto, H.; Neckers, L. The therapeutic target Hsp90 and cancer hallmarks. *Curr. Pharm. Des.* **2013,** *19*, 347-365.

5. Hanahan, D.; Weinberg, R. A. Hallmarks of cancer: the next generation. *Cell* **2011,** *144*, 646-674.

6. Dollins, D. E.; Warren, J. J.; Immormino, R. M.; Gewirth, D. T. Structures of GRP94-nucleotide complexes reveal mechanistic differences between the Hsp90 chaperones. *Mol. Cell* **2007,** *28*, 41-56.

7. Khandelwal, A.; Crowley, V. M.; Blagg, B. S. Natural product inspired N-terminal Hsp90 inhibitors: from bench to bedside? *Med. Res. Rev.* **2016,** *36*, 92-118.

8. Travers, J.; Sharp, S.; Workman, P. HSP90 inhibition: two-pronged exploitation of cancer dependencies. *Drug Discov. Today* **2012,** *17*, 242-252.

9. Bhat, R.; Tummalapalli, S. R.; Rotella, D. P. Progress in the discovery and development of heat shock protein 90 (Hsp90) inhibitors. *J. Med. Chem.* **2014,** *57*, 8718-8728.

10.   Neckers, L.; Workman, P. Hsp90 molecular chaperone inhibitors: are we there yet? *Clin. Cancer Res.* **2012,** *18*, 64-76.

11.   Chen, B.; Piel, W. H.; Gui, L.; Bruford, E.; Monteiro, A. The HSP90 family of genes in the human genome: insights into their divergence and evolution. *Genomics* **2005,** *86*, 627-637.

12.   Taldone, T.; Patel, P. D.; Patel, M.; Patel, H. J.; Evans, C. E.; Rodina, A.; Ochiana, S.; Shah, S. K.; Uddin, M.; Gewirth, D.; Chiosis, G. Experimental and structural testing module to analyze paralogue-specificity and affinity in the Hsp90 inhibitors series. *J. Med. Chem.* **2013,** *56*, 6803-6818.

13.   Song, H. Y.; Dunbar, J. D.; Zhang, Y. X.; Guo, D.; Donner, D. B. Identification of a protein with homology to Hsp90 that binds the type 1 tumor necrosis factor receptor. *J. Biol. Chem.* **1995,** *270*, 3574-3581.

14.   Lee, A. S. Glucose-regulated proteins in cancer: molecular mechanisms and therapeutic potential. *Nat. Rev. Cancer* **2014,** *14*, 263-276.

15.   Ghosh, S.; Shinogle, H. E.; Galeva, N. A.; Dobrowsky, R. T.; Blagg, B. S. Endoplasmic Reticulum-resident Heat Shock Protein 90 (HSP90) Isoform Glucose-regulated Protein 94 (GRP94) Regulates Cell Polarity and Cancer Cell Migration by Affecting Intracellular Transport. *J. Biol. Chem.* **2016,** *291*, 8309-8323.

16.   Marzec, M.; Eletto, D.; Argon, Y. GRP94: An HSP90-like protein specialized for protein folding and quality control in the endoplasmic reticulum. *Biochim. Biophys. Acta* **2012,** *1823*, 774-787.

17.   Patel, P. D.; Yan, P.; Seidler, P. M.; Patel, H. J.; Sun, W.; Yang, C.; Que, N. S.; Taldone, T.; Finotti, P.; Stephani, R. A.; Gewirth, D. T.; Chiosis, G. Paralog-selective Hsp90 inhibitors define tumor-specific regulation of HER2. *Nat. Chem. Biol.* **2013,** *9*, 677-684.

18.   Wu, S.; Hong, F.; Gewirth, D.; Guo, B.; Liu, B.; Li, Z. The molecular chaperone gp96/GRP94 interacts with Toll-like receptors and integrins via its C-terminal hydrophobic domain. *J. Biol. Chem.* **2012,** *287*, 6735-6742.

19.   Suntharalingam, A.; Abisambra, J. F.; O'Leary, J. C.; Koren, J.; Zhang, B.; Joe, M. K.; Blair, L. J.; Hill, S. E.; Jinwal, U. K.; Cockman, M.; Duerfeldt, A. S.; Tomarev, S.; Blagg, B. S.; Lieberman, R. L.; Dickey, C. A. Glucose-regulated protein 94 triage of mutant myocilin through endoplasmic reticulum-associated degradation subverts a more efficient autophagic clearance mechanism. *J. Biol. Chem.* **2012,** *287*, 40661-40669.

20.   Muth, A.; Crowley, V.; Khandelwal, A.; Mishra, S.; Zhao, J.; Hall, J.; Blagg, B. S. Development of radamide analogs as Grp94 inhibitors. *Bioorg. Med. Chem.* **2014,** *22*, 4083-4098.

21.   Crowley, V. M.; Khandelwal, A.; Mishra, S.; Stothert, A. R.; Huard, D. J.; Zhao, J.; Muth, A.; Duerfeldt, A. S.; Kizziah, J. L.; Lieberman, R. L.; Dickey, C. A.; Blagg, B. S. Development of Glucose Regulated Protein 94-Selective Inhibitors Based on the BnIm and Radamide Scaffold. *J. Med. Chem.* **2016,** *59*, 3471-3488.

22.   Mishra, S. J.; Ghosh, S.; Stothert, A. R.; Dickey, C. A.; Blagg, B. S. Transformation of the Non-Selective Aminocyclohexanol-Based Hsp90 Inhibitor into a Grp94-Seletive Scaffold. *ACS Chem. Biol.* **2017,** *12*, 244-253.

23.   Rachidi, S.; Sun, S.; Wu, B. X.; Jones, E.; Drake, R. R.; Ogretmen, B.; Cowart, L. A.; Clarke, C. J.; Hannun, Y. A.; Chiosis, G.; Liu, B.; Li, Z. Endoplasmic reticulum heat shock protein gp96 maintains liver homeostasis and promotes hepatocellular carcinogenesis. *J. Hepatol.* **2015,** *62*, 879-888.

24.   Hua, Y.; White-Gilbertson, S.; Kellner, J.; Rachidi, S.; Usmani, S. Z.; Chiosis, G.; Depinho, R.; Li, Z.; Liu, B. Molecular chaperone gp96 is a novel therapeutic target of multiple myeloma. *Clin. Cancer Res.* **2013,** *19*, 6242-6251.

25.   Stothert, A. R.; Suntharalingam, A.; Huard, D. J.; Fontaine, S. N.; Crowley, V. M.; Mishra, S.; Blagg, B. S.; Lieberman, R. L.; Dickey, C. A. Exploiting the interaction between Grp94 and aggregated myocilin to treat glaucoma. *Hum. Mol. Genet.* **2014,** *23*, 6470-6480.

26.   Duerfeldt, A. S.; Peterson, L. B.; Maynard, J. C.; Ng, C. L.; Eletto, D.; Ostrovsky, O.; Shinogle, H. E.; Moore, D. S.; Argon, Y.; Nicchitta, C. V.; Blagg, B. S. Development of a Grp94 inhibitor. *J. Am. Chem. Soc.* **2012,** *134*, 9796-9804.

27.   Rosser, M. F.; Nicchitta, C. V. Ligand interactions in the adenosine nucleotide-binding domain of the Hsp90 chaperone, GRP94. I. Evidence for allosteric regulation of ligand binding. *J. Biol. Chem.* **2000,** *275*, 22798-22805.

28.   Patel, H. J.; Patel, P. D.; Ochiana, S. O.; Yan, P.; Sun, W.; Patel, M. R.; Shah, S. K.; Tramentozzi, E.; Brooks, J.; Bolaender, A.; Shrestha, L.; Stephani, R.; Finotti, P.; Leifer, C.; Li, Z.; Gewirth, D. T.; Taldone, T.; Chiosis, G. Structure-activity relationship in a purine-scaffold compound series with selectivity for the endoplasmic reticulum Hsp90 paralog Grp94. *J. Med. Chem.* **2015,** *58*, 3922-3943.

29.   Murray, C. W.; Carr, M. G.; Callaghan, O.; Chessari, G.; Congreve, M.; Cowan, S.; Coyle, J. E.; Downham, R.; Figueroa, E.; Frederickson, M.; Graham, B.; McMenamin, R.; O'Brien, M. A.; Patel, S.; Phillips, T. R.; Williams, G.; Woodhead, A. J.; Woolford, A. J. Fragment-based drug discovery applied to Hsp90. Discovery of two lead series with high ligand efficiency. *J. Med. Chem.* **2010,** *53*, 5942-5955.

30.   Woodhead, A. J.; Angove, H.; Carr, M. G.; Chessari, G.; Congreve, M.; Coyle, J. E.; Cosme, J.; Graham, B.; Day, P. J.; Downham, R.; Fazal, L.; Feltell, R.; Figueroa, E.; Frederickson, M.; Lewis, J.; McMenamin, R.; Murray, C. W.; O'Brien, M. A.; Parra, L.; Patel, S.; Phillips, T.; Rees, D. C.; Rich, S.; Smith, D. M.; Trewartha, G.; Vinkovic, M.; Williams, B.; Woolford, A. J. Discovery of (2,4-dihydroxy-5-isopropylphenyl)-[5-(4-methylpiperazin-1-ylmethyl)-1,3-dihydrois oindol-2-yl]methanone (AT13387), a novel inhibitor of the molecular chaperone Hsp90 by fragment based drug design. *J. Med. Chem.* **2010,** *53*, 5956-5969.

31.   Tso, S. C.; Qi, X.; Gui, W. J.; Wu, C. Y.; Chuang, J. L.; Wernstedt-Asterholm, I.; Morlock, L. K.; Owens, K. R.; Scherer, P. E.; Williams, N. S.; Tambar, U. K.; Wynn, R. M.; Chuang, D. T. Structure-guided development of specific pyruvate dehydrogenase kinase inhibitors targeting the ATP-binding pocket. *J. Biol. Chem.* **2014,** *289*, 4432-4443.

32.   Llauger-Bufi, L.; Felts, S. J.; Huezo, H.; Rosen, N.; Chiosis, G. Synthesis of novel fluorescent probes for the molecular chaperone Hsp90. *Bioorg. Med. Chem. Lett.* **2003,** *13*, 3975-3978.

33.   Bagratuni, T.; Wu, P.; Gonzalez de Castro, D.; Davenport, E. L.; Dickens, N. J.; Walker, B. A.; Boyd, K.; Johnson, D. C.; Gregory, W.; Morgan, G. J.; Davies, F. E. XBP1s levels are implicated in the biology and outcome of myeloma mediating different clinical outcomes to thalidomide-based treatments. *Blood* **2010,** *116*, 250-253.

5. The Development of TRAP1-selective Inhibitors

Introduction

The 90 kDa heat shock protein (Hsp90) family is comprised of four different isoforms: Hsp90α and Hsp90β reside in the cytosol, Grp94 is localized to the endoplasmic reticulum (ER), and TRAP1 is found in the mitochondria. Together, these proteins act as molecular chaperones that are responsible for the maturation of over 300 Hsp90-dependent (client) proteins through its protein folding machinery.[1-3] Hsp90 client proteins are associated with all ten hallmarks of cancer, including important anticancer targets such as Her2, Raf, and BCR-Abl.[4-5] Small molecule inhibition of Hsp90 results in disruption of the Hsp90 chaperone cycle and degradation of client proteins via the ubiquitin-proteasome pathway. Therefore, Hsp90 inhibition provides a multifaceted attack against cancer with a single agent through simultaneous disruption of multiple oncogenic signaling nodes.[6-7]

Seventeen small molecule inhibitors of Hsp90 have entered into clinical trials, all of which exhibit *pan*-Hsp90 inhibitory activity.[8] Unfortunately, these inhibitors have demonstrated toxicities, including ocular, gastrointestinal, and cardiotoxicity, which have dampened enthusiasm for Hsp90 as a therapeutic target.[9-10] Recently, several studies have sought to elucidate the roles played by individual Hsp90 isoforms through the identification of client proteins that are dependent upon specific isoforms.[11-12] The hERG channel was shown to be solely dependent upon the Hsp90α isoform, suggesting that inhibition of this isoform could be a contributing factor to the cardiotoxicity observed in the clinic.[13] Additionally, Grp94-dependent client proteins have been identified, as well as disease states that rely upon this isoform, including glaucoma, metastasis, and multiple myeloma.[14-18] These data suggest that identification of the roles played by individual

Hsp90 isoforms could prove useful for the therapeutic treatment of different disease states. However, the pursuit of these inhibitors is hindered by the high sequence identity present in the N-terminal ATP-binding site among all four Hsp90 isoforms. Grp94 is the most unique of the four isoforms, and Hsp90α and Hsp90β are most similar. The sequence similarity of TRAP1 resides between Grp94 and the cytosolic isoforms, and differs from Hsp90β by only four residues within its N-terminal ATP-binding site.[19]

TRAP1 is predominantly localized to the mitochondria within cells and serves a cytoprotective role within this organelle.[20] TRAP1 is highly expressed in cancerous cells, but is expressed at basal levels in normal cells.[21] Genetic knockdown of TRAP1 activated apoptosis that culminates in the release of apoptogenic proteins into the cytosol, which initiates the caspase cascade and cell death. Further investigations into the role played by TRAP1 in mitochondrial apoptosis revealed that TRAP1 antagonizes the functions of cyclophilin D (CypD), which maintains mitochondrial integrity. CypD is a component of the mitochondrial membrane transition pore (MTP).[22] When formed, the MTP results in mitochondrial membrane depolarization, which leads to activation of mitochondrial apoptosis. Formation of the MTP releases calcium ions from the mitochondria which, in turn, triggers the release of calcium from the ER and activation of the unfolded protein response (UPR) in the ER.[23] The UPR results in activation of the pro-apoptotic transcription factor, C/EBP homologous protein (CHOP), which then activates apoptosis.[24-27] Therefore, selective TRAP1 inhibition can induce apoptosis through activation of the pro-apoptotic protein CHOP, and consequently, provide a viable therapeutic opportunity for the treatment of cancer.

Identification of TRAP1-selective Inhibitors

Due to the limited number of solved TRAP1 co-crystal structures, the development of TRAP1-selective inhibitors has been hindered. Prior co-crystal structures have been solved with purine-

based inhibitors (non-hydrolysable ATP mimics or purine-based inhibitors), and as such, the development of resorcinol-based TRAP1-selective inhibitors has been underexplored. Nonetheless, these structures have provided some insight into mechanisms by which TRAP1 selectivity can be achieved.

The first co-crystal structure of TRAP1 solved with a non-hydrolysable ATP mimic, confirmed high identity within the N-terminal nucleotide binding pocket compared to the cytosolic Hsp90 isoforms (**Figure 5.1a**).[28] In fact, TRAP1 and Hsp90β differ by only four residues within their
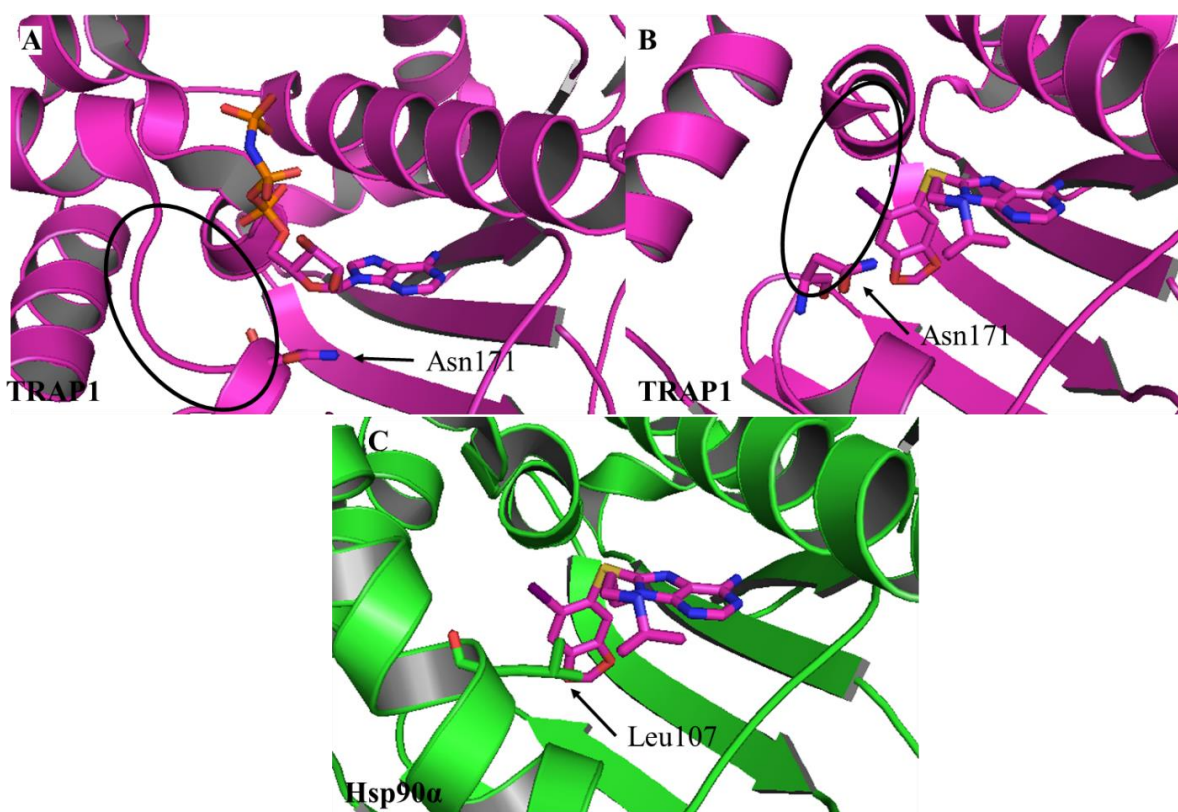

Figure 5.1. TRAP1 co-crystal structures reveal differences that can be exploited for TRAP1 selectivity. (**a**) Non-hydrolysable ATP mimic co-crystallized with TRAP1 (PDBID: 4IPE) demonstrating ordered lid (oval) and Asn171. (**b**) PU-H71 bound to TRAP1 (PDBID: 4Z1F) highlighting disordered lid (oval) and Asn171. (**c**) PU-H71 bound to Hsp90α (PDBID: 2FWZ) highlighting Leu107 in place of Asn171 present in TRAP1.

ATP-binding sites. More recently, a purine-based *pan*-Hsp90 inhibitor, **PU-H71**, was co-crystallized with TRAP1 and revealed differences between TRAP1 and the other Hsp90 isoforms that could potentially be utilized to gain TRAP1 selectivity (**Figure 5.1b**).[29]

Similar to the cytosolic Hsp90 isoforms, TRAP1 possesses a lid that closes over the N-terminal nucleotide pocket upon ATP binding.[20] The most notable difference between these two TRAP1 co-crystal structures is the lid. When co-crystallized with ATP, the lid was ordered (**Figure 5.1a**); however, when co-crystallized with **PU-H71**, the lid was disordered (**Figure 5.1b**). Interestingly, mechanistic studies into the TRAP1 ATPase cycle revealed the lid-closed conformation binds ATP with ~10-fold higher affinity as compared to the cytosolic Hsp90 isoforms in similar lid-closed conformations.[30] Therefore, stabilization of the lid via a small molecule can take advantage of this higher affinity conformation. The only residue that differs between TRAP1 and the cytosolic Hsp90 isoforms that appears to be useful for the development of TRAP1-selective inhibitors is Asn171, which is located just before the TRAP1 lid, whereas the cytosolic isoforms and Grp94 possess a Leu residue at this position (**Figure 5.1c**). Therefore, stabilization of the lid via interactions with Asn171 could produce TRAP1 selectivity.
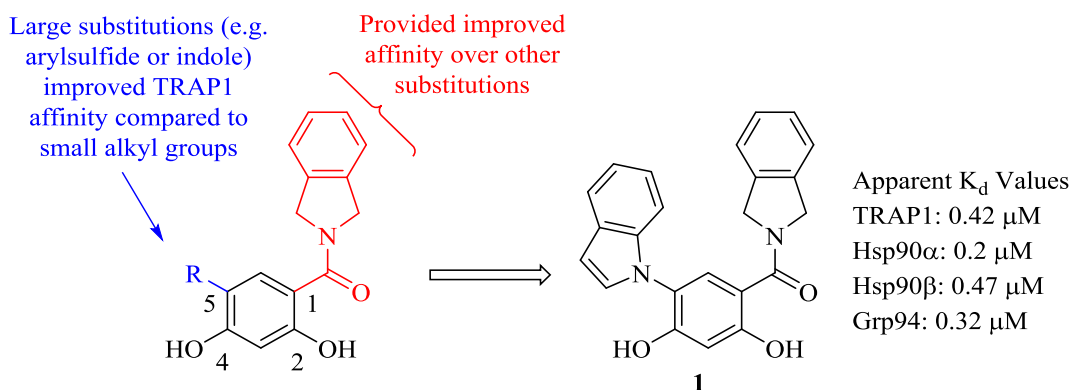

Figure 5.2. Structural features that improve TRAP1 affinity and lead compound (**1**) utilized to develop TRAP1-selective inhibitors.

Due to a lack of structural information regarding the binding modes of resorcinol-based Hsp90 inhibitors in the TRAP1 ATP-binding site, a small library (~170) of resorcinol-based Hsp90 inhibitors was screened in a fluorescence polarization assay. Hits identified from this screen revealed structural characteristics associated with TRAP1 affinity. As highlighted in **Figure 5.2**,

inhibitors derived from the isoindoline-containing scaffold exhibited the highest affinity for TRAP1. Furthermore, large substitutions at the 5-position increased TRAP1 affinity, as compared to small alkyl substitutions. The *pan*-Hsp90 inhibitor **1** was chosen as a lead compound for conversion into a TRAP1-selective inhibitor due to its high affinity for TRAP1 (apparent K_d = 0.42 μM).
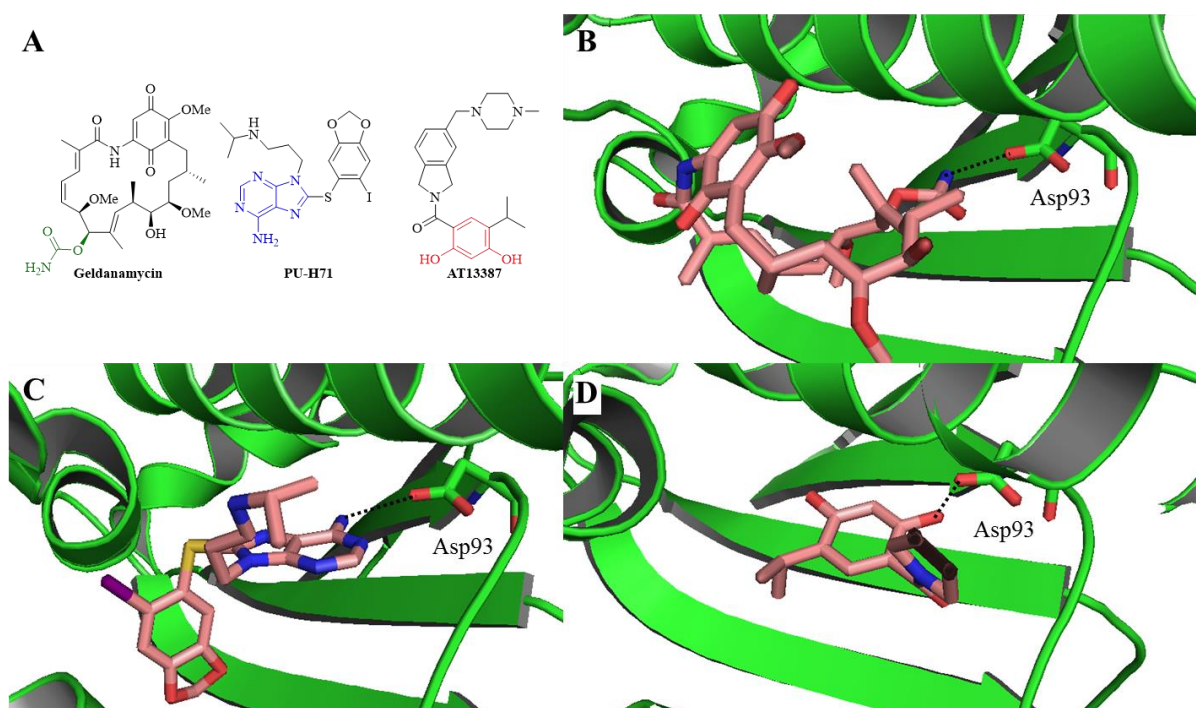

Figure 5.3. Hsp90 inhibitory scaffold interact with a conserved Asp residue in order to gain affinity. (**a**) Representative structures from 3 Hsp90 inhibitor scaffolds. Pharmacophores that interact with Asp residue are colored. (**b-d**) Interactions between pharmacophores and Asp93 of Hsp90α for the three scaffolds. (PDBIDs: 1YET, 2FWZ, and 2XAB).

In order to convert compound **1** into a TRAP1-selective inhibitor, modifications were sought based upon structural information from the other three Hsp90 isoforms. A key interaction between all known Hsp90 inhibitory scaffolds and the N-terminal ATP-binding pocket that is responsible for significant affinity is the interaction between the pharmacophore (colored moieties, **Figure 5.3a**) and a conserved Asp residue at the base of the binding pocket.[31-32] In fact, Hsp90 function in cells can be abolished with a single mutation of Asp to Asn.[33] Therefore, development of a

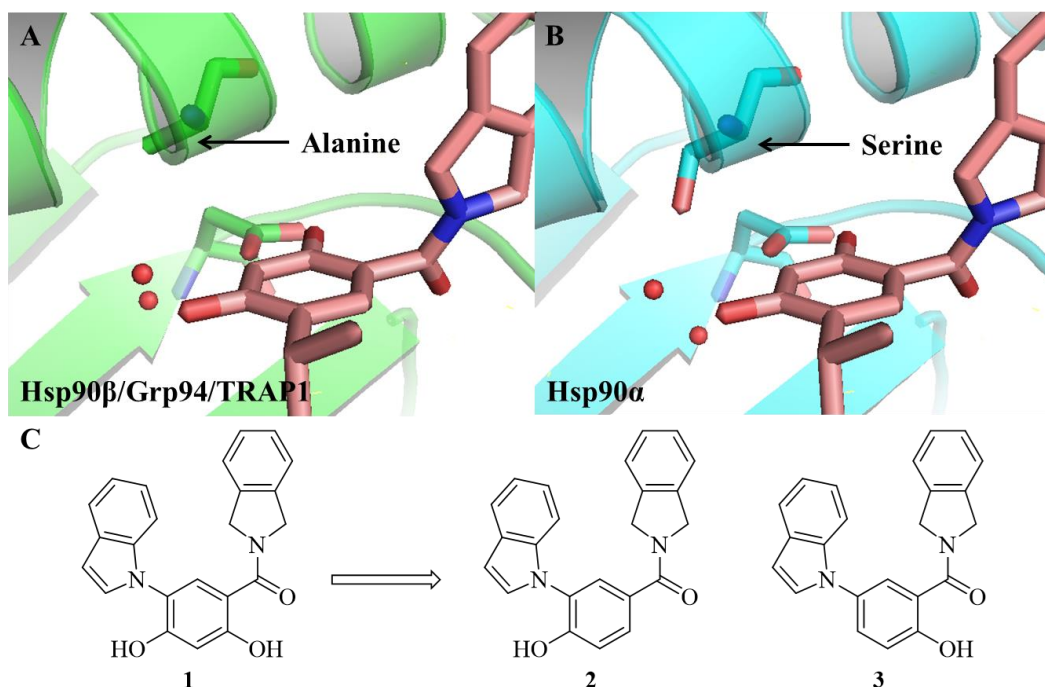**Figure 5.4.** Design of TRAP1-selective inhibitors. (**a**) Hsp90β, Grp94, and TRAP1 possess an Ala residue near the resorcinol binding region. (**b**) Hsp90α is the only isoform to possess a Ser residue at this position. (**c**) Compounds **2** and **3** were proposed to reduce affinity for Hsp90α.

TRAP1-selective inhibitor must maintain this interaction for high affinity; however, since this interaction is conserved among all four Hsp90 isoforms, other subtle differences must be utilized to diminish binding to other isoforms.

Similar to Hsp90β and Grp94, TRAP1 possesses an Ala residue (Ala120 for TRAP1) at the base of the ATP-binding pocket (**Figure 5.4a**); whereas Hsp90α possesses a Ser residue at this position (**Figure 5.4b**). Therefore, in order to reduce affinity for Hsp90α, compounds **2** and **3** (**Figure 5.4c**) were proposed to eliminate interactions with the Ser residue in Hsp90α. Compounds

Scheme 5.1. Synthesis of **2** and **3**
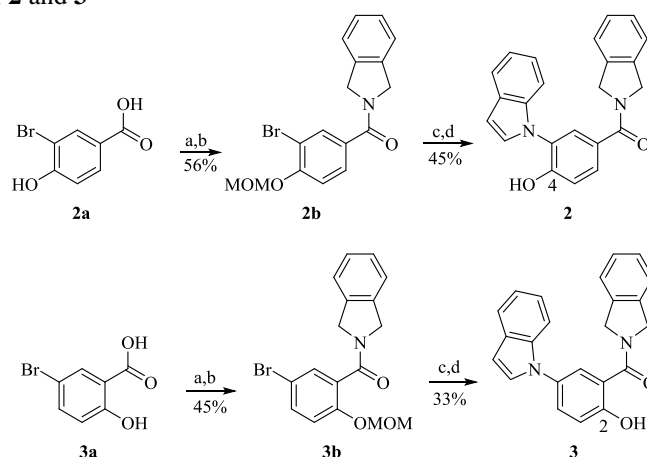
Conditions: (**a**) isoindoline hydrochloride, EDCI, HOBT, Hunig's base, DCM; (**b**) MOMCl, Hunig's base, DCM; (**c**) indole, CuI, (±)-*trans*-1,2-diaminocyclohexane; K$_3$PO$_4$, Toluene; (**d**) *p*-TsOH, MeOH

2 and **3** were synthesized from commercially available benzoic acids (**Scheme 5.1**). EDCI-

mediated amide bond coupling between isoindoline and **2a** or **3a**, followed by methoxymethyl

(MOM) ether protection of the phenol, provided intermediates **2b** and **3b**, respectively. The

Table 5.1. Evaluation of **2** and **3** via fluorescence polarization against the Hsp90 isoforms.

Entry	Structure	Apparent K_d TRAP1 (µM)	Apparent K_d Hsp90α (µM)	Apparent K_d Hsp90β (µM)	Apparent K_d Grp94 (µM)	Fold TRAP1 Selective		
						Hsp90α	Hsp90β	Grp94
1		0.42 ± 0.1	0.2 ± 0.05	0.47±0.02	0.32±0.02	2[a]	n/a	2[b]
2		2.5 ± 0.05	>100	>100	>100	>40	>40	>40
3		>100	>100	n.d.	n.d.	n/a	n/a	n./a

Apparent K_d values are the average of two independent experiments ± SEM. n.d. = not determined. n/a = non-selective. [a] selective for Hsp90α. [b] selective for Grp94.

resulting aryl bromides were subjected to a copper-catalyzed cross coupling reaction with indole, followed by removal of the MOM protecting group to provide phenols **2** and **3**.

Evaluation of these analogues in a fluorescence polarization assay against TRAP1 revealed that **2** exhibited TRAP1 affinity (apparent K_d = 2.5 µM, **Table 5.1**), whereas **3** did not. These data suggest that the 4-phenol provides affinity through an interaction with Asp158 within the TRAP1 binding site.

Evaluation of **2**, via fluorescence polarization, against the other three Hsp90 isoforms revealed that this compound exhibits minimal affinity at 100 µM. Due to the importance of the 4-phenol's interaction with the conserved Asp residue, the isoindoline amide is proposed to occupy the opposite side of the binding site as compared to previously reported co-crystal structures with this scaffold (described in Chapter 4). This orientation projects the amide carbonyl into close proximity with Asn171 to form a hydrogen bond, further increasing TRAP1 affinity. Similar to Grp94, TRAP1 possesses a 2 amino acid insertion into its primary sequence (residues 191 and 192), which appears to produce a secondary binding pocket that accounts for the ability of TRAP1 to accommodate the isoindoline ring in this region (**Figure 5.5**).[19] The residues that appear to comprise this pocket in TRAP1 are similar to the S2 sub-pocket of Grp94. However, their spatial arrangement likely differs from that of Grp94, due to the smaller insertion of amino acids (2 for TRAP1 vs. 5 for Grp94), which can lead to decreased affinity of **2** for Grp94. Since no amino acid insertions occur in Hsp90α and Hsp90β, this region cannot accommodate such molecules and reduced affinity for these isoforms.
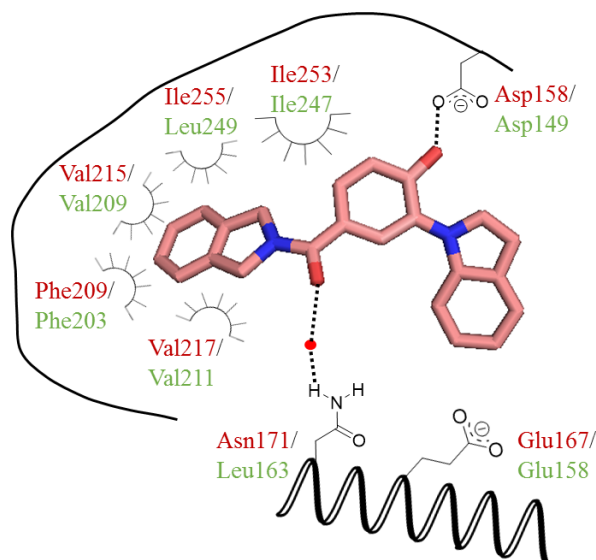
Figure 5.5. Proposed binding mode of **2** in TRAP1 and Grp94. TRAP1 residues are listed in red and Grp94 residues are listed in green. Black dotted lines are proposed hydrogen bonds. Red circle is a water molecule.

Evidence to support the existence of this pocket in TRAP1 is based on the purine-based Grp94-selective inhibitors that utilize the S2 sub-pocket (e.g. **PU-H54**, Chapter 4). Some of these inhibitors exhibit low micromolar affinity for TRAP1, suggesting the presence of this pocket, but differs slightly from the S2 sub-pocket in Grp94 since these compounds exhibit Grp94 selectivity.[34-35] In addition, Asn171 of TRAP1 is replaced by Leu in the 3 other Hsp90 isoforms, and therefore, orientation of the amide carbonyl toward this region is likely detrimental (**Figure 5.5**).
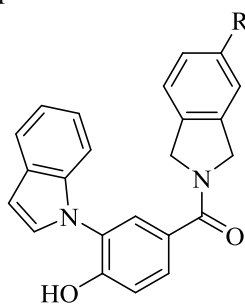
Further evidence to support this proposed binding mode was pursued through modification of the isoindoline ring. In previous studies, modifications of this region improved or maintained

Scheme 5.2. Synthesis of **4-8**.
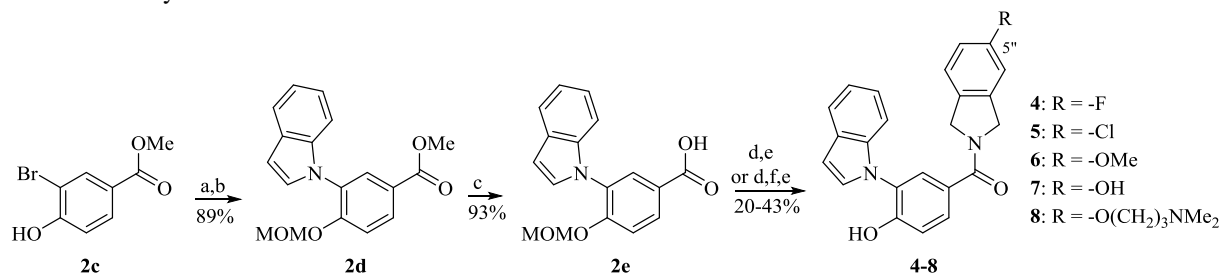
Conditions: (**a**) MOMCl, Hunig's base, DCM; (**b**) indole, CuI, (±)-*trans*-1,2-diaminocyclohexane; K₃PO₄, Tolueen; (**c**) LiOH, THF/Water/MeOH; (**d**) substituted isoindoline, EDCI, HOBT, Hunig's base, DCM; (**e**) *p*-TsOH, MeOH; (**f**) 3-dimethylamino-propyl chloride hydrochloride, K₂CO₃, ⁿBu₄N⁺I⁻, DMF

Table 5.2. Evaluation of **4-8** via fluorescence polarization.

Entry	R	Apparent K_d TRAP1 (µM)
4	-F	>100
5	-Cl	>100
6	-OMe	>100
7	-OH	>100
8	-O(CH$_2$)$_3$NMe$_2$	>100

Apparent K_d values are the average of two independent experiments.

affinity for Hsp90, and consequently was used to modulate the pharmacokinetic properties of such inhibitors since these modifications project toward the solvent exposed region of the binding pocket.[36] However, due to the proposed binding mode of **2**, which projects the isoindoline ring into a hydrophobic pocket, these substitutions likely reduce TRAP1 affinity and support an alternative binding mode for this scaffold with TRAP1. Compounds **4-8** were designed for such investigation, and their preparation is outlined in **Scheme 5.2**. Commercially available methyl ester **2c** was converted to the MOM ether and then subjected to a copper-catalyzed cross coupling reaction with indole to provide **2d**. Saponification of the methyl ester provided the corresponding benzoic acid, **2e**, which was subjected to an EDCI-mediated amide bond coupling with isoindolines **4a**-**7a**, followed by acidic deprotection of the MOM ether to provide phenols **4-8**. Prior to cleavage of the MOM ether, **7** was reacted with 3-dimethylamino-propyl chloride hydrochloride in the presence of potassium carbonate and tetrabutylammonium iodide to provide **8** after removal of the MOM protecting group. Evaluation of these analogues via fluorescence polarization revealed that substitutions at the 5"-position significantly reduced affinity for TRAP1

(TRAP1 apparent K_d >100 µM) compared to **2**, further supporting the proposed binding mode of this scaffold projecting the isoindoline ring into a hydrophobic pocket (**Table 5.2**).

Due to the loss in affinity upon modification of the isoindoline ring, structure-activity relationship studies were performed on the indole ring to further understand the requirements for TRAP1 affinity and selectivity. Synthesis of these analogues was performed in a manner similar to the synthesis of **2** (**Scheme 5.1**). The analogues were then evaluated for their affinity and selectivity against TRAP1, Hsp90α, and Grp94. Hsp90β was excluded due to its high identity with Hsp90α (>95%). Compounds that exhibited TRAP1 affinity and selectivity over Hsp90α and Grp94 were then evaluated against Hsp90β to confirm selectivity.

As observed in **Table 5.3**, modifications to the 2'- and 3'-positions (**9-11**) resulted in a significant loss of affinity for TRAP1. Based on the proposed binding mode, this region of the binding pocket appears to be sterically restricted by Gly160, Ile161, and Gly162, and modifications at these positions produce detrimental steric interactions that reduce TRAP1 affinity (**Figure 5.6**). Modification of the 4'-, 5'-, 6'-, and 7'-positions were subsequently pursued as these positions appeared less sterically encumbered and potentially more amenable to substitution. Upon their synthesis, compounds **12-34** were evaluated via fluorescence polarization for TRAP1 affinity and selectivity. Many of these inhibitors exhibited good affinity and selectivity for TRAP1 (**Table 5.3**) and revealed trends for binding TRAP1.
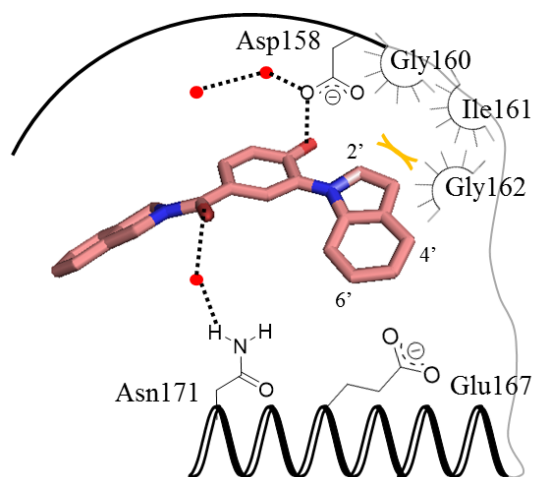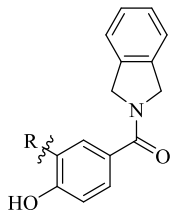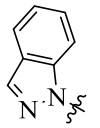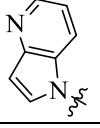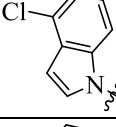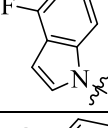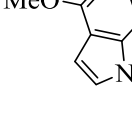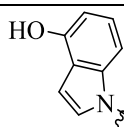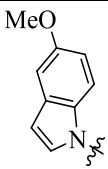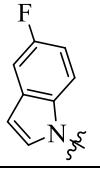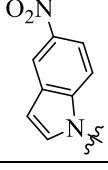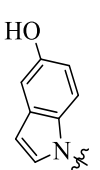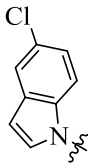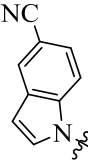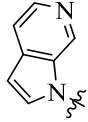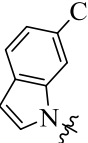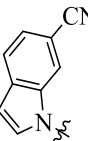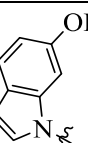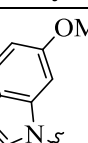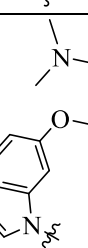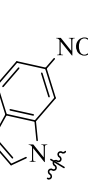
Figure 5.6. Proposed binding model of **2** in the TRAP1 binding site. Modifications to the 2'- and 3'-positions produce steric interactions with Gly160, Ile161, and Gly162 (yellow lines). Black dotted lines represent proposed hydrogen bond interactions. Red circles are water molecules.
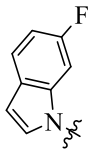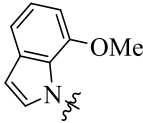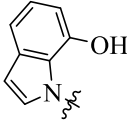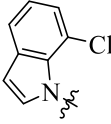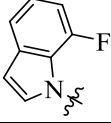
Table 5.3. Evaluation of 9-34 via fluorescence polarization.

Entry	R =	Apparent K_d TRAP1 (µM)	Apparent K_d Hsp90α (µM)	Apparent K_d Hsp90β (µM)	Apparent K_d Grp94 (µM)	Fold TRAP1 Selective		
						Hsp90α	Hsp90β	Grp94
2	n/a	2.5 ± 0.05	>100	>100	>100	>40	>40	>40
9		78 ± 7	>100	>100	>100	n/a	n/a	n/a
10		>100	>100	n.d.	>100	n/a	n/a	n/a

Entry	R =	Apparent K_d TRAP1 (µM)	Apparent K_d Hsp90α (µM)	Apparent K_d Hsp90β (µM)	Apparent K_d Grp94 (µM)	Fold TRAP1 Selective		
						Hsp90α	Hsp90β	Grp94
11		13.2 ± 1.3	>100	n.d.	>100	>8	n/a	>8
12		2.9 ± 0.7	>100	n.d.	22.3 ± 1.1	>34	n/a	7
13		4.56 ± 0.2	>100	>100	>100	>22	>22	>22
14		>50	>100	n.d.	>100	n/a	n/a	n/a
15		>50	>100	n.d.	>100	n/a	n/a	n/a
16		1.41 ± 0.2	>100	>100	>100	>71	>71	>71
17		2.46 ± 0.8	>100	>100	>100	>40	>40	>40
18		2.66 ± 0.4	>100	>100	>100	>38	>38	>38
19		>50	>100	n.d.	>100	n/a	n/a	n/a
20		1.9 ± 0.3	31.3 ± 4.8	n.d.	5.9 ± 0.8	17	n.d.	3

Entry	R =	Apparent K_d TRAP1 (μM)	Apparent K_d Hsp90α (μM)	Apparent K_d Hsp90β (μM)	Apparent K_d Grp94 (μM)	Fold TRAP1 Selective		
						Hsp90α	Hsp90β	Grp94
21		>50	>100	n.d.	>100	n/a	n/a	n/a
22		3.5 ± 0.8	>100	>100	>100	>29	>29	>29
23		21.6 ± 5.6	>100	n.d.	n.d.	5	n.d.	n.d.
24		6.0 ± 0.8	>100	>100	>100	>17	>17	>17
25		>50	>100	n.d.	>100	n/a	n/a	n/a
26		2.4 ± 0.2	>100	n.d.	8.7 ± 0.6	>40	n.d.	4
27		>50	>100	n.d.	>100	n/a	n/a	n/a
28		>50	>100	n.d.	>100	n/a	n/a	n/a
29		>50	>100	n.d.	>100	n/a	n/a	n/a

Entry	R =	Apparent K_d TRAP1 (μM)	Apparent K_d Hsp90α (μM)	Apparent K_d Hsp90β (μM)	Apparent K_d Grp94 (μM)	Fold TRAP1 Selective		
						Hsp90α	Hsp90β	Grp94
30	F (indole)	>50	>100	n.d.	>100	n/a	n/a	n/a
31	OMe (indole)	3.43 ± 0.2	2.86 ± 0.4	n.d.	>100	n.s	n.d	>29
32	OH (indole)	2.56 ± 0.1	5.48 ± 0.9	n.d.	>100	2	n.d.	>40
33	Cl (indole)	>50	>100	n.d.	>100	n/a	n/a	n/a
34	F (indole)	>50	>100	n.d.	>100	n/a	n/a	n/a

Apparent K_d values are the average of two independent experiments ± SEM. n.d. = not determined. n/a = not applicable; n.s. = non-selective.

Evaluation of the analogues that contain modifications at the 4'-position (**12-16**) suggested that halogen or hydrogen bond donating groups were beneficial, but size-dependent, as the chloro (**13**) and phenol (**16**) exhibited good affinity and maintained selectivity for TRAP1, while the fluoro (**14**) and methoxy (**15**) did not. The phenol substituent produced a ~2-fold increase in TRAP1 affinity and an apparent K_d of 1.41 μM along with >70-fold TRAP1 selectivity. Alternatively, favorable substitutions at the 5'-position appeared to result from small or hydrogen bond accepting groups, as the methyl ether (**17**) and fluoro (**18**) exhibited good affinities (TRAP1 apparent K_d's = 2.46 μM and 2.66 μM, respectively) and selectivities for TRAP1. Incorporation of the hydrogen bond donating phenol at the 5'-position (**20**) maintained TRAP1 affinity (TRAP1 apparent K_d = 1.9 μM), but with a loss in selectivity versus Grp94 (~3-fold). A similar effect was observed with the 6'-phenol (**26**, apparent K_d = 2.4 μM, 4-fold selective over Grp94). This trend suggests that
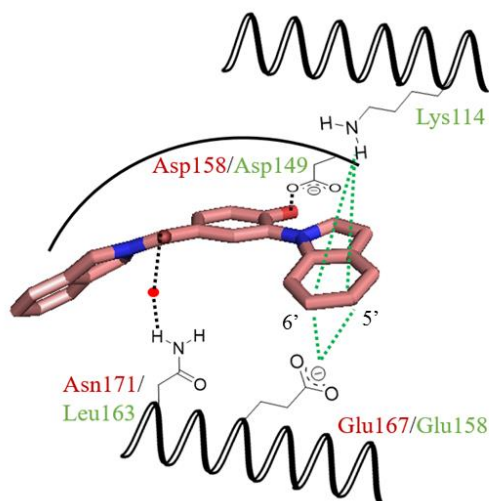
Figure 5.7. Proposed interactions between the 5'- and 6'-positions of **2** and the polar residues of Grp94. Residues are numbered according to their respective isoforms (Red = TRAP1, Green = Grp94). Black dotted lines are prosed hydrogen bonds present in TRAP1. Green dotted lines are proposed hydrogen bonds between substitutions at the 5'- and 6'-positions with Grp94 residues that result in decreased selectivity. Water molecules are represented by red circles.

hydrogen bond donating groups at the 5'- and 6'-positions exhibit affinity for Grp94 likely through interactions with polar residues at the solvent exposed region of the binding pocket (e.g. Glu158, **Figure 5.7**).[16] Other modifications to the 6'-position exhibited a similar trend as that observed for the 4'-position, wherein halogen or hydrogen bond donating abilities were important for affinity, as the 6'-chloro (**24**) substitution maintained TRAP1 affinity and selectivity. However, these interactions were also size dependent as suggested by the poor affinity manifested by the fluoro (**30**) substitution (apparent K_d >50 µM). Lastly, hydrogen bond accepting and donating groups (**31** and **32**) at the 7'-position maintained affinity (TRAP1 apparent K_d's 3.43 µM and 2.56 µM, respectively), but this was accompanied by a complete loss of selectivity, as increased affinity for Hsp90α was observed.

Scheme 5.3. Synthesis of **36-39**.
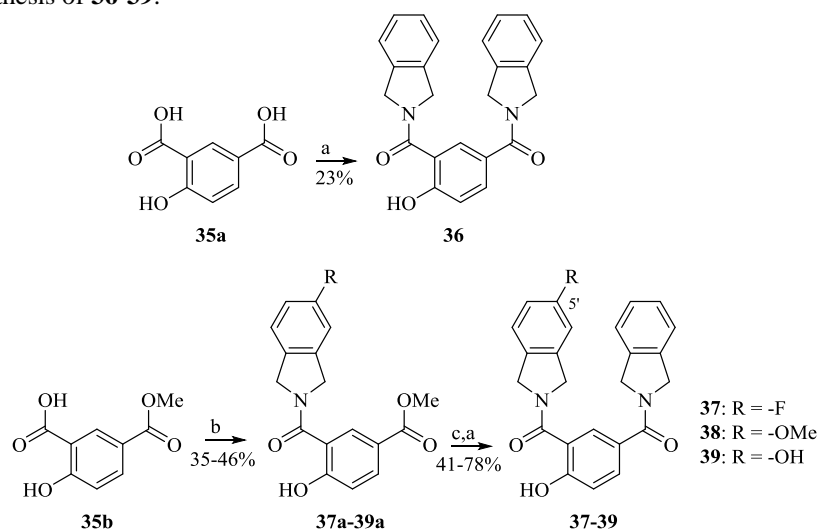
Conditions: (**a**) isoindoline hydrochloride, EDCI, HOBT, Hunig's base, DCM; (**b**) **4a**, **6a**, or **7a**; EDCI, HOBT, Hunig's base, DCM; (**c**) LiOH, THF/Water/MeOH

While the structure-activity relationship studies performed on the indole ring provided insight into the binding requirements for TRAP1 selectivity and affinity, these studies did not provide inhibitors with significant affinity. Therefore, other modifications to this scaffold were pursued. Based on the structure-activity relationship trends of **2**, the indole was proposed to occupy the same region of the binding pocket in which the isoindoline amide had previously been observed to bind.[36] Previous studies determined that incorporation of the isoindoline ring produced significant affinity for the *pan*-Hsp90 inhibitor **AT13387**. Therefore, a bis-isoindoline inhibitor (**36**) was proposed as a mechanism to increase TRAP1 affinity.[37] Synthesis of these analogues is outlined in **Scheme 5.3**. The unsubstituted bis-isoindoline (**36**) was synthesized from 4-hydroxyisophthalic acid (**35a**) via EDCI-mediated amide coupling with isoindoline. Compounds **37-39** which possess various substitutions about the isoindoline ring were synthesized from 2-hydroxy-5-(methoxycarbonyl)benzoic acid (**35b**) and corresponding isoindolines, followed by saponification of the methyl ester and subsequent coupling with isoindoline to provide the desired analogues **36-39**.

214

Table 5.4. Evaluation of **36-39** via fluorescence polarization.

Entry	R	Apparent K_d TRAP1 (µM)	Apparent K_d Hsp90α (µM)	Apparent K_d Hsp90β (µM)	Apparent K_d Grp94 (µM)	Fold TRAP1 Selective		
						Hsp90α	Hsp90β	Grp94
36	-H	0.41±0.03	>100	>100	56.5 ± 4.4	>244	>244	138
37	-F	0.19±0.06	>100	>100	13.8 ± 1.2	>526	>526	73
38	-OMe	0.86±0.05	>100	n.d.	n.d.	>116	n.d	n.d.
39	-OH	0.18±0.02	>100	>100	7.3 ± 0.2	>556	>556	41
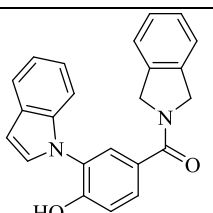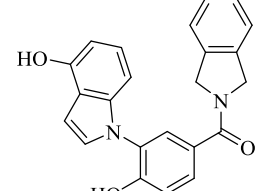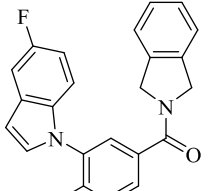
Apparent K_d values are the average of two independent experiments ± SEM. n.d. = not determined.

Upon their preparation, compounds **36-39** were evaluated for TRAP1 affinity and selectivity (**Table 5.4**). Gratifyingly, bis-isoindoline **36** exhibited increased TRAP1 affinity (apparent K_d 0.41 µM) compared to **2**. Compound **36** also exhibited >240-fold selectivity over the cytosolic Hsp90 isoforms and ~140-fold selectivity versus Grp94. Incorporation of hydrogen or halogen bond donating groups (**37** and **39**) at the 5'-position improved affinity (TRAP1 apparent K_d's 0.19 µM and 0.18 µM, respectively), whereas incorporation of the hydrogen bond accepting methyl ether (**38**) resulted in ~2-fold loss in TRAP1 affinity (apparent K_d 0.86 µM) compared to **36**. Unfortunately, the increased affinity for TRAP1 exhibited by **37** and **39** was accompanied by a significant increase in affinity for Grp94 (Grp94 apparent K_d's 13.8 µM and 7.3 µM, respectively) resulting in reduced TRAP1 selectivity. Similar to the trends observed for hydrogen bond donating groups with the indole-isoindoline scaffold (e.g. **20** and **26**), such modifications resulted in decreased TRAP1 selectivity (**Figure 5.7**).

Biological Evaluation of TRAP1-selective Inhibitors

Based on the cytoprotective role played by TRAP1 in cancer, compounds that exhibited TRAP1 affinity and selectivity were evaluated for anti-proliferative activity against cancer cell lines. Prostate (PC3-MM2), colorectal (HCT116), and cervical (HeLa) cancer cell lines were chosen as they have been used to study the roles of TRAP1.[38-40] As seen in **Table 5.5**, the indole-isoindoline inhibitor **2** exhibited modest GI_{50} values against these cell lines. Surprisingly, the bis-isoindoline inhibitors, **36** and **37**, did not exhibit any anti-proliferative activity against these cell lines until high micromolar concentrations, which is likely a consequence of reduced cell permeability or low mitochondrial permeability. In contrast, the chloro-substituted indole inhibitor **24** exhibited improved GI_{50} values against these cell lines as compared to **2**. Therefore, compound **24** was chosen for further investigation for the induction of apoptosis via TRAP1-selective inhibition.

Table 5.5. Evaluation of TRAP1-selective inhibitors in cells.

Entry	Structure	PC3-MM2 (Prostate)	HCT116 (Colorectal)	HeLa (Cervical)
2		47.5 ± 3.9	30.7 ± 5.6	44.7 ± 4.7
16		42.2 ± 5.8	54.0 ± 2.4	52.7 ± 2.4
18		29.5 ± 1.2	39.0 ± 4.1	29.8 ± 1.4

Entry	Structure	PC3-MM2 (Prostate)	HCT116 (Colorectal)	HeLa (Cervical)
24		17.5 ± 2.9	12.2 ± 2.6	13.9 ± 1.8
36		>100	>100	>100
37		>100	61.4 ± 5.9	50.3 ± 4.7
DN401		4.4 ± 0.7	3.6 ± 0.4	3.0 ± 0.9

GI$_{50}$ values are the average of two independent experiments ± SEM.

As seen in **Figure 5.8**, western blot analysis of HeLa cells treated with compound **24** and the previously reported TRAP1-selective inhibitor, **DN401**, exhibited induction of the pro-apoptotic protein CHOP, suggesting that these compounds induce apoptosis. Flow cytometry analysis of HeLa cells treated with **24** or **DN401** supported that these compounds result cell death due to the increased intensity of fluorescence upon staining with propidium iodide.[41] Release of DNA from the nucleus suggests that the induction of CHOP, via TRAP1 inhibition, results in activation of apoptosis. Furthermore, **24** did not induce the degradation of Akt, a client protein dependent upon
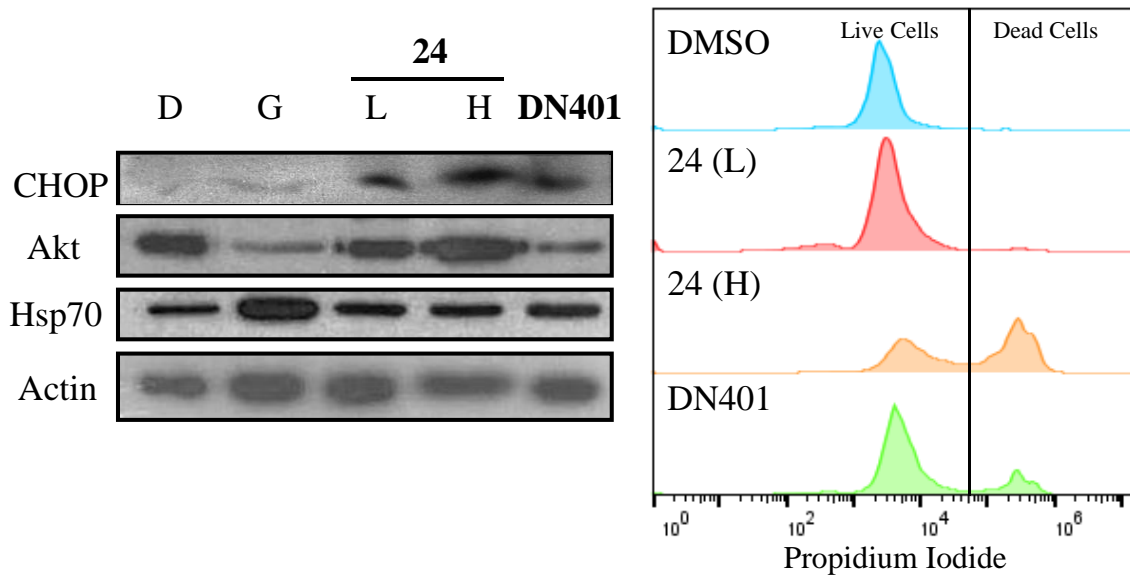
Figure 5.8. Compound **24** exhibited TRAP1-selective inhibition in cells. Left: Western blot analysis of HeLa cells treated with vehicle control (D, DMSO, 0.25% final concentration), a *pan*-Hsp90 inhibitor (G, geldanamycin, 0.5 μM), **24** (L = ½ GI$_{50}$, H = 5x GI$_{50}$), or **DN401** (8-fold TRAP1-selective inhibitor, 20 μM). Right: Flow cytometry analysis of HeLa cells treated with vehicle control (DMSO), **24**, or **DN401** after staining with propidium iodide.

cytosolic Hsp90 isoforms, nor did it induce the HSR as monitored by Hsp70 levels. This pattern contrasts the effects of the natural product and *pan*-Hsp90 inhibitor **GDA**, which produced both the degradation of Akt, and induction of Hsp70. As observed previously, **DN401** produced degradation of Akt, which suggests that in addition to inhibition of TRAP1, **DN401** also inhibits the cytosolic Hsp90 isoforms.[40] These data suggest that **24** exhibited TRAP1 selectivity in a cellular environment and activated apoptosis without the liabilities associated with *pan*-Hsp90 inhibitors.

Conclusions and Future Directions

Identification of scaffolds that exhibit selective inhibition of individual Hsp90 isoforms represents a significant advancement in Hsp90 drug discovery. Through screening of a small library of Hsp90 inhibitors, **1** was identified to exhibit TRAP1 affinity. Subsequent investigation of the roles played by the phenols led to the discovery of **2**, which exhibited a TRAP1 apparent K$_d$

of 2.5 µM and was >40-fold selective for TRAP1 versus the other Hsp90 isoforms. Structure-activity relationship studies on the indole region of **2** led to the identification of trends necessary for TRAP1 binding, but did not produce improved affinity. Alternatively, substitution of the indole moiety with an isoindoline amide (**36**) resulted in increased TRAP1 affinity (apparent $K_d = 0.41$ µM) and selectivity (>138-fold). These inhibitors were then evaluated for anti-proliferative activity against cervical, colorectal, and prostate cancer cell lines. Unfortunately, **36** and similar inhibitors did not produce anti-proliferative effects until high micromolar concentrations. However, substituted indoles (e.g. **24**) exhibited moderate anti-proliferative activities against these cancers. Further evaluation of **24**, via western blot analysis, demonstrated induction of the pro-apoptotic protein CHOP without degradation of the cytosolic Hsp90-dependent client protein, Akt, nor induction of Hsp70. Treatment with **24** resulted in cell death as monitored by flow cytometry suggesting that this inhibitor exhibits apoptotic activity in cells, via TRAP1-selective inhibition, without the detriments exhibited by *pan*-Hsp90 inhibitors. These inhibitors provide novel small molecule tools for further study of the roles played by TRAP1 in cancer and other diseases. In addition, this scaffold provides excellent leads for the further development of TRAP1-selective inhibitors that could improve TRAP1 affinity and selectivity. Future studies aimed to improve the cellular activity of the bis-isoindoline scaffold (e.g. **36**) would be beneficial as this scaffold exhibits excellent affinity via fluorescence polarization, but this activity did not translate into cellular studies. Additional structural information, via the solution co-crystal structures of **2** and/or **36** in complex with TRAP1, would greatly assist the design of future TRAP1-selective inhibitors. These inhibitors will expedite the discovery and validation of TRAP1-dependent processes in cancer and other maladies.

Experimental Section

Chemistry General. **Chemistry General.** ^{1}H NMR were recorded at 400 (Bruker AVIIIHD 400 MHz NMR with a broadband X-channel detect gradient probe) or 500 MHz (Avance AVIII 500 MHz spectrometer with a dual carbon/proton cryoprobe) and ^{13}C NMR were recorded at 125 MHz (Bruker AVIII spectrometer equipped with a cryogenically cooled carbon observe probe); chemical shifts are reported in δ (ppm) relative to the internal standard (CDCl$_3$, 7.26 ppm for ^{1}H and 77.2 for ^{13}C). HRMS spectra were recorded with a LCT Premier with ESI ionization. All biologically tested compounds were determined to be >95% pure. TLC analysis was performed on glass backed silica gel plates and visualized by UV light. All solvents were reagent grade and used without further purification.

Synthetic Procedures.
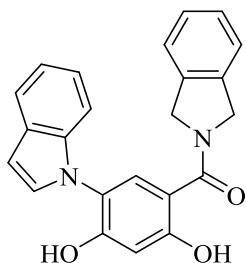
(2,4-Dihydroxy-5-(1H-indol-1-yl)phenyl)(isoindolin-2-yl)methanone (**1**). A dry 10-20 mL microwave vial was charged with (5-bromo-2,4-bis(methoxymethoxy)phenyl)(isoindolin-2-yl)methanone (100 mg, 0.23 mmol, 1 equiv.), indole (42 mg, 0.36 mmol, 1.5 equiv.), CuI (5 mg, 0.02 mmol, 0.1 equiv.), and K$_3$PO$_4$ (126 mg, 0.59 mmol, 2.5 equiv.). The vial was then evacuated and backfilled (3x) with argon followed by the addition of dry toluene (3 mL) and (±)-*trans*-1,2-diaminocyclohexane (0.01 mL, 0.1 mmol, 0.4 equiv.). Argon was bubbled through the solvent for 5 minutes and the vial was sealed and heated at 115˚C for 36 h. The reaction was cooled to rt and partitioned between EtOAc (10 mL) and water (10 mL). The aqueous layer extracted with EtOAc

(2 x 10 mL). The combined organic layers were dried over Na_2SO_4, concentrated, and the residue was passed through a plug of silica gel. The crude material was dissolved in MeOH (3 mL) and *p*-toluylsulfonic acid was added. The reaction stirred at rt for 12 h and quenched with saturated $NaHCO_3$. The aqueous layer was extracted with EtOAc (2 x 10 mL), dried, and concentrated. The residue was purified by flash chromatography (EtOAc/Hexanes, 1:1) to provide **1** as a yellow amorphous solid (57 mg, 65%). ^{1}H NMR (400 MHz, $CDCl_3$) δ 12.01 (s, 1H), 7.76 – 7.71 (m, 1H), 7.62 (s, 1H), 7.33 – 7.26 (m, 4H), 7.26 – 7.24 (m, 1H), 7.24 – 7.21 (m, 2H), 7.21 – 7.18 (m, 1H), 6.79 – 6.71 (m, 2H), 5.04 (s, 4H). ^{13}C NMR (126 MHz, $CDCl_3$) δ 169.7, 161.6, 157.0, 137.2, 129.3, 128.4, 128.2, 127.7, 122.4, 122.1 (2C), 120.8 (2C), 120.0 (2C), 117.8, 110.3, 108.8, 104.7, 102.7 (2C), 77.1 (2C). HRMS (ESI) *m/z* [M]$^+$ for $C_{23}H_{18}N_2O_3$ 370.1317, found 370.1320.

General Procedure for the synthesis of 2b and 3b.

Hunig's base (6 equiv.) was added to a stirred solution of **2a** or **3a** (1 equiv.), EDCI (3 equiv.), isoindoline hydrochloride (3 equiv.), and HOBT (3 equiv.) in DCM (0.1 M). The reaction was stirred for 12 h before the addition of 1 N HCl. The organic layer was separated and washed with saturated $NaHCO_3$ and brine then dried over Na_2SO_4 and concentrated. The residue was used without further purification. The residue was dissolved in dry DCM (~0.1M) and cooled to 0˚C. Hunig's base was added (3 equiv.) followed by chloromethyl methyl ether (2 equiv.). The reaction was allowed to warm to room temperature and stirred for 12 h. Water was added, the organic layer separated, and the aqueous layer was extracted with DCM (2 x) The organic layers were combined, dried (Na_2SO_4), and concentrated. The residue was purified via flash chromatography (EtOAc/Hexanes, 3:7) to provide **2b** or **3b**.
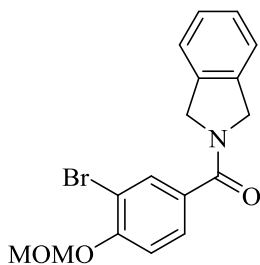
(3-Bromo-4-(methoxymethoxy)phenyl)(isoindolin-2-yl)methanone (**2b**), off white amorphous solid (4.8 g, 56%). ^{1}H NMR (500 MHz, CDCl$_3$) δ 7.82 (d, *J* = 2.1 Hz, 1H), 7.51 (dd, *J* = 8.5, 2.1 Hz, 1H), 7.36 − 7.26 (m, 3H), 7.21 (d, *J* = 8.5 Hz, 1H), 7.17 (d, *J* = 7.4 Hz, 1H), 5.30 (s, 2H), 5.00 (s, 2H), 4.82 (s, 2H), 3.54 (s, 3H). ^{13}C NMR (126 MHz, CDCl$_3$) δ 168.6, 155.3, 136.5, 136.4, 132.6, 131.4, 128.0, 127.8, 127.7, 123.1, 122.6, 115.5, 112.8, 95.1, 56.7, 55.2, 52.8. HRMS (ESI) *m/z* [M+Na]$^+$ for C$_{17}$H$_{16}$BrNO$_3$Na 384.0211, found 384.0255.
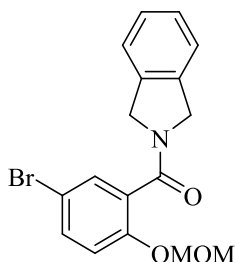

(5-Bromo-2-(methoxymethoxy)phenyl)(isoindolin-2-yl)methanone (**3b**). white amorphous solid (372 mg, 45%) ^{1}H NMR (400 MHz, CDCl$_3$) δ 7.50 − 7.43 (m, 2H), 7.38 − 7.26 (m, 3H), 7.18 − 7.07 (m, 2H), 5.17 (s, 2H), 4.99 (s, 2H), 4.64 (s, 2H), 3.44 (s, 3H). ^{13}C NMR (126 MHz, CDCl$_3$) δ 166.6, 152.3, 136.4, 136.3, 133.5, 130.6, 129.8, 128.0, 127.8, 123.3, 122.7, 117.4, 114.9, 95.3, 56.6, 53.6, 52.2. HRMS (ESI) *m/z* [M]$^+$ for C$_{17}$H$_{16}$BrNO$_3$ 361.0314, found 361.0314.

**General Procedure for the Synthesis of 2, 10, 13-22, 24-34.**

A dry 10-20 mL microwave vial was charged with **2b** (100 mg, 0.28 mmol, 1 equiv.), the corresponding indole (1.5 equiv.), CuI (5 mg, 0.02 mmol, 0.1 equiv.), and potassium phosphate tribasic (147 mg, 0.69 mmol, 2.5 equiv.). The vial was then evacuated and backfilled (3x) with

argon followed by the addition of dry toluene (3 mL) and (±)-*trans*-1,2-diaminocyclohexane (0.01

mL, 0.1 mmol, 0.4 equiv.). Argon was bubbled through the solvent for 5 minutes and the vial was

sealed and heated to 115˚C for 36 h. The reaction was cooled to rt and partitioned between EtOAc

(10 mL) and water (10 mL). The aqueous layer was extracted with EtOAc (2 x 10 mL). The

combined organic layers were dried over Na_2SO_4, concentrated and the residue was passed through

a plug of silica gel. The crude material was dissolved in MeOH (3 mL) and *p*-toluylsulfonic acid

(10 eq.) was added. The reaction was stirred at rt for 12 h and was quenched with saturated

$NaHCO_3$. The aqueous layer was extracted with EtOAc (2 x 10 mL), dried, and concentrated. The

residue was purified by flash chromatography (EtOAc/Hexanes, 1:1) to provide **2, 10, 13-22, 24-**

34.
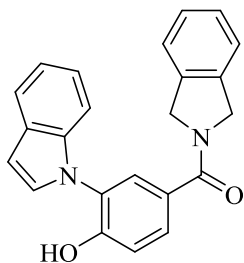
(4-Hydroxy-3-(1H-indol-1-yl)phenyl)(isoindolin-2-yl)methanone (**2**). Off white amorphous

solid (44 mg, 45%). ^{1}H NMR (400 MHz, CDCl$_3$) δ 7.67 – 7.63 (m, 1H), 7.57 – 7.51 (m, 2H), 7.32

– 7.26 (m, 3H), 7.25 – 7.20 (m, 2H), 7.19 – 7.09 (m, 4H), 6.68 (dt, *J* = 3.2, 0.9 Hz, 1H), 4.96 (s,

2H), 4.86 (s, 2H). ^{13}C NMR (126 MHz, CDCl$_3$) δ 169.5, 154.0, 136.7, 136.4, 136.2, 128.9, 128.7,

128.6, 128.6, 128.0, 127.7, 127.6, 126.0, 123.1, 122.7, 122.5, 121.2, 120.6, 117.3, 110.7, 103.9,

55.3, 52.8. HRMS (ESI) *m/z* [M+Na]$^+$ for C$_{23}$H$_{18}$N$_2$O$_2$Na 377.1266, found 377.1276.
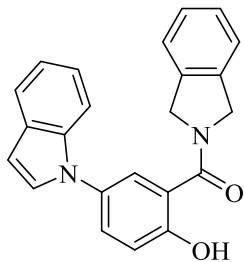
(2-Hydroxy-5-(1H-indol-1-yl)phenyl)(isoindolin-2-yl)methanone (**3**). A dry 10-20 mL microwave vial was charged with **3b** (100 mg, 0.28 mmol, 1 equiv.), indole (1.5 equiv.), CuI (5 mg, 0.02 mmol, 0.1 equiv.), and potassium phosphate tribasic (147 mg, 0.69 mmol, 2.5 equiv.). The vial was then evacuated and backfilled (3x) with argon followed by the addition of dry toluene (3 mL) and (±)-*trans*-1,2-diaminocyclohexane (0.01 mL, 0.1 mmol, 0.4 equiv.). Argon was bubbled through the solvent for 5 minutes and the vial was sealed and heated to 115°C for 36 h. The reaction was cooled to rt and partitioned between EtOAc (10 mL) and water (10 mL). The aqueous layer was extracted with EtOAc (2 x 10 mL). The combined organic layers were dried over Na_2SO_4, concentrated and the residue was passed through a plug of silica gel. The crude material was dissolved in MeOH (3 mL) and *p*-toluylsulfonic acid (10 equiv.) was added. The reaction stirred at rt for 12 h and was quenched with saturated $NaHCO_3$. The aqueous layer was extracted with EtOAc (2 x 10 mL), dried, and concentrated. The residue was purified by flash chromatography (EtOAc/Hexanes, 1:1) to provide **3** as a white amorphous solid (32 mg, 33%) ^{1}H NMR (400 MHz, $CDCl_3$) δ 11.13 (s, 1H), 7.77 – 7.70 (m, 2H), 7.52 (dd, *J* = 8.7, 2.6 Hz, 1H), 7.46 (dq, *J* = 8.2, 0.9 Hz, 1H), 7.36 – 7.27 (m, 5H), 7.25 – 7.16 (m, 3H), 6.71 (dd, *J* = 3.2, 0.9 Hz, 1H), 5.11 (s, 4H). ^{13}C NMR (126 MHz, $CDCl_3$) δ 170.1, 159.5, 130.5, 128.6, 128.4, 124.9, 124.7, 124.0, 123.0, 122.9, 121.7, 120.9, 120.8, 119.7, 118.6, 117.7, 110.6, 110.4, 104.2, 103.7, 90.9, 55.2, 50.5. HRMS (ESI) *m/z* [M+Na]+ for $C_{23}H_{18}N_2O_2Na$ 377.1266, found 377.1247.
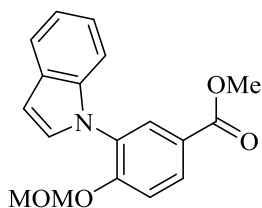
Methyl 3-(1H-indol-1-yl)-4-(methoxymethoxy)benzoate (**2d**). Chloromethyl methyl ether (1.9 mL, 26 mmol, 3 equiv.) was added to a stirred solution of methyl 3-bromo-4-hydroxybenzoate (2g, 8.7 mmol, 1 equiv.) and Hunig's base (6 mL, 34 mmol, 4 equiv.) in dry DCM (90 mL) at 0˚C. The reaction was stirred at rt for 12 h. Water (100 mL) was added, the organic layer separated, and the aqueous layer was extracted with DCM (2 x 50 mL). The organic layers were combined, dried (Na$_2$SO$_4$), concentrated, and used without further purification. The residue (2.3 g, 8.2 mmol, 1 eq.), indole (1.4 g, 12.3 mmol, 1.5 equiv.), CuI (156 mg, 0.8 mmol, 0.1 equiv.), and K$_3$PO$_4$ (4.36 g, 20.5 mmol, 2.5 equiv.) were added to a dry 120 mL sealed tube. The tube was evacuated and backfilled with argon (3 x) followed by the addition of dry toluene (80 mL) and (±)-*trans*-1,2-diaminocyclohexane (0.4 mL, 3.2 mmol, 0.4 equiv.). Argon was bubbled through the solvent for 5 minutes and the tube was sealed and heated at 115˚C for 36 h. The tube was cooled to rt and partitioned between EtOAc (100 mL) and water (100 mL). The aqueous layer was extracted with EtOAc (2 x 50 mL). The combined organic layers were dried (Na$_2$SO$_4$), concentrated, and purified via flash chromatography (EtOAc/Hexanes, 3:7) to provide **2d** as a white amorphous solid (2.39 g, 89% yield). ^{1}H NMR (400 MHz, CDCl$_3$) δ 8.12 (d, J = 1.4 Hz, 1H), 8.08 (dd, J = 8.7, 2.8 Hz, 1H), 7.69 (dd, J = 6.5, 1.9 Hz, 1H), 7.39 (d, J = 8.7 Hz, 1H), 7.27 (d, J = 3.4 Hz, 1H), 7.24 − 7.12 (m, 3H), 6.69 (d, J = 3.3 Hz, 1H), 5.15 (s, 2H), 3.91 (s, 3H), 3.36 (s, 3H). ^{13}C NMR (126 MHz, CDCl$_3$) δ 166.1, 156.0, 136.8, 130.4, 129.8, 129.0, 128.8, 128.6, 124.2, 122.1, 120.9, 120.2, 115.5, 110.7, 103.1, 94.8, 56.6, 52.2. HRMS (ESI) *m/z* for [M+Na]$^+$ for C$_{18}$H$_{17}$NO$_4$Na 334.1055, found 334.1056.
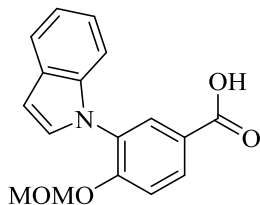
3-(1H-Indol-1-yl)-4-(methoxymethoxy)benzoic acid (**2e**). LiOH (1.84 g, 77 mmol, 10 equiv.) was added to a stirred solution of **2d** (2.39 g, 7.7 mmol, 1 equiv.) in a THF:MeOH:Water mixture (2:1:1, 0.1 M). The reaction was heated at 70˚ for 12 h. Upon cooling to rt, 3 N HCl was added dropwise until the pH was ~7 followed by the addition of EtOAc (50 mL). The aqueous layer was extracted with EtOAc (2 x 50 mL). The organic layers were combined, dried, and concentrated to provide **2e** (2.12 g 93%). ^{1}H NMR (500 MHz, CDCl$_3$) δ 8.13 (d, *J* = 2.1 Hz, 1H), 8.09 (dd, *J* = 8.7, 2.2 Hz, 1H), 7.71 – 7.65 (m, 1H), 7.38 (d, *J* = 8.7 Hz, 1H), 7.27 (d, *J* = 1.2 Hz, 1H), 7.23 – 7.13 (m, 3H), 6.68 (dd, *J* = 3.3, 0.8 Hz, 1H), 5.14 (s, 2H), 3.35 (s, 3H). ^{13}C NMR (126 MHz, CDCl$_3$) δ 168.3, 156.3, 136.9, 130.9, 130.3, 129.1, 128.9, 128.6, 124.3, 122.2, 121.0, 120.2, 115.6, 110.8, 103.2, 94.8, 56.7. HRMS (ESI) *m/z* [M+H]$^+$ for C$_{17}$H$_{16}$NO$_4$ 298.1079, found 298.1071.

General procedure for the synthesis of 4-7.

Hunig's base (6 equiv.) was added to a stirred solution of **2e** (1 equiv.), EDCI (3 equiv.), HOBT (3 equiv.) and a substituted isoindoline (3 equiv.) in DCM (0.1 M) and stirred at rt for 12 h. 1 N HCl was added and the organic layer was separated and washed with saturated NaHCO$_3$ and brine. The organic layer was dried (Na$_2$SO$_4$), concentrated, and used without further purification. The residue was dissolved in MeOH and *p*-toluylsulfonic acid was added. The reaction stirred for 12 h at rt. The reaction was quenched with saturated NaHCO$_3$ and extracted with EtOAc (3 x 20 mL). The combined organic layers were dried (Na$_2$SO$_4$), concentrated, and purified by flash chromatography (EtOAc/Hexanes, 1:1) to provide **4-7**.
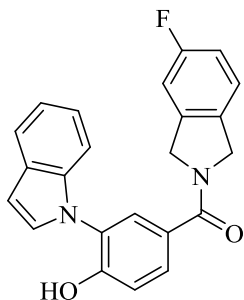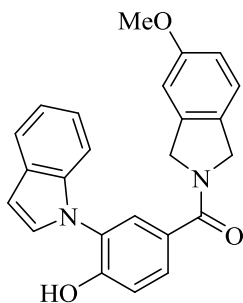
(5-Fluoroisoindolin-2-yl)(4-hydroxy-3-(1H-indol-1-yl)phenyl)methanone (**4**) white amorphorous solid (15 mg, 24%). ^{1}H NMR (400 MHz, CDCl$_3$) δ 7.68 (dt, *J* = 7.5, 1.3 Hz, 1H), 7.57 (t, *J* = 2.8 Hz, 2H), 7.27 (d, *J* = 3.3 Hz, 1H), 7.23 – 7.19 (m, 2H), 7.18 – 7.11 (m, 2H), 7.10 – 6.83 (m, 3H), 6.73 – 6.70 (m, 1H), 4.95 (d, *J* = 12.1 Hz, 2H), 4.84 (d, *J* = 9.8 Hz, 2H). ^{13}C NMR (126 MHz, CDCl$_3$) δ 169.7, 154.3, 136.7, 131.8, 131.6, 129.0, 128.7, 128.4, 128.4, 127.8, 127.5, 126.2, 124.4, 124.3, 123.9, 123.8, 122.4, 121.1, 120.4, 117.3, 115.4, 115.2, 115.1, 114.9, 110.7, 110.3, 110.1, 109.8, 109.6, 103.5, 55.2, 54.7, 52.8, 52.2. HRMS (ESI) *m/z* [M+H]$^+$ for C$_{23}$H$_{18}$FN$_2$O$_2$ 373.1352, found 373.1340.
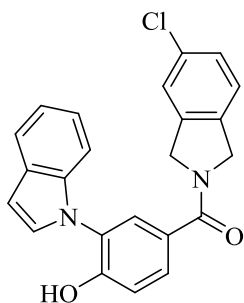
(5-Chloroisoindolin-2-yl)(4-hydroxy-3-(1H-indol-1-yl)phenyl)methanone (**5**), tan amorphous solid (28 mg, 43%). ^{1}H NMR (400 MHz, CDCl$_3$) δ 7.73 – 7.68 (m, 1H), 7.64 – 7.56 (m, 2H), 7.30 (d, *J* = 16.6 Hz, 1H), 7.25 – 7.16 (m, 6H), 6.76 (dd, *J* = 3.2, 0.8 Hz, 1H), 4.97 (d, *J* = 7.0 Hz, 2H), 4.84 (s, 2H). ^{13}C NMR (126 MHz, CDCl$_3$) δ 169.4, 154.0, 138.2, 136.7, 134.8, 129.2, 128.8, 128.8, 128.7, 128.4, 128.4, 128.1, 127.7, 124.3, 123.7, 123.4, 122.8, 121.3, 120.8, 117.4, 115.4, 110.6,

104.1, 54.9, 54.8, 52.6, 52.4. HRMS (ESI) *m/z* [M+Na]$^+$ for C$_{23}$H$_{17}$ClN$_2$O$_2$Na 411.0876, found 411.0887.

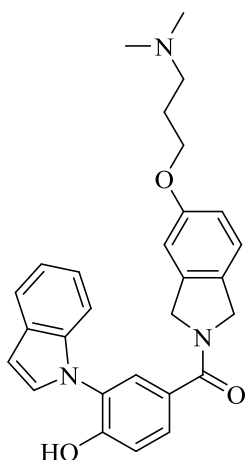*(4-Hydroxy-3-(1H-indol-1-yl)phenyl)(5-methoxyisoindolin-2-yl)methanone* (**6**), off white amorphous solid (18 mg, 28%). ^{1}H NMR (400 MHz, CDCl$_3$) δ 7.76 − 7.69 (m, 1H), 7.62 (dd, *J* = 8.4, 2.1 Hz, 1H), 7.59 (d, *J* = 2.1 Hz, 1H), 7.25 − 7.17 (m, 6H), 6.90 − 6.80 (m, 2H), 6.76 (dd, *J* = 3.2, 0.8 Hz, 1H), 5.63 (s, 1H), 4.95 (d, *J* = 14.4 Hz, 2H), 4.82 (d, *J* = 11.7 Hz, 2H), 3.80 (d, *J* = 13.2 Hz, 3H). ^{13}C NMR (126 MHz, CDCl$_3$) δ 169.6, 159.9, 159.6, 154.1, 137.7, 137.6, 136.7, 129.0, 128.7, 128.4, 128.3, 128.2, 128.1, 127.5, 126.2, 123.8, 123.3, 122.5, 121.1, 120.5, 117.3, 114.3, 114.2, 110.7, 107.8, 107.7, 103.6, 55.6, 55.4, 54.8, 53.0, 52.3. HRMS (ESI) *m/z* [M+Na]$^+$ for C$_{24}$H$_{20}$N$_2$O$_3$Na 407.1372, found 407.1386.
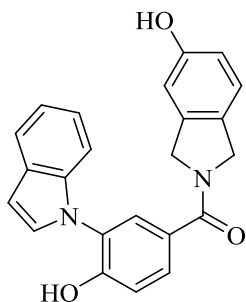
(4-Hydroxy-3-(1H-indol-1-yl)phenyl)(5-hydroxyisoindolin-2-yl)methanone (**7**), tan amorphous solid (43 mg, 69%). ^{1}H NMR (400 MHz, CDCl$_3$) δ 7.65 (d, *J* = 7.7 Hz, 1H), 7.53 (d, *J* = 11.4 Hz, 2H), 7.27 (s, 1H), 7.25 − 6.93 (m, 5H), 6.77 − 6.58 (m, 3H), 4.87 (s, 2H), 4.76 (d, *J* = 6.7 Hz, 2H). ^{13}C NMR (126 MHz, CDCl$_3$) δ 169.5, 156.9, 154.0, 136.7, 128.9, 128.7, 128.6, 127.6, 123.8,

123.4, 122.7, 122.7, 121.2, 120.6, 117.3, 115.4, 115.3, 110.7, 109.6, 109.2, 103.8, 54.9, 52.9.

HRMS (ESI) m/z [M+H]$^+$ for $C_{23}H_{19}N_2O_3$ 371.1396, found 371.1387.

*(5-(3-(Dimethylamino)propoxy)isoindolin-2-yl)(4-hydroxy-3-(1H-indol-1-*

yl)phenyl)methanone (**8**). A 2-5 mL microwave vial was charged with (3-(1H-indol-1-yl)-4-(methoxymethoxy)phenyl)(5-hydroxyisoindolin-2-yl)methanone (50 mg, 0.12 mmol, 1 equiv.), 3-dimethylamino-1-propyl chloride hydrochloride (29 mg, 0.18 mmol, 1.5 equiv.), K_2CO_3 (50 mg, 0.36 mmol, 3 equiv.), $^nBu_4N^+I^-$ (cat.), and dry DMF (2 mL). The vial was sealed and heated at 90°C for 36 h. The reaction was cooled to rt and 1 N HCl (5 mL) was added followed by EtOAc (10 mL). The organic layer was washed with water (5 x 20 mL), dried (Na$_2$SO$_4$), concentrated, and used without further purification. The residue was dissolved in MeOH and *p*-toluylsulfonic acid was added and stirred for 12 h at rt. The reaction was quenched with saturated NaHCO$_3$ and extracted with EtOAc (3 x 10 mL). The combined organic layers were dried (Na$_2$SO$_4$) and concentrated. The residue was purified via flash chromatography (MeOH/10% ammoniated DCM, 1:49) to provide **8** as a clear oil (15 mg, 20%). ^{1}H NMR (400 MHz, CDCl$_3$) δ 7.69 (dt, J = 7.2, 1.3 Hz, 1H), 7.62 – 7.56 (m, 2H), 7.25 (s, 1H), 7.23 – 7.00 (m, 5H), 6.85 – 6.65 (m, 3H), 4.93 (d, J = 10.0 Hz, 3H), 4.80 (d, J = 10.7 Hz, 2H), 3.96 (dt, J = 18.2, 6.3 Hz, 2H), 2.45 (q, J = 7.7 Hz, 2H), 2.23 (d, J = 4.5 Hz, 6H), 1.93 (q, J = 7.5 Hz, 2H). ^{13}C NMR (126 MHz, CDCl$_3$) δ 169.4, 159.2,

154.0, 136.8, 129.4, 129.3, 129.0, 129.0, 128.6, 128.6, 127.8, 126.4, 124.1, 123.6, 123.2, 121.6, 121.1, 117.6, 115.1, 110.9, 108.8, 108.6, 104.8, 75.1, 66.8, 56.6, 55.1, 53.3, 45.6, 30.1. HRMS (ESI) *m/z* [M+H]$^+$ for $C_{28}H_{30}N_3O_3$ 456.2287, found 456.2289.
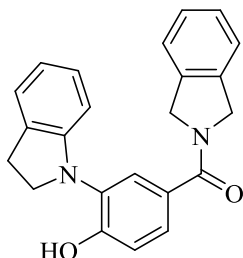
(4-Hydroxy-3-(indolin-1-yl)phenyl)(isoindolin-2-yl)methanone (**9**). A microwave vial was charged with **2b** (27 mg, 0.07 mmol, 1 equiv.), indoline (0.01 mL, 0.07 mmol, 1 equiv.), SPhos (3 mg, 0.007 mmol, 0.1 equiv.), Pd(OAc)$_2$ (1 mg, 0.003 mmol, 0.05 equiv.), and sodium *tert*-butoxide (10 mg, 0.1 mmol, 1.4 equiv.). The tube was evacuated and backfilled with argon (3 x) followed by the addition of toluene (1 mL). The resulting mixture was heated at 115 °C for 16 h, cooled to rt, and diluted with water (5 mL) and EtOAc (5 mL). The aqueous layer was extracted with EtOAc (2 x 10 mL). The combined organic layers were dried (Na$_2$SO$_4$), concentrated, and used as obtained. The residue was dissolved in MeOH and *p*-toluylsulfonic acid (10 equiv.) was added. The reaction was stirred at rt for 12 h, quenched with saturated NaHCO$_3$, and extracted with EtOAc (3 x 5 mL). The combined organic layers were dried (Na$_2$SO$_4$), concentrated, and purified by flash chromatograph (EtOAc/Hexanes, 1:1) to provide **9** as a light brown amorphous solid (13 mg, 49%). ^{1}H NMR (400 MHz, CDCl$_3$) δ 7.52 (d, *J* = 2.0 Hz, 1H), 7.47 (dd, *J* = 8.3, 2.1 Hz, 1H), 7.30 (d, *J* = 6.2 Hz, 3H), 7.22 (d, *J* = 7.5 Hz, 1H), 7.12 (d, *J* = 8.4 Hz, 1H), 7.09 − 7.03 (m, 1H), 6.83 (td, *J* = 7.4, 1.0 Hz, 1H), 6.48 (s, 1H), 6.35 (d, *J* = 7.8 Hz, 1H), 4.98 (s, 2H), 4.82 (s, 2H), 3.75 (t, *J* = 8.1 Hz, 2H), 3.18 (t, *J* = 8.1 Hz, 2H). ^{13}C NMR (126 MHz, CDCl$_3$) δ 168.9, 154.8, 136.3, 130.7, 128.9, 128.4, 127.8, 127.5, 127.5, 127.0, 124.9, 124.3, 123.1, 121.4, 121.0, 120.3, 116.9,

115.0, 110.3, 109.8, 105.0, 55.9, 55.1, 29.7, 29.1. HRMS (ESI) *m/z* [M+H]$^+$ for C$_{23}$H$_{21}$N$_2$O$_2$ 357.1603, found 357.1594.
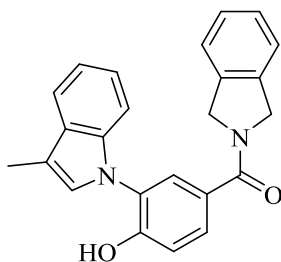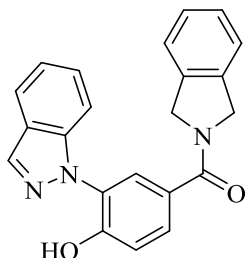

4-Hydroxy-3-(3-methyl-1H-indol-1-yl)phenyl)(isoindolin-2-yl)methanone (**10**), off white amorphous solid (63 mg, 62%). ^{1}H NMR (400 MHz, CDCl$_3$) δ 7.67 − 7.62 (m, 1H), 7.62 − 7.55 (m, 2H), 7.34 − 7.26 (m, 3H), 7.22 (d, *J* = 2.0 Hz, 1H), 7.18 (ddt, *J* = 8.5, 7.1, 1.1 Hz, 4H), 7.02 (q, *J* = 1.1 Hz, 1H), 5.00 (s, 2H), 4.87 (s, 2H), 2.39 (d, *J* = 1.1 Hz, 3H). ^{13}C NMR (126 MHz, CDCl$_3$) δ 169.4, 153.4, 136.9, 136.4, 136.3, 129.6, 129.1, 128.5, 128.0, 127.7, 127.4, 126.2, 126.0, 123.1, 123.0, 122.6, 120.3, 119.5, 117.1, 114.1, 110.4, 55.3, 52.9, 9.8. HRMS (ESI) *m/z* [M+Na]$^+$ for C$_{24}$H$_{20}$N$_2$O$_2$Na 391.1422, found 391.1440.

**General procedure for the synthesis of 11, 12, and 23.**

A dry 10-20 mL microwave vial was charged with **2b** (100 mg, 0.28 mmol, 1 equiv.), indazole, 4-azaindole, or 6-azaindole (1.5 equiv.), CuI (3 mg, 0.01 mmol, 0.05 equiv.), and K$_3$PO$_4$ (147 mg, 0.69 mmol, 2.5 equiv.). The vial was then evacuated and backfilled (3x) with argon followed by the addition of dry toluene (3 mL) and (*1R,2R*)-*N,N'*-dimethyl-1,2-diaminocyclohexane (8 mg, 0.05 mmol, 0.2 equiv.). Argon was bubbled through the solvent for 5 minutes and the vial was sealed and heated at 115˚C for 36 h. The reaction was cooled to rt and portioned between EtOAc (10 mL) and water (10 mL). The aqueous layer was extracted with EtOAc (2 x 10 mL). The combined organic layers were dried over Na$_2$SO$_4$, concentrated and the residue was passed through a plug of silica gel. The crude material was dissolved in MeOH (3 mL), *p*-toluylsulfonic acid (10

equiv.) was added and stirred at rt for 12 h. The reaction was quenched with saturated NaHCO$_3$ and the aqueous layer was extracted with EtOAc (2 x 10 mL), dried, and concentrated. The residue was purified by flash chromatography (EtOAc/Hexanes, 1:1) to provide **11, 12, and 23.**

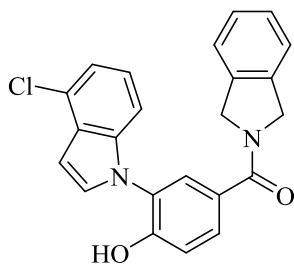*(4-Hydroxy-3-(1H-indazol-1-yl)phenyl)(isoindolin-2-yl)methanone* (**11**) off white amorphous solid (23 mg, 23%). ^{1}H NMR (400 MHz, CDCl$_3$) δ 10.09 (s, 1H), 8.29 (d, J = 0.9 Hz, 1H), 8.00 (d, J = 2.1 Hz, 1H), 7.92 (dq, J = 8.6, 0.9 Hz, 1H), 7.86 (dt, J = 8.2, 1.0 Hz, 1H), 7.57 − 7.47 (m, 2H), 7.38 − 7.27 (m, 4H), 7.24 (d, J = 8.4 Hz, 1H), 7.18 (d, J = 7.4 Hz, 1H), 5.06 (s, 2H), 4.92 (s, 2H). ^{13}C NMR (126 MHz, CDCl$_3$) δ 169.7, 151.8, 139.2, 136.8, 136.7, 135.5, 129.0, 128.6, 128.3, 128.0, 126.9, 126.4, 124.7, 123.3, 123.0, 122.8, 122.2, 120.9, 118.8, 111.6, 55.7, 53.2. HRMS (ESI) *m/z* [M+Na]$^+$ for C$_{22}$H$_{17}$N$_3$O$_2$Na 378.1218, found 378.1222.
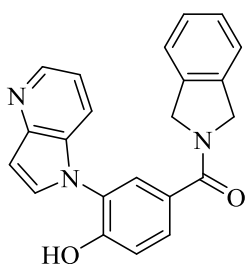

(4-Hydroxy-3-(1H-pyrrolo[3,2-b]pyridin-1-yl)phenyl)(isoindolin-2-yl)methanone (**12**) brown amorphous solid (15 mg, 15%). ^{1}H NMR (400 MHz, CDCl$_3$) δ 8.19 (dd, J = 4.9, 1.3 Hz, 1H), 7.63 − 7.52 (m, 1zH), 7.41 (d, J = 3.4 Hz, 1H), 7.34 − 7.28 (m, 2H), 7.28 − 7.25 (m, 2H), 7.18 (d, J = 7.3 Hz, 1H), 7.05 (dd, J = 8.3, 4.8 Hz, 1H), 6.45 (dd, J = 3.4, 0.9 Hz, 1H), 5.01 (s, 2H), 4.90 (s, 2H). ^{13}C NMR (126 MHz, CDCl$_3$) δ 169.3, 155.0, 145.6, 142.1, 136.1, 136.0, 132.7, 130.0, 128.6,

127.8, 127.7, 127.5, 127.3, 125.6, 122.8, 122.3, 119.2, 118.2, 116.8, 102.9, 55.1, 52.7. HRMS (ESI) m/z [M+H]$^+$ for $C_{22}H_{18}N_3O_2$ 356.1399, found 356.1392.
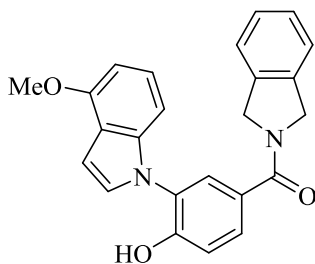

(3-(4-Chloro-1H-indol-1-yl)-4-hydroxyphenyl)(isoindolin-2-yl)methanone (**13**), tan amorphous solid (48 mg, 45%). ^{1}H NMR (400 MHz, CDCl$_3$) δ 7.60 − 7.53 (m, 2H), 7.34 (d, $J = 3.3$ Hz, 1H), 7.31 (d, $J = 6.9$ Hz, 2H), 7.25 (d, $J = 7.0$ Hz, 1H), 7.20 − 7.08 (m, 5H), 6.79 (dd, $J = 3.3, 0.7$ Hz, 1H), 4.99 (s, 2H), 4.88 (s, 2H). ^{13}C NMR (126 MHz, CDCl$_3$) δ 169.5, 154.1, 137.5, 136.3, 136.1, 129.6, 128.7, 128.0, 127.7, 127.5, 127.4, 126.3, 125.9, 123.0 (2C), 122.5, 120.2, 117.3, 109.5 (2C), 102.0, 55.3, 52.9. HRMS (ESI) m/z [M+H]$^+$ for $C_{23}H_{18}ClN_2O_2$ 389.1059, found 389.1039.
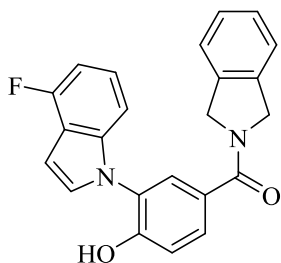
(3-(4-Fluoro-1H-indol-1-yl)-4-hydroxyphenyl)(isoindolin-2-yl)methanone (**14**), off white amorphous solid (23 mg, 22%). ^{1}H NMR (500 MHz, CDCl$_3$) δ 7.56 (d, J = 2.1 Hz, 1H), 7.52 (dd, J = 8.4, 2.1 Hz, 1H), 7.29 (d, J = 6.8 Hz, 2H), 7.24 (d, J = 3.5 Hz, 2H), 7.15 (d, J = 7.7 Hz, 1H), 7.12 − 7.05 (m, 2H), 7.00 (d, J = 8.2 Hz, 1H), 6.85 − 6.77 (m, 1H), 6.75 (d, J = 3.2 Hz, 1H), 4.97 (s, 2H), 4.85 (s, 2H). ^{13}C NMR (126 MHz, CDCl$_3$) δ 169.5, 156.3 (d, J = 247.2 Hz), 154.1, 129.0, 128.9, 128.5, 128.0, 127.9, 127.6, 127.3, 122.9, 122.8, 122.8, 122.4, 117.3, 115.3, 106.8, 106.8,

105.2, 105.0, 99.3, 55.2, 52.8. HRMS (ESI) *m/z* [M+H]$^+$ for $C_{23}H_{18}FN_2O_2$ 373.1352, found 373.1355.

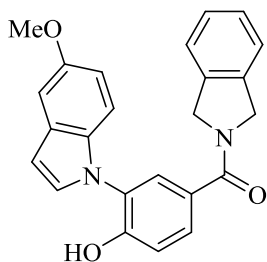*(4-Hydroxy-3-(4-methoxy-1H-indol-1-yl)phenyl)(isoindolin-2-yl)methanone* (**15**), brown amorphous solid (27 mg, 25%). ^{1}H NMR (500 MHz, CDCl$_3$) δ 7.56 (s, 1H), 7.44 (d, J = 8.5 Hz, 1H), 7.29 (d, J = 11.4 Hz, 2H), 7.19 − 7.09 (m, 4H), 6.84 (d, J = 8.4 Hz, 2H), 6.79 (d, J = 3.3 Hz, 1H), 6.57 (d, J = 7.6 Hz, 1H), 4.97 (s, 2H), 4.83 (d, J = 23.9 Hz, 2H), 3.96 (s, 3H). ^{13}C NMR (126 MHz, CDCl$_3$) δ 170.9, 158.7, 153.4, 138.1, 136.2, 136.0, 129.0, 128.5, 127.9, 127.9, 127.5, 127.4, 123.4, 122.9, 122.4, 122.4, 117.3, 115.2, 104.0, 100.9, 100.4, 55.4, 55.2, 52.7. HRMS (ESI) *m/z* [M+Na]$^+$ for $C_{24}H_{20}N_2O_3Na$ 407.1372, found 407.1391.
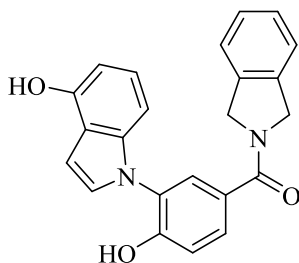
(4-Hydroxy-3-(4-hydroxy-1H-indol-1-yl)phenyl)(isoindolin-2-yl)methanone (**16**) tan amorphous solid (37 mg, 36%). ^{1}H NMR (500 MHz, CDCl$_3$) δ 7.64 (dd, J = 8.4, 2.0 Hz, 1H), 7.60 (d, J = 2.1 Hz, 1H), 7.53 − 7.50 (m, 2H), 7.34 − 7.28 (m, 2H), 7.24 − 7.15 (m, 3H), 7.10 (t, J = 8.0 Hz, 1H), 6.88 (d, J = 8.6 Hz, 1H), 6.79 (d, J = 8.3 Hz, 1H), 6.61 (d, J = 7.6 Hz, 1H), 5.02 (s, 2H), 4.86 (d, J = 28.6 Hz, 2H). ^{13}C NMR (126 MHz, CDCl$_3$) δ 171.5, 161.6, 157.3, 129.2, 128.9, 128.7,

128.6, 128.5, 127.5, 122.1, 121.2, 117.7, 115.2, 111.7, 111.7, 111.6, 105.8, 103.3, 102.1, 101.8, 101.2, 55.2, 52.8. HRMS (ESI) m/z [M+H]$^+$ for $C_{23}H_{19}N_2O_2$ 371.1396, found 371.1405.
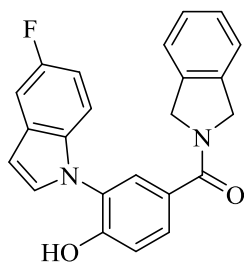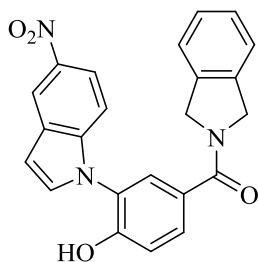

(4-Hydroxy-3-(5-methoxy-1H-indol-1-yl)phenyl)(isoindolin-2-yl)methanone　　(**17**),　　white amorphous solid (42 mg, 40%). ^{1}H NMR (400 MHz, CDCl$_3$) δ 7.57 – 7.49 (m, 2H), 7.32 – 7.26 (m, 2H), 7.24 (t, J = 3.1 Hz, 2H), 7.17 – 7.08 (m, 4H), 6.87 – 6.81 (m, 1H), 6.60 (dd, J = 3.2, 0.8 Hz, 1H), 4.96 (s, 2H), 4.85 (s, 2H), 3.83 (s, 3H). ^{13}C NMR (126 MHz, CDCl$_3$) δ 169.5, 154.6, 153.9, 136.2, 136.0, 131.9, 129.4, 129.1, 128.2, 128.2, 127.9, 127.6, 127.3, 126.2, 122.9, 122.4, 117.2, 112.6, 111.5, 103.3, 102.7, 55.9, 55.2, 52.7. HRMS (ESI) m/z [M+H]$^+$ for $C_{24}H_{21}N_2O_3$ 385.1552, found 385.1564.

(3-(5-Fluoro-1H-indol-1-yl)-4-hydroxyphenyl)(isoindolin-2-yl)methanone (**18**) off white amorphous solid (39 mg, 38%). ^{1}H NMR (400 MHz, CDCl$_3$) δ 7.54 (d, J = 2.1 Hz, 1H), 7.50 (dd, J = 8.4, 2.2 Hz, 1H), 7.30 (d, J = 3.3 Hz, 1H), 7.28 (d, J = 2.0 Hz, 2H), 7.26 (s, 2H), 7.13 (dd, J = 8.8, 4.1 Hz, 2H), 7.09 (d, J = 8.4 Hz, 1H), 6.89 (td, J = 9.1, 2.5 Hz, 1H), 6.60 (dd, J = 3.2, 0.8 Hz, 1H), 4.95 (s, 2H), 4.85 (s, 2H). ^{13}C NMR (126 MHz, CDCl$_3$) δ 169.7, 159.2, 157.4, 154.1, 136.2, 136.0, 133.3, 130.6, 129.0, 128.9, 128.4, 128.1, 128.0, 127.7, 127.4, 126.1, 123.0, 122.5, 117.2,

111.6, 111.5, 110.8, 110.6, 105.9, 105.7, 103.3, 103.3, 55.3, 52.8. HRMS (ESI) *m/z* [M+Na]$^+$ for

C$_{23}$H$_{17}$FN$_2$O$_2$Na 395.1172, found 395.1174.

(4-Hydroxy-3-(5-nitro-1H-indol-1-yl)phenyl)(isoindolin-2-yl)methanone (**19**), yellow

amorphous solid (15 mg, 14%). ^{1}H NMR (500 MHz, CDCl$_3$) δ 8.64 (d, J = 2.2 Hz, 1H), 8.09 (dd,

J = 9.1, 2.2 Hz, 1H), 7.74 − 7.63 (m, 2H), 7.44 (d, J = 8.5 Hz, 1H), 7.42 (d, J = 3.3 Hz, 1H), 7.37

− 7.27 (m, 3H), 7.24 (d, J = 9.1 Hz, 1H), 7.19 (d, J = 7.5 Hz, 1H), 6.86 (d, J = 3.4 Hz, 1H), 5.03 (s,

2H), 4.90 (s, 2H). ^{13}C NMR (126 MHz, CDCl$_3$) δ 168.5, 153.6, 139.6, 136.1, 132.2, 130.8, 128.8,

128.0, 127.9, 127.8, 127.7, 127.5, 123.0, 122.4, 118.2, 117.8, 116.0, 110.8, 105.3, 55.1, 52.8.

HRMS (ESI) *m/z* [M]$^+$ for C$_{23}$H$_{17}$N$_3$O$_4$ 399.1219, found 399.1215.

(4-Hydroxy-3-(5-hydroxy-1H-indol-1-yl)phenyl)(isoindolin-2-yl)methanone (**20**), brown

amorphous solid (32 mg, 31%). ^{1}H NMR (500 MHz, CDCl$_3$) δ 7.54 (s, 1H), 7.44 (d, J = 8.5 Hz,

2H), 7.30 (s, 2H), 7.22 (d, J = 3.2 Hz, 1H), 7.13 (d, J = 7.8 Hz, 1H), 7.06 (d, J = 8.3 Hz, 1H), 6.85

(d, J = 8.5 Hz, 2H), 6.76 (dd, J = 8.7, 2.5 Hz, 1H), 6.54 (d, J = 3.2 Hz, 1H), 4.97 (s, 2H), 4.83 (d,

J = 21.5 Hz, 2H). ^{13}C NMR (126 MHz, CDCl$_3$) δ 172.5, 162.1, 158.8, 148.3, 147.0, 144.8, 142.7,

136.5, 135.1, 133.5, 132.8, 132.7, 130.8, 129.0, 128.1, 127.3, 127.0, 115.2, 109.8, 105.5, 103.2, 55.2, 53.4. HRMS (ESI) *m/z* [M+H]$^+$ for C$_{23}$H$_{19}$N$_2$O$_3$ 371.1396, found 371.1403.
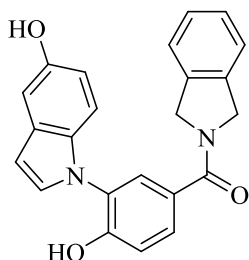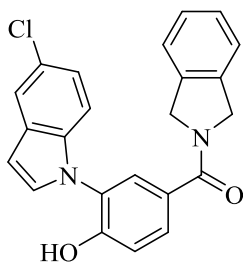

(3-(5-Chloro-1H-indol-1-yl)-4-hydroxyphenyl)(isoindolin-2-yl)methanone (**21**) tan amorphous solid (29 mg, 27%). ^{1}H NMR (500 MHz, CDCl$_3$) δ 7.59 (d, J = 2.1 Hz, 1H), 7.55 – 7.49 (m, 2H), 7.44 – 7.40 (m, 1H), 7.29 (d, J = 3.2 Hz, 2H), 7.17 – 7.07 (m, 4H), 6.88 – 6.79 (m, 1H), 6.59 (d, J = 3.1 Hz, 1H), 4.96 (s, 2H), 4.85 (s, 2H). ^{13}C NMR (126 MHz, CDCl$_3$) δ 169.6, 154.1, 136.1, 135.1, 130.3, 129.6, 129.0, 128.3, 127.9, 127.9, 127.6, 127.3, 125.9, 122.9, 122.5, 122.4, 120.2, 117.2, 115.2, 111.9, 102.9, 55.2, 52.7. HRMS (ESI) *m/z* [M+H]$^+$ for C$_{23}$H$_{18}$ClN$_2$O$_2$ 389.1057, found 389.1072.
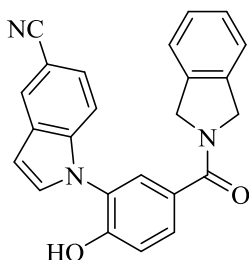
1-(2-Hydroxy-5-(isoindoline-2-carbonyl)phenyl)-1H-indole-5-carbonitrile (**22**), yellow amorphous solid (48 mg, 46%). ^{1}H NMR (400 MHz, CDCl$_3$) δ 7.98 (d, J = 1.7 Hz, 1H), 7.57 – 7.50 (m, 2H), 7.43 – 7.35 (m, 2H), 7.33 – 7.21 (m, 5H), 7.18 – 7.07 (m, 2H), 6.72 (d, J = 2.9 Hz, 1H), 4.96 (s, 2H), 4.85 (s, 2H). ^{13}C NMR (126 MHz, CDCl$_3$) δ 169.2, 153.9, 138.1, 135.9, 135.8, 131.2, 128.5, 128.2, 127.9, 127.8, 127.5, 127.2, 126.3, 125.2, 124.9, 122.8, 122.3, 120.5, 117.0,

111.7, 103.7, 102.9, 55.0, 52.6. HRMS (ESI) *m/z* [M+Na]$^+$ for C$_{24}$H$_{17}$N$_3$O$_2$Na 402.1218, found 402.1236.
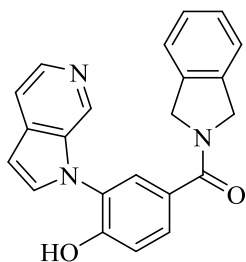
(4-Hydroxy-3-(1H-pyrrolo[2,3-c]pyridin-1-yl)phenyl)(isoindolin-2-yl)methanone (**23**), tan amorphous solid (24 mg, 24%). ^{1}H NMR (400 MHz, DMSO-*d$_6$*) δ 10.72 (s, 1H), 8.54 (s, 1H), 8.18 (d, *J* = 5.4 Hz, 1H), 7.74 (d, *J* = 3.2 Hz, 1H), 7.69 (d, *J* = 2.1 Hz, 1H), 7.65 (dd, *J* = 8.4, 2.2 Hz, 1H), 7.62 (dd, *J* = 5.4, 1.1 Hz, 1H), 7.39 (d, *J* = 6.6 Hz, 1H), 7.28 (s, 3H), 7.19 (d, *J* = 8.4 Hz, 1H), 6.72 (dd, *J* = 3.1, 0.8 Hz, 1H), 4.89 (d, *J* = 24.8 Hz, 4H). ^{13}C NMR (126 MHz, DMSO-*d$_6$*) δ 167.9, 153.6, 138.5, 137.2, 136.0, 134.1, 133.4, 133.0, 132.8, 128.5, 127.8, 127.4, 127.3, 127.1, 124.8, 122.8, 122.8, 116.6, 115.0, 101.8, 54.4, 52.2. HRMS (ESI) *m/z* [M+H]$^+$ for C$_{22}$H$_{18}$N$_3$O$_2$ 356.1399, found 356.1411.

(3-(6-Chloro-1H-indol-1-yl)-4-hydroxyphenyl)(isoindolin-2-yl)methanone (**24**), off white amorphous solid (45 mg, 42%). ^{1}H NMR (400 MHz, CDCl$_3$) δ 7.57 – 7.52 (m, 3H), 7.31 – 7.26 (m, 3H), 7.24 (d, *J* = 1.9 Hz, 1H), 7.23 – 7.22 (m, 1H), 7.18 (d, *J* = 7.2 Hz, 1H), 7.13 – 7.06 (m, 2H), 6.64 (dd, *J* = 3.3, 0.9 Hz, 1H), 4.97 (s, 2H), 4.89 (s, 2H). ^{13}C NMR (126 MHz, CDCl$_3$) δ 169.5, 154.0, 137.1, 136.2, 136.0, 129.7, 128.6, 128.2, 128.0, 127.9, 127.6, 127.3, 127.1, 125.6,

122.9, 122.5, 121.8, 120.9, 117.2, 110.8, 103.4, 55.3, 52.8. HRMS (ESI) *m/z* [M+Na]⁺ for

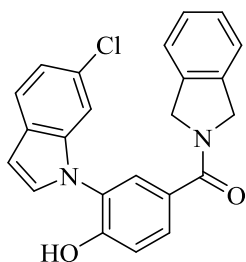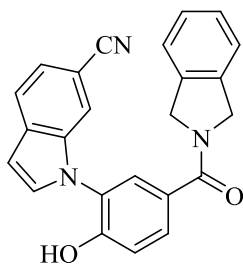C₂₃H₁₇ClN₂O₂Na 411.0876, found 411.0875.

1-(2-Hydroxy-5-(isoindoline-2-carbonyl)phenyl)-1H-indole-6-carbonitrile (**25**), off white

amorphous solid (32 mg, 31%). ¹H NMR (400 MHz, CDCl₃) δ 7.70 – 7.67 (m, 1H), 7.59 – 7.52

(m, 3H), 7.47 (dd, J = 3.2, 1.2 Hz, 1H), 7.33 (dt, J = 8.2, 1.4 Hz, 1H), 7.29 (s, 1H), 7.22 (s, 0H),

7.18 (d, J = 7.0 Hz, 1H), 7.12 – 7.08 (m, 1H), 6.76 – 6.69 (m, 1H), 4.97 (s, 2H), 4.88 (s, 2H). ¹³C

NMR (126 MHz, CDCl₃) δ 169.4, 154.1, 135.9, 135.6, 132.7, 131.9, 129.0, 128.7, 127.9, 127.9,

127.7, 127.3, 125.2, 122.8, 122.5, 121.7, 121.6, 120.7, 117.0, 116.1, 104.2, 103.8, 55.2, 52.8.

HRMS (ESI) *m/z* [M+Na]⁺ for C₂₄H₁₇N₃O₂Na 380.1399, found 380.1382.
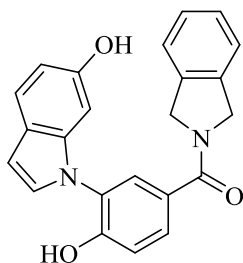
(4-Hydroxy-3-(6-hydroxy-1H-indol-1-yl)phenyl)(isoindolin-2-yl)methanone (**26**), brown

amorphous solid (25 mg, 24%). ¹H NMR (500 MHz, CDCl₃) δ 7.43 (d, J = 2.1 Hz, 1H), 7.39 (d, J

= 8.5 Hz, 1H), 7.33 (dd, J = 8.4, 2.1 Hz, 1H), 7.27 (s, 1H), 7.27 – 7.19 (m, 2H), 7.13 (d, J = 7.4

Hz, 1H), 6.98 (d, J = 3.3 Hz, 1H), 6.90 (d, J = 8.4 Hz, 1H), 6.69 (dd, J = 8.5, 2.2 Hz, 1H), 6.52 (d,

J = 3.2 Hz, 1H), 6.39 (d, J = 2.1 Hz, 1H), 4.91 (s, 2H), 4.76 (s, 2H). ¹³C NMR (126 MHz, CDCl₃)

δ 170.1, 153.7, 153.0, 137.3, 136.0, 135.7, 127.9, 127.9, 127.6, 127.6, 127.4, 127.0, 126.4, 122.9,

122.5 (2C), 121.6, 117.2, 110.9, 103.8, 96.4, 55.1, 52.8. HRMS (ESI) *m/z* [M+Na]$^+$ for C$_{23}$H$_{18}$N$_2$O$_3$Na 393.1215, found 393.1225.
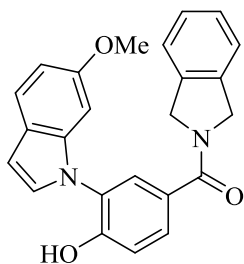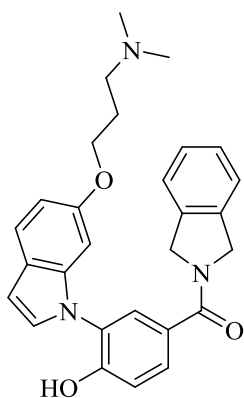

(4-Hydroxy-3-(6-methoxy-1H-indol-1-yl)phenyl)(isoindolin-2-yl)methanone (**27**), off white amorphous solid (17 mg, 16%). ^{1}H NMR (500 MHz, CDCl$_3$) δ 7.54 (d, J = 1.9 Hz, 1H), 7.52 (d, J = 8.6 Hz, 1H), 7.45 – 7.39 (m, 1H), 7.29 (d, J = 8.5 Hz, 2H), 7.25 – 7.21 (m, 1H), 7.14 (dt, J = 4.0, 2.4 Hz, 2H), 6.82 (td, J = 8.8, 1.8 Hz, 2H), 6.68 (d, J = 2.2 Hz, 1H), 6.61 (dd, J = 3.2, 1.0 Hz, 1H), 4.98 (s, 2H), 4.87 (s, 2H). ^{13}C NMR (126 MHz, CDCl$_3$) δ 169.5, 156.8, 154.1, 137.4, 136.2, 136.0, 129.0, 128.5, 127.9, 127.8, 127.4, 126.0, 122.9, 122.7, 122.4, 121.6, 117.3, 115.2, 110.4, 103.5, 94.2, 55.7, 55.2, 52.8. HRMS (ESI) *m/z* [M+Na]$^+$ for C$_{24}$H$_{20}$N$_2$O$_3$Na 407.1372, found 407.1383.

(3-(6-(3-(Dimethylamino)propoxy)-1H-indol-1-yl)-4-hydroxyphenyl)(isoindolin-2-yl)methanone (**28**), brown oil (8 mg, 6%). ^{1}H NMR (400 MHz, CDCl$_3$) δ 7.69 – 7.62 (m, 2H), 7.53 (d, J = 8.6 Hz, 1H), 7.42 (d, J = 8.4 Hz, 1H), 7.35 – 7.27 (m, 3H), 7.20 – 7.14 (m, 2H), 6.85 – 6.81 (m, 1H), 6.74 (d, J = 2.2 Hz, 1H), 6.60 (dd, J = 3.3, 0.8 Hz, 1H), 5.03 (s, 2H), 4.90 (s, 3H), 3.98 (t, J = 6.4 Hz, 2H), 2.47 – 2.40 (m, 2H), 2.23 (s, 6H), 1.97 – 1.92 (m, 2H). ^{13}C NMR (126 MHz,

CDCl$_3$) δ 168.9, 156.0, 153.7, 137.6, 130.7, 128.0, 128.0, 127.9, 127.6, 127.3, 127.3, 123.0, 122.9, 122.8, 122.4, 121.3, 116.5, 110.4, 103.0, 95.4, 95.0, 66.8, 56.5, 56.5, 45.6, 45.5, 29.7, 27.7. HRMS (ESI) *m/z* [M]$^+$ for C$_{28}$H$_{29}$N$_3$O$_3$ 455.2209, found 455.2193.
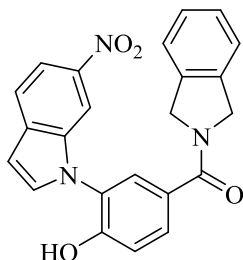

(4-Hydroxy-3-(6-nitro-1H-indol-1-yl)phenyl)(isoindolin-2-yl)methanone (**29**), yellow amorphous solid (13 mg, 12%). ^{1}H NMR (500 MHz, CDCl$_3$) δ 8.24 (s, 1H), 8.04 (td, J = 8.7, 8.3, 2.1 Hz, 1H), 7.70 (d, J = 8.6 Hz, 1H), 7.67 − 7.52 (m, 3H), 7.48 − 7.43 (m, 1H), 7.28 (d, J = 8.2 Hz, 3H), 7.16 − 7.11 (m, 1H), 6.77 (d, J = 3.3 Hz, 1H), 4.99 (s, 2H), 4.97 (s, 2H). ^{13}C NMR (126 MHz, CDCl$_3$) δ 169.3, 154.0, 143.4, 135.4, 134.8, 133.5, 131.3, 129.1, 127.7, 127.2, 125.1, 124.4, 120.9, 119.8, 117.3, 115.6, 114.9, 114.6, 111.2, 110.9, 108.0, 103.8, 55.4, 52.8. HRMS (ESI) *m/z* [M+Na]$^+$ for C$_{23}$H$_{17}$N$_3$O$_4$Na 422.1117, found 422.1115.
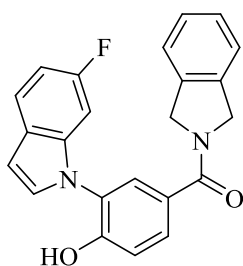
(3-(6-Fluoro-1H-indol-1-yl)-4-hydroxyphenyl)(isoindolin-2-yl)methanone (**30**), white amorphous solid (22 mg, 13%). ^{1}H NMR (500 MHz, CDCl$_3$) δ 7.57 − 7.51 (m, 3H), 7.28 (d, J = 8.5 Hz, 2H), 7.25 (d, J = 3.4 Hz, 2H), 7.16 (d, J = 7.4 Hz, 1H), 7.10 (d, J = 8.3 Hz, 1H), 6.94 − 6.86 (m, 2H), 6.64 (d, J = 3.3 Hz, 1H), 4.97 (s, 2H), 4.86 (s, 2H). ^{13}C NMR (126 MHz, CDCl$_3$) δ 169.5, 160.1 (d, J = 238.1 Hz), 154.0, 136.0, 129.3, 129.0, 128.4, 127.9, 127.6, 127.2, 125.9, 125.0,

123.0, 122.4, 121.6, 117.2, 115.2, 108.9, 103.3, 97.2, 55.2, 52.7. HRMS (ESI) *m/z* [M+Na]⁺ for

C₂₃H₁₇FN₂O₂Na 395.1172, found 395.1186.
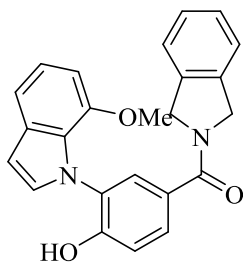
(4-Hydroxy-3-(7-methoxy-1H-indol-1-yl)phenyl)(isoindolin-2-yl)methanone (**31**), white

amorphous solid (40 mg, 38%). ¹H NMR (400 MHz, CDCl₃) δ 7.53 – 7.43 (m, 2H), 7.27 (s, 1H),

7.23 (dd, *J* = 7.9, 0.8 Hz, 3H), 7.12 (d, *J* = 7.2 Hz, 1H), 7.08 (d, *J* = 3.2 Hz, 1H), 7.05 – 6.99 (m,

2H), 6.64 – 6.59 (m, 2H), 4.93 (s, 2H), 4.85 (s, 2H), 3.64 (s, 3H). ¹³C NMR (126 MHz, CDCl₃) δ

169.9, 154.5, 147.5, 136.4, 136.2, 131.1, 130.2, 128.5 (2C), 128.3, 127.9, 127.6, 127.2, 126.7,

123.0, 122.4, 121.1, 116.3, 114.0, 104.0, 103.9, 55.7, 55.3, 52.8. HRMS (ESI) *m/z* [M+Na]⁺ for

C₂₄H₂₀N₂O₃Na 407.1372, found 407.1382.
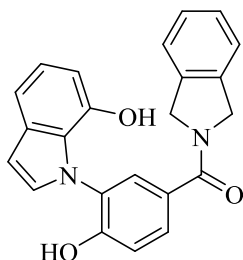
(4-Hydroxy-3-(7-hydroxy-1H-indol-1-yl)phenyl)(isoindolin-2-yl)methanone (**32**), brown

amorphous solid (19 mg, 19%). ¹H NMR (500 MHz, CDCl₃) δ 7.63 – 7.60 (m, 1H), 7.54 – 7.49

(m, 2H), 7.36 – 7.28 (m, 3H), 7.20 – 7.14 (m, 2H), 7.09 (dd, J = 6.2, 3.3 Hz, 1H), 6.90 – 6.86 (m,

2H), 6.66 (d, J = 7.3 Hz, 1H), 5.02 (s, 2H), 4.83 (s, 2H). ¹³C NMR (126 MHz, CDCl₃) δ 170.2,

160.8, 157.2, 156.6, 145.1, 135.9, 135.4, 135.3, 132.0, 131.7, 129.2, 127.7, 126.8, 126.7, 120.5,

115.2, 109.3, 108.9, 106.5, 100.3, 100.2, 55.1, 52.6. HRMS (ESI) *m/z* [M+Na]$^+$ for C$_{23}$H$_{18}$N$_2$O$_3$Na 393.1215, found 393.1220.
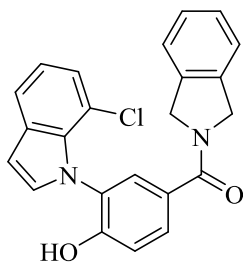
(3-(7-Chloro-1H-indol-1-yl)-4-hydroxyphenyl)(isoindolin-2-yl)methanone (**33**), yellow amorphous solid (35 mg, 33%). ^{1}H NMR (500 MHz, CDCl$_3$) δ 7.60 − 7.55 (m, 1H), 7.44 (d, J = 8.4 Hz, 2H), 7.35 − 7.27 (m, 3H), 7.21 − 7.12 (m, 2H), 7.12 − 7.04 (m, 2H), 6.84 (d, J = 8.4 Hz, 2H), 5.01 (s, 2H), 4.85 (d, J = 21.5 Hz, 2H). ^{13}C NMR (126 MHz, CDCl$_3$) δ 171.1, 158.7, 136.4, 136.1, 131.3, 129.4, 129.0 (2C), 128.9, 127.8, 127.6, 127.5, 127.2, 124.0, 122.9, 122.4, 121.3, 120.0, 116.4, 115.5 (2C), 104.4, 55.3, 52.8. HRMS (ESI) *m/z* [M+Na]$^+$ for C$_{23}$H$_{17}$ClN$_2$O$_2$Na 411.0876, found 411.0878.
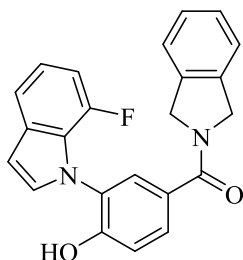
(3-(7-Fluoro-1H-indol-1-yl)-4-hydroxyphenyl)(isoindolin-2-yl)methanone (**34**), brown amorphous solid (32 mg, 31%). ^{1}H NMR (500 MHz, CDCl$_3$) δ 7.54 (q, J = 2.0 Hz, 1H), 7.53 − 7.46 (m, 1H), 7.39 (dd, J = 7.9, 3.3 Hz, 1H), 7.29 − 7.23 (m, 3H), 7.20 − 7.13 (m, 2H), 7.07 − 6.96 (m, 2H), 6.88 − 6.79 (m, 1H), 6.66 (d, J = 3.0 Hz, 1H), 4.95 (s, 2H), 4.86 (s, 2H). ^{13}C NMR (126 MHz, CDCl$_3$) δ 169.8, 154.4, 150.0 (d, J = 246.1), 136.3, 136.0, 130.7, 128.4, 127.8, 127.6, 127.6,

127.5, 127.3, 122.9, 122.4, 120.4, 120.4, 116.8, 116.7, 116.5, 108.0, 107.9, 103.8, 55.1, 52.7.

HRMS (ESI) *m/z* [M+Na]$^+$ for C$_{23}$H$_{17}$FN$_2$O$_2$Na 395.1172, found 395.1179.
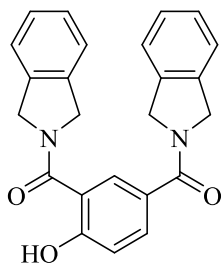
(4-Hydroxy-1,3-phenylene)bis(isoindolin-2-ylmethanone) (**36**). Hunig's base (1.2 mL, 6.6 mmol, 12 equiv.) was added to a stirred solution of 4-hydroxyisophthalic acid (100 mg, 0.55 mmol, 1 equiv.), EDCI (632 mg, 3.3 mmol, 6 equiv.), HOBT (445 mg, 3.3 mmol, 6 equiv.) and isoindoline hydrochloride (513 mg, 3.3 mmol, 6 equiv.) in DCM (0.05 M) and stirred at rt for 12 h. 1 N HCl was added and the organic layer was separated and washed with saturated NaHCO$_3$ and brine. The organic layer was dried (Na$_2$SO$_4$), concentrated, and purified by flash chromatography (EtOAc/Hexanes, 1:1) to provide **36** as a tan amorphous solid (48 mg, 23%). ^{1}H NMR (400 MHz, CDCl$_3$) δ 7.99 (d, *J* = 2.1 Hz, 1H), 7.67 (dd, *J* = 8.6, 2.1 Hz, 1H), 7.40 – 7.27 (m, 7H), 7.20 (d, *J* = 7.5 Hz, 1H), 7.09 (d, *J* = 8.6 Hz, 1H), 5.13 (s, 4H), 5.05 (s, 2H), 4.88 (s, 2H). ^{13}C NMR (126 MHz, CDCl$_3$) δ 169.8, 169.3, 161.8, 136.3, 136.1, 131.7 (2C), 128.0 (2C), 127.8 (2C), 127.5, 126.4, 122.8, 122.5 (2C), 122.4, 117.7 (2C), 116.7, 55.1 (2C), 52.7 (2C). HRMS (ESI) *m/z* [M+Na]$^+$ for C$_{24}$H$_{20}$N$_2$O$_3$ 407.1372, found 407.1358.

General procedure for the synthesis of 37a-39a.

Hunig's base (6 equiv.) was added to a stirred solution of 2-hydroxy-5-(methoxycarbonyl)benzoic acid (1 equiv.), EDCI (3 equiv.), HOBT (3 equiv.) and a substituted isoindoline (3 equiv.) in DCM (0.1 M) and stirred at rt for 12 h. 1 N HCl was added and the organic layer was separated and washed with saturated NaHCO$_3$ and brine. The organic layer was dried

(Na$_2$SO$_4$), concentrated, and purified by flash chromatography (EtOAc/Hexanes, 1:1) to provide **37a**-**39a**.
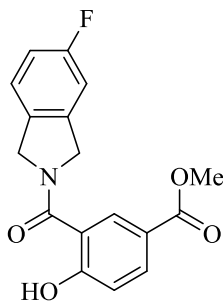
Methyl 3-(5-fluoroisoindoline-2-carbonyl)-4-hydroxybenzoate (**37a**) white amorphous solid (17 mg, 35%). ^{1}H NMR (400 MHz, CDCl$_3$) δ 11.76 (s, 1H), 8.41 (d, J = 2.1 Hz, 1H), 8.06 (dd, J = 8.7, 2.1 Hz, 1H), 7.26 (s, 1H), 7.09 – 6.99 (m, 3H), 5.12 (s, 4H), 3.93 (s, 3H). ^{13}C NMR (126 MHz, CDCl$_3$) δ 169.8, 166.4, 164.6, 146.8, 144.9, 143.9, 134.5 (2C), 130.4, 120.3, 118.2 (2C), 101.0, 92.9, 53.4, 52.2 (2C). HRMS (ESI) *m/z* [M+H]$^+$ for C$_{17}$H$_{15}$FNO$_4$ 316.0985, found 316.0977.
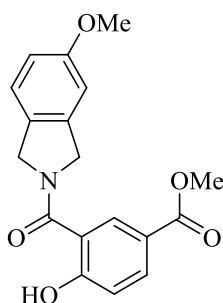
Methyl 4-hydroxy-3-(5-methoxyisoindoline-2-carbonyl)benzoate (**38a**), white amorphous solid (23 mg, 46%). ^{1}H NMR (400 MHz, CDCl$_3$) δ 11.89 (s, 1H), 8.43 (d, J = 2.1 Hz, 1H), 8.06 (dd, J = 8.7, 2.0 Hz, 1H), 7.22 (s, 1H), 7.05 (d, J = 8.7 Hz, 1H), 6.87 (d, J = 8.4 Hz, 2H), 5.09 (s, 4H), 3.93 (s, 3H), 3.82 (s, 3H). ^{13}C NMR (126 MHz, CDCl$_3$) δ 172.7, 169.7, 166.4, 164.6, 145.9, 135.6, 134.4, 131.6, 130.5, 121.9, 120.2, 118.2, 112.5, 100.0, 67.4, 64.2, 55.5, 52.2. HRMS (ESI) *m/z* [M+H]$^+$ for C$_{18}$H$_{18}$NO$_5$ 328.1185, found 328.1175.
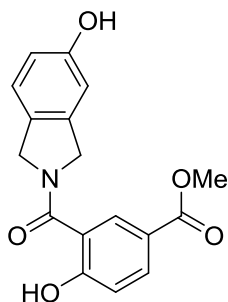
Methyl 4-hydroxy-3-(5-hydroxyisoindoline-2-carbonyl)benzoate (**39a**), off white amorphous solid (19 mg, 40%). ^{1}H NMR (400 MHz, CDCl$_3$) δ 8.30 (d, J = 2.1 Hz, 1H), 8.00 (dd, J = 8.7, 2.1 Hz, 1H), 7.24 (s, 1H), 6.99 (d, J = 8.6 Hz, 1H), 6.71 (d, J = 30.1 Hz, 2H), 4.96 (s, 4H), 3.88 (s, 3H). ^{13}C NMR (126 MHz, CDCl$_3$) δ 172.3, 172.1, 165.3, 155.2, 134.0, 130.3, 127.3, 125.0, 122.9, 119.6, 117.7, 114.3, 110.7, 108.6, 100.0, 56.2, 53.7, 52.1. HRMS (ESI) *m/z* [M+H]$^+$ for C$_{17}$H$_{16}$NO$_5$ 314.1028, found 314.1040.

General procedure for the synthesis of 37-39.

LiOH (10 eq.) was added to a stirred solution of **37a-39a** (1 equiv.) in a THF:MeOH:Water mixture (2:1:1, 0.1 M). The reaction was heated to 70°C for 12 h then cooled to rt. 3 N HCl was added dropwise until the pH was ~7 followed by the addition of EtOAc. The organic layer was separated and the aqueous layer was extracted with EtOAc. The organic layers were combined, dried, and concentrated and used as obtained. The residue was dissolved in DCM to which isoindoline (3 equiv.), EDCI (3 equiv.), HOBT (3 equiv.), and Hunig's base (6 equiv.) were added. The reaction stirred at rt for 12 h. 1 N HCl was added and the organic layer was separated and washed with saturated NaHCO$_3$ and brine. The organic layer was dried (Na$_2$SO$_4$), concentrated, and purified by flash chromatography (EtOAc/Hexanes, 1:1) to provide **37-39**.
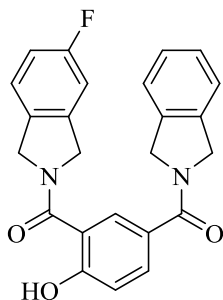
(5-Fluoroisoindolin-2-yl)(2-hydroxy-5-(isoindoline-2-carbonyl)phenyl)methanone (**37**), white amorphous solid (15 mg, 70%). ^{1}H NMR (400 MHz, CDCl$_3$) δ 11.36 (s, 1H), 7.97 (d, *J* = 2.1 Hz, 1H), 7.72 – 7.63 (m, 1H), 7.42 – 7.27 (m, 4H), 7.24 – 7.18 (m, 1H), 7.09 (d, *J* = 8.6 Hz, 1H), 7.01 (d, *J* = 8.6 Hz, 2H), 5.08 (d, *J* = 21.1 Hz, 6H), 4.88 (s, 2H). ^{13}C NMR (126 MHz, CDCl$_3$) δ 169.9, 169.3, 161.9, 136.3, 136.2, 131.9 (2C), 131.8, 128.2, 128.1 (2C), 128.0, 127.9, 127.6, 127.6, 126.5, 123.0, 122.5, 117.8, 117.8 (2C), 116.7, 55.2, 52.8. HRMS (ESI) *m/z* [M+Na]$^+$ for C$_{24}$H$_{19}$FN$_2$O$_3$Na 425.1277, found 425.1273.
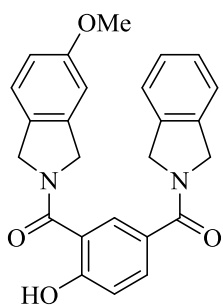
(4-Hydroxy-3-(5-methoxyisoindoline-2-carbonyl)phenyl)(isoindolin-2-yl)methanone (**38**) tan amorphous solid (12 mg, 41%). ^{1}H NMR (400 MHz, CDCl$_3$) δ 11.48 (s, 1H), 7.98 (d, *J* = 2.1 Hz, 1H), 7.66 (dd, *J* = 8.5, 2.1 Hz, 1H), 7.39 – 7.27 (m, 3H), 7.20 (d, *J* = 7.3 Hz, 2H), 7.08 (d, *J* = 8.5 Hz, 1H), 6.89 – 6.73 (m, 2H), 5.05 (s, 6H), 4.87 (s, 2H), 3.81 (s, 3H). ^{13}C NMR (126 MHz, CDCl$_3$) δ 170.2, 169.8, 162.3, 136.8, 136.6, 132.2, 128.6, 128.3, 128.0, 126.8, 123.8, 123.4, 122.9, 118.2, 117.2, 114.9, 107.9, 55.9, 55.6, 53.2. HRMS (ESI) *m/z* [M+Na]$^+$ for C$_{25}$H$_{22}$N$_2$O$_4$Na 437.1477, found 437.1481.
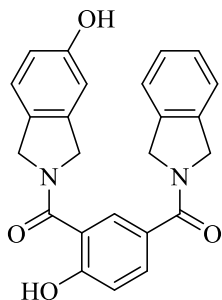
(4-Hydroxy-3-(5-hydroxyisoindoline-2-carbonyl)phenyl)(isoindolin-2-yl)methanone (**39**) tan amorphous solid (19 mg, 78%). ^{1}H NMR (400 MHz, CDCl$_3$) δ 7.93 (d, J = 2.1 Hz, 1H), 7.65 (d, J = 2.1 Hz, 1H), 7.39 − 7.28 (m, 5H), 7.20 (d, J = 7.4 Hz, 1H), 7.09 (s, 1H), 6.82 (s, 1H), 5.07 (s, 2H), 4.91 (d, J = 11.0 Hz, 4H), 4.81 (d, J = 6.6 Hz, 2H). ^{13}C NMR (126 MHz, CDCl$_3$) δ 169.8, 169.8, 169.5, 169.4, 161.9, 131.5, 128.5, 128.0, 127.9, 127.7, 127.6, 123.1, 123.0, 122.6, 122.5, 117.7, 55.3, 53.4, 53.0, 52.1. HRMS (ESI) *m/z* [M]$^+$ for C$_{24}$H$_{21}$N$_2$O$_4$ 387.1471, found 387.1476.

Fluorescence polarization. The assay was performed in 96-well black, flat-bottom plates with a final volume of 100 μL. 25 μL of assay buffer (20 mM HEPES, pH 7.3, 50 mM KCl, 5 mM MgCl2, 20 mM Na2MoO4, 2 mM DTT, 0.1 mg/mL BGG, and 0.01% NP-40) were added, followed by 25 μL of assay buffer containing 6 nM FITC-GDA (fluorescent tracer, stock in DMSO, diluted in assay buffer) and 50 μL of assay buffer containing 10 nM of either Grp94, Hsp90β, or Hsp90α or 20 nM TRAP1 were added to each well. For each plate, wells containing buffer only (background), tracer in buffer only (low polarization control) and protein, tracer, and 1% DMSO (final concentration, high polarization control) were included. Compounds were then added with a final concentration of DMSO = 1%. Plates were incubated at 4 ˚C with rocking for 24 h. Polarization values (in mP units) were measured at 37 ˚C with an excitation filter at 485 nm and an emission filter at 528 nm. Polarization values were correlated to % tracer bound and compound concentrations. The concentration at which the tracer was 50% displaced by compound of interested were calculated and reported as apparent Kd's.

Cell Culture. PC3-MM2, HeLa, and HCT116 (ATCC) were grown in a water jacketed incubator at 37˚C with 5% CO_2 in DMEM (PC3-MM2), EMEM (HeLa), or McCoy's (HCT116) media supplemented with 10% FBS and 1% penicillin/streptomycin.

Anti-proliferation. Cells were counted via Trypan blue exclusion and seeded in 96-well plates at 2000 cells/0.1 mL/well then returned to the incubator for 24 h. Compounds in DMSO (1% final concentration) or vehicle were administered and the plates were returned to the incubator for 72 h. The % viable cells was determined using the MTS/PMS cell proliferation kit (Promega) per the manufacturer's instructions. Cells treated with vehicle were normalized to 100% viable and compound treated cells were adjusted accordingly. GI_{50} values were calculated via GraphPad Prism and reported as the average of 2 independent experiments.

Western Blot Analysis. HeLa were counted as described above and seeded at 100,000 cells/mL in 10 cm dishes. The dishes were returned to the incubator for 24 h at which point compounds or vehicle were added (0.25% DMSO final concentration) and incubated together for 24 h. Cells were harvested in cold PBS and lysed using MPER (Thermo Scientific) supplemented with protease inhibitors (Roche) according to the manufacturer's instructions. Cell lysates were obtained by centrifugation at 14,000 rpm for 10 min. Protein concentrations were determined using the Pierce BCA assay kit with serum albumin as the standard and following the manufacturer's instructions. Equal amounts of protein were separated via SDS-PAGE under reducing conditions then transferred to PVDF membranes and immunoblotted with the corresponding primary antibodies for CHOP (Cell Signaling), Akt (Santa Cruz Biotechnology), Hsp70 (Enzo Life Sciences), and Actin (Santa Cruz Biotechnology). Membranes were then incubated with the correct HRP-conjugated secondary antibody (Rabbit for Akt and Hsp70; Mouse for CHOP and Actin), developed with a chemiluminescent substrate (Bio-Rad), and visualized.

Flow Cytometry. HeLa cells were counted and seeded at 100,000 cells/mL in a 24 well plate and returned to the incubator for 24 h. Compounds or DMSO were then administered (0.25% DMSO final concentration) and returned to the incubator for 12 h. The cells were then washed with PBS, trypsinized, and diluted with media (2 x volume of trypsin). Propidium iodide (5 mM stock in DMSO) was added to each sample for a final concentration of 5 µM. Samples were incubated for 10 min at rt with rocking before analysis. 60 µL of each sample were analyzed via an Accuri C6 flow cytometer.

References

1.   Travers, J.; Sharp, S.; Workman, P. HSP90 inhibition: two-pronged exploitation of cancer dependencies. *Drug Discov. Today* **2012,** *17*, 242-252.

2.   Taipale, M.; Jarosz, D. F.; Lindquist, S. HSP90 at the hub of protein homeostasis: emerging mechanistic insights. *Nat. Rev. Mol. Cell Biol.* **2010,** *11*, 515-528.

3.   Picard, D. Hsp90 Interactors. https://www.picard.ch/downloads.

4.   Miyata, Y.; Nakamoto, H.; Neckers, L. The therapeutic target Hsp90 and cancer hallmarks. *Curr. Pharm. Des.* **2013,** *19*, 347-365.

5.   Hanahan, D.; Weinberg, R. A. Hallmarks of cancer: the next generation. *Cell* **2011,** *144*, 646-674.

6.   Neckers, L.; Workman, P. Hsp90 molecular chaperone inhibitors: are we there yet? *Clin. Cancer Res.* **2012,** *18*, 64-76.

7.   Khandelwal, A.; Crowley, V. M.; Blagg, B. S. Natural product inspired N-terminal Hsp90 inhibitors: from bench to bedside? *Med. Res. Rev.* **2016,** *36*, 92-118.

8.   Bhat, R.; Tummalapalli, S. R.; Rotella, D. P. Progress in the discovery and development of heat shock protein 90 (Hsp90) inhibitors. *J. Med. Chem.* **2014,** *57*, 8718-8728.

9.   Rajan, A.; Kelly, R. J.; Trepel, J. B.; Kim, Y. S.; Alarcon, S. V.; Kummar, S.; Gutierrez, M.; Crandon, S.; Zein, W. M.; Jain, L.; Mannargudi, B.; Figg, W. D.; Houk, B. E.; Shnaidman, M.; Brega, N.; Giaccone, G. A phase I study of PF-04929113 (SNX-5422), an orally bioavailable heat shock protein 90 inhibitor, in patients with refractory solid tumor malignancies and lymphomas. *Clin. Cancer Res.* **2011,** *17*, 6831-6839.

10.   Roman, D.; VerHoeve, J.; Schadt, H.; Vicart, A.; Walker, U. J.; Turner, O.; Richardson, T. A.; Wolford, S. T.; Miller, P. E.; Zhou, W.; Lu, H.; Akimov, M.; Kluwe, W. Ocular toxicity of AUY922 in pigmented and albino rats. *Toxicol. Appl. Pharmacol.* **2016,** *309*, 55-62.

11.   Liu, W.; Vielhauer, G. A.; Holzbeierlein, J. M.; Zhao, H.; Ghosh, S.; Brown, D.; Lee, E.; Blagg, B. S. KU675, a Concomitant Heat-Shock Protein Inhibitor of Hsp90 and Hsc70 that Manifests Isoform Selectivity for Hsp90alpha in Prostate Cancer Cells. *Mol. Pharmacol.* **2015,** *88*, 121-130.

12.   Ghosh, S.; Shinogle, H. E.; Galeva, N. A.; Dobrowsky, R. T.; Blagg, B. S. Endoplasmic Reticulum-resident Heat Shock Protein 90 (HSP90) Isoform Glucose-regulated Protein 94 (GRP94) Regulates Cell Polarity and Cancer Cell Migration by Affecting Intracellular Transport. *J. Biol. Chem.* **2016,** *291*, 8309-8323.

13.   Peterson, L. B.; Eskew, J. D.; Vielhauer, G. A.; Blagg, B. S. The hERG channel is dependent upon the Hsp90α isoform for maturation and trafficking. *Mol. Pharm.* **2012,** *9*, 1841-1846.

14.   Stothert, A. R.; Suntharalingam, A.; Huard, D. J.; Fontaine, S. N.; Crowley, V. M.; Mishra, S.; Blagg, B. S.; Lieberman, R. L.; Dickey, C. A. Exploiting the interaction between Grp94 and aggregated myocilin to treat glaucoma. *Hum. Mol. Genet.* **2014,** *23*, 6470-6480.

15.   Crowley, V. M.; Khandelwal, A.; Mishra, S.; Stothert, A. R.; Huard, D. J.; Zhao, J.; Muth, A.; Duerfeldt, A. S.; Kizziah, J. L.; Lieberman, R. L.; Dickey, C. A.; Blagg, B. S. Development of

Glucose Regulated Protein 94-Selective Inhibitors Based on the BnIm and Radamide Scaffold. *J. Med. Chem.* **2016,** *59*, 3471-3488.

16.   Crowley, V.; Huard, D.; Lieberman, R.; Blagg, B. Second Generation Grp94-selective Inhibitors Provide Opportunities for the Inhibition of Metastatic Cancer. *Chem. Eur. J.* **2017,** *In Press.*

17.   Hua, Y.; White-Gilbertson, S.; Kellner, J.; Rachidi, S.; Usmani, S. Z.; Chiosis, G.; Depinho, R.; Li, Z.; Liu, B. Molecular chaperone gp96 is a novel therapeutic target of multiple myeloma. *Clin. Cancer Res.* **2013,** *19*, 6242-6251.

18.   Khandelwal, A. C., V. M.; Blagg, B. S. Resorcinol-Based Grp94-Selective Inhibitors. *ACS Med. Chem. Lett.* **2017,** *8*, 1013-1018.

19.   Gewirth, D. T. Paralog Specific Hsp90 Inhibitors - A Brief History and a Bright Future. *Curr. Top. Med. Chem.* **2016,** *16*, 2779-2791.

20.   Altieri, D. C.; Stein, G. S.; Lian, J. B.; Languino, L. R. TRAP-1, the mitochondrial Hsp90. *Biochim. Biophys. Acta* **2012,** *1823*, 767-773.

21.   Song, H. Y.; Dunbar, J. D.; Zhang, Y. X.; Guo, D.; Donner, D. B. Identification of a protein with homology to Hsp90 that binds the type 1 tumor necrosis factor receptor. *J. Biol. Chem.* **1995,** *270*, 3574-3581.

22.   Kang, B. H.; Plescia, J.; Dohi, T.; Rosa, J.; Doxsey, S. J.; Altieri, D. C. Regulation of tumor cell mitochondrial homeostasis by an organelle-specific Hsp90 chaperone network. *Cell* **2007,** *131*, 257-270.

23.   Park, H. K.; Lee, J. E.; Lim, J.; Kang, B. H. Mitochondrial Hsp90s suppress calcium-mediated stress signals propagating from mitochondria to the ER in cancer cells. *Mol. Cancer* **2014,** *13*, 148.

24.   Oyadomari, S.; Mori, M. Roles of CHOP/GADD153 in endoplasmic reticulum stress. *Cell Death Differ.* **2004,** *11*, 381-389.

25.   Li, Y.; Guo, Y.; Tang, J.; Jiang, J.; Chen, Z. New insights into the roles of CHOP-induced apoptosis in ER stress. *Acta Biochim. Biophys. Sin (Shanghai)* **2014,** *46*, 629-640.

26.   Lei, Y.; Wang, S.; Ren, B.; Wang, J.; Chen, J.; Lu, J.; Zhan, S.; Fu, Y.; Huang, L.; Tan, J. CHOP favors endoplasmic reticulum stress-induced apoptosis in hepatocellular carcinoma cells via inhibition of autophagy. *PLoS One* **2017,** *12*, e0183680.

27.   Marciniak, S. J.; Yun, C. Y.; Oyadomari, S.; Novoa, I.; Zhang, Y.; Jungreis, R.; Nagata, K.; Harding, H. P.; Ron, D. CHOP induces death by promoting protein synthesis and oxidation in the stressed endoplasmic reticulum. *Genes Dev.* **2004,** *18*, 3066-3077.

28.   Lavery, L. A.; Partridge, J. R.; Ramelot, T. A.; Elnatan, D.; Kennedy, M. A.; Agard, D. A. Structural asymmetry in the closed state of mitochondrial Hsp90 (TRAP1) supports a two-step ATP hydrolysis mechanism. *Mol. Cell* **2014,** *53*, 330-343.

29.   Lee, C.; Park, H. K.; Jeong, H.; Lim, J.; Lee, A. J.; Cheon, K. Y.; Kim, C. S.; Thomas, A. P.; Bae, B.; Kim, N. D.; Kim, S. H.; Suh, P. G.; Ryu, J. H.; Kang, B. H. Development of a mitochondria-targeted Hsp90 inhibitor based on the crystal structures of human TRAP1. *J. Am. Chem. Soc.* **2015,** *137*, 4358-4367.

30.   Leskovar, A.; Wegele, H.; Werbeck, N. D.; Buchner, J.; Reinstein, J. The ATPase cycle of the mitochondrial Hsp90 analog Trap1. *J. Biol. Chem.* **2008,** *283*, 11677-11688.

31.   Roe, S. M.; Prodromou, C.; O'Brien, R.; Ladbury, J. E.; Piper, P. W.; Pearl, L. H. Structural basis for inhibition of the Hsp90 molecular chaperone by the antitumor antibiotics radicicol and geldanamycin. *J. Med. Chem.* **1999,** *42*, 260-266.

32.   Zubriene, A.; Gutkowska, M.; Matuliene, J.; Chaleckis, R.; Michailoviene, V.; Voroncova, A.; Venclovas, C.; Zylicz, A.; Zylicz, M.; Matulis, D. Thermodynamics of radicicol binding to human Hsp90 alpha and beta isoforms. *Biophys. Chem.* **2010,** *152*, 153-163.

33.   Panaretou, B.; Prodromou, C.; Roe, S. M.; O'Brien, R.; Ladbury, J. E.; Piper, P. W.; Pearl, L. H. ATP binding and hydrolysis are essential to the function of the Hsp90 molecular chaperone in vivo. *EMBO J.* **1998,** *17*, 4829-4836.

34.   Patel, P. D.; Yan, P.; Seidler, P. M.; Patel, H. J.; Sun, W.; Yang, C.; Que, N. S.; Taldone, T.; Finotti, P.; Stephani, R. A.; Gewirth, D. T.; Chiosis, G. Paralog-selective Hsp90 inhibitors define tumor-specific regulation of HER2. *Nat. Chem. Biol.* **2013,** *9*, 677-684.

35.   Patel, H. J.; Patel, P. D.; Ochiana, S. O.; Yan, P.; Sun, W.; Patel, M. R.; Shah, S. K.; Tramentozzi, E.; Brooks, J.; Bolaender, A.; Shrestha, L.; Stephani, R.; Finotti, P.; Leifer, C.; Li, Z.; Gewirth, D. T.; Taldone, T.; Chiosis, G. Structure-activity relationship in a purine-scaffold compound series with selectivity for the endoplasmic reticulum Hsp90 paralog Grp94. *J. Med. Chem.* **2015,** *58*, 3922-3943.

36.   Woodhead, A. J.; Angove, H.; Carr, M. G.; Chessari, G.; Congreve, M.; Coyle, J. E.; Cosme, J.; Graham, B.; Day, P. J.; Downham, R.; Fazal, L.; Feltell, R.; Figueroa, E.; Frederickson, M.; Lewis, J.; McMenamin, R.; Murray, C. W.; O'Brien, M. A.; Parra, L.; Patel, S.; Phillips, T.; Rees, D. C.; Rich, S.; Smith, D. M.; Trewartha, G.; Vinkovic, M.; Williams, B.; Woolford, A. J. Discovery   of   (2,4-dihydroxy-5-isopropylphenyl)-[5-(4-methylpiperazin-1-ylmethyl)-1,3-dihydrois oindol-2-yl]methanone (AT13387), a novel inhibitor of the molecular chaperone Hsp90 by fragment based drug design. *J. Med. Chem.* **2010,** *53*, 5956-5969.

37.   Murray, C. W.; Carr, M. G.; Callaghan, O.; Chessari, G.; Congreve, M.; Cowan, S.; Coyle, J. E.; Downham, R.; Figueroa, E.; Frederickson, M.; Graham, B.; McMenamin, R.; O'Brien, M.

A.; Patel, S.; Phillips, T. R.; Williams, G.; Woodhead, A. J.; Woolford, A. J. Fragment-based drug discovery applied to Hsp90. Discovery of two lead series with high ligand efficiency. *J. Med. Chem.* **2010,** *53*, 5942-5955.

38.   Lisanti, S.; Garlick, D. S.; Bryant, K. G.; Tavecchio, M.; Mills, G. B.; Lu, Y.; Kossenkov, A. V.; Showe, L. C.; Languino, L. R.; Altieri, D. C. Transgenic Expression of the Mitochondrial Chaperone TNFR-associated Protein 1 (TRAP1) Accelerates Prostate Cancer Development. *J. Biol. Chem.* **2016,** *291*, 25247-25254.

39.   Maddalena, F.; Simeon, V.; Vita, G.; Bochicchio, A.; Possidente, L.; Sisinni, L.; Lettini, G.; Condelli, V.; Matassa, D. S.; Li Bergolis, V.; Fersini, A.; Romito, S.; Aieta, M.; Ambrosi, A.; Esposito, F.; Landriscina, M. TRAP1 protein signature predicts outcome in human metastatic colorectal carcinoma. *Oncotarget* **2017,** *8*, 21229-21240.

40.   Park, H. K.; Jeong, H.; Ko, E.; Lee, G.; Lee, J. E.; Lee, S. K.; Lee, A. J.; Im, J. Y.; Hu, S.; Kim, S. H.; Lee, J. H.; Lee, C.; Kang, S.; Kang, B. H. Paralog Specificity Determines Subcellular Distribution, Action Mechanism, and Anticancer Activity of TRAP1 Inhibitors. *J. Med. Chem.* **2017,** *60*, 7569-7578.

41.   Riccardi, C.; Nicoletti, I. Analysis of apoptosis by propidium iodide staining and flow cytometry. *Nat. Protoc.* **2006,** *1*, 1458-1461.